To: NATIONAL AERONAUTICS AND SPACE ADMINISTRATION
WASHINGTON, D. C. 20546

ANNUAL REPORT

Crystal Growth of Device Quality GaAs in Space

(NSG-7331)

Period April 1, 1979 to March 31, 1980

Submitted by:

Professor Harry C. Gatos and Dr. Jacek Lagowski
Department of Materials Science and Engineering
Massachusetts Institute of Technology
Cambridge, Massachusetts 02139

May 1980

TABLE OF CONTENTS

	Page No.
SUMMARY	2
INTRODUCTION	4
CRYSTAL GROWTH	4
Electroepitaxy	4
Electroepitaxial Growth Velocity	7
Electroepitaxy of Multicomponent Systems	10
New Experimental Systems for Electroepitaxy	12
Melt Growth	14
Growth Apparatus	14
Characteristics of Melt-Grown GaAs	21
CHARACTERIZATION	29
Deep-Level Transient Spectroscopy	29
Derivative Photocapacitance Spectroscopy	31
SEM-Cathodoluminescence	33
GROWTH-PROPERTY RELATIONSHIPS	33
Electronic Properties of GaAs on a Microscale	33
Compensation of InP	39
REFERENCES	43
APPENDIX	44
Preprints and reprints of publications since last annual report	

SUMMARY

Our experimental and theoretical effort continues to be aimed at the establishment of relationships among crystal growth parameters, materials properties, electronic properties and device applications of GaAs. Toward this goal we undertook the development of new approaches to the preparation and characterization of GaAs. This extensive ground-based program constitutes a necessary step for insuring successful processing of GaAs under zero-gravity conditions. Furthermore, due to its unique scope combining crystal-growth characterization, and device-related properties and phenomena, this program bears directly on the exploitation of the potential of GaAs in device applications.

Our crystal growth effort includes electroepitaxy as a non-conventional and extremely promising approach to liquid phase epitaxy and melt growth of bulk GaAs crystal. We have substantially advanced the understanding of fundamental processes involved in electroepitaxial growth. Our quantitative model of electroepitaxial growth in terms of electromigration and the Peltier effect has been successfully extended to the growth of ternary and quarternary compounds predicting high growth rates and remarkable stabilization of the composition of electroepitaxial layers.

High growth rates attained by electroepitaxy confirmed out prediction that interface kinetic phenomena have only negligible effects on electroepitaxial growth. Thus, it is now experimentally verified that electroepitaxy enables the extension of the LPE process to high growth rates so far obtained only in melt growth. As clearly demonstrated by our growth-property studies, high growth rates result in a remarkable improvement of the carrier recombination characteristics of epitaxial layers.

In our melt-growth studies we have completed the construction and testing of an advanced system for horizontal and/or vertical growth of GaAs. Successful

growth of bulk GaAs under precisely controlled growth conditions has been initiated. Crystals recently obtained were extensively characterized on a macro- and micro-scale.

Our effort to establish a "state of the art" characterization facility has been highly successful. A modified system for Deep Level Transient Capacitance Spectroscopy was set up, suitable for the determination of bulk levels and interface states. Scanning Electron Microscopy-cathodoluminescence studies were initiated in the temperature range of 80K to 700K. These newly introduced techniques, together with our recently developed methods such as IR scanning absorption, derivative photovoltage and photocapacitance spectroscopies, transport techniques and SEM-electron beam-induced current now permit the unique characterization of all essential electronic parameters of GaAs on a macro- and a micro-scale.

The importance of micro-characterization in establishing growth-property relationships of GaAs was recently demonstrated through our studies of carrier concentration and compensation microprofiles in melt-grown material. These studies showed clearly that, unlike those of elemental semiconductors (Si, Ge), the electronic characteristics of GaAs are controlled by amphoteric doping and deviations from stoichiometry rather than by impurity segregation.

We also initiated preliminary characterization studies on InP which very recently received considerable attention as a material competitive with GaAs in microwave and optoelectronic applications. Although such studies introduce a new element to our program, we believe that they are essential for proper assessment of the relative potential of GaAs versus other compound semiconductors in future applications.

INTRODUCTION

During the last three years we have made significant advancements in the electroepitaxial growth of GaAs, in the electronic characterization on a microscale, and in the study of growth-property relationships relevant to GaAs applications. We have also initiated the study of melt growth of bulk GaAs crystals. Our program on "Crystal Growth of Device Quality GaAs in Space" has been widely exposed to the scientific and engineering community of leading industrial and educational institutions, and we have succeeded in establishing direct contacts which have proven extremely valuable in assessing the present status, major problems and future prospectives of GaAs growth and applications.

Table I summarizes the most important among the above developments. A more detailed discussion is given in our publications and earlier annual reports. Presently we will outline the most recent developments, i.e., since April 1, 1979.

CRYSTAL GROWTH

Electroepitaxy

Electroepitaxy represents a novel approach to liquid phase epitaxy (LPE) of semiconductor compounds in which growth is achieved by passing an electric current through the substrate solution interface while the overall temperature of the system is maintained constant.

The prospect of achieving precise control of the crystal growth process by simply controlling the current density stimulated extensive experimental and theoretical studies of electroepitaxy.

In our earlier theoretical investigations of binary systems a model of the growth kinetics and impurity segregation has been developed.[1-4] This model defines the contribution of the Peltier effect at the solid-solution interface and that of solute electromigration to the overall growth process. Thus, it has been shown that electromigration of solute species to the growth interface is the primary means of mass transport required for supersaturation and continued growth; the contribution of electromigration to growth is dominant

TABLE I

PROGRESS TO DATE - SUMMARY OF MAJOR DEVELOPMENTS

	Development	Comments	Reference
ELECTROEPITAXIAL GROWTH	1. Growth Kinetics Model 2. Dopant Segregation Model 3. Growth Model of Multicomponent Systems	Quantitative understanding of the role of electromigration and of the Peltier effect in the electroepitaxy of binary & multicomponent systems	1,2 3,4 5
	4. Improvement in Defect Structure and Electronic Characteristics	Reduction of micro-defect density has been achieved in electroepitaxial growth high growth rates	6
MELT GROWTH	1. Construction of Advanced GaAs Melt-Growth System	Advanced system has been designed & constructed for horizontal and/or vertical growth of GaAs. The system provides unique feasibility for controlling & monitoring growth parameters. Successful growth of GaAs has been initiated.	
CHARACTERIZATION	1. IR Scanning Absorption	Quantitative method has been developed for microprofiling of carrier concentration & compensation ratio through free carrier absorption	7
	2. Derivative Surface Photovoltage Spectroscopy	A new approach has been developed for the determination of deep levels, band structure & shallow impurities	8,9
	3. Derivative Photocapacitance Spectroscopy	Wavelength modulated photocapacitance spectroscopy has been developed for the determination of deep levels	10
	4. Deep Level Transient Capacitance Spectroscopy	DLTS system has been set up suitable for determination of bulk levels & interface states	11
	5. Transport Techniques	New approach has been developed for reliable determination of electron concentration & compensation ratio from electron mobility & free carrier absorption	12,13,14
	6. SEM-Cathodoluminescence	Advanced variable temperature system has been set up for cathodoluminescence microprofiling of defects, impurities & carrier concentration	

	7. SEM-Electron Beam Induced Current	Variable temperature system has been set up for instantaneous profiling of diffusion length	
PROPERTIES & PHENOMENA	1. Electronic Properties of Melt-Grown GaAs	It has been shown that presently available melt-grown GaAs is highly inhomogeneous in microscale; it exhibits noticeable compensation & high density of deep levels	9,13,15,16
	2. Interaction Between Epitaxial Layer & Substrate	It has been demonstrated that outdiffusion of recombination centers from the substrate into LPE layers during growth process takes place. Growth conditions have been formulated to minimize outdiffusion.	17
	3. Growth-Property Relationship in Epitaxial Growth	It has been found that growth rate variations have significant effect on formation of recombination centers in GaAs.	18
	4. Relationships Between Electronic Properties & Melt-Growth Conditions	Microprofiles of electron & ionized impurity concentrations in melt-grown GaAs have been obtained for the first time. It is shown that electronic properties of GaAs in microscale are governed by amphoteric doping & deviation from stoichiometry rather than impurity segregation.	7
	5. Minority Carrier Mobility	Minority carrier mobility in p-type GaAs has been computed as a function of carrier concentration & temperature	19
	6. Interface States	Surface states on GaAs-anodic oxide interface were determined with a modified version of DLTS	11
INTERACTION WITH INDUSTRIAL ORGANIZATIONS	1. Workshop	Workshop has been held with representatives of leading industrial & educational institutions devoted to the assessment of present status, major problems & future prospects for GaAs growth & applications	16
	2. Exposure of the Program to Scientific Community	Present program & its major developments have been exposed to scientific community through a series of seminars given in industrial organizations (for example: RCA, Texas Instruments, Hewlett-Packard, Hughes Int'l., Xerox, Eastman Kodak ...), presentations at scientific meetings and/or direct contacts with individual scientists.	
	3. Working Contacts	Preliminary contacts have been established with certain industrial organizations in the area of GaAs characterization, growth & device applications.	

in the absence of significant convection in the liquid. The presence of convection in the solution enhances the contribution of the Peltier effect (cooling or heating at the growth interface) with pronounced concentration gradients which increase mass transport by diffusion.

The presence of electromigration and of the Peltier effect render electroepitaxial growth sensitive to the direction and density of the electric current, to the electrical resistivity of the solution, to the conductivity type (n or p) of the substrate and to the thickness of the substrate; as has been shown, these parameters provide a high flexibility in controlling and studying the growth process which is unattainable in standard LPE.

Our present studies were addressed to three important aspects: (1) the feasibility of achieving high growth velocities comparable to melt growth in GaAs; (2) the theoretical and experimental analysis of electroepitaxial growth of GaAs-related multicomponent systems; (3) the development of new advanced systems for electroeptiaxial growth.

Electroepitaxial Growth Velocity

The experimental results of electroepitaxial growth velocity as a function of electric current density are given in Figures 1 and 2. Figure 1 presents the results obtained on substrates with (100) orientation commonly employed in LPE growth, while Fig. 2 corresponds to substrates with (111) orientation. Only slight differences are seen between (111) and (100) orientations, and these differences are within variations expected from slight systematic differences in electron concentration of the employed substrate materials (leading to differences in Peltier effect contributions to the growth velocity). It is thus apparent that the electroepitaxial growth velocity is insensitive to substrate orientation. Furthermore, growth velocity increases linearly with

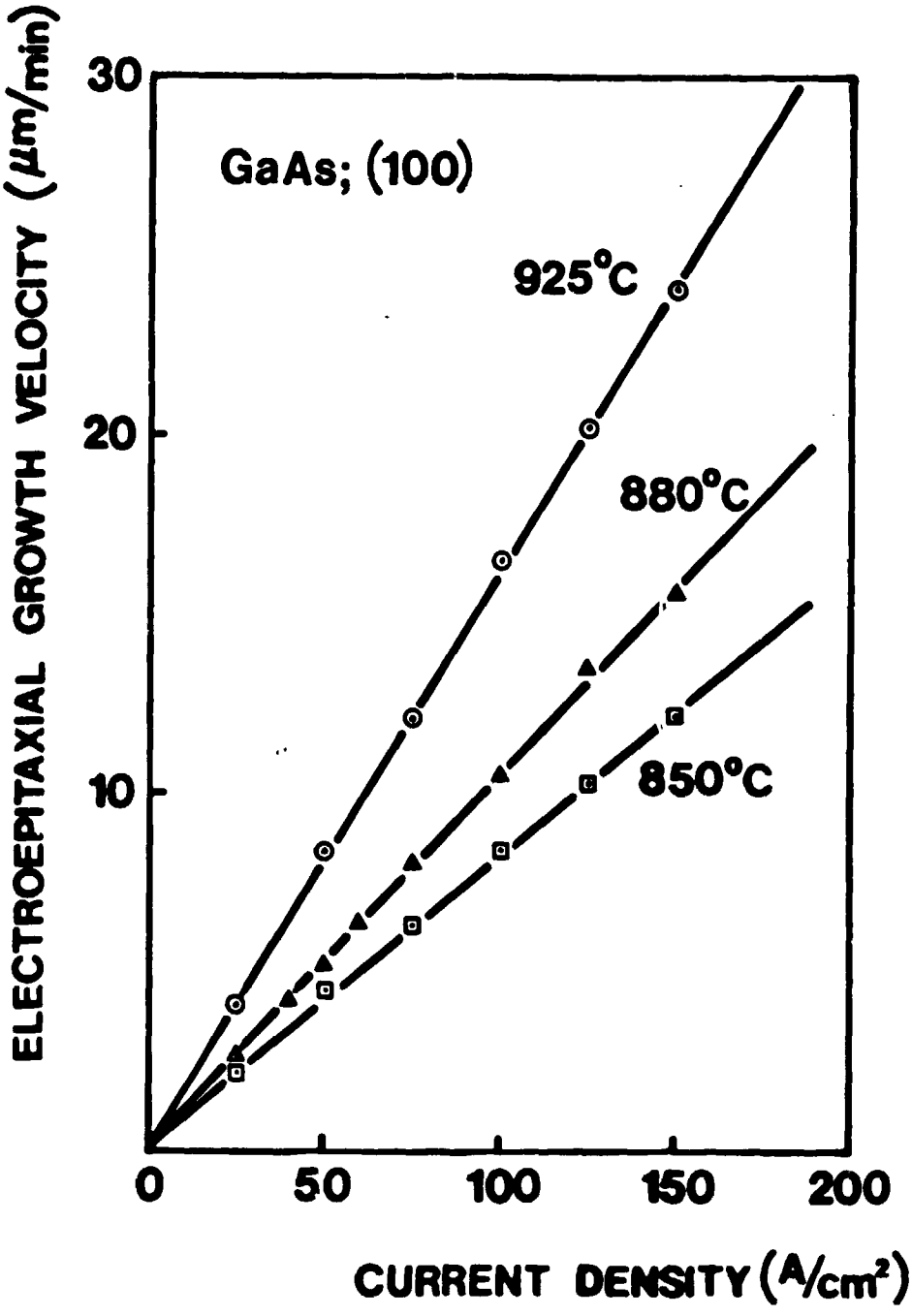

Fig. 1 Electroepitaxial growth velocity versus electric current density for GaAs grown on n-type substrates ($9.10^{17}cm^{-3}$) of (100) orientation.

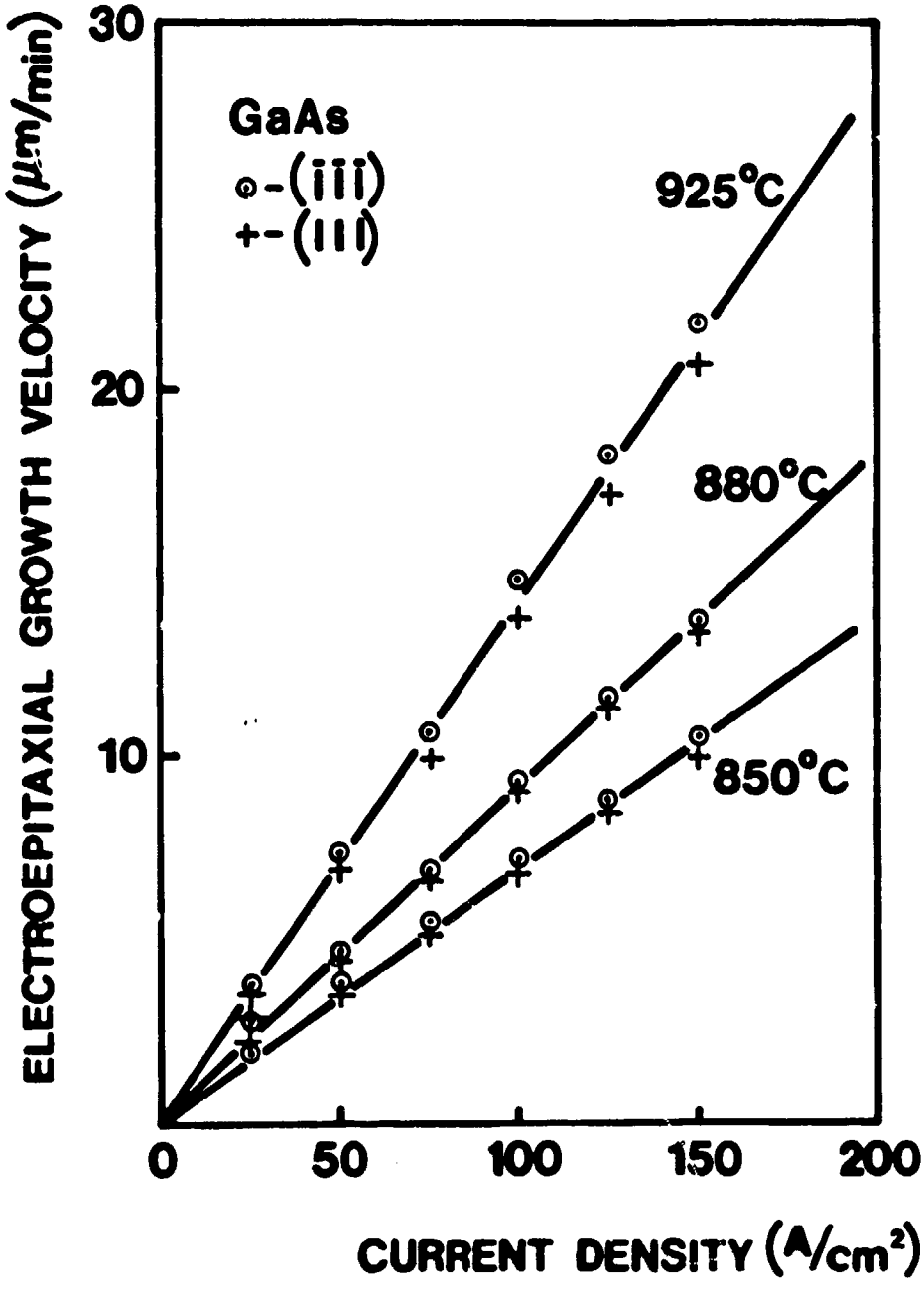

Fig. 2 Electroepitaxial growth velocity versus electric current density for GaAs grown on n-type substrates (1.1 x $10^{18}cm^{-3}$) of (111) orientation.

electric current density, even for high current densities, which provides direct evidence of the negligible role of interface kinetic phenomena. It should be noted that the highest growth velocity obtained at 925° for a current density of 150 A/cm^2 is about 0.1 inches/hr, i.e., comparable to typical growth rates of GaAs from the melt (0.3 to 0.5 inch/hr) by directional solidification.

Electroepitaxy of Multicomponent Systems

Our recent study of the electroepitaxy of multicomponent compounds has shown that the same phenomena which dominate the electroepitaxial growth of binary compounds are also of fundamental importance in this case. Thus, a theoretical electroepitaxial growth model of multicomponent systems was developed[5] based on electromigration in the solution and on the Peltier effect at the growth interface. Quantitative relationships were derived for the dependence of the growth velocity and the composition of the layers on the current density and other growth parameters. The model was successfully used for the analysis of experimental results on the electroepitaxial growth of $Ga_{1-x}Al_xAs$, and it enabled to explain the observed remarkable stabilization of the composition in the direction of growth under constant density. It was also found that the composition of the solid can be precisely varied by varying the current density. Experimentally determined compositional changes of $Ga_{1-x}Al_xAs$ are shown in Figure 3 as a function of current density. The dashed line is computed from the theoretical model of multicomponent-system electroepitaxy. It should be noted, in conjunction with the present results, that multicomponent systems play a key role in optoelectronic device structures and their technology relies exclusively on epitaxial growth. Standard LPE provides only limited flexibility in controlling the microscopic growth velocity; thus, precise control of the composition of ternary and quarternary compound layers is still a problem. The unique advantages of electroepitaxy in this respect are quite evident.

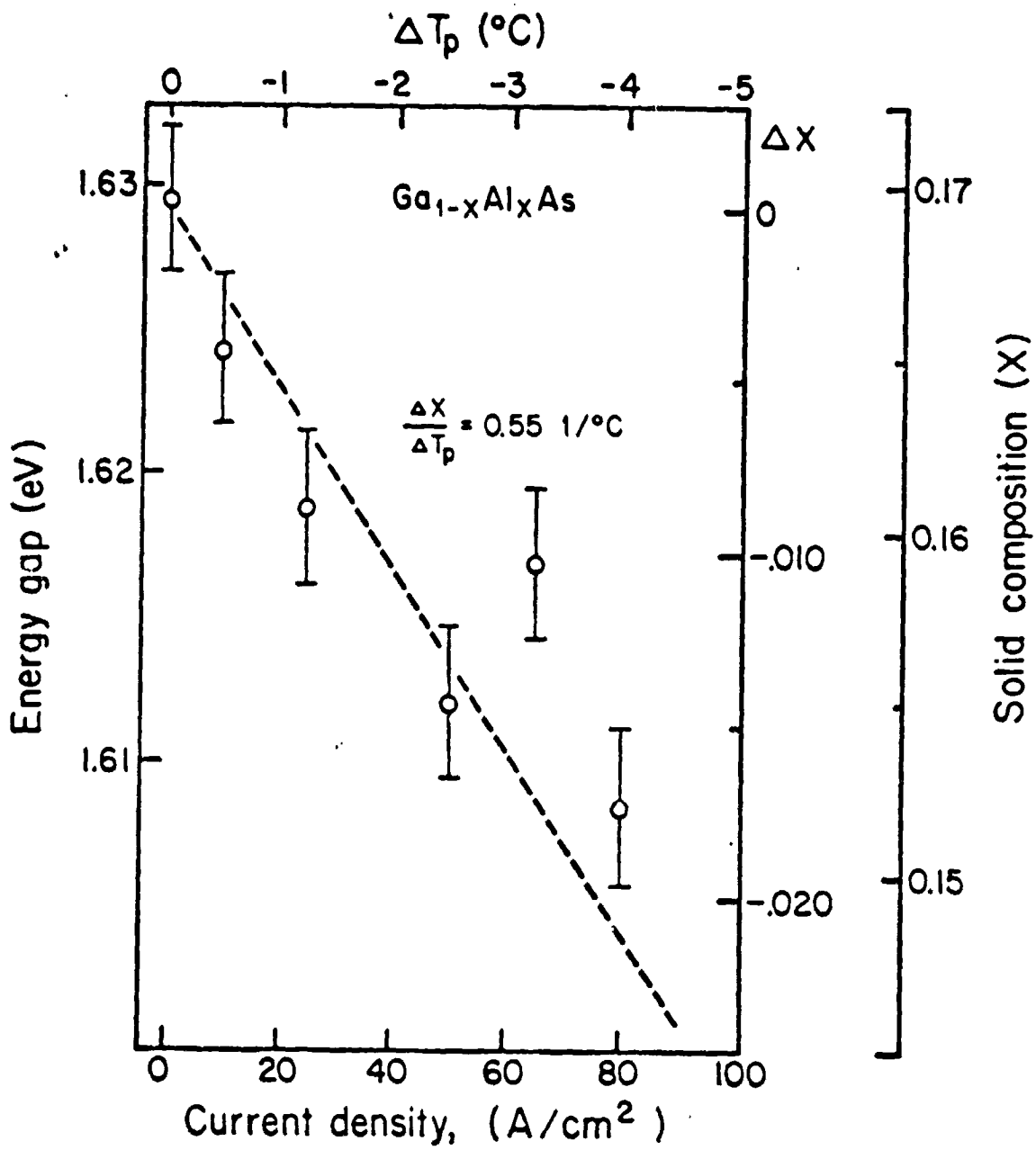

Fig. 3 The energy gap and corresponding compositional changes of electroepitaxially grown $Ga_{1-x}Al_xAs$ as a function of current density (lower horizontal scale) and of Peltier effect-induced change in interface temperature ΔT_p (upper scale). Dashed line represents theoretical dependence predicted by our electroepitaxy model of multicomponent systems.

New Experimental Systems for Electroepitaxy

During the last year we initiated the design and construction of two highly advanced systems for electroepitaxial growth of thick GaAs layers and of improved quality heterostructure layers.

The first of these systems incorporates a configuration of "rotating substrate" (see figure 4), originally proposed and studied in conjunction with electroepitaxy at the Institute of Inorganic Chemistry, Siberian branch of the Soviet Academy of Sciences. As shown schematically in figure 4, the GaAs substrate is mounted on a rotating shaft and growth from equilibrated Ga-As solution is performed by passing electric current through the solution-substrate interface. The vertical motion of the graphite boat brings the substrate into contact with solution, makes possible pulling of the substrate with respect to the solution during the growth, and permits the separation of the substrate from the solution after growth is terminated. Rapid spinning of the substrate (~100 RPM) provides a convenient means for an effective removal of the residual solution from the surface of the grown GaAs layer. We believe that this approach (which in essence incorporates all of the convenient features of Czochralski-type arrangement in epitaxial growth) will enable extension of the electroepitaxial growth to thick layer, and possibly to the growth of high quality, bulk GaAs crystals. Construction of the apparatus has already been completed. Extensive work on testing and calibrating the system is in progress; preliminary first growth experiments were carried out and yielded promising results.

The second electroepitaxy system, which is in the final states of construction, was designed for the growth of ultra-high quality layers and heterostructures. It combines our own experience in current-contolled LPE with the advanced

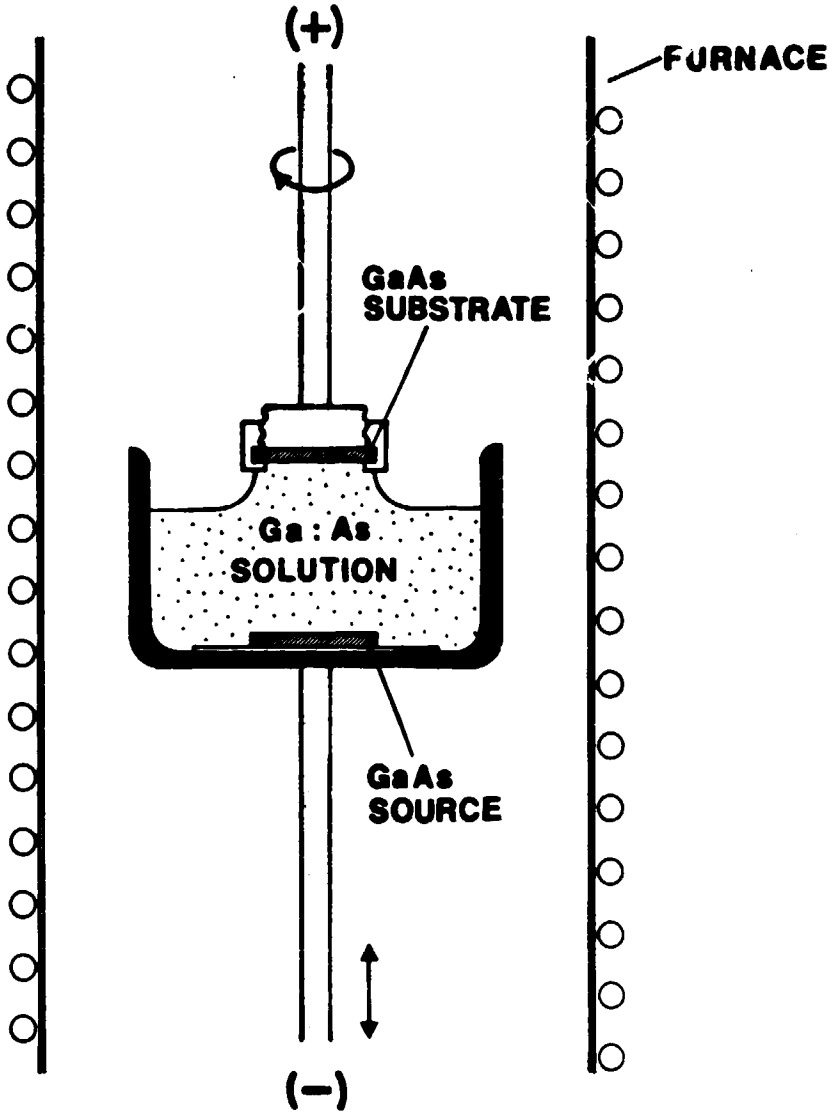

Fig. 4 Schematic representation of a boat design for electro-epitaxy in "rotating substrate" configuration.

know-how of industrial organizations (RCA, Nippon T & T, Fujitsu Labs) leading in the field of thermal LPE.

Figures 5, 6, and 7 depict three essential subsystems of the new apparatus, i.e., the electronics system, the ambient gas system and the electroepitaxial boat, respectively. The electronic system utilizes a microprocessor which enables computer programming and controlling of the growth process. Detailed temperature control monitoring is considered a key factor for consistent and reproducible growth of a multicomponent layer.

Significant improvements were also introduced in the ambient gas purification system (figure 6) which, according to a new design, includes H_2 and N_2 purifiers and sorption pumps eliminating oil contamination of standard mechanical pumps.

The multi-well boat (figure 7) was designed on the basis of the latest experience of RCA with modifications permitting the passage of electric current through the solution-substrate interface. This boat enables the growth electroepitaxially, and/or thermally, of four layers of the desired composition and/or doping characteristics, and it will be employed for electroepitaxial growth of heterostructure layers and device structures. Growth experiments will be carried out in the very near future.

Melt Growth

Growth Apparatus

During the last ye. we completed the construction and testing of an advanced system for horizontal and/or vertical growth of GaAs. An overall view of this melt-growth apparatus is given in figures 8 and 9 in the horizontal and vertical operation mode, respectively.

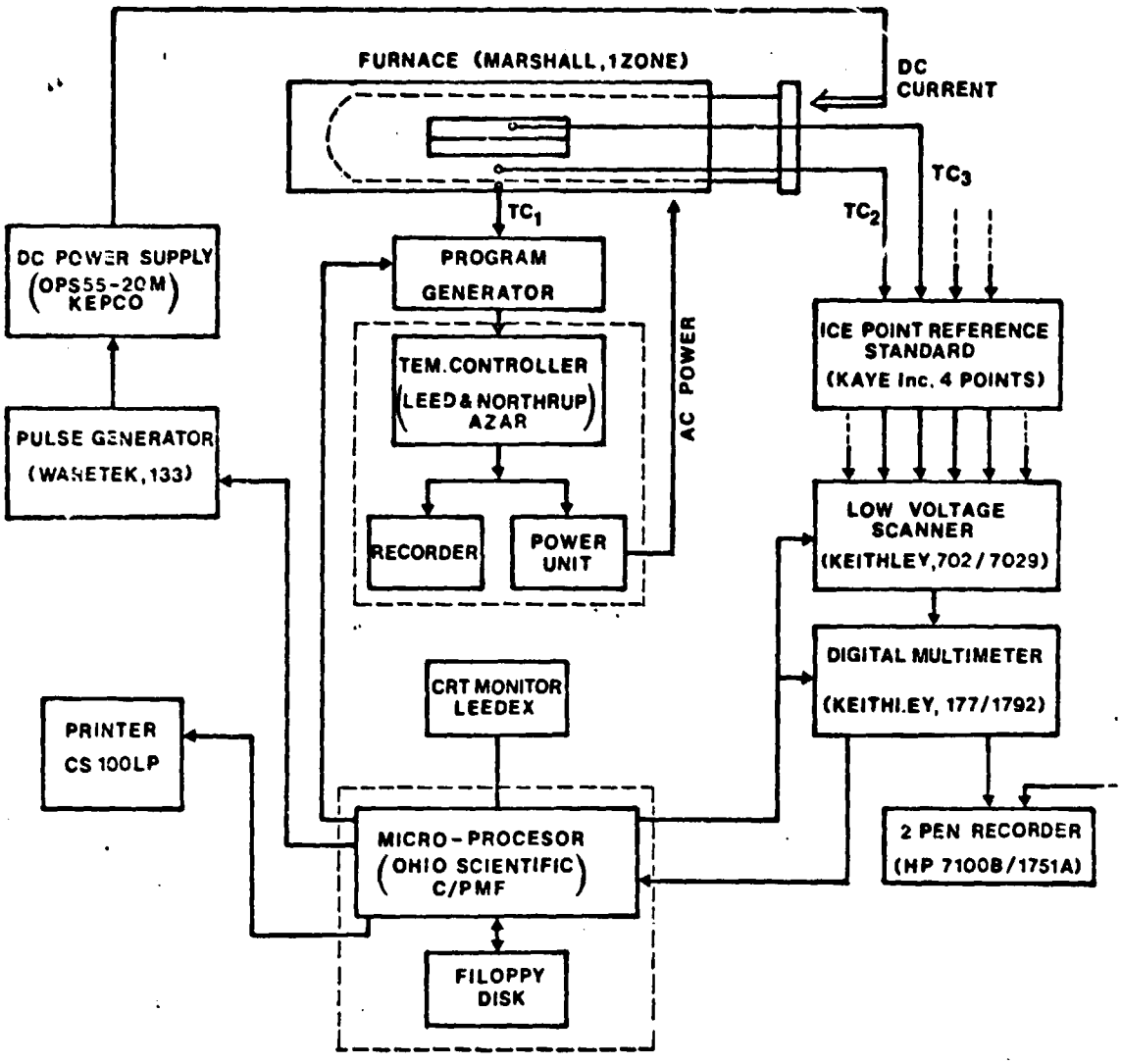

Fig. 5 Block diagram of electronic system of our electroepitaxy apparatus for growth of high quality multicomponent layers.

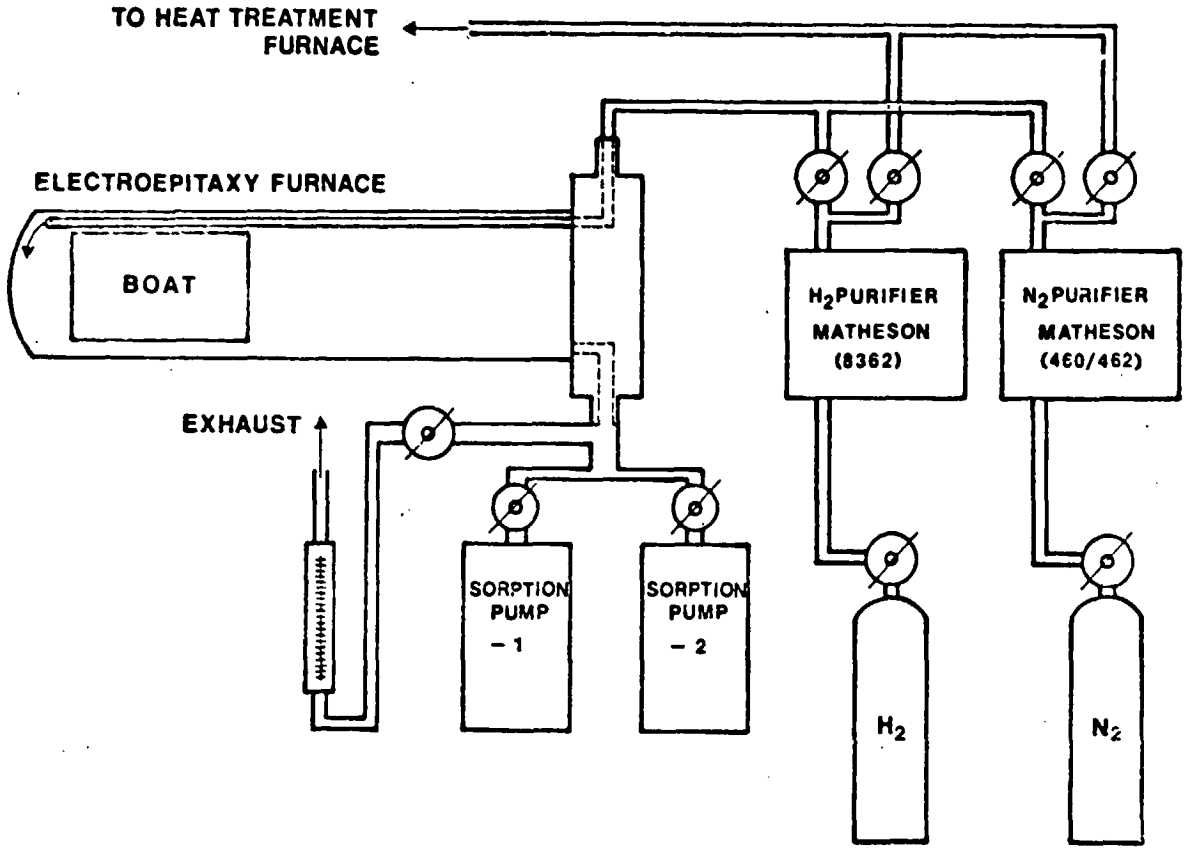

Fig. 6 Gas purification system utilized in our new electro-epitaxy apparatus.

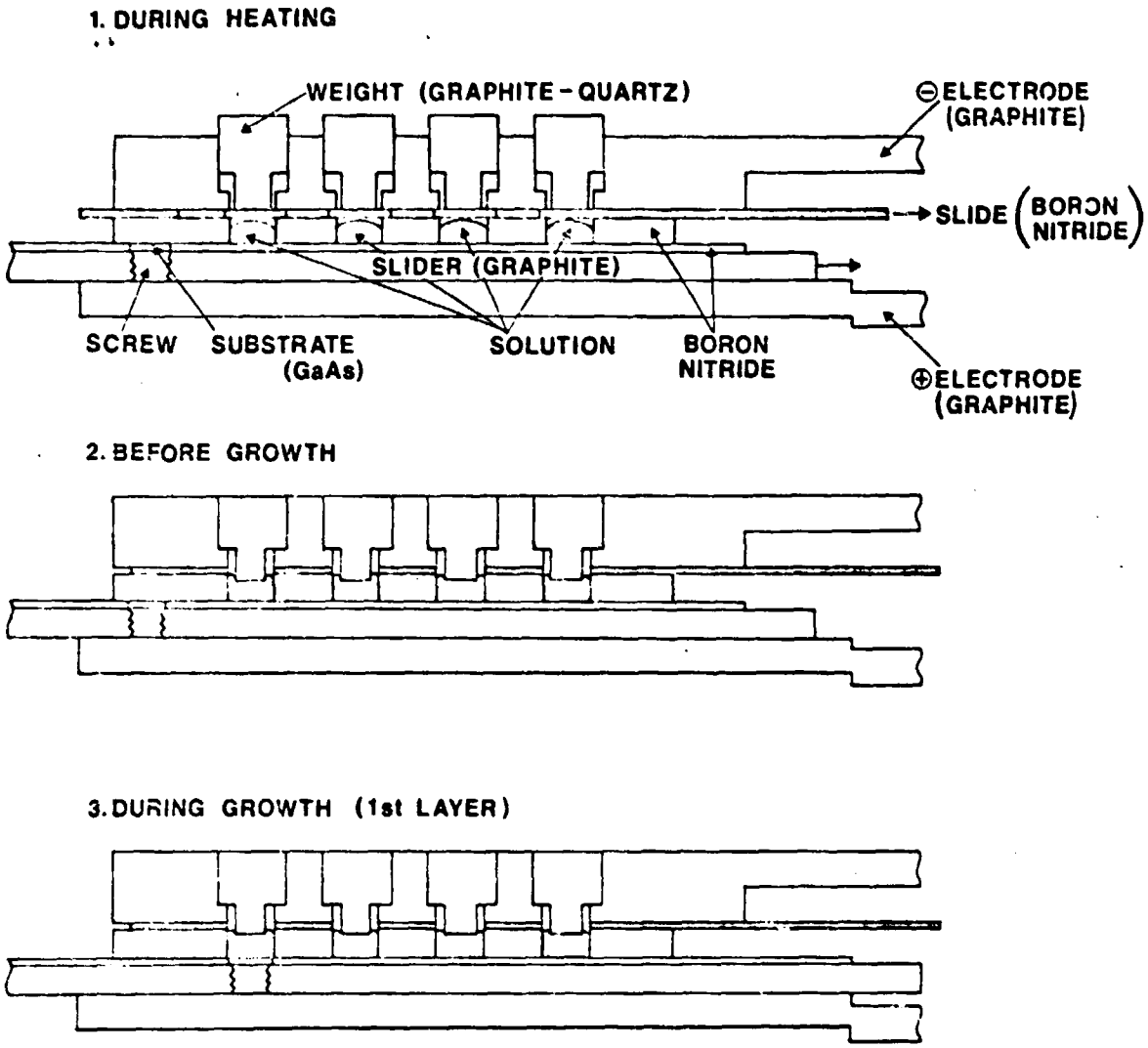

Fig. 7 Electroepitaxial boat for growth of multicomponent layers and heterostructure devices.

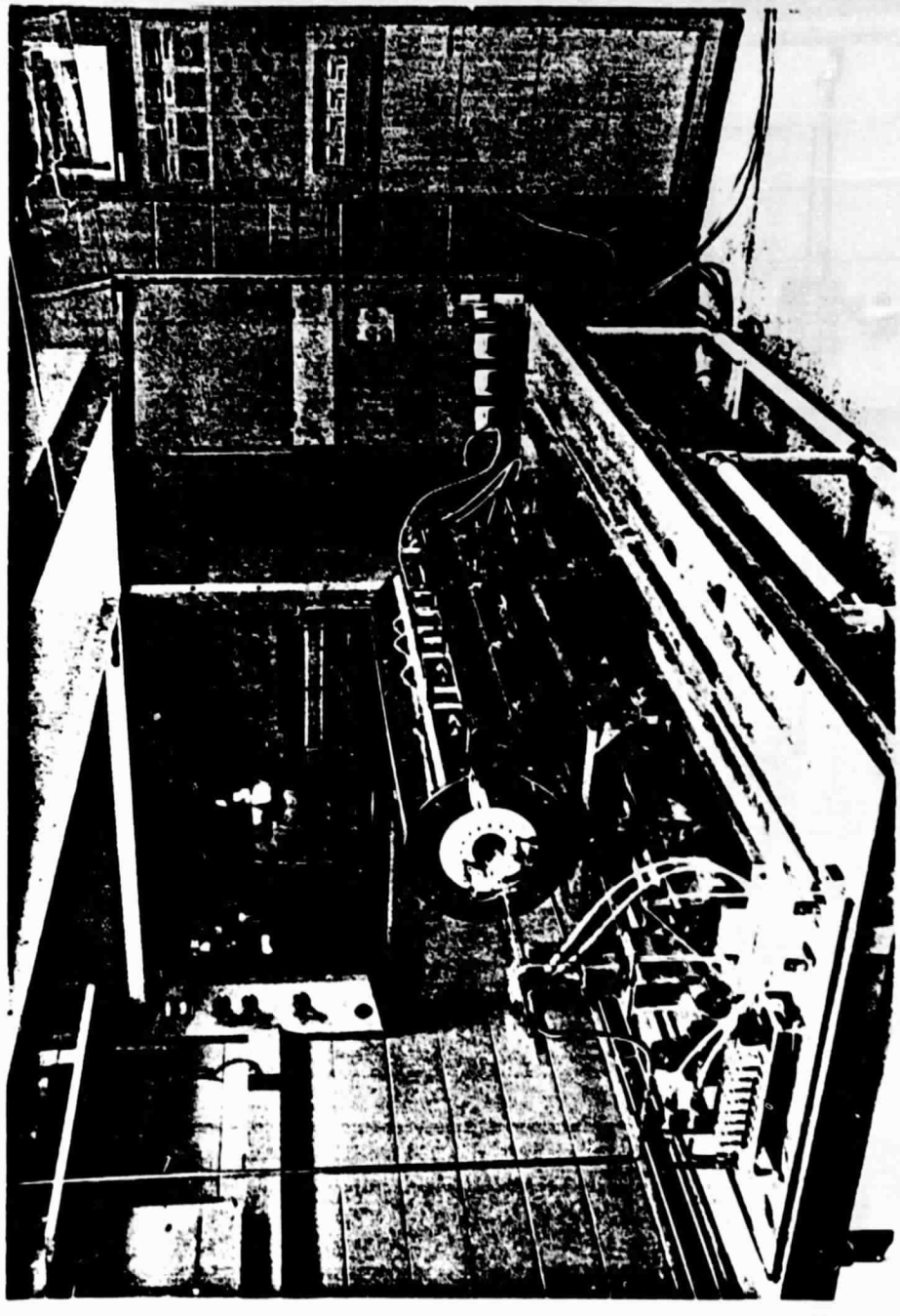

Fig. 8 An overall view of our melt-growth apparatus operating in horizontal position

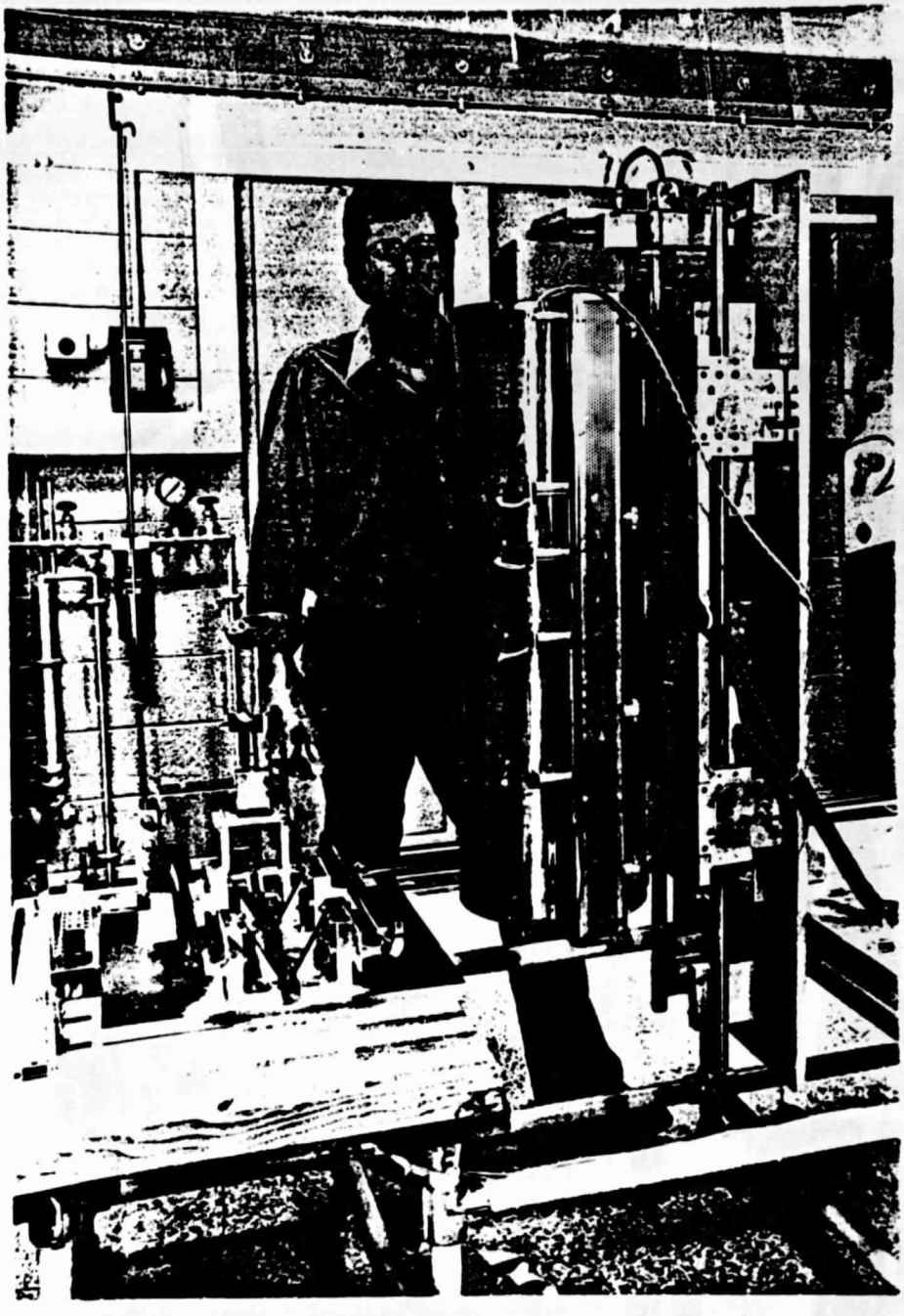

Fig. 9 Melt-growth apparatus of Fig. 8 rearranged to operate in vertical mode.

To satisfy unique thermal requirements the furnace system was constructed with four independently controlled resistance windings, an internal gas cooling system for enhanced heat extraction, and a heat pipe in the low temperature zone for improved thermal stability and "flat" temperature profile. Power taps on the windings permit tailoring of the thermal profile in each zone. The furnace is supported by a carriage assembly which rides on two parallel rails mounted on a two-piece main frame. The main frame permits positioning the system at any orientation from horizontal to vertical (figures 8 and 9). Furnace motion is accomplished by a variable speed cable drive system pulling the carriage assembly. Drive rates range from 0.05 cm/hr to to 6 cm/hr. All of the support systems (power inputs, gas feeds, sensor outputs and cable drive) have been designed to enable operation in any configuration without major modifications.

A 15-channel chart recorder provides continuous monitoring of the thermal conditions throughout the system. Digital readouts enable visual monitoring of system temperatures. Four adjustable voltage sources permit high sensitivity thermal measurements to be made by offsetting the thermocouple potential. During the testing procedures emphasis was placed on temperature control. All detectable sources of temperature instabilities in the sensor and control circuits have been systematically isolated and stabilized. Air circulation effects in the furnace tube which tend to flatten the temperature profile, were minimized by the use of zirconia and alumina insulation between the quartz process tube and the furnace interior wall. Long-term temperature stability is typically better than $\pm$0.02°C.

During the initial growth experiments three major problems related to the actual growth process were identified and solved. The first of these involved temperature control in the "cold zone". Since the temperature in

this zone determines the arsenic vapor pressure and thus the melt stoichiometry and growth temperature, it is essential that it be maintained very stable. It was found that heat transfer within the ampoule was acting as a "short circuit" path between the high and low temperature zones. The transfer caused erratic temperature control in the low temperature zone leading to depletion of arsenic in the melt and collapse of the ampoule due to the decreased pressure inside the ampoule. External control of the "cold zone" was abandoned in favor of control at the coldest point on the ampoule end wall. Implementation of this change led to a thermal stability of $\pm$0.01 to $\pm$0.02°C.

The second problem was related to the accurate positioning of the initial solid-liquid growth interface without visibility through the furnace wall. To solve this problem a series of partial seed melting experiments were performed which led to the establishment of an experimental procedure which makes possible positioning of the interface (through controlling of the exterior temperature profile) with a precision of $\pm$1 mm.

A third practical problem was related to surface tension effects which complicate seeding of the crystal due to a tendency of GaAs melt to detach itelf from the seed crystal. This problem was overcome by redesigning the boat configuration, which now permits reproducible seeding and growth of single crystals of GaAs.

Finally, a new ampoule design was generated which permits the reuse of the most complex portion of the ampoule. This design reduces the time and costs of rebuilding the ampoule for each run.

Characteristics of Melt-Grown GaAs

The initial melt-growth experiments were designed for testing the growth system rather than for studying growth-property relationships. Nevertheless,

these experiments were quite successful in yielding bulk GaAs with electronic properties (e.g., mobility, compensation and homogeneity) comparable to commercially available material of similar electron concentration.

The electronic properties of two crystals are given in Table II. It should be noted that characterization of these crystals was based on the utilization of our advanced characterization facility, Thus, the compensation ratio was determined from carrier concentration and electron mobility with our transport technique.[12,13] The homogeneity of the material was assessed with IR Scanning absorption.[7] A typical electron concentration microprofile of the end portion (most inhomogeneous) of crystal 1 is presented in figure 10. It is seen that local changes of electron concentration are $\pm$20%, i.e., typical for presently available melt-grown GaAs.[13]

A first derivative surface photovoltage spectrum characteristic of crystal 1 is shown in figure 11. The well resolved subbandgap Si-peak permitted the identification of Si as the dominating impurity. The density of dislocations was determined from etch-pit densities (figure 12) and was confirmed by SEM-cathodoluminescence scanning. The cathodoluminescence image of a sample prepared from crystal 1 is shown in figure 13. The dark spots in this image correspond to dislocation regions characterized by enhanced non-radiative recombination. The room temperature cathodoluminescence spectrum of the same sample (dashed and dotted lines correspond to different points on the sample) is shown in figure 14. Both the position of the peak (band-to-band transitions) and its half-width are consistent with literature data on cathodoluminescence characteristics of GaAs of similar electron concentration.

The low electron concentration of crystal 2 permitted the determination of the deep level characteristics utilizing deep level transient capacitance spectroscopy. A typical DLTS spectrum is shown in figure 15, indicating the

Table II

Properties of Melt-Grown GaAs Single Crystals

	Carrier Concentration (cm^{-3})	Mobility (cm^2/Vs)	Compensation	Microscale Homogeneity $\Delta n/n_{av}$	Dominating Impurity	Deep Levels	Dislocation Density (cm^{-3})
Run 5 Crystal 1	$n = 6.7 \cdot 10^{17}$	3500	0.4	±20%	Si	-	10^5
Run 6 Crystal 2	$n = 2.7 \cdot 10^{17}$	3300	0.37	±10%	Si	$E_c - E_t = 0.81eV$ $1 \times 10^{16} cm^{-3}$ (oxygen)	

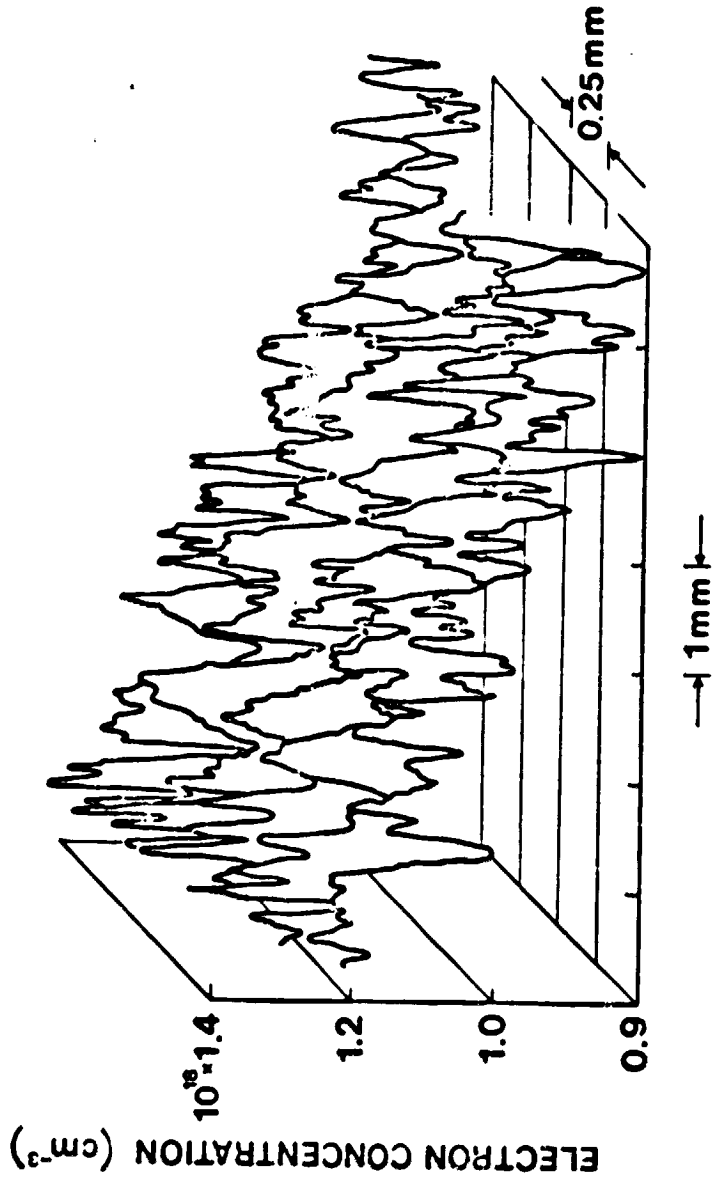

Fig. 10 Electron concentration microprofile of melt-grown GaAs (crystal 1; see text).

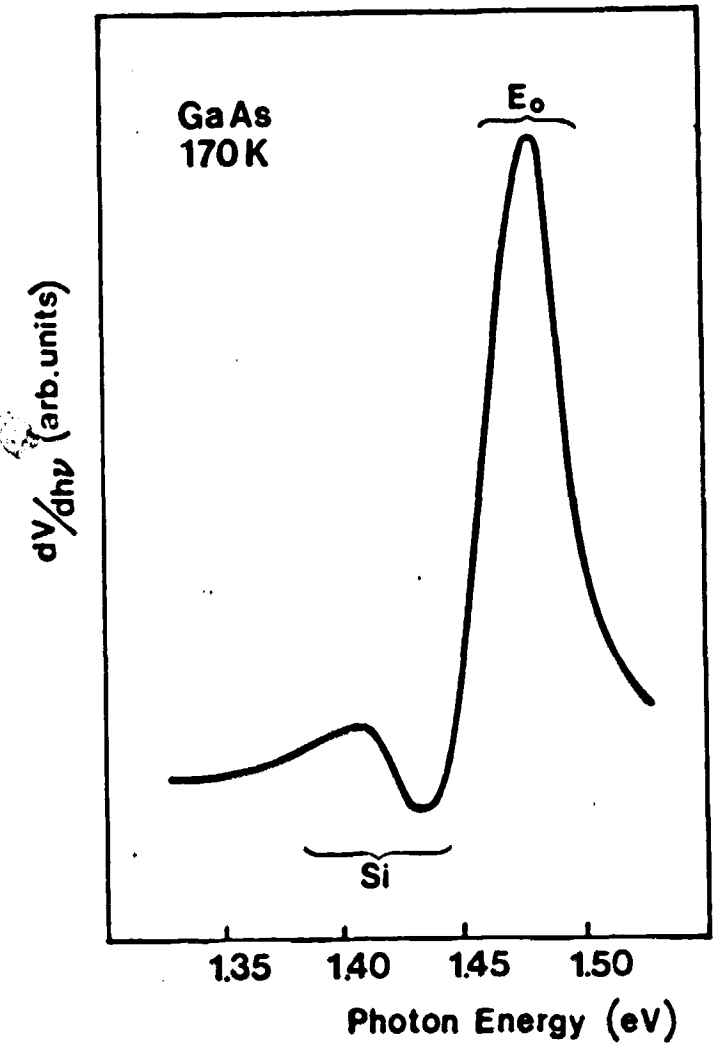

Fig. 11 First derivative photovoltage spectrum of melt-grown GaAs (see text).

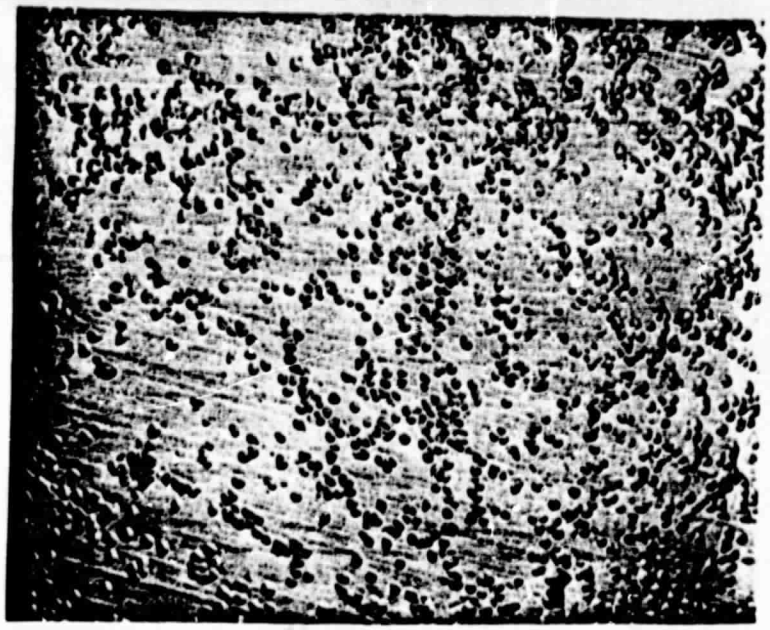

Fig. 12 Dislocation-etched pits of melt-grown crystal 1 as revealed by chemical etching.

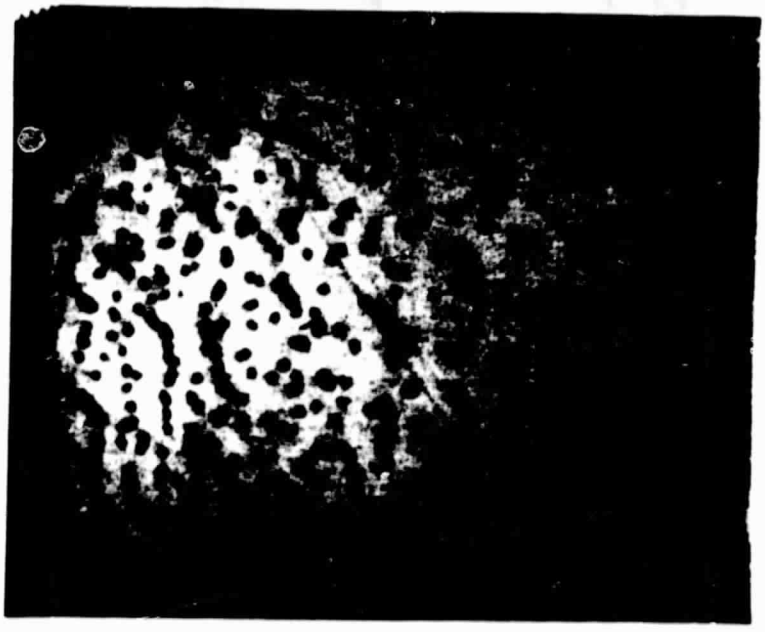

Fig. 13 Dislocation pattern of melt-grown crystal 1 as revealed by SEM-cathodoluminescence. Note that Figs. 12 and 13 correspond to neighboring segments of crystal 1.

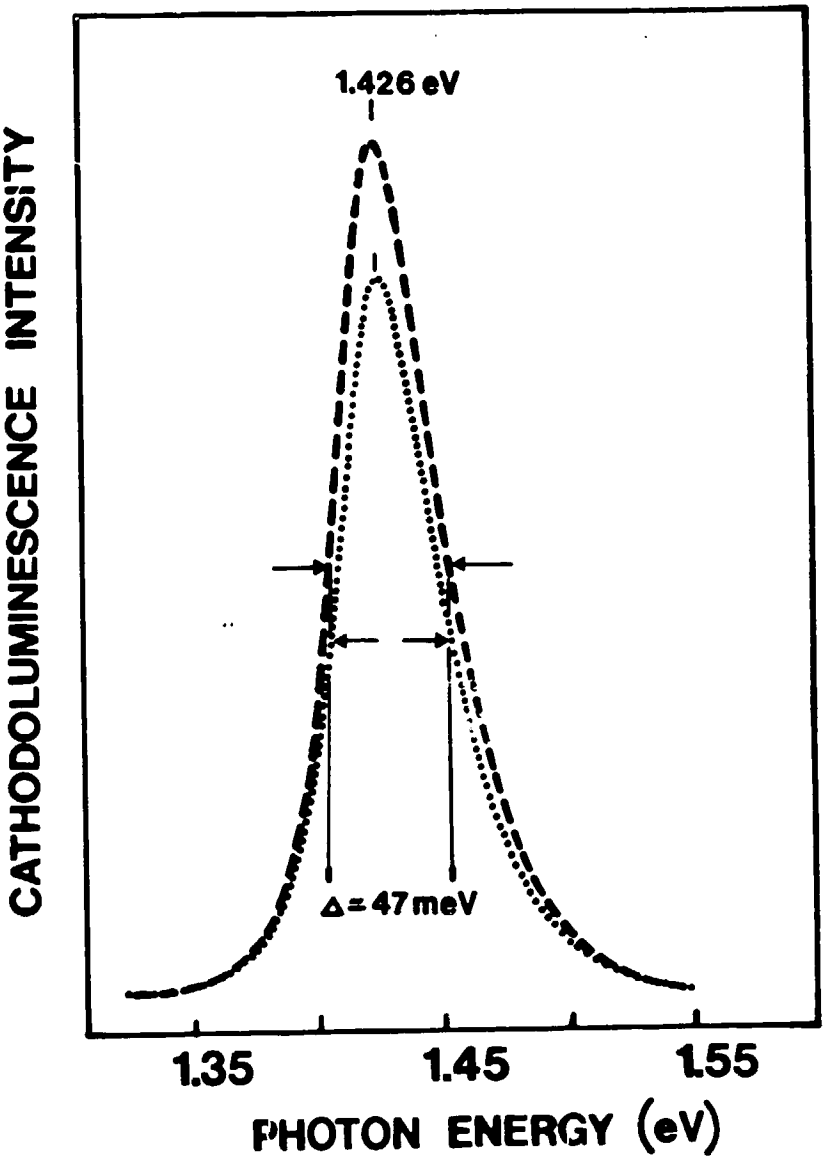

Fig. 14 Room temperature cathodoluminescence spectra of crystal 1 measured at two points separated by 25 μm (dotted and dashed lines, respectively).

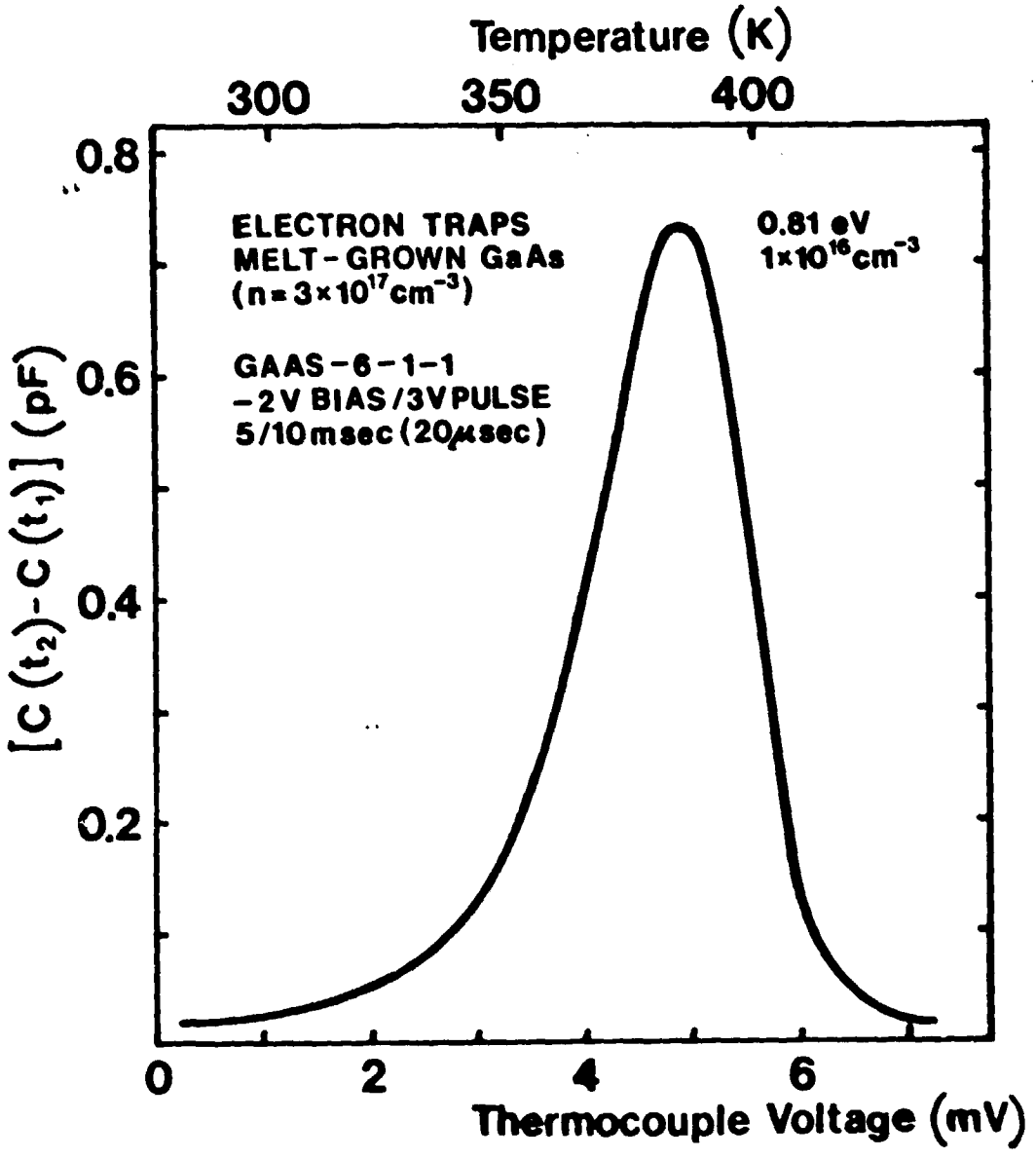

Fig. 15 Deep Level Transient Capacitance spectrum of melt-grown GaAs crystal 2 showing oxygen-related level at 0.81 eV below conduction band.

presence of an electron tap 0.81 eV below the conduction band. This trap coincides with a level commonly interpreted as related to oxygen. The concentration of these traps is determined to be about $10^{16}cm^{-3}$, i.e., typical for melt-grown GaAs. The characterization effort outlined above constitutes an assessment of the electronic properties of the first GaAs single crystals grown with our newly constructed melt-growth apparatus. These properties represent an initial reference point for our future research on growth-property relationships.

CHARACTERIZATION

Deep-Level Transient Spectroscopy

Deep-level transient spectroscopy (DLTS) is presently used as a standard characterization technique of wide bandgap semiconductors.[20] This technique is capable of displaying the spectrum of traps in a crystal in the form of peaks (emerging from a flat baseline) as a function of temperature. From the position and the height of the peaks one determines the energy position of the levels, the capture cross-section, and concentration. Since the DLTS method is sensitive, rapid, and easy to analyze, it is extremely useful as one of the basic techniques for establishing the relationships between growth conditions and the properties of GaAs. The block diagram of our recently constructed DLTS system is shown in figure 16. The basic capacitance measurements are performed with a modified 1 MHz commercial capacitance meter. The rate window is implemented by a double boxcar averager. In this approach, the emission rate, e_2, corresponding to the maximum height of the DLTS peak, is precisely defined by settings of gates in the boxcar averager. The values of e_2 at different gate settings and the temperatures corresponding to the peak maxima allow determination of the thermal activation energy of traps. The measurements for testing the system were performed on MS structures (Schottky barrier)

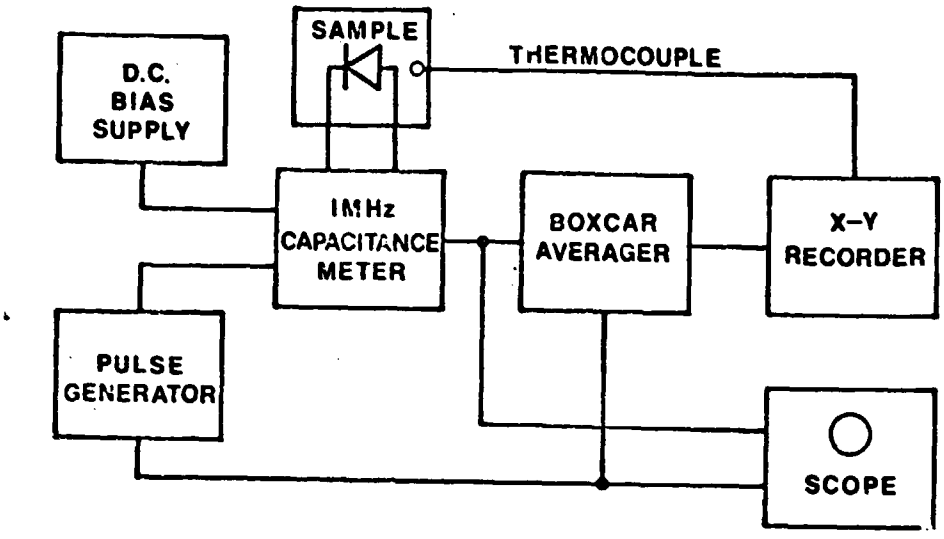

Fig. 16 Block diagram of our Deep Level Transient Spectroscopy system.

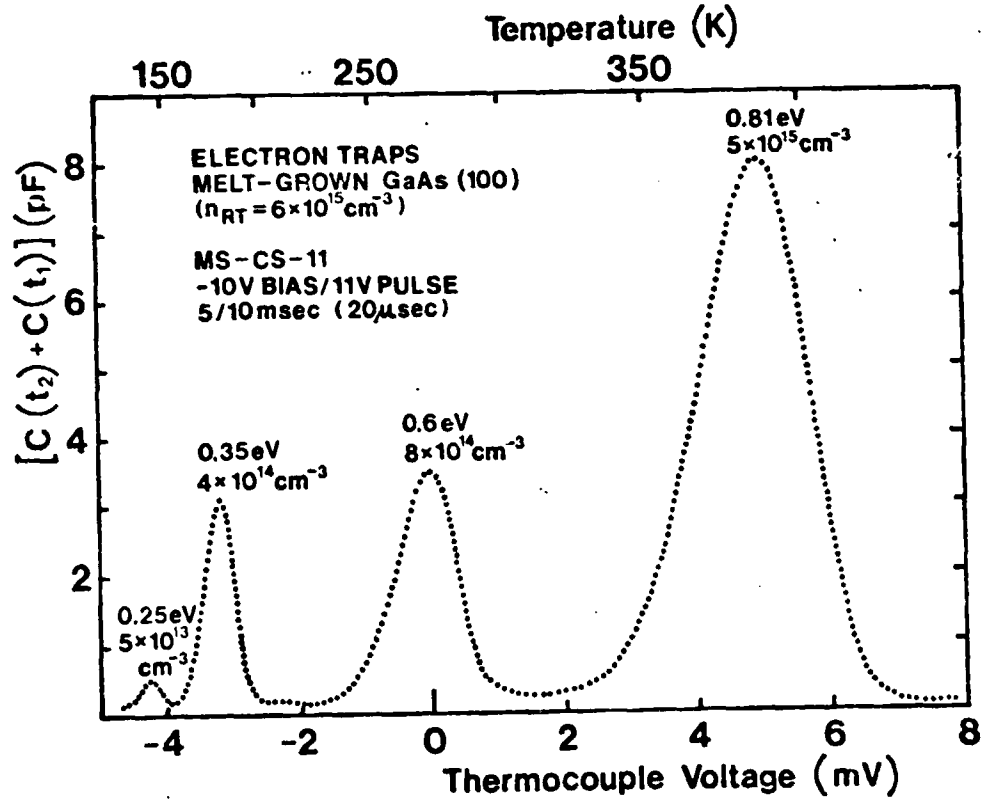

Fig. 17 Typical Deep Level Transient Capacitance spectrum of commercially available undoped (n-type, $6.10^{15}cm^{-3}$) melt-grown GaAs. DLTS peaks correspond to electron traps located at 0.25, 0.35, 0.6 and 0.81 eV below conduction band. Note that in our melt-grown GaAs (crystal 2, Fig. 15) only an oxygen related peak (0.81 eV) was observed.

prepared on commercially available melt-grown GaAs ($n = 6 \times 10^{15} cm^{-3}$). A typical transient capacitance spectrum is shown in figure 17. This spectrum reveals four peaks which can be considered as characteristic of the melt-grown GaAs.[21]

The DLTS technique was also employed for the investigation of MOS-GaAs structures.[11] Preliminary results have shown that measurements of transient capacitance spectra of MOS structures vs. filling pulse magnitude provide a convenient means for identification of interface states and bulk levels. Thus, as shown in figure 18, besides the DLTS peak corresponding to 0.8 eV bulk level (observed also in MS structures) an additional peak is observed at high filling pulse voltages. This additional peak can be accounted for on the basis of an interface state with a discrete energy at 0.65 eV below the conduction band edge. Further investigation of interface states is in progress.

Derivative Photocapacitance Spectroscopy

The capacitance measuring system discussed above has also been utilized in conjunction with wavelength modulation of the incident light as a new convenient and simple approach to the determination of photoionization characteristics of deep levels.[10] The advantages of wavelength modulation for studying deep levels have recently been demonstrated in our derivative surface photovoltage spectroscopy as applied to GaAs MOS structures.[8,9] The newly developed derivative wavelength modulated photocapacitance spectroscopy is applicable to MOS as well as to structures simpler than MOS, e.g., metal-semiconductor Schottky barriers and p-n junctions. In the course of these studies the technique was successfully employed for the determination of deep levels in melt-grown GaAs and the Cr level in high resistivity GaAs.

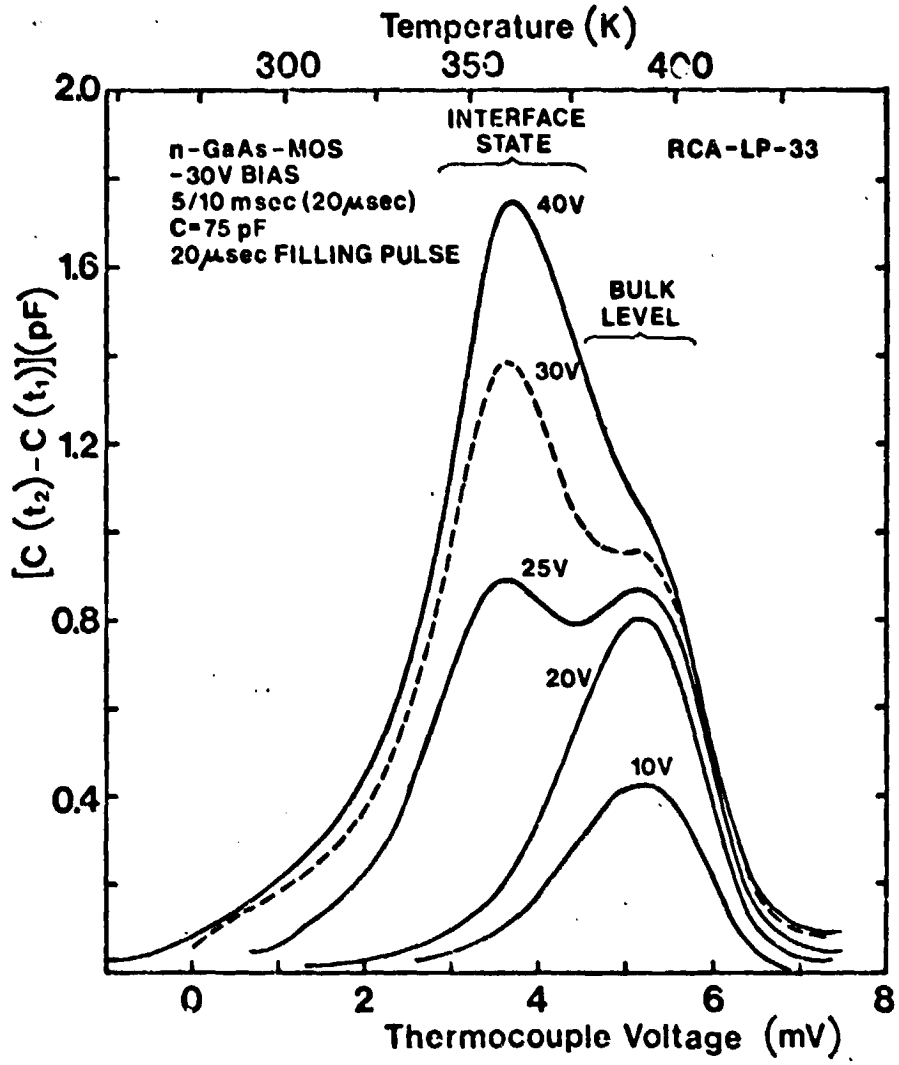

Fig. 18 DLTC spectra of MOS structure (prepared on epitaxially grown GaAs by anodic oxidation process) showing interface states and bulk levels. Note the dominating character of DLTS peak due to the interface states for high voltages of the filling pulse.

SEM-Cathodoluminescence

A cathodoluminescence measuring system has been assembled to perform experiments in dispersive and non-dispersive modes at temperatures ranging from 80-700 K. The system consists of an optical microscope (incorporated into our scanning electron microscope apparatus), of a monochromator and a photomultiplier which serves as a detector of light emitted by the sample irradiated by the electron beam.

The image shown in figure 13 is a non-dispersive mode representation of cathodoluminescence of Si-doped melt-grown GaAs (crystal 1), discussed earlier. Emission spectra (dispersive mode) of the same sample were given in figure 14. The non-dispersive mode studies provide an instantaneous means for qualitative imaging of recombination inhomogeneities. Quantitative dispersive mode analysis enables the determination of carrier concentration microprofiles and/or microprofiling of radiative recombination centers. In the course of the present studies the relationship between the half-width of the emission peak and the carrier concentration was used to develop a simple procedure for quantitative electron concentration microprofiling of n-type GaAs. Typical results obtained with a commercially available melt-grown Te-doped GaAs are given in figure 19. It is seen that the crystal exhibits large carrier concentration inhomogeneities (n varies by a factor of 2) in agreement with our results obtained with IR absorption scanning. However, it is also seen that cathodoluminescence scanning allows the identification of inhomogeneities with extremely high spatial resolution of about 1 μm. The advantage of cathodoluminescence over optical excitation techniques is in this respect unquestionable.

GROWTH-PROPERTY RELATIONSHIPS

Electronic Properties of GaAs on a Microscale

Utilizing our tunable laser IR absorption scanning technique we

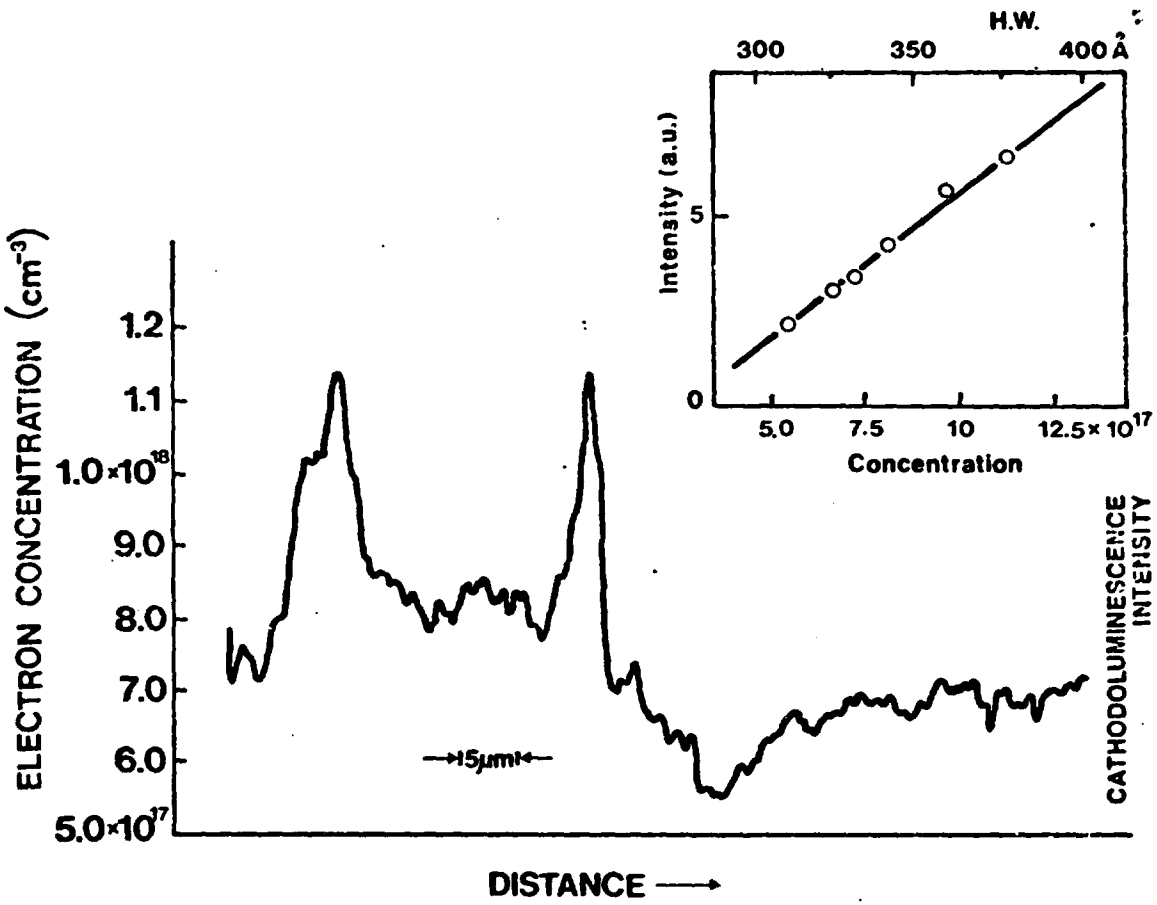

Fig. 19 High spatial resolution microprofile of electron concentration of Te-doped commercial GaAs. The insert shows a calibrating curve of the half-width (H.W.) of band-to-band luminescence peak versus electron concentration.

achieved, for the first time, the simultaneous microprofiling of semiconductor free carrier, donor and acceptor concentrations.[7] A number of techniques utilizing spreading resistance, Schottky barriers, EBIC, electroreflectance and IR absorption or topography have previously been developed for profiling the carrier concentration in semiconductors. However, these techniques essentially fail to distinguish between changes in impurity concentration and in compensation ratio. The present method is an application of our recent quantitative studies of the free carrier absorption in GaAs and InP as a means of determining the compensation ratio. The principle of the method is understood by considering the absolute value and the wavelength dependence of the free carrier absorption coefficient are experimentally measured quantities which contain only two unknown parameters, namely the electron concentration $n = N_D - N_A$ and the compensation ratio $\theta = N_A/N_D$. (N_D and N_A are the concentrations of ionized donors and acceptors, respectively.)

Microprofiles of free carrier, donor and acceptor concentrations obtained with melt-grown (horizontal Bridgman) Ge- and Si-doped GaAs are presented in figures 20 and 21, respectively. The inhomogeneities seen in these figures, although of an amplitude larger than average, are typical of all crystals obtained from several sources. Actually, as a general rule, all presently available melt-grown GaAs is highly compensated and exhibits pronounced variations in free carrier concentration.

A striking feature of the results of figure 20 is that the electron concentration exhibits large fluctuations of a magnitude comparable to its average value, while the total concentration of ionized impurities remains essentially constant. It is also seen in figure 20 that the spatial variations of donor and acceptor concentration are out of phase, i.e., maxima in N_D coincide with minima of N_A.

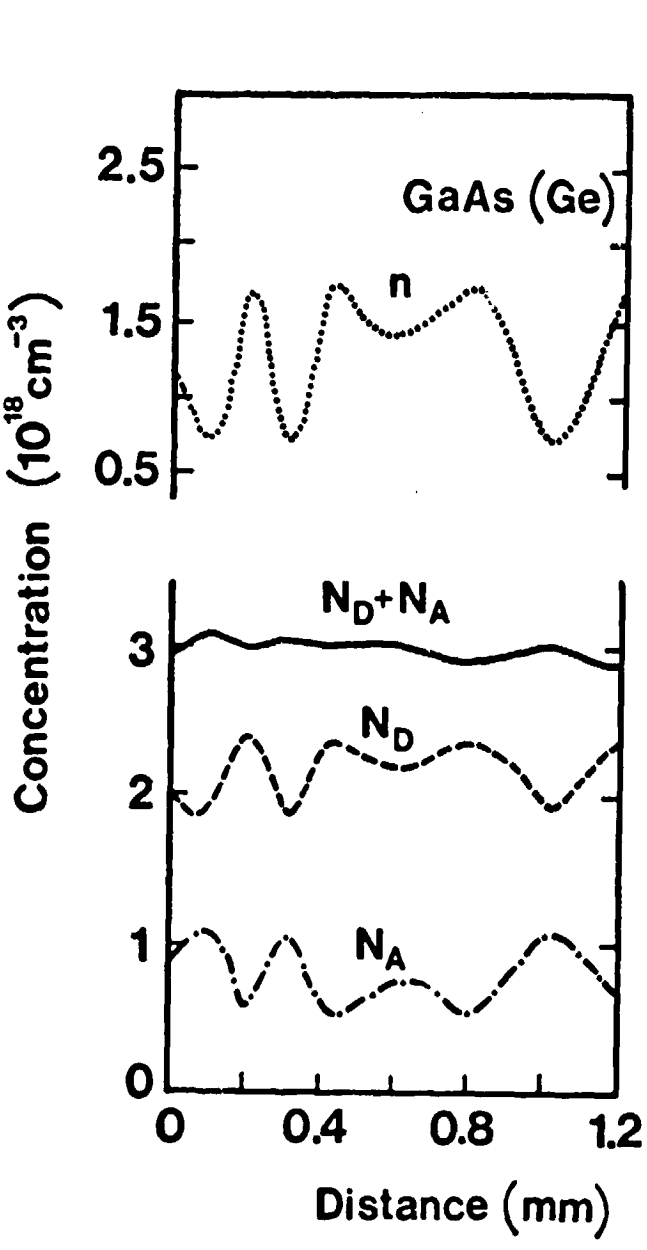

Fig. 20 Electron concentration and ionized impurity microprofiles of Ge-doped melt-grown GaAs.

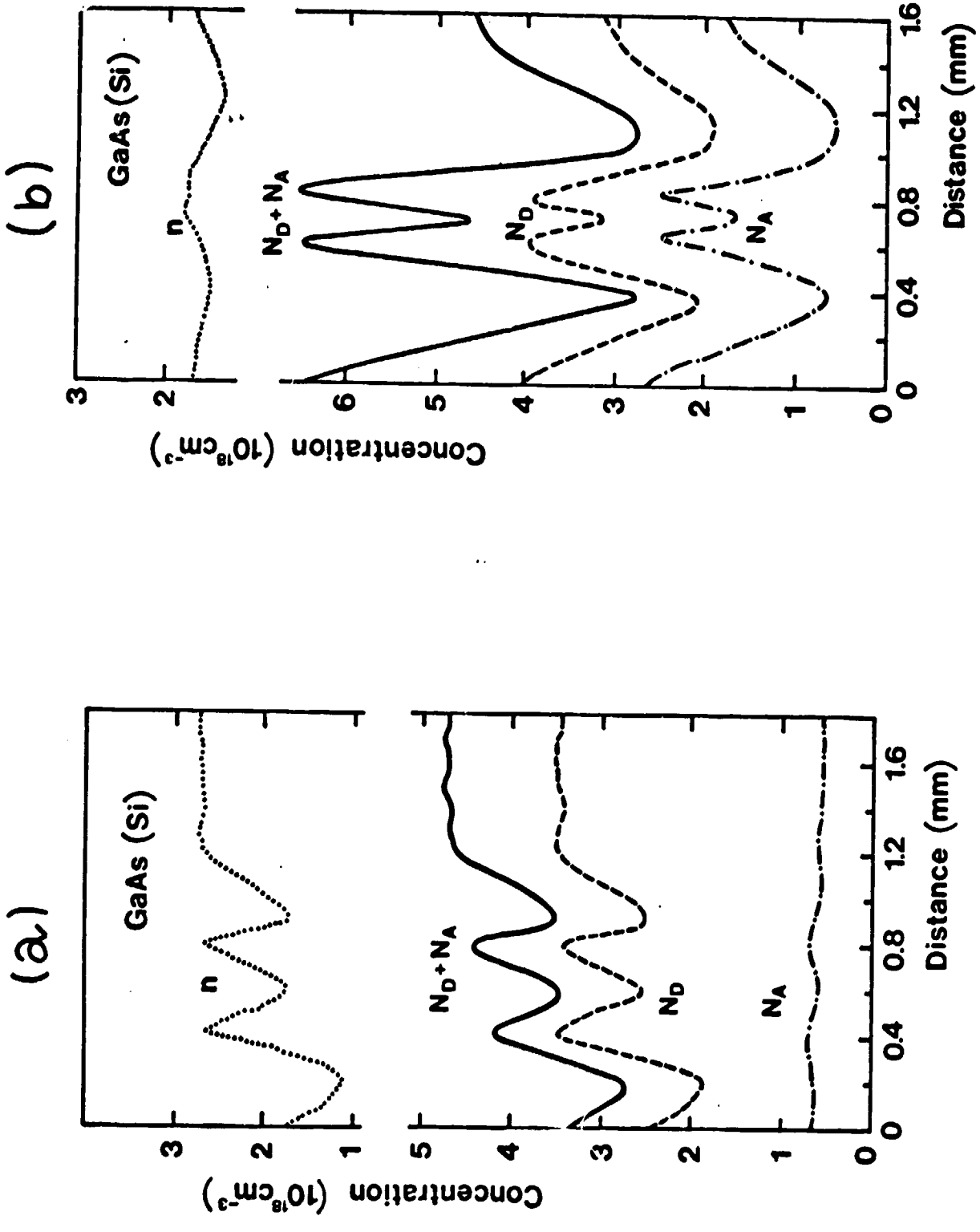

Fig. 21 Electron concentration and ionized impurity microprofiles of Si-doped melt-grown GaAs. (a) and (b) correspond to different segments of the same crystal.

The variations of donor and acceptor concentration shown in figure 20 cannot be explained on the basis of standard impurity segregation behavior controlled by the crystal growth velocity or the diffusion boundary layer thickness, and they must be associated with factors affecting the relative concentration of Ga and As vacancies or stoichiometry of GaAs.

Similarly, the free carrier concentration profiles in Si-doped GaAs cannot be accounted for by standard segregation behavior. Thus, in figure 21 the donor and acceptor concentration changes are not nearly so pronounced. The results of figure 21 were obtained from the same Si-doped crystal as those of figure 4a, but a different segment. In this case, the fluctuations of the free carrier, the donor and the total ionized impurity ($N_D + N_A$) concentrations are of similar nature and magnitude, but the ionized acceptor concentration undergoes relatively small variations.

It is apparent from figures 20 and 21 that fluctuations in the individual profiles of carrier, donor, acceptor and total ionized impurity concentration can readily be mistaken as related to standard impurity segregation behavior as they resemble well established impurity segregation variations, particularly in elemental semiconductors. Thus, all of these microprofiles must be simultaneously considered in assessing the origin of inhomogeneities in compound semiconductors.

Such simultaneous analysis performed on the basis of IR scanning absorption showed clearly that the electronic characteristics of GaAs on a microscale are controlled by amphoteric doping and deviations from stoichiometry rather than by impurity segregation. This conclusion is not necessarily limited to GaAs, but most likely it is valid for other semiconductor compounds as well.

Our preliminary cathodoluminescence study of InP has demonstrated striking differences between microscale variations of free carrier and impurity

concentrations. Typical results obtained with a p-type, $10^{17}cm^{-3}$, sample of melt-grown InP are shown in figure 22, and they are labeled as I, II, and III. In each case two spectral dependences are given as measured for the neighboring points (separated by about 25 μm). In figure 22 I, the band-to-band luminescence peak (B-B) does not vary, while a significant increase in a lower energy peak involving impurity level transitions (B-L) is observed. In case II, the band-to-band peak increases while the peak involving the impurity level decreases noticeably. In case III, the band-to-band transition is enhanced, while the impurity level transitions remain unchanged. Thus, it is evident that the spatial variations of band-to-band luminescence and of impurity level luminescence in InP are not interrelated. The sensitivity of the band-to-band transition to concentration of free carriers, and of the impurity luminescence to impurity concentration leads to the conclusion that in InP, like in GaAs, the concentration of free carriers and the concentration of impurities does not follow the standard pattern established by crystal growth dependent segregation behavior, but rather it is controlled by growth patterns affecting amphoteric doping and stoichiometry, which cannot be as yet unambiguously defined.

Compensation of InP

We have recently initiated preliminary characterization studies on InP which has been receiving increased attention as a material competitive to GaAs in a number of applications. Thus, we have extended our theoretical calculation of electron mobility and free carrier absorption of GaAs to the case of InP, and we have performed rigorous experimental study of DC and high frequency AC transport phenomena. Detailed results of this study are given in a forthcoming publication.[14]

It is, however, of importance to underscore that according to our own results and the analysis of literature data, melt-grown InP exhibits much

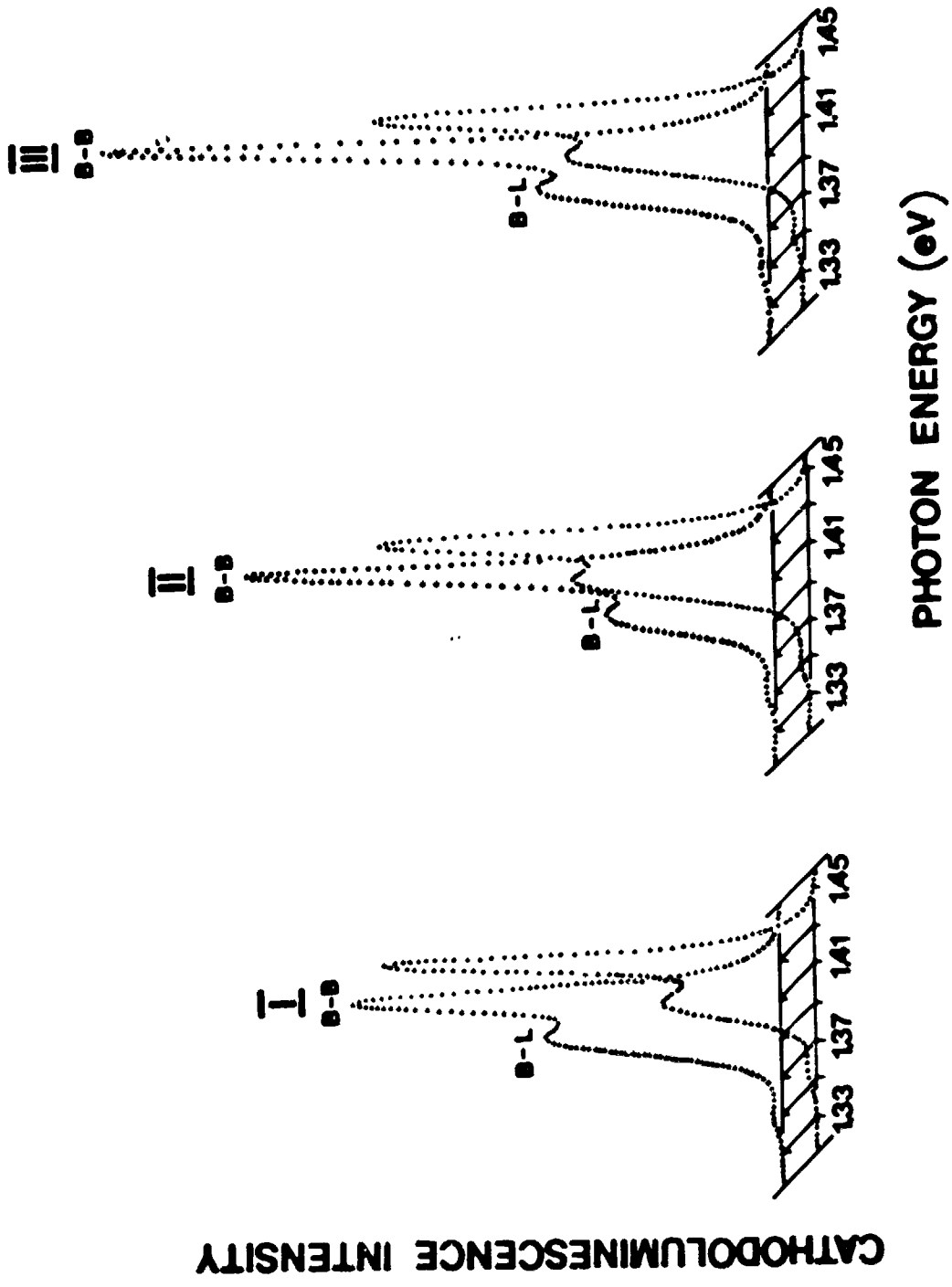

Fig. 22 SEM-cathodoluminescence spectra of melt-grown p-type (about 10^{17} cm^{-3}) InP (see text).

lower compensation than that encountered in melt-grown GaAs. This difference is evident in figure 23 where the normal range of $N_{i_{imp}}/n$ is plotted as a function of electron concentration for commercially available high-quality GaAs and for InP. In the low electron-concentration region the melt-grown GaAs is highly compensated, with a total concentration of ionized impurities exceeding by an order of magnitude the free carrier concentration. InP, on the other hand, even at low concentrations can be obtained by melt growth with a concentration of ionized impurities of the same order of magnitude as the electron concentration. This marked difference is probably related, in part, to the lower melting point of InP (1062°C for InP and 1238°C for GaAs) and thus to the lower concentration of native point defects; point defects in compound semiconductors are known to participate in the formation of compensation centers. Furthermore, the covalent radii of In and P differ by about 40%, whereas those of Ga and As are about the same; thus, a dopant impurity is more likely to occupy preferentially In or P sites in InP than Ga or As sites in GaAs (amphoteric or compensating doping).

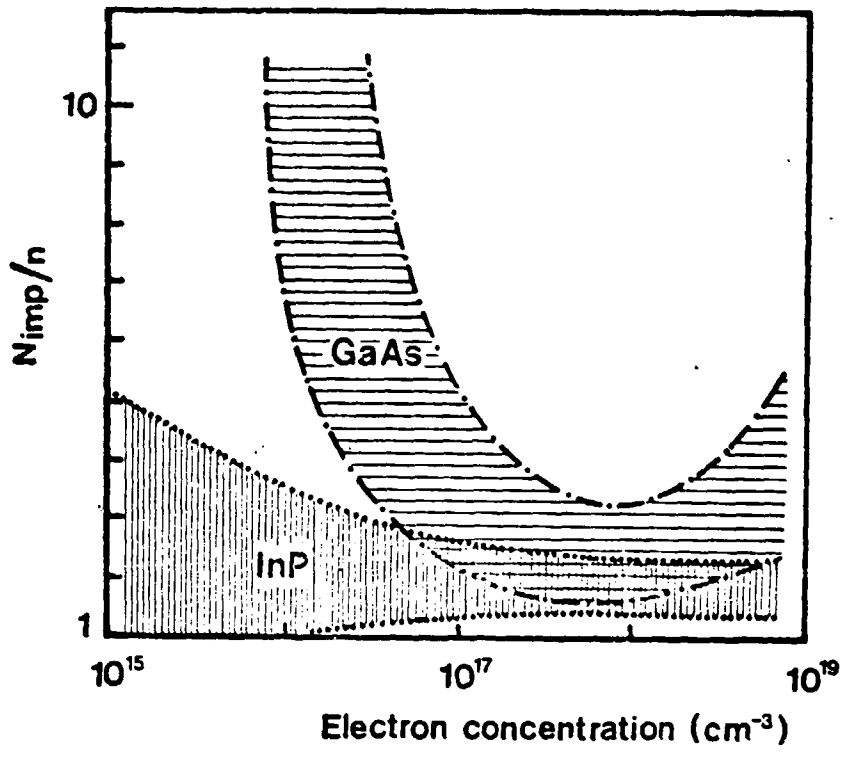

Fig. 23 Normal range of N_{imp}/n as a function of electron concentration in available melt-grown InP and GaAs, determined from our analysis of electron mobility and compensation ratio.

REFERENCES

1. L. Jastrzebski, J. Lagowski, H.C. Gatos and A.F. Witt, "Model of Liquid Phase Electroepitaxial Growth: GaAs," presented at Fourth American Conf. on Crystal Growth, July 1978, Gaithersburg, Maryland.

2. L. Jastrzebski, J. Lagowski, H.C. Gatos and A.F. Witt, "Liquid-Phase Electroepitaxy: Growth Kinetics," J. Appl. Phys. 49, 5909 (1978).

3. L. Jastrzebski, J. Lagowski, H.C. Gatos and A.F. Witt, "Dopant Segregation in Liquid Phase Electroepitaxy; GaAs," presented at Fourth American Conf. on Crystal Growth, July 1978, Gaithersburg, Maryland.

4. J. Lagowski, L. Jastrzebski and H.C. Gatos, "Liquid Phase Electroepitaxy: Dopant Segregation," J. Appl. Phys., 51, 364 (1980).

5. T. Bryskiewicz, J. Lagowski and H.C. Gatos, "Electroepitaxy of Multicomponent Systems," J. Appl. Phys. 51, 988 (1980)

6. Y. Imamura, L. Jastrzebski and H.C. Gatos, "Defect Structure and Electronic Characteristics of GaAs Layers Grown by Electroepitaxy and Thermal LPE," J. Electrochem. Soc. 126, 1381 (1979).

7. L. Jastrzebski, J. Lagowski, W. Walukiewicz and H.C. Gatos, "Determination of Carrier Concentration and Compensation Microprofiles in GaAs," submitted to J. Appl. Phys.

8. J. Lagowski, W. Walukiewicz, M.M.G. Slusarczuk and H.C. Gatos, "Derivative Surface Photovoltage Spectroscopy; A New Approach to the Study of Absorption in Semiconductors; GaAs," J. Appl. Phys. 50, 5059 (1979).

9. M.M.G. Slusarczuk, "Study of Electronic and Optical Properties of Gallium Arsenide Surfaces and Interfaces," Doctor's Thesis, MIT, 1979.

10. E. Kamieniecki, J. Lagowski and H.C. Gatos, "Wavelength Modulated Photocapacitance Spectroscopy," J. Appl. Phys. 1980, in press.

11. E. Kamieniecki, T.E. Kazior, J. Lagowski and H.C. Gatos, "A Study of GaAs-Native Oxide Interface States by Transient Capacitance," to be presented at 7th Annual Conf. on the Physics of Compound Semiconductor Interfaces, Estes Park, Colorado, January 1980.

12. W. Walukiewicz, J. Lagowski, L. Jastrzebski, M. Lichtensteiger and H.C. Gatos, "Determination of Compensation Ratios in Semiconductors from Electron Mobility and Free Carrier Absorption; GaAs," 153d Electrochem. Soc. Meeting, Seattle, Washington, 1978.

13. W. Walukiewicz, J. Lagowski, L. Jastrzebski, M. Lichtensteiger and H.C. Gatos, "Electron Mobility and Free-Carrier Absorption in GaAs: Determination of the Compensation Ratio," J. Appl. Phys. 50, 899 (1979).

14. W. Walukiewicz, J. Lagowski, L. Jastrzebski, P. Rava, M. Lichtensteiger, C.H. Gatos and H.C. Gatos, "Electron Mobility and Free-Carrier Absorption

in InP; Determination of the Compensation Ratio," J. Appl. Phys., in press.

15. J. Lagowski, "Microcharacterization of GaAs for Device Applications," Proc. 3rd Biennial Univ./Industry/Gov. Microelectronic Symp., May 1979, Lubbock, Texas, IEEE Conf. Record, p. 1.

16. H.C. Gatos, J. Lagowski and L. Jastrzebski, "Present Status of GaAs," NASA Contractor Report 3093, January 1979.

17. L. Jastrzebski, J. Lagowski and H.C. Gatos, "Outdiffusion of Recombination Centers from the Substrate into LPE Layers; GaAs," J. Electrochem. Soc. 126, 2231 (1979).

18. L. Jastrzebski, J. Lagowski and H.C. Gatos, "Effect of Growth Kinetics on Formation of Recombination Centers in GaAs," presented at 155th Annual Meeting of Electrochem. Soc., May 1979, Boston.

19. W. Walukiewicz, J. Lagowski, L. Jastrzebski and H.C. Gatos, "Minority-Carrier Mobility in p-Type GaAs," J. Appl. Phys. 50, 5040 (1979).

20. D.W. Lang, "Deep-Level Transient Spectroscopy," J. Appl. Phys. 45, 3023 (1974).

21. A. Mircea and A. Mitonneau, "A Study of Electron Traps," J. Appl. Phys. 8, 15 (1975).

APPENDIX

PUBLICATIONS

Reprints and preprints of papers which appeared in the literature or were submitted for publication since our last annual report are appended. They provide a more detailed account of some of the work discussed in the text of the present report.

Defect Structure and Electronic Characteristics of GaAs Layers Grown by Electroepitaxy and Thermal LPE

Y. Imamura,[1] L. Jastrzebski, and H. C. Gatos*

Department of Materials Science and Engineering, Massachusetts Institute of Technology, Cambridge, Massachusetts 02139

ABSTRACT

A comparative study was carried out on the defect structure and electronic properties of GaAs layers grown under similar conditions by electroepitaxy (electromigration controlled) and by thermal LPE. It was found that the density of certain microdefects, commonly present in GaAs layers, is significantly smaller (about an order of magnitude) in electroepitaxially grown than in thermally grown layers. It was also found that electroepitaxial layers exhibit greater carrier mobility and diffusion length than the thermally grown layers; in addition, electroepitaxially grown p-n junctions exhibited lower saturation current than the thermally grown junctions. The differences in the characteristics of two types of layers are attributed to corresponding differences in the nature of the driving forces for growth.

Growth of semiconductor compounds from solution can be initiated and sustained by passing electric current through the growth interface while the over-all temperature of the system is kept constant. Electroepitaxial growth has been successfully achieved with InSb (1), GaAs (2, 3), GaAlAs (4, 5), InP (6), HgCdTe (7), and garnet layers (8). The advantages of electroepitaxy in obtaining controlled doping (2, 9), improved electronic structures (9, 5), and in studying growth and segregation (10) have already been reported. A theoretical model of growth kinetics has been recently formulated (11) which defines the contribution of the solute electromigration and that of the Peltier effect (at the solid-solution interface) to the over-all growth process. According to the model, the contribution of electromigration is dominant in the absence of convection in the solution, whereas the contribution of the Peltier effect can be dominant in the presence of convection. This model was found to be in excellent agreement with experiment data on the kinetics of the electroepitaxial growth of GaAs from Ga-As solutions.

Under electromigration control it has been shown that growth takes place under nearly equilibrium (isothermal) conditions (11) Consistent with this result it has been found that the surface morphology of electroepitaxial layers (attained under electromigration control) do not exhibit terracing commonly observed on layers grown by standard (thermal) LPE (12). In the light of these results, the present study was undertaken and aimed at the comparison of the defect structure and electrical properties of GaAs layers grown by thermal cooling and by electromigration controlled electroepitaxy under similar over-all conditions.

Experimental

Electroepitaxial growth of GaAs was performed in a standard LPE apparatus modified to permit controlled current flow through the solution-substrate interface (2, 13). Ga-As solutions doped with Ge (2%) were used; their height in the growth cell was from 10 to 14 mm. Growth was carried out on a 0.5 cm^2 area of (100) oriented 300 μm thick GaAs substrates which were either Cr-doped (semi-insulating in room temperature) or Si-doped ($n = 2 \times 10^{18}$ cm^{-3}). Electrical contact to the substrate was made with a 150 μm thick layer of Ga (13). To insure electromigration controlled growth, convective interference was eliminated as described elsewhere (13).

Prior to growth, the Ga-As solution was thermally equilibrated over a dummy substrate at 900°C. After bringing the solution into contact with the substrate, the temperature of the system was increased by 3°C to dissolve the substrate surface layer which might have been depleted in As during the thermal equilibration period (14).

Epitaxial layers ranging in thickness from 20 to 40 μm were grown by employing current densities of 2, 5, 10, 20, 40, and 50 A/cm^2 with the substrate having a positive polarity or by decreasing the temperature 10°C at a rate ranging from 0.1° to 2°C/min; this cooling range was chosen to obtain the same microscopic growth rates as those obtained by the employed current densities.

The microscopic growth rate was determined by interface demarcation (15); current pulses (80 A/cm^2) of 0.5 sec duration and at intervals of a few minutes to one hour were passed through the growth interface during thermal cooling or they were superimposed to the base current during electroepitaxy.[2] The microscopic growth rate was found to be essentially constant during the first hour of growth; only layers grown under constant growth rate were used in the present analysis.

After growth the electric contact to the base of the substrate was removed by lapping. To determine the growth rate, the substrate and epilayer were cleaved and etched in AB etchant for about 20 sec; interference contrast microscopy was used to measure the spacing between interface demarcation lines. Samples for carrying out Hall-effect measurements and for p-n junction characterization were obtained by cleaving the substrate and the epilayer into 1 × 1 mm squares; electrical contacts were made with In or Sn by heating at 400°C for 10 min in a H_2 atmosphere; layers grown on semi-insulating substrates were used for the Hall-effect measurements. Saturation currents were determined from the *I-V* characteristics of the diodes (p-type epilayers on n-type substrates). The diffusion length was determined from the dependence of the electron-beam-induced current (in an SEM) on the distance of the p-n junction employing a 30 kV accelerating voltage (16).

* Electrochemical Society Active Member.

[1] Present address: Electrical Communication Laboratories, Nippon Telegraph and Telephone Public Corporation, Tokyo 180, Japan.

Key words: semiconductor, defect, doping.

[2] By changing their duration and frequency it was established that current pulses do not affect the over-all growth process or the properties of the material grown.

Crystallographic defects present in the epilayers were revealed by 5 min etching in nonstirred AB etchant at 10°-15°C. Because the presence of terraces on thermally grown surfaces interfered with the observation of etch pits, these layers were lapped with a 5 μm particle diam abrasive and mechanical-chemical polished prior to etching. Electroepitaxially grown layers were etched without any pretreatment. To examine defect distribution in the growth direction, the epilayers were 1° angle-lapped, mechanical-chemical polished with (commercial) bleach solution for 40 to 80 sec; they were then etched in AB etchant for 5 min at 10°-15°C. This process was repeated a few times to obtain the statistical defect distribution through the epilayer. Determination of etch pit densities on as-grown epitaxial layers and on angle-lapped surfaces showed that the lapping process did not introduce defects in the material; in addition the location of the substrate-epilayer interface could be determined with an accuracy of from 1 to 2 μm by etching angle-lapped and cleaved surfaces.

Microscopic defects.—Four types of crystallographic defects were observed in electroepitaxially and in thermally grown layers similar to those previously reported in the literature. Typical examples of these defects in a thermally grown layer with an average velocity of 1 μm/min (1°C/min) are presented in Fig. 1. The conical pits shown in Fig. 1a have been attributed to dislocations which intersect the (001) surfaces at 90° (17). The flat-bottom rounded pits in Fig. 1b are similar in shape to the saucer pits (S-pits) observed in GaP (18); their origin is not clear; they are probably associated with agglomerates of defects or residual impurities (18). The shallow line defects in Fig. 1c are attributed to dislocation segments lying along the (100) surfaces (17). The boat-shaped defects (Fig. 1d), oriented along <110> directions, are related to the presence of Ge, since they are not present in the substrates and they were not observed in epilayers which were Sn- or Te-doped; they could be attributed to either dislocation loops or to stacking faults (19, 20). Apparently, the formation of these pits is due to the segregation of Ge atoms at crystallographic defects.

The above defects were found to be homogeneously distributed in the planes of growth (excepting at the edges). The distribution of the conical defects in all epilayers was the same as in the substrates in the initial stages of growth; their density decreased by more than one order of magnitude after a few microns of growth. This finding indicates that the propagation of dislocation from the substrates to the epitaxial layers is significantly suppressed during LPE growth. Suppression of dislocation propagation (by a factor of about four), although not as pronounced, has been reported during LPE growth on low dislocation density substrates (21).

The distribution of the flat-bottom defects in the growth direction is shown in Fig. 2. The density of these pits is highest near the substrate-epilayer interface and decreases below their density in the substrates as growth proceeds. The increase of the flat-bottom pit density at the interface might be related to

Fig. 1a

Fig. 1b

Fig. 1c

Fig. 1d.

Fig. 1. Typical microdefects observed in an epilayer grown by thermal cooling. See text. (2000×)

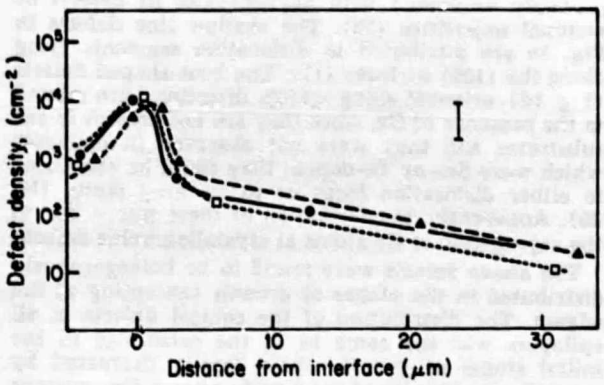

Fig. 2. Distribution of flat-bottom or S pits (Fig. 1b) along the growth direction in layers grown: ● thermally; ▲ with 20 A/cm²; □ with 50 A/cm². Vertical bar indicates standard deviation.

segregation of defects at the surface of the substrate during the heating cycle. For example, As vacancies on the substrate due to As sublimation during heating, prior to growth, could enhance this effect (14). The density of the conical and the flat-bottom pits in the epilayers does not depend on the growth velocity and is the same in thermally or electroepitaxially grown layers.

The density of the shallow line defects is shown in Fig. 3; it is highest near the substrate-epilayer interface; these microdefects were not observed in the substrates or in the epilayers beyond 7 μm of growth. Their density decreases with increasing current density; in layers grown at 50 A/cm² current their density was found to be about one order of magnitude smaller than in the epilayers grown thermally at comparable growth velocity.

The largest difference between thermal LPE and electroepitaxy was found with regard to the boat-shaped pits. Their distribution is presented in Fig. 4; the defect density in thermally grown layers with the maximum and minimum velocity employed in this study (0.2 and 5 μm/min) is shown together with results obtained for layers grown at 10, 20, and 50 A/cm². The boat-shaped defect density is significantly smaller in electroepitaxial layers than in thermally obtained layers (grown with comparable growth rates) and is decreasing with increasing current density. Near the interface the density of the boat-shaped pits in the thermally grown layers is about two orders of magnitude greater than in the layers grown at 50 A/cm² current. With continued growth the density of these defects decreases significantly in the thermally grown layers towards the values found in the electroepitaxial layers.

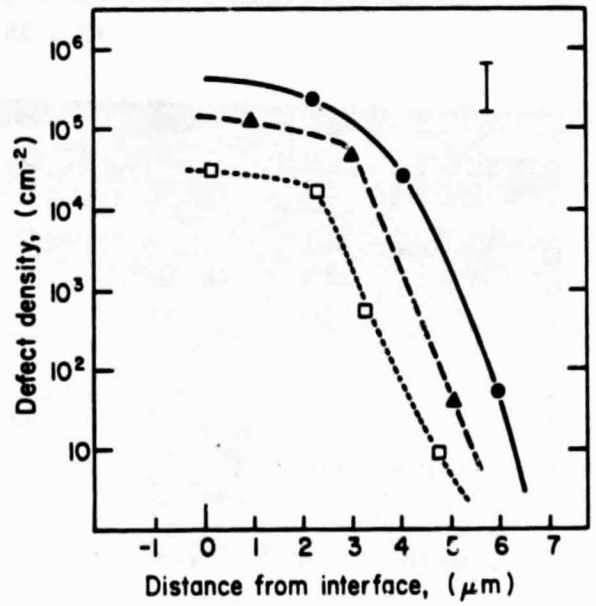

Fig. 3. Distribution of line defects (Fig. 1c) along the growth direction in layers grown: ● thermally; ▲ with 20 A/cm²; □ with 50 A/cm². Vertical bar indicates standard deviation.

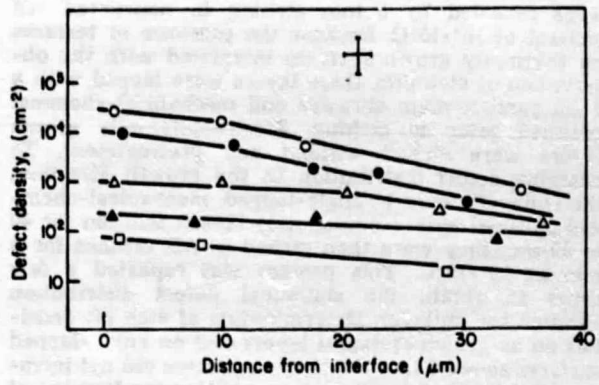

Fig. 4. Distribution of boat-shaped defects (Fig. 1d) along the growth direction in layers grown: ○ thermally with minimum growth velocity (0.2 μm/min); ● thermally with maximum growth velocity (5 μm/min); △ with 5 A/cm²; ▲ with 20 A/cm²; □ with 50 A/cm². Vertical and horizontal bars represent standard deviation.

Electrical properties.—The carrier concentration, mobility, and diffusion length in the layers grown by electroepitaxy and under the same conditions by thermal LPE are presented in Table I; each pair of layers grown at similar rates was obtained in a single run from the same solution. The variations of the carrier concentration in the layers make a direct comparison of the mobility in different layers rather difficult; for this reason the values of the mobilities were normalized to a concentration of 2×10^{18} cm^{-3} and are shown in Table I. Normalization was obtained using the experimental relationship between mobility and hole concentration (9). It is seen that the normalized mobility is slightly but consistently higher in the electroepitaxial layers than in those grown with the same velocity by thermal LPE. The ratio of mobility in the electroepitaxial layers and in the corresponding thermally grown layers appears to increase with increasing growth velocity.

The diffusion length in all layers grown by electroepitaxy is higher than in the corresponding thermally grown layers. In both types of layers the diffusion length increases with increasing growth velocity. With increasing current density, the ratio of the diffusion length in electroepitaxially and thermally grown layers is increasing. It is apparent that the observed difference in diffusion length for the two types of lay-

Table I. Electrical properties of layers grown by electroepitaxy and thermal LPE

Current density and cooling rate	Growth rate (μm/min)	Carrier concentration (10^{18} cm^3)	Mobility (±8%) (cm²/V-sec)			Diffusion length (±10%) (μm)
			Measured	Normalised	Ratio	
2 A/cm² 0.09°C/min	0.20 0.35	2.0 1.8	105 110	105 100	1.05	6.5 6.0
10 A/cm² 0.35°C/min	0.9 1.1	1.9 2.3	125 100	118 115	1.03	7.5 8.5
20 A/cm² 0.7°C/min	2.3 2.0	2.4 2.0	96 10[illegible]	114 105	1.09	8.0 7.0
40 A/cm² 1.5°C/min	4.5 4.0	2.3 2.1	125 115	137 121	1.13	9.5 8.0
80 A/cm² 2.0°C/min	5.6 5.2	2.0 2.3	115 85	115 98	1.18	10.0 7.5

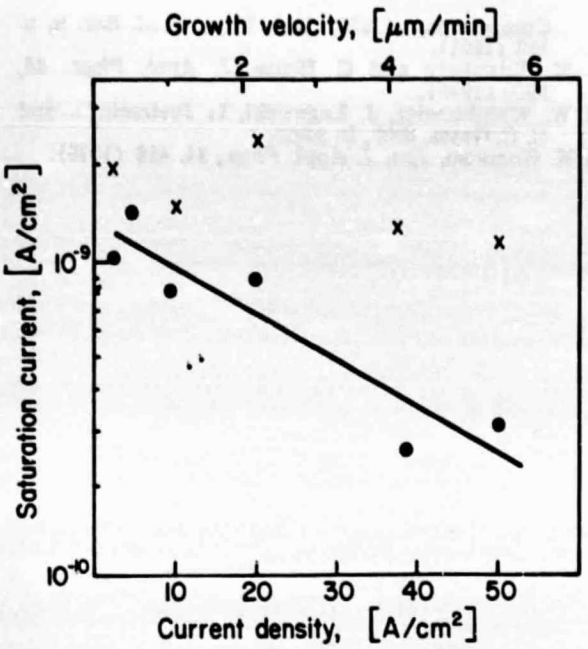

Fig. 5. Saturation current of p-n junctions as a function of growth velocity for thermally grown layers, x, and as a function of current density for electroepitaxial layers, ●.

ers cannot be attributed to changes in the carrier diffusion due to minority carrier mobility variations (22); it must be due to changes in the lifetime. The increase of lifetime in the electroepitaxially grown layers compared with that in the thermally grown layers indicates that electroepitaxy provides material with a smaller concentration of recombination centers.

The dependence of the saturation current of the p-n junction on the growth velocity and/or current density for the layers grown by electroepitaxy and by thermal cooling is presented in Fig. 5. With increasing current density (up to 50 A/cm²) the saturation current of the grown junctions decreases by about one order of magnitude, while for the same changes of the growth velocity in thermal LPE the saturation current remains practically constant. The value of the saturation current increases with increasing concentration of electrically active defects (in the junction plane) leading to leakage current (21). The lower saturation current in the electroepitaxial junctions and its decrease with increasing current density, indicates that the density of electrically active defects in the electroepitaxially grown layers is lower than in the thermally grown layers, and it decreases with current density. This decrease in the density of electrically active defects in the junction plane contributing to the leakage current, could be associated with the observed lower density of boat-shaped defects in the initial stages of growth in the electroepitaxial layers than in the thermally grown layers.

Summary and Conclusions

The micro-defect structure was studied in the layers grown by electroepitaxy and by thermal LPE under the same conditions, i.e., same solutions and growth velocities. It was found that the density of defects related to dislocations lying in the plane of growth and the density of boat-shaped Ge-related defects, especially in the initial stages of growth, is lower in the electroepitaxially grown layers than in the layers thermally grown under comparable conditions. It was also established that their density decreases in both types of layers with increasing current density, or growth velocity. Higher values of carrier mobility and of minority carrier diffusion length and lower values of saturation current of p-n junctions were found in the electroepitaxial layers as compared to those in thermally grown layers; these values were found to improve with increasing current density. In view of this finding it appears likely that the observed defects are electrically active and that their decreased density in electroepitaxially grown layers leads to improved electrical properties.

The pronounced differences in the defect structure observed in the layers grown by electroepitaxy and those grown by thermal LPE cannot be attributed to specific growth conditions. Rather, they must be associated with fundamental differences in the growth mechanisms involved in the two growth methods. Since quantitative models of nucleation and of defect formation have not been established for these methods, the present results will be considered in the light of some general features characterizing the methods.

In electroepitaxy (electromigration-controlled) supersaturation takes place in the immediate vicinity of the growth interface and growth is controlled by the rate of transfer of solute, under the electric field, to the interface. Under these conditions, growth takes place under nearly equilibrium (isothermal) conditions (11). On the other hand, in thermal LPE a supersaturation takes place in the entire solution. Thus, the As distribution in the solution and the interfacial phenomena are different in electroepitaxy and in thermal LPE. Growth under a constant and uniform flux of solute driven to the growth interface by an electric field must be less susceptible to defect formation than growth under thermal LPE conditions.

Acknowledgment

The authors are indebted to the National Science Foundation and the National Aeronautics and Space Administration for financial support.

Manuscript submitted July 24, 1978; revised manuscript received Feb. 14, 1979.

Any discussion of this paper will appear in a Discussion Section to be published in the June 1980 JOURNAL. All discussions for the June 1980 Discussion Section should be submitted by Feb. 1, 1980.

Publication costs of this article were assisted by the Massachusetts Institute of Technology.

REFERENCES

1. M. Kumagawa, A. F. Witt, M. Lichtensteiger, and H. C. Gatos, *This Journal*, 120, 583 (1973).
2. D. J. Lawrence and L. F. Eastman, *J. Cryst. Growth*, 30, 267 (1975); *J. Electronic Mater.*, 6, 1 (1976).
3. L. Jastrzebski, H. C. Gatos, and A. F. Witt, *This Journal*, 123, 1121 (1976).
4. J. Daniele, *Appl. Phys. Lett.*, 27, 373 (1975).
5. J. Daniele, D. A. Commack, and P. M. Asbeck, *J. Appl. Phys.*, 48, 914 (1977).
6. A. Abdul-Fadl and E. K. Stefanakos, *J. Cryst. Growth*, 39, 341 (1977).
7. P. E. Vanier, F. H. Pollack, and P. M. Reccah, 20th Electronic Mat. Conf., June 28-30 (1978).
8. L. Jastrzebski, H. C. Gatos, and A. F. Witt, *This Journal*, 124, 633 (1977).
9. L. Jastrzebski and H. C. Gatos, "GaAs and Related Compounds," (St. Louis 1976) Inst. Phys. Conf. Ser. 33b, p. 88 (1977).
10. L. Jastrzebski and H. C. Gatos, *J. Cryst. Growth*, 42, 309 (1977).
11. L. Jastrzebski, J. Lagowski, H. C. Gatos, and A. F. Witt, *J. Appl. Phys.*, In press (December 1978).
12. Y. Imamura, L. Jastrzebski, and H. C. Gatos, *This Journal*, 125, 1560 (1978).
13. L. Jastrzebski, Y. Imamura, and H. C. Gatos, *ibid.*, 125, 1140 (1978).
14. J. Hallais, A. Mircea-Roussel, J. P. Farges, and G. Poibland, "GaAs and Related Compounds," (St. Louis 1976), Inst. Phys. Conf. Ser. 33b, p. 220 (1977).
15. M. Lichtensteiger, A. F. Witt, and H. C. Gatos, *This Journal*, 118, 1013 (1971).
16. L. Jastrzebski, J. Lagowski, and H. C. Gatos, *Appl. Phys. Lett.*, 27, 537 (1975).

17. M. S. Abrahams and C. J. Buiocchi, *J. Appl. Phys.*, 36, 2855 (1965).
18. G. A. Rozgonyi, A. R. Von Neida, T. Izuka, and S. E. Haszko, ibid., 43, 3141 (1972).
19. D. J. Stirland and B. W. Straugham, *Thin Solid Films*, 31, 139 (1976).
20. A. M. Huber and G. Champier, "GaAs and Related Compounds," (1970) Inst. Phys. Conf. Ser. 9, p. 118 (1971).
21. M. Ettenberg and C. Neuse, *J. Appl. Phys.*, 46, 3500 (1975).
22. W. Walukiewicz, J. Lagowski, L. Jastrzebski, and H. C. Gatos, ibid., In press.
23. R. Komatsu, *Jpn. J. Appl. Phys.*, 14, 419 (1975).

Reprinted from JOURNAL OF THE ELECTROCHEMICAL SOCIETY
Vol. 126, No. 8, August 1979
Printed in U.S.A.

Reprinted from JOURNAL OF THE ELECTROCHEMICAL SOCIETY
Vol. 126, No. 12, December 1979
Printed in U.S.A.

Outdiffusion of Recombination Centers from the Substrate into LPE Layers; GaAs

L. Jastrzebski,[1] J. Lagowski, and H. C. Gatos*

Department of Materials Science and Engineering, Massachusetts Institute of Technology, Cambridge, Massachusetts 02139

ABSTRACT

Experimental results are presented showing that outdiffusion of recombination centers from the GaAs substrate into the epitaxial layer takes place during growth. Such outdiffusion decreases the carrier lifetime in the epitaxial layer to much lower values than the radiative recombination limit. Furthermore, it introduces a lifetime gradient across the epitaxial layer which depends critically on the growth velocity and thermal treatment. High rates of growth (such as those attainable in electroepitaxy) and high cooling rates can minimize the adverse effects of normally available substrates on the epitaxial layers; however, good quality substrates are essential for the consistent growth of device quality layers.

It has been established that the performance of many compound semiconductor devices is adversely affected by nonradiative recombination centers. Their presence in the device active region leads to a decrease in the device efficiency [as in the case of solar cells (1)]. Furthermore, the recombination-enhanced diffusion of such centers (2) causes a slow degradation of the device performance [as in the case of semiconductor lasers (3)].

The nonradiative recombination centers in GaAs are usually associated with residual impurities such as oxygen (4), transition metals (5), and nonstoichiometric point defects (6). The origin of nonstoichiometric defects is not fully understood, although in GaAs it has been attributed to the solidus of the phase diagram (7) and/or to As depletion of the substrate during the heating cycle prior to epitaxial growth (8). Growth at low temperatures and backmelting of the substrate prior to growth (9) tend to reduce the concentration of nonstoichiometric defects and improve the quality of the grown epitaxial layer.

Poor quality GaAs substrate material is a source of defects which can diffuse into the epitaxial layer during the growth process. The available melt-grown GaAs substrates are in most instances highly compensated (10), exhibit large carrier concentration inhomogeneities (11), and contain high concentration of nonradiative recombination centers (12, 13).

The present work is concerned with the outdiffusion of recombination centers from GaAs substrates into GaAs LPE layers. Minority carrier diffusion length and lifetime profiles obtained with EBIC-mode (SEM) measurements are employed for the study of such outdiffusion. Growth conditions required to minimize

* Electrochemical Society Active Member.
[1] Present address: RCA Research Laboratories, David Sarnoff Research Center, Princeton, New Jersey 08540.
Key words: growth, semiconductor, lasers.

the outdiffusion of recombination centers are pointed out.

Experimental

Epitaxial growth and sample preparation.—LPE growth of GaAs was carried out employing classical thermal cooling techniques and electromigration-controlled electroepitaxy (14, 15). Cd-doped ($p \simeq 2 \times 10^{17}$ cm^{-3}) 300 μm thick (100) substrates were used. Epitaxial growth was performed in a two-well graphite boat. In one of the wells the substrates were backmelted (about 25 μm) with an under-saturated solution to remove the As depleted layer formed during the heating cycle. After backmelting the substrate was positioned in the second well containing 2.5g of an undoped Ga-As solution with a GaAs source on top. In the electroepitaxy experiments layers ranging in thickness from 10 to 100 μm were grown at 900°C on an area of 0.5 cm^2 at a rate of about 6 μm/min by passing an electric current of 60 A/cm^2 for a period of 2-20 min. Growth was terminated by turning the current off. In the thermal growth experiments the growth was performed from equilibrated solutions by cooling from 910° to 900°C at a rate of 1°C/min.

In both procedures, after growth was completed, the system was kept at the growth temperature for time periods ranging from 1 min to 3 hr with the grown layer in contact with the solution. The experiment was terminated by quenching the system to room temperature with an initial cooling rate (from 900° to 700°C) of about 70°C/min. The solution was left over the epitaxial layer or wiped by the moving slider prior to cooling.

After cooling, if the excess Ga-GaAs mixture was not wiped, it was removed from the epitaxial layer surface by boiling in HCl; the epilayer was cleaved and etched in AB etchant for about 30 sec. Interference contrast microscopy was employed to determine the thickness of the epitaxial layers. Whenever necessary, the part of the epitaxial layer grown during cooling to room temperature (about 5-10 μm in thickness) was etched away in 5 parts H_2SO_4 + 1 H_2O + 1 H_2O_2. Ohmic contacts were soldered on the substrate and the epilayer employing Sn and In in an H_2 atmosphere.

The epitaxial layers were n-type with a carrier concentration of about 5×10^{16} cm^{-3}. Schottky barriers required for EBIC-mode measurements were made by evaporating aluminum or gold on the surfaces of the epitaxial layer.

Minority carrier diffusion length and lifetime.—Measurements of the minority carrier diffusion length were performed utilizing electron beam excitation as shown schematically in Fig. 1. The diffusion length was obtained from the dependence of the electron beam-induced current (EBIC) on the distance between the generation position and the collecting Schottky barrier or the p-n junction (16). Reabsorption of photons resulting from radiative recombination in general introduces uncertainties in the determination of the minority carrier diffusion length. However, in the present case, such uncertainties are of no consequence, since the lifetime of the minority carriers was significantly lower (up to two orders of magnitude) than the radiative recombination limit. A 35 keV electron beam energy was used in all experiments to minimize the effect of surface recombination on the measured diffusion length (17).

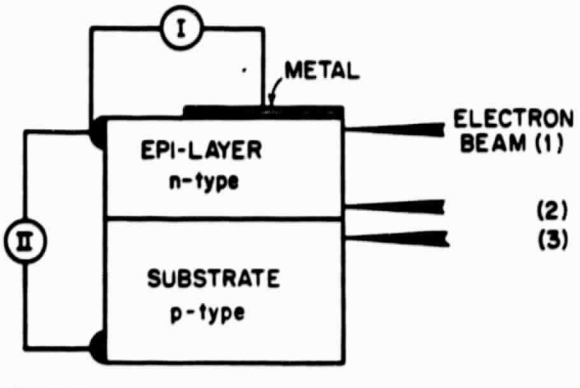

Fig. 1. Schematic representation of the experimental configuration for the determination of the minority carrier diffusion length by the EBIC method; see text.

The configuration shown in Fig. 1 made possible the determination of the diffusion length, L_p, of the minority carriers in the epitaxial layer near the epilayer surface (with the electron beam at position 1 and with current circuit I), and near the substrate (with the electron beam in position 2 and with current circuit II); the minority carrier diffusion length was also determined in the p-type substrates (with the electron beam in position 3 and with current circuit II).

Values of lifetime, τ, were estimated from the standard relationship, $L = \left(\frac{kT}{e}\mu\tau\right)^{1/2}$, where μ is the minority carrier mobility and kT/e equals 0.026V at 300°K. In p-type GaAs (substrates in the present case) the electron mobility can be noticeably smaller than the mobility of electrons in n-type material of similar free carrier concentration (18). Accordingly, in evaluating the electron lifetime in the substrates recently calculated theoretical values of electron mobility in p-type GaAs were used (18). In these calculations the contribution of electron scattering by heavy holes and the difference in screening energies between holes and electrons have been taken into account. In the case of holes their mobility as majority or minority carriers is expected to be similar at room temperature and for free carrier concentrations below 10^{17} cm^{-3} (since screening effects and carrier-carrier scattering are not significant). Accordingly, in evaluating the hole lifetime in epitaxial layers, the hole mobility value of $\mu_p \simeq 300$ cm^2/V-sec was used, *i.e.*, the hole mobility in p-type GaAs with hole concentration of 5×10^{16} cm^{-3} (19), which is similar to the electron concentration in the epitaxial layers.

Results and Discussion

Substrate.—The minority carrier lifetime in the substrate material was found to be about 10^{-10} sec, *i.e.*, two orders of magnitude smaller than the lifetime value expected from band-to-band radiative recombination (20). It was also determined that the substrate material is highly inhomogeneous with local lifetime fluctuations exceeding a factor of 4. These findings clearly indicate that the lifetime in the substrates is controlled entirely by nonradiative recombination and thus the substrate must contain a high, nonuniform, concentration of recombination centers.

Outdiffusion of recombination centers from the substrate.—The lifetime in the epitaxial layers was measured as a function of position on a given plane parallel to the surface, as a function of distance from the substrate-epitaxial layer interface, and as a function of time the layer was kept at the growth temperature.

Typical results of the lifetime measurements as a function of position on a plane parallel to the surface of the epitaxial layer are given in Fig. 2. The upper curve corresponds to positions near the surface of the epitaxial layer. The layer was 40 μm thick; it was grown electroepitaxially and was kept 20 min at the growth temperature (from the beginning of growth to the beginning of cooling). It is evident from Fig. 2 that lifetime inhomogeneities of a similar nature are present near the substrate-epitaxial interface and near the surface of the layer; however, near the surface the lifetime values are significantly higher. It should be noted that even the highest values of lifetime are well below the values (of the order of 10^{-7} sec) expected from radiative band-to-band recombination (20).

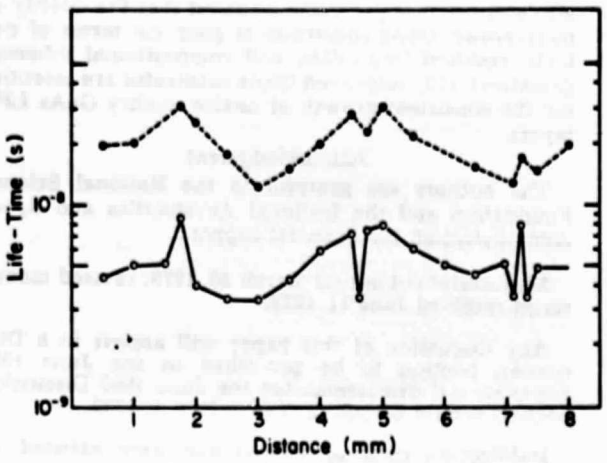

Fig. 2. Minority carrier lifetime profiles along two planes parallel to the growth interface; ○—near the original growth interface (position 2 in Fig. 1); ●—near surface of epitaxial layer (position 1 in Fig. 1).

The above behavior of the minority carrier lifetime can be understood if one considers that the substrate represents a source of recombination centers which diffuse into the epitaxial layer during the growth process and thermal treatment. On this basis, the difference between the lifetime near the epitaxial layer surface and the lifetime near the epitaxial layer-substrate interface should decrease with increasing exposure time of the system to the growth temperature. Similarly, the lifetime in the epitaxial layer should decrease with increasing exposure time to the growth temperature. As is seen from Fig. 3, such behavior is indeed found in electroepitaxially and in thermally grown layers. The lifetime in both electroepitaxially and thermally grown layers behaves similarly upon exposure to high temperature after growth, as it is dominated by recombination at outdiffused centers.

The fact that recombination centers outdiffuse from the substrate into the epitaxial layers is further supported by the results shown in Fig. 4. Here the lifetime measured near the epitaxial layer surface is plotted as a function of thickness of the epitaxial layers, all of which have been exposed to a high temperature (growth temperature) for the same period of time (20 min). The layers were grown by electroepitaxy and at the same growth rate of about 6 μm/min. It is seen that the lifetime increases by about two orders of magnitude (near the surface) as the distance from the substrate (thickness of the layer) increases from 5 to 90 μm.

If the simplified assumption is made that the lifetime is inversely proportional to the concentration of the recombination centers, the data of Fig. 3 and 4 can be used to estimate the diffusion constant of the recombination centers. Thus, treating the substrate-epitaxial layer interface as a limited diffusion source (21) the lifetime becomes

$$\frac{1}{\tau} \sim \frac{1}{\sqrt{Dt}} \exp\left(-\frac{x^2}{4Dt}\right) \qquad [1]$$

where x is the distance from the substrate-epitaxial layer interface, t is the time, and D is the diffusion constant of recombination centers. From this expression the solid line in Fig. 3 is obtained by taking x = constant and the solid line in Fig. 4 by taking t = constant. From these plots a value for the diffusion constant of the recombination centers of approximately 5×10^{-9} cm²/sec is obtained (900°C). The same value of 5×10^{-9} cm²/sec has been reported for point defect diffusion in GaAs (gallium vacancies) at 1000°C (22).

It is important to note that the observed lifetime behavior which is consistent with the above diffusion model, cannot be explained on the basis of impurity segregation effects. A recent experimental and theoretical analysis of impurity segregation in GaAs during electroepitaxy (23) has shown that the maximum changes of the dopant segregation coefficients do not exceed 40%, i.e., they are two orders of magnitude smaller than the changes required to account for the presently reported lifetime behavior.

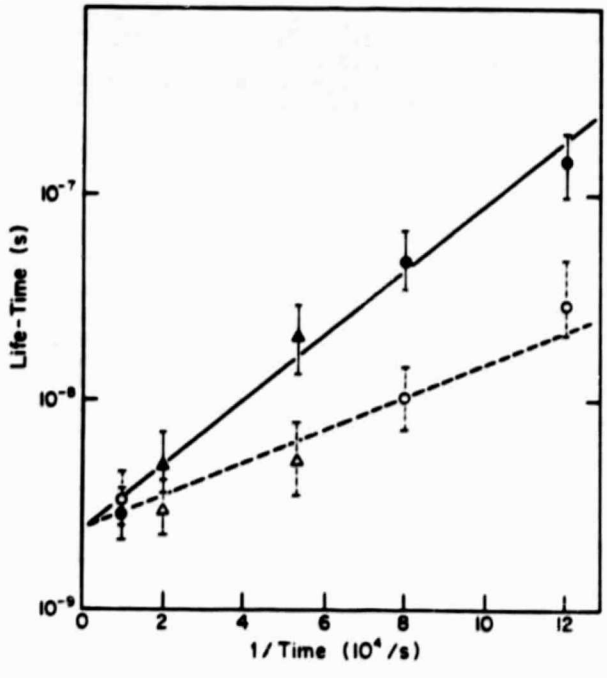

Fig. 3. Minority carrier lifetime as a function of time at the growth temperature (900°C); △, ○ near the original growth interface; ▲, ●—near the surface of the epitaxial layer; circles correspond to layers grown by electroepitaxy and triangles to thermally grown layers; all layers were 40 μm thick.

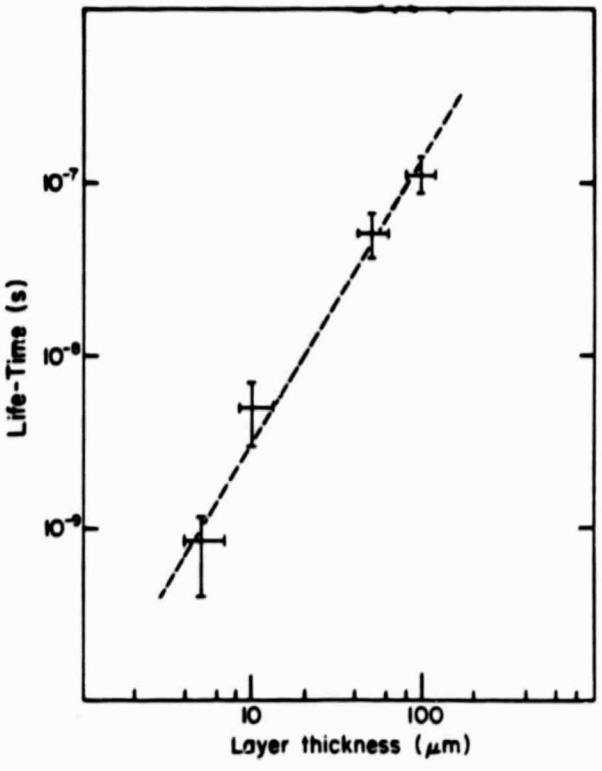

Fig. 4. Minority carrier lifetime near the surface of the layers as a function of the layer thickness.

Growth velocity and the effects of outdiffusion.—The diffusion constant of impurities and point defects decreases exponentially with decreasing temperature, and thus lowering the growth temperature should drastically reduce the effects of outdiffusion from the substrate. However, there are limitations to the lowering of the growth temperature as the attainable growth rate decreases significantly and single crystal growth becomes problematic.

On the other hand, it is evident that the effects of outdiffusion can be reduced if the growth velocity, R, is much greater than the velocity of the diffusion front propagation v_D. In a diffusion process a constant concentration profile can be approximated as $x^2/4Dt$ = const.; consequently, $v_D = dx/dt$ = const. $\sqrt{D/t}$. Thus, the condition $R >> v_D$ can be expressed as

$$R >> \left(\frac{D}{t}\right)^{1/2} \quad [2a]$$

or

$$R >> \frac{D}{t} \quad [2b]$$

Equation [2a] represents the case where growth is performed for certain time t and Eq. [2b] represents the case where the growth of a layer of a thickness d is required.

In the present case the outdiffusion constant of recombination centers was found to be 5×10^{-9} cm^2/sec. Thus, according to Eq. [2b], for a layer 40 μm thick the growth rate required to reduce significantly the effect of outdiffusion is $R >> 0.75$ μm/min. In the present experiments the electroepitaxial growth velocity was about 6 μm/min, which is high enough to satisfy the above condition for reducing significantly the effects of outdiffusion of recombination centers. Accordingly, it is not surprising that, without a postgrowth heat-treatment epitaxial layers 40 μm thick were consistently grown with a lifetime of about 10^{-7} sec.

The growth velocity in thermal LPE is limited by the slow solute transport to the growth interface and by the fact that the relatively small supercooling must be used to prevent spurious nucleation in the solution (24). These limitations are overcome in electroepitaxy (15).

Summary and Conclusions

It was found that outdiffusion of recombination centers from a substrate to the epitaxial layer takes place during liquid phase epitaxial growth. From the study of the time dependence of the diffusion process a diffusion constant of 5×10^{-9} cm^2/sec at 900°C was obtained for the outdiffusion of recombination centers. This value is the same as that reported for the diffusion constant of Ga vacancies in GaAs at 1000°C. It should be noted that outdiffusion of point defects from the substrate has recently been suggested (25) on the basis of measurements on the distribution of residual deep levels in LPE GaAs crystals employing photocapacitance in conjunction with step-etching.

According to the present results, the recombination of minority carriers at the outdiffused defects constitutes the limiting factor for the minority carrier lifetime in the epitaxial layers. It has also been shown that the substrate-epitaxial layer interaction during the growth process can be reduced by increasing the growth velocity. Thus utilizing high growth velocities attainable in electroepitaxy, an improvement of as much as two orders of magnitude in the minority carrier lifetime was observed. The present results could account for the improved characteristics of GaAs lasers grown under high growth velocities (26).

Thus, the recombination characteristics of excited carriers in epitaxial layers are significantly influenced by compositional and structural defects in the substrate. Since it is generally accepted that the quality of melt-grown GaAs substrates is poor (in terms of defects, residual impurities, and compositional inhomogeneities) (13) improved GaAs substrates are essential for the consistent growth of device quality GaAs LPE layers.

Acknowledgment

The authors are grateful to the National Science Foundation and the National Aeronautics and Space Administration for financial support.

Manuscript submitted March 26, 1979; revised manuscript received June 11, 1979.

Any discussion of this paper will appear in a Discussion Section to be published in the June 1980 JOURNAL. All discussions for the June 1980 Discussion Section should be submitted by Feb. 1, 1980.

Publication costs of this article were assisted by Massachusetts Institute of Technology.

REFERENCES

1. See, for example, J. H. Reynolás and A. Meulenbert, Jr., *J. Appl. Phys.*, 45, 2582 (1974).
2. D. V. Lang and L. C. Kimerling, *Phys. Rev. Lett.*, 33, 489 (1974).
3. P. Petroff, W. D. Johnston, Jr., and R. L. Hartman, *Appl. Phys. Lett.*, 25, 226 (1974), and H. Kressel and H. F. Lockwood, *J. Phys.*, 35, 223 (1974).
4. M. Ishii, H. Kan, and W. Susaki, *Appl. Phys. Lett.*, 29, 375 (1976).
5. A. G. Milnes, Private communication.
6. J. A. Van Vechten, *J. Electron. Mater.*, 4, 1159 (1975).
7. G. M. Bloom, *J. Cryst. Growth*, 36, 125 (1976).
8. See, for example, R. Zucca, in "Proceedings 6th International Symposium on GaAs and Related Compounds, St. Louis, 1976, p. 228, Inst. of Physics, London (1977).
9. L. Jastrzebski and H. C. Gatos, *J. Cryst. Growth*, 42, 309 (1977).
10. W. Walukiewicz, J. Lagowski, L. Jastrzebski, M. Lichtensteiger, and H. C. Gatos, *J. Appl. Phys.*, 50, 899 (1979).
11. L. Jastrzebski, J. Lagowski, W. Walukiewicz and H. C. Gatos, submitted to *J. Appl. Phys.*
12. A. M. Sekela, D. L. Feucht, and A. G. Milnes, in "Proceedings of the Symposium on GaAs and Related Compounds, Deauville, France, 1974" Conf. Ser. 24, p. 245, Inst. of Physics, London and Bristol (1974).
13. H. C. Gatos, J. Lagowski, and L. Jastrzebski, "Present Status of GaAs," NASA Report 3093, January 1979.
14. L. Jastrzebski, Y. Imamura, and H. C. Gatos, *This Journal*, 125, 1140 (1978).
15. L. Jastrzebski, J. Lagowski, H. C. Gatos, and A. F. Witt, *J. Appl. Phys.*, 49, 5909 (1978).
16. D. B. Wittry and D. F. Kyser, ibid., 36, 1387 (1965).
17. L. Jastrzebski, J. Lagowski, and H. C. Gatos, *Appl. Phys. Lett.*, 27, 537 (1975).
18. W. Walukiewicz, J. Lagowski, L. Jastrzebski, and H. C. Gatos, *J. Appl. Phys.*, In press.
19. J. D. Wiley, in "Semiconductors and Semimetals," Vol. 10, R. K. Willardson and A. C. Beer, Editors, Chap. 2, Academic Press, New York (1975).
20. See, for example, "Gallium Arsenide, Growth, Properties and Applications," F. P. Kesamanly and D. N. Nasledova, Editors, Chap. 5, Izdatelstvo Nauka, Moscow (1973) in Russian.
21. S. M. Sze, "Physics of Semiconductor Devices," p. 82, Wiley-Interscience, New York (1969).
22. J. Blanc, *J. Appl. Phys.*, 45, 1948 (1974).
23. J. Lagowski, L. Jastrzebski, and H. C. Gatos, Submitted to *J. Appl. Phys.*
24. A. Ju. Malinin and O. B. Nevsky, *J. Electronic Mater.*, 7, 757 (1978).
25. T. Okumura and T. Ikoma, *J. Cryst. Growth*, 45, 459 (1978).
26. M. Ettenberg and H. Kressel, *Appl. Phys. Lett.*, 26, 478 (1975).

Liquid-phase electroepitaxy: Dopant segregation

J. Lagowski, L. Jastrzebski,[a] and H. C. Gatos
Department of Materials Science and Engineering, Massachusetts Institute of Technology, Cambridge, Massachusetts 02139

(Received 21 May 1979; accepted for publication 20 August 1979)

A theoretical model is presented which accounts for the dopant segregation in liquid-phase electroepitaxy in terms of dopant transport in the liquid phase (by electromigration and diffusion), the growth velocity, and the Peltier effect at the substrate-solution interface. The contribution of dopant electromigration to the magnitude of the effective segregation coefficient is dominant in the absence of convection; the contribution of the Peltier effect becomes significant only in the presence of pronounced convection. Quantitative expressions which relate the segregation coefficient to the growth parameters also permit the determination of the diffusion constant and electromigration mobility of the dopant in the liquid phase. The model was found to be in good agreement with the measured segregation characteristics of Sn in the electroepitaxial growth of GaAs from Ga-As solutions. For Sn in Ga-As solution at 900 °C the diffusion constant was found to be 4×10^{-5} cm^2/s and the electromigration velocity (toward the substrate with a positive polarity) 2×10^{-5} cm/s at a current density of 10 A/cm^2.

PACS numbers: 68.55. + b, 61.70.Tm

INTRODUCTION

It has been recognized for many years that the dopant distribution in semiconductors could be controlled by passage of electric current through the solid-melt interface during crystal growth.[1-5] Peltier cooling (or heating) in the vicinity of the interface[1,2] and/or electromigration in the liquid phase[3-5] have been considered as contributing factors to changes in the crystal growth velocity and/or the impurity segregation. In the case of the growth of bulk single crystals from the melt the proposed approaches utilizing electric current have been proven of limited applicability because of convection instabilities in the melt and other interfering processes caused by Joule heating.

In the liquid-phase-epitaxy (LPE) configuration, where the dimensions of the substrate and the solution are relatively small, the effects of Joule heating resulting from dc can be minimized. Actually, it has been demonstrated that electroepitaxy (LPE growth by passing dc through the substrate-solution interface) can provide control of the growth velocity[7,8] as well as of the dopant segregation[9-12] and defect structure in the grown layers.[13] In standard, thermal LPE, such control is still a complex problem.

Recently a quantitative model has been developed for the kinetics of electroepitaxial growth.[8] The model defines the contribution of the Peltier effect (Peltier cooling or heating at the growth interface) and that of solute electromigration to the overall growth process; it also provides expressions which relate directly the growth velocity to growth parameters. This model was found to be in excellent agreement with extensive experimental data on the electroepitaxial growth of GaAs.[8]

In the present study of a theoretical model is presented for segregation of dopants in electroepitaxial growth. This model combines the characteristics of growth kinetics and segregation phenomena involving transport of dopants in solution (electromigration and diffusion) and Peltier cooling (or heating) at the interface. The segregation model is applied to the analysis of the experimental results obtained on the dopant segregation in electroepitaxial growth of GaAs from Sn-doped Ga-As solutions.

ELECTROEPITAXIAL GROWTH PROCESS

In thermal LPE, growth is initiated by lowering the temperature of an equilibrated substrate-solution system by ΔT (i.e., $T_0 \rightarrow T_0 - \Delta T$) and thus bringing about supersaturation which leads to solidification taking place preferentially (although not always exclusively) on the substrate. The depletion (or accumulation) of the solute at the growth interface creates a concentration gradient in the solution and thus solute transport for the growth process is provided by diffusion.[14] External control of diffusion is hardly possible and consequently control of the overall growth process is limited to the control of ΔT as a function of time.

In electroepitaxy, the substrate-solution system is kept at the equilibrium temperature T_0, while an electric current is passed through the solution-substrate interface.[8] Since the substrate (e.g., GaAs) and the solution (e.g., Ga-As solution) are dissimilar conductors, the electric current (in the appropriate direction) leads to Peltier cooling at their interface which in turn leads to supersaturation and growth as in standard LPE. At the same time, current flow (in the appropriate direction) results in electromigration of the solute toward the substrate due to electron-momentum exchange and/or electrostatic field forces.[15] Such electromigration leads also to supersaturation at the substrate-solution interface and thus to crystal growth. Thus, Peltier cooling as well as solute electromigration can contribute to the overall electroepitaxial growth velocity v. It has been shown[8] by taking into consideration solute transport through diffusion and electromigration that

$$v = v_T f_k(E,\delta,t) + v_E, \tag{1}$$

[a]Present address: RCA, David Sarnoff Research Center, Princeton, N.J. 08540.

 0021-8979/80/010364-09$01.10

where v_T is the contribution to the overall velocity by diffusion transport and v_E is the contribution by electromigration; these velocities are expressed as follows:

$$v_T = \frac{\Delta T_p}{C_s - C_l} \left.\frac{dC}{dT}\right|_L \left(\frac{D}{\pi t}\right)^{1/2}, \tag{2a}$$

$$v_E = \mu E \frac{C_l}{C_s - C_l}, \tag{2b}$$

where ΔT_p is the temperature decrease due to Peltier cooling, C_s and C_l are the concentration of the solute in the solid and at the substrate-solution interface, respectively; D is the diffusivity of the solute in the solution; μ is the mobility of the solute under the electric field E; $dC/dT|_L$ is the slope of the liquidus line. The function f_k in Eq. (1) accounts for solute transport by processes other than diffusion (e.g., convective flow) and in metallic solutions of primary interest here[8] $f_k = 1$ in the absence of convection, and $f_k = (\pi D t)^{1/2}/\delta$ in the presence of convection, where δ is the thickness of the diffusion boundary layer.

In the absence of convection ($f_k = 1$) the Peltier contribution, v_T, decreases with time, whereas v_E is independent of time [Eq.(2b)]; thus after the initial transient period the overall growth velocity is practically constant, and it is controlled by the solute electromigration. Since Peltier cooling is usually small (of the order of 1 °C), C_l in Eq. (2b) can be taken to be equal to C_0, and the electromigration growth velocity becomes

$$v_E = \mu E \frac{C_0}{C_s - C_0}, \tag{3}$$

where C_0 is the equilibrium solute concentration at the constant growth temperature T_0.

In the presence of convection, f_k is inversely proportional to δ which in turn decreases with increasing convective flow. Thus, in the presence of convection the contribution of Peltier cooling to the overall growth velocity can be significant.

The agreement of the above model with experimental results has been discussed in detail elsewhere.[8]

SEGREGATION MODEL

In considering dopant segregation in electroepitaxy it is assumed that the dopant concentration in the solution is small enough so that it has no appreciable effect on the phase diagram of the host system as well as on the electromigration and diffusion of the solute; i.e., it is assumed that the impurity has no effect on the crystal growth velocity.

Two representative cases will be analyzed: (1) convection in the solution is virtually absent; in this case the growth kinetics is controlled by electromigration and the growth velocity, $v = v_E$, is independent of time; (2) convection is present in the solution; in this case the role of the Peltier effect becomes significant, and after a transient period of $t \simeq \delta^2/D$ growth proceeds essentially under steady-state conditions. Both of these cases are readily attainable experimentally as discussed elsewhere.[8,16]

In developing the model of dopant segregation in electroepitaxy, a similar approach is used to that employed in the theoretical treatment of growth kinetics. Thus, segregation will be related to mass-transport considerations involving electromigration and diffusion of impurities in the solution and the advancement of the growth interface. Diffusion of impurities within the solid and also interface phenomena (e.g., adsorbed layers on the substrate) will not be taken into consideration.

The incorporation of impurities into the solid will be described by introducing an interface segregation coefficient $k_0 = C_{is}/C_i|_{x=0}$ where C_{is} and $C_i|_{x=0}$ are the impurity concentration in the solid and in the solution at the interface, respectively.

The pertinent equations are the transport equation and the relationship ensuring conservation of fluxes at the interface.

The transport equation is expressed as

$$D_i \frac{\partial^2 C_i}{\partial x^2} + (v + \mu_i E)\frac{\partial C_i}{\partial x} = \frac{\partial C_i}{\partial t}, \tag{4a}$$

where D_i is the diffusion coefficient of the impurity in the solution, C_i is the impurity concentration in the solution, x is the distance from the interface, v is the growth velocity, μ_i is the mobility of the impurity (under an electric field) in the solution, and t is the time. The sign of the electromigration velocity $\mu_i E$ depends on the direction of current flow; in the present case $\mu_i E$ is taken as positive when impurities electromigrate toward the interface.

Conservation of fluxes at the interface is expressed as

$$vC_{is} - (v + \mu_i E)C_i|_{x=0} = D_i \left.\frac{dC_i}{dx}\right|_{x=0} \tag{4b}$$

The boundary conditions describing impurity concentration are:

$$C_i = C_{io} \quad \text{for } t = 0 \tag{4c}$$

$$C_i = C_{io} \text{ for } x = \infty \text{ (absence of convection)} \tag{4d}$$

or

$$C_i = C_{io} \text{ for } x > \delta \text{ (presence of convection).} \tag{4e}$$

The initial temperature of the system is T_0; upon current flow the temperature changes, due to Peltier effect, to $T_1 = T_0 + \Delta T_p$. Accordingly, upon current flow the interface segregation coefficient k changes from $k_0(T = T_0)$ to $k^1(T_1) = k_0 + \partial k/\partial T|_{T_0}\Delta T_p$. For the two cases defined above (absence and presence of convection in the solution) the solution of Eq. (4) and, thus the effective segregation coefficient $k_{\text{eff}} = C_{is}/C_{io}$, can be obtained in an analytical form. The Laplace transform procedure of solving Eq. (4) in the absence of convection is given in the Appendix. In the presence of convection, the steady state solution obtained in Ref. 5 will be adopted here.

Absence of convection electromigration-controlled growth

According to the derivation given in the Appendix, the effective segregation coefficient is given by

$$k_{\text{eff}} = k_0^1 \left\{1 - \frac{1}{2}\operatorname{erfc}[\beta(D_i t)^{1/2}]\right.$$

$$+\frac{\beta-\alpha}{2(\alpha+\beta)}\operatorname{erfc}[-\beta(D_i t)^{1/2}]$$
$$+\frac{\alpha}{\alpha+\beta}\exp[D_i t(\alpha^2-\beta^2)]\operatorname{erfc}[\alpha(D_i t)^{1/2}]\Big\}, \quad (5)$$

$$\alpha=\frac{1}{D_i}\left((k_0^{\frac{1}{2}}-1)v+\frac{v-\mu_i E}{2}\right); \quad \beta=\frac{v+\mu_i E}{2D_i}.$$

It is of interest to note that if the impurity transport is not affected by the electric field ($\mu_i = 0$) and for $\Delta T_p = 0$, Eq. (5) reduces to

$$k_{\text{eff}}=\frac{1}{2}\left\{1+\operatorname{erf}\left[\frac{v}{2}\left(\frac{t}{D_i}\right)^{1/2}\right]+(2k_0-1)\right.$$
$$\left.\times\exp\left(k_0(k_0-1)\frac{v^2 t}{D_i}\right)\operatorname{erfc}\left[\frac{(2k_0-1)v}{2}\left(\frac{t}{D_i}\right)^{1/2}\right]\right\}. \quad (6)$$

Equation (6) is identical to the standard expression for diffusion-controlled segregation under conditions of constant growth velocity.[17]

The complex form of Eq. (5) reduces to much simpler forms in the cases of high or low electric fields. For a high electric field, and under the assumption that $\mu_i E t \gg 2(D_i t)^{1/2}$, Eq. (5) reduces to

$$k_{\text{eff}}\simeq k_0^{\frac{1}{2}}\left\{1+\frac{\mu_i E}{k_0^{\frac{1}{2}} v}\left[1-\exp\left(-\frac{k_0^{\frac{1}{2}} v\mu_i E}{D_i}t\right)\right]\right\}. \quad (7)$$

Thus, the effective segregration coefficient increases exponentially with time to a value $k_{\text{eff}} = k_0^{\frac{1}{2}} + \mu_i E/v$. Such behavior is expected only in nonmetallic solutions (e.g., electroepitaxial growth of garnets[18]) where the electric field can be of the order of V/cm.

In metallic-type solutions (such as those employed in epitaxial growth of III-V compounds) the values of $\mu_i E$ lie between 10^{-5} and 10^{-4} cm/s; accordingly, the low-field condition, $\mu_i E t^{1/2} \ll D_i^{1/2}$, is applicable. The approximate solution for low electric fields can be obtained from Eq. (5) by expanding the erfc and the exponential functions around zero [for small z, $\operatorname{erfc} z \simeq 1-(2/\pi^{1/2})z$] and by neglecting the products proportional to E^n with $n > 1$. Since ΔT_p is proportional to the electric current density and thus to the electric field E, the linearization of Eq. (5) leads to the expression

$$k_{\text{eff}}=k_0\left[1+2\left(\frac{t}{\pi D_i}\right)^{1/2}\mu_i E-2\left(\frac{t}{\pi D_i}\right)^{1/2}\right.$$
$$\left.\times v(k_0-1)\right]+\left.\frac{\partial k_0}{\partial T}\right|_{T_0}\Delta T_p \quad (8)$$

or

$$k_{\text{eff}}/k_0 = 1+\Delta^E+\Delta^v+\Delta^T \quad (9)$$

where Δ^E, Δ^v, and Δ^T are the contributions of the electromigration of impurities of the growth velocity and of the Peltier effect, respectively.

$$\Delta^E=2\left(\frac{t}{\pi D_i}\right)^{1/2}\mu_i E; \quad \Delta^v=2\left(\frac{t}{\pi D_i}\right)^{1/2}v(1-k_0);$$
$$\Delta^T=\frac{1}{k_0}\left.\frac{\partial k_0}{\partial T}\right|_{T_0}\Delta T_p. \quad (10)$$

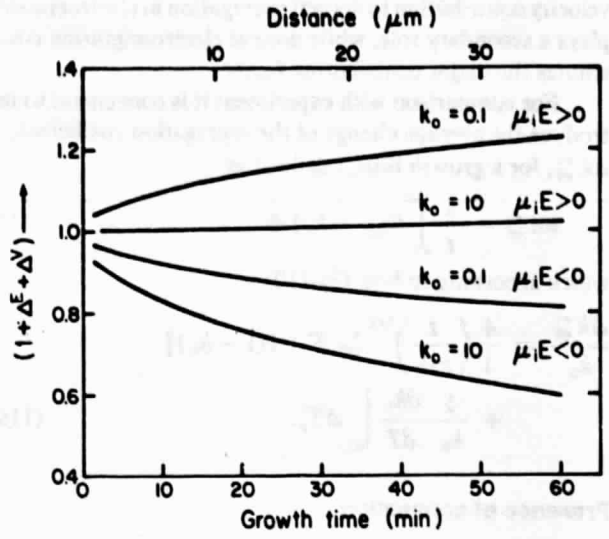

FIG. 1. Time dependence of the effective segregation coefficient k_{eff}/k_0 calculated from Eqs. (9) and (10) for electroepitaxial growth of GaAs from Ga-rich solution at 900 °C under conditions of negligible Peltier cooling at the interface ($\Delta T_p \simeq 0$). Dopant is electromigrating toward the substrate ($\mu_i E > 0$) or away from the substrate ($\mu_i E < 0$) with a velocity $|\mu_i E| = 10^{-5}$ cm/s. Other parameters used in calculations: $D_i = 10^{-5}$ cm^2/s, electromigration velocity of As; $\mu E = 1.3\times 10^{-5}$ cm/s, distance from the original growth interface is shown on the upper scale.

It is apparent that if $k_0 \gg 1$, the effect of growth velocity can be more significant than the effect of electromigration since the ratio of $|\Delta^E/\Delta^v|$ becomes very small (the depletion of the impurity at the interface due to segregation becomes large compared to the amount of impurity transported to the interface by electromigration). Similarly, if $k_0 < 1$, k_{eff} does not necessarily increase with growth velocity, as it does in thermal LPE, because the sign of the electromigration term, Δ^E, is independent of the value of k_0 but depends on the electromigration direction (i.e., it is positive if impurities migrate toward the growth interface and negative if they migrate away from the interface). Finally, the sign of the Peltier term, Δ^T, is determined by the direction of currrent flow (for a given conductivity type of substrate) and by the temperature dependence of the segregation coefficient.

The time dependence of $1+\Delta^E+\Delta^v$ calculated from Eqs. (9) and (10) is shown in Fig. 1 for electroepitaxial growth of GaAs from a Ga-rich solution at 900 °C and for a dopant electromigrating with a velocity $|\mu E| = 10^{-5}$ cm/s. It is seen that in both instances, i.e., $k_0 \ll 1$ and $k_0 \gg 1$, the value of $1+\Delta^E+\Delta^v$ is greater than unity (and thus k_{eff} is greater than k_0) when impurities electromigrate toward the interface ($\mu_i E > 0$), and it is smaller than 1 (k_{eff} smaller than k_0) when impurities electromigrate away from the interface. Such behavior can be generally expected in electroepitaxy unless the electromigration velocity is lower than $|v(k_0-1)|$ and/or when the thermal contribution Δ^T is significant. In most actual cases k_0 is less than unity and also v is expected to be much smaller than $\mu_i E$. (Note that v is typically one order of magnitude smaller than the electromigration velocity of the solute [see Eq. (3)]. Thus, the growth

velocity contribution to dopant segregation in electroepitaxy plays a secondary role, while dopant electromigration constitutes the major contributing factor.

For comparison with experiment it is convenient to introduce the average change of the segregation coefficient, $\Delta k_{\text{eff}}^{\text{av}}$, for a growth time, t defined as

$$\Delta k_{\text{eff}}^{\text{av}} = \frac{1}{t}\int_t^0 (k_{\text{eff}} - k_0)\, dt. \tag{11}$$

which according to Eqs. (8)–(10) is

$$\frac{\Delta k_{\text{eff}}^{\text{av}}}{k_0} = \frac{4}{3}\left(\frac{t}{\pi D_l}\right)^{1/2}[\mu_l E + v(1-k_0)] + \frac{1}{k_0}\frac{\partial k_0}{\partial T}\bigg|_{T_0}\Delta T_p. \tag{11a}$$

Presence of convection

The expression for steady-state segregation when convection is present in the solution can be obtained by solving Eq. (4) with a boundary condition of Eq. (4e) for time $t > \delta^2/D_l$. By following the procedure given in Ref. 5 it can be readily shown that

$$k_{\text{eff}} = k_0^1\left(1+\frac{\mu_l E}{v}\right)\left[k_0^1 + \left(1+\frac{\mu_l E}{v} - k_0^1\right) \times \exp\left(-\frac{(v+\mu_l E)\delta}{D_l}\right)\right]^{-1}. \tag{12}$$

when Peltier cooling is neglected $k_0^1 = k_0$, and Eq. (12) is the same as that originally derived in Ref. (5). In addition, if the impurities exhibit no mobility in an electric field ($\mu_l = 0$) Eq. (12) converts into the standard Burton-Prim-Slichter expression [19] for the effective segregation coefficient.

For a low electric field approximation, valid in metallic solutions as those presently being considered, Eq. (12) becomes:

$$k_{\text{eff}} = k_0\left(1 + \frac{\delta}{D_l}\mu_l E - \frac{\delta}{D_l}v(k_0-1)\right) + \frac{\partial k_0}{\partial T}\bigg|_{T_0}\Delta T_p. \tag{13}$$

It is seen that in Eq. (13) the impurity segregation coefficient can be expressed in a form similar to that of Eq. (9), appropriately modified to include the thickness of boundary layer thickness, δ.

The calculated dependence of k_{eff}/k_0 on the boundary layer thickness δ is shown in Fig. 2, for the same parameters as used in Fig. 1. It is seen that for larger δ of the direction of change in segregation coefficient is determined primarily by the sign of electromigration velocity $\mu_l E$. However, the magnitude of $\Delta^E + \Delta^v$ decreases with decreasing δ and thus for $\delta \to 0$ (strong convection) the Peltier term, Δ^T, which is indepndent of δ, becomes dominant.

General features of impurity segregation in electroepitaxy

The essential features of impurity segregation in electroepitaxy from metallic solutions can be summarized as follows: (a) The segregation behavior can be analyzed in terms of the additive contributions of electromigration, growth velocity, and change in interface temperature; these contributions depend linearly on the electric current. (b) The growth velocity component reflects a dependence of the segregation coefficient on growth velocity similar to that encountered in a standard segregation behavior. (c) Impurity electromigration leads to an increase or decrease of the segregation coefficient depending on the direction of electromigration rather than the sign of $(k_0 - 1)$. (d) In the absence of convection in the solution, the contributions of electromigration and growth velocity to k_{eff} depend on time as $t^{1/2}$; the Peltier contribution is independent of time. (e) The presence of convection leads to steady-state contributions from electromigration and growth velocity which are proportional to the boundary layer thickness, δ; the Peltier contribution is independent of δ; accordingly, with increasing convection (decreasing δ), the relative contribution of Peltier effect is enhanced.

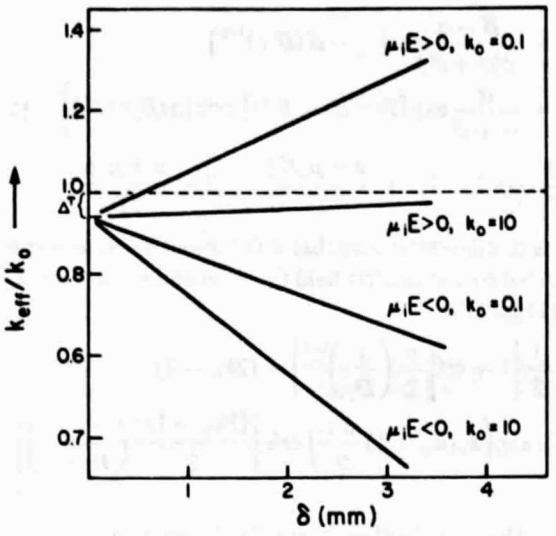

FIG. 2. Dependence of k_{eff}/k_0 on the boundary layer thickness, δ, calculated from Eq. (13) for electroepitaxial growth of GaAs from Ga-rich solution at 900 °C. ΔT_p was taken as -3 °C; $(1/k_0)(\partial k_0/\partial T) = 2\times 10^{-2}$. Other parameters are as in Fig. 1.

In the present treatment of impurity segregation in electroepitaxy from equilibrated solutions two types of transients were not considered; (a) the relatively fast transients associated with the establishment of a new interface temperature under the influence of the Peltier effect; typical time constants of these transients are of the order of 1 s; (b) the relatively slower transients (with time constants of the order of 1 min) during which the growth velocity relaxes to a value $v \simeq v_E^1$ (see Ref. 8). These cases require a numerical approach and they will not be pursued at present.

EXPERIMENTAL PROCEDURE

Electroepitaxial growth experiments were carried out from Sn-doped Ga-As solutions in a standard LPE apparatus (horizontal graphite boat) modified to permit passage of electric current through the solution-substrate interface as described elsewhere. [16]

The effect of electric current on changes in the impurity segregation coefficient was studied in the absence and in the presence of convection in the solution. Thus, growth was performed in a configuration in which convectional flow in the solution was either essentially eliminated as described in Ref. 16 or was intentionally introduced by superimposing a 2.5 °C/cm horizontal temperature gradient across the solution. The magnitude of convection was further varied by varying the solution height (Grashoff number). The value of the solute boundary layer thickness was obtained from an analysis of the growth velocity using the procedure described in Ref. 8.

Semi-insulating (at room temperature) Cr-doped substrates were used; their thickness ranged from 250 to 1500 μm. The desired value of the interfacial temperature decrease (due to Peltier cooling), for a given current, was obtained by selecting the proper thickness for the substrate. As reported in Ref. 8 varying the thickness of Cr-doped substrates from 250 μm to 1.5 mm, ΔT_p is varied from 0.5 to 3.0 °C for the same current density of 10 A/cm^2. In order to remove the As-depleted substrate surface formed during the heating cycle, the substrates were back-etched prior to growth by a 3 °C undersaturated solution.

The electronic characterization of the grown layers included the determination of carrier concentration on macroscale and microscale and the compensation ratio, $\theta = N_A/N_D$, where N_A and N_D are the concentration of the ionized acceptors and donors, respectively. The compensation ratio in LPE layers of GaAs ranges from 0.1 to 0.8. Sn introduces shallow donors and compensating deep acceptors with θ typically ~ 0.3 in layers grown at 700 °C.[20] Accordingly, for a reliable analysis of impurity segregation, knowledge of the θ values is required. In the present study, θ was determined by recently developed theoretical and experimental methods based on electron mobility and free carrier absorption.[21] When the electron concentration, n, and the compensation ratio, θ, are known, one can determine the concentration of ionized donors, N_D, and acceptors, N_A. Since

$$\theta = \frac{N_A}{N_D} \quad \text{and} \quad n = N_D - N_A, \tag{14a}$$

it is apparent that

$$N_D = \frac{n}{1-\theta} \quad \text{and} \quad N_A = n\frac{\theta}{1-\theta}. \tag{14b}$$

In nondegenerate material the value of N_D, given by expression (14b), can be used as the total concentration of donor impurities. In degenerate material ($n > 6\times 10^{17}$ cm^{-3}) a correction must be introduced accounting for the occupational statistics of impurity levels.

Charge carrier concentration profiles in the electroepitaxial layers perpendicular to the growth direction were determined by ir absorption scanning[22,23] which provides a spatial resolution of about 20 μm.

For the analysis of the Peltier effect contribution to the segregation coefficient, knowledge of the temperature dependence of k_0 is required. The values of k_0 for Sn were estimated from measurements on epitaxial layers grown thermally (no electromigration involved) by ramp cooling from a temperature of $T_0 + 2.5$ °C to a temperature of $T_0 - 2.5$ °C. The cooling rate was varied betwen 0.1 and 3 °C/min; this rate was found to have no effect on the segregation coefficient during thermal growth.[12] The values of k_0 obtained for different temperatures were used to determine $(1/k_0)(dk/dT)$ which at 900 °C was estimated to be $+0.01$ °C^{-1} (at 900 °C k_0 was aout 5×10^{-4}).

In the analysis of the experimental data the average value of the effective segregation coefficient will be used for donor-type impurities:

$$\frac{\Delta k_{\text{eff}}^{\text{av}}}{k_0} = \frac{k_{\text{eff}}^{\text{av}}}{k_0} - 1 = \frac{N_D(J)}{N_D(J=0)} - 1, \tag{15}$$

where $N_D(J)$ and $N_D(J=0)$ are the average donor concentration in an electroepitaxially grown layer and in a thermally grown layer, respectively. (J denotes the current density).

RESULTS AND DISCUSSION

Absence of convection

It was found that the carrier concentration in the electroepitaxial layers, grown from solutions in which convection was essentially eliminated, was very uniform in the direction normal to the growth direction. Typical electron concentration profiles obtained by ir scanning are shown in Fig. 3. The layers were grown from 3.5% Sn-doped solution at 950 °C with current densities of 15 and 50 A/cm^2, applied for a period of 30 min. Except for the layer edges (not shown in Fig. 3) the electron concentration in the growth plane does not change by more than 1%.

The effect of current density on the change of the average segregation coefficient is shown in Fig. 4. Growth was carried out for 20 min from 2.5% Sn-doped solutions at 900 °C. Two substrate thicknesses were used, 300 and 1000 μm; the corresponding values of ΔT_p were -2.5 and -8 °C, respectively, for 40 A/cm^2. It is seen that the segregation coefficient increases linearly with current density. For the thicker substrate, the values of $\Delta k_{\text{eff}}^{\text{av}}/k_0$ are slightly lower due to the higher contribution from Peltier cooling [last term in Eq. (11)]. However, the difference between the

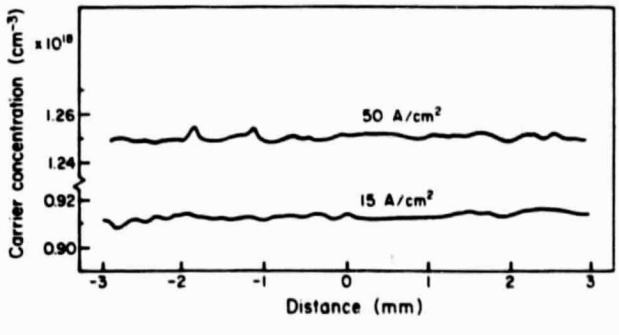

FIG. 3. Electron concentration profile perpendicular to the growth direction for Sn-doped electroepitaxial layers (see text).

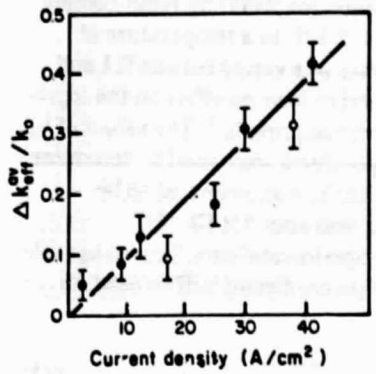

FIG. 4. Relative change of the effective segregation coefficient $\Delta k_{\text{eff}}^{\text{av}}/k_0$ versus current density for Sn-doped layers grown electroepitaxially at 900 °C in the absence of convection on Cr-doped substrates 300 μm thick (▼) and 1000 μm thick (▽), respectively (corresponding values of ΔT_p were − 2.5 and − 8 °C). Growth was carried out for 20 min.

results obtained with thick and thin substrates (in spite of the difference in ΔT_p) is rather minor, which indicates that segregation is controlled by impurity electromigration and the growth velocity.

The electroepitaxial growth velocity contribution to the results of Fig. 4 estimated from expression (11) does not exceed 15%. It is thus apparent that the observed segregation coefficient changes induced by the electric current are due to electromigration of Sn in the solution. The increase of segregation coefficient indicates that electromigration of Sn is directed toward the positive polarity of the substrate, which is consistent with reported electrotransport direction of Sn in liquid gallium.[15,24] Using expression (11) a value of $1/D_l^{1/2}[\mu_l E + v(1-k_0)] \simeq 3.8\times10^{-3}\,\text{s}^{-1/2}$ is obtained from the slope of the line of Fig. 4 for a current density of 10 A/cm^2.

The experimental results of the dependence of the average segregation coefficient on time are given in Fig. 5. Growth was performed with a current density of 30 A/cm^2 and with substrates of 300 μm thickness. Other experimental conditions were identical to those employed in the experiments of Fig. 4. Using the value of $1/D_l^{1/2}[\mu_l E + v(1-k_0)] \simeq 3.8\times10^{-3}\,\text{s}^{-1/2}$ (as determined above) the theoretical dependence of $\Delta k_{\text{eff}}^{\text{av}}/k_0$ on time was calculated from expresssion (11). The calculated curve is shown in Fig. 5. It is seen that the theoretical behavior is in good agreement with experiment.

On the basis of the above results it is apparent that the dependence of the effective distribution coefficient on current density for constant growth time as well as the dependence of the effective distribution coefficient on time for constant current density are quantitatively accounted for by the present model of segregation in electroepitaxy. It is also apparent that the electric current effect on Sn segregation in the GaAs : Ga-As solution system is due almost entirely to Sn electromigration.

Presence of convection

The electroepitaxial layers grown in the presence of convection were found to exhibit a pronounced variation in electron concentration in the direction perpendicular to the growth direction. Typical results obtained with ir scanning are shown in Fig. 6. The layers were grown at 950 °C with a current density of 30 A/cm^2 from 3.5% Sn-doped solutions; the solution heights were 0.6 and 1.2 cm, and the substrates were 300 μm thick.

For relatively small convectional flow (0.6 cm solution height) the variation in impurity concentration across the layer is about 10% and increases to 20% with increasing convectional flow (1.2 cm solution height). These changes reflect an increase in the variation of the solute boundary layer thickness along the substrate with increasing convectional flow in the solution. It has been reported earlier that

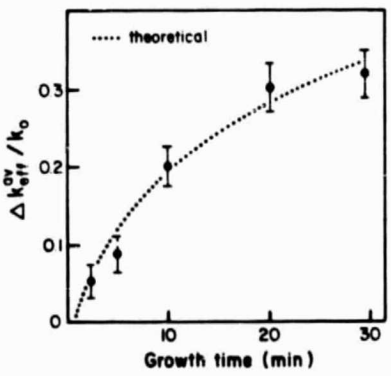

FIG. 5. Growth time dependence of the relative change in segregation coefficient $k_{\text{eff}}^{\text{av}}/k_0$ for layers electroepitaxially grown with current density 30 A/cm^2 in the absence of convection. The substrate thickness was 300 μm; other parameters the same as in Fig. 4. Dotted line is calculated from Eq. (11) (see text).

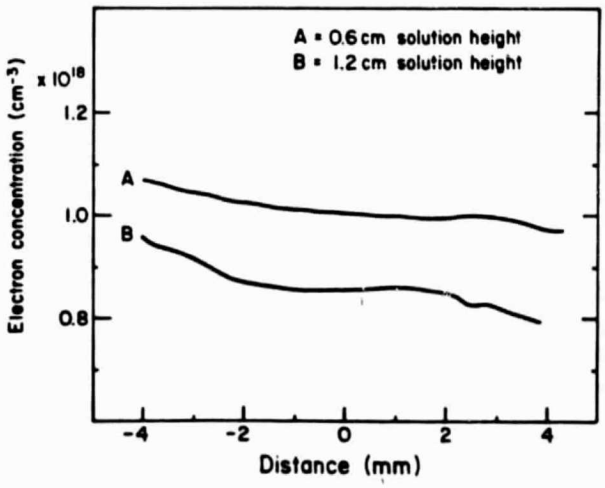

FIG. 6. Electron concentration profile of electroepitaxial layers grown in the presence of convection. The layers were grown a 950 °C with a current density of 30 A/cm^2. Cr-doped substrates were used with a thickness of 300 μm.

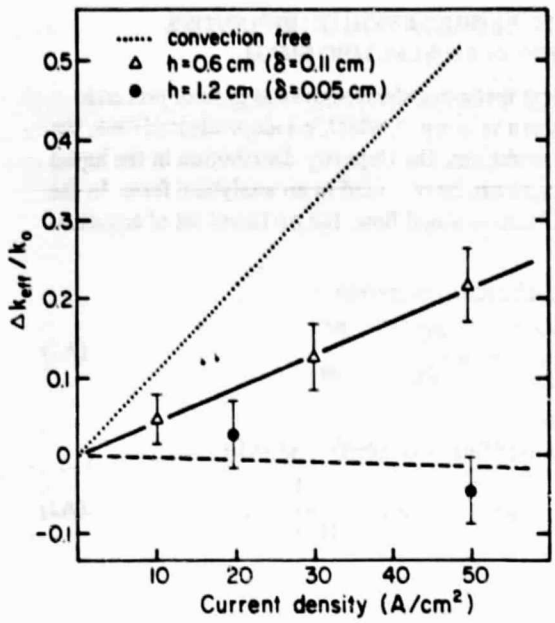

FIG. 7. Change in Sn segregation coefficient $\Delta k_{eff}/k_0$ as a function of current density in the presence of convection (see text).

variations in solute-boundary layer thickness can also lead to variations in the thickness of the grown layers. [16]

The experimental results of the steady-state segregation coefficient as a function of current density are shown in Fig. 7 for two values of solution height, 0.6 and 1.2 cm; the corresponding values of δ, as estimted from the growth velocity, are 0.11 and 0.05 cm, respectively. Growth was performed on 1.5-mm-thick substrates at 900 °C from 2.5% Sn-doped solutions. For comparison, the changes of the average segregation coefficient obtained under convection-free conditions is also shown in Fig. 7.

Thus, consistent with the theoretical model, the magnitude of segregation coefficient changes in electroepitaxy is noticeably reduced in the presence of convection. It should also be noted that with increasing convection (decreasing δ) the current-induced change of the segregation coefficient becomes negative (Fig. 5). Such behavior is readily understood in the light of expression (13): The contribution from electromigration and from growth velocity decreases with decreasing δ, to the extent that the thermal contribution Δ^T becomes dominant. However, Δ^T is negative ($\Delta T_p < 0$).

From Eq. (13) and the experimental data of Fig. 7, $\mu_i E/D_i$ can be obtained. Thus, considering that $(1/k_0)(\partial k/\partial T) \simeq 10^{-2}$ 1/ C, $\Delta T_p/J \simeq 0.3$ C/A cm^2; $\delta = 0.11$ and 0.05 cm, the value of $\mu_i E/D_i|_{10\ A/cm^2} \simeq 0.6$ cm^{-1} is obtained from the slopes of the two curves of Fig. 7.

This value, together with the parameters determined earlier, yields $D_i \simeq 4 \times 10^{-5}$ cm^2/s and $\mu_i E|_{10\ A/cm^2} \simeq 2.3 \times 10^{-5}$ cm/s for Sn in Ga-As solution. Both values seem quite reasonable.

The effect of increasing convection flow on the changes of the segregation coefficient is shown in Fig. 8. The layers were grown under constant current density (40 A/cm^2) on 300-μm-thick substrates ($\Delta T_p = -3$ °C) at 900 °C from 2.5% Sn-doped solution with heights ranging from 0.3 to 1.2 cm, corresponding to a range of δ from 2.0 to 0.5 mm. The dotted line represents the dependence calculated from the theoretical model [Eq. (13)] using parameters as determined above. The contribution of the Peltier effect ot the segregation coefficient changes is small, compared with the contribution of electromigration. However, the effect of electromigration decreases (consistent with theory) with the decreasing thickness of the solute-boundary layer (increasing convection in the solution); thus, for sufficiently large solution heights a change in the sign of Δk_{eff} is observed (see also Fig. 9).

The effect of Peltier cooling on the changes of the segregation coefficient in the presence of strong convection in the solution is shown in Fig. 9. Growth was performed at 900 °C with a current density of 40 A/cm^2 from 2.5% Sn-doped solution with a height of 1.2 cm ($\delta \simeq 0.05$ cm) on substrates with thicknesses ranging from 200 m to 1.5 mm, corresponding to a range of ΔT_p values from -2 to -13 °C. As predicted from the model, for small values of ΔT_p, the change of the segregation coefficient is controlled by electromigration, but with increasing substrate thickness (ΔT_p) the contribution of the Peltier effect becomes comparable to that of electromigration; for thick substrates (> 1 mm) the Peltier effect becomes dominant and leads to a change in the sign of Δk_{eff}.

SUMMARY

Dopant segregation in liquid-phase electroepitaxy was investigated employing GaAs epitaxial layers grown from Sn-doped Ga-As solutions over a broad range of experimental conditions. The results were analyzed on the basis of a

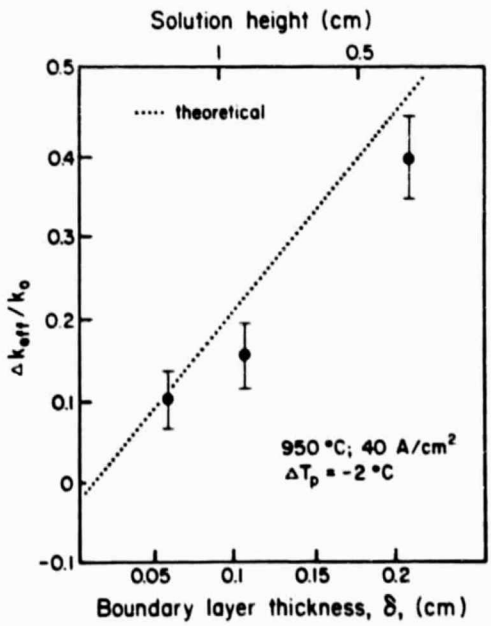

FIG. 8. The change in Sn segregation coefficient $\Delta k_{eff}/k_0$ versus boundary layer thickness, δ, for layer grown under a current density of 40 A/cm^2. Points are experimental, dotted line is calculated from Eq. (13) (see text).

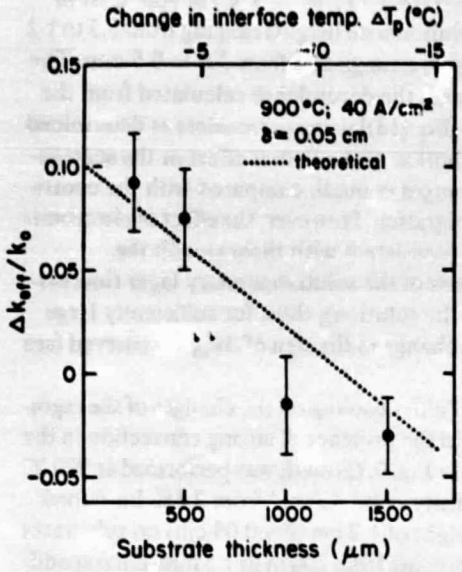

FIG. 9. Change in Sn segregation coefficient $\Delta k_{eff}/k_o$ versus thickness of substrate (or change in interface temperature, ΔT_p, caused by Peltier effect) for layer growth in the presence of convection.

theoretical model which relates quantitatively the dopant segregation coefficient and growth parameters such as temperature, convection flow in the solution, and current density or growth velocity. In the theoretical analysis dopant transport in the liquid phase by diffusion as well as by electromigration was taken into consideration.

Consistent with the theoretical model it was found that, in the absence of convection in the liquid, the effective segregation coefficient of Sn increases with increasing current density and also increases with increasing time (for constant current density). This behavior is encountered when the electromigration term is positive, i.e., when electromigration of the dopant proceeds toward the growth interface. The effective distribution coefficient decreases with increasing current density if the electromigration term is negative.

In the presence of convection, the effective segregation coefficient decreases with increasing magnitude of convective flow (as assessed by the height of the solution) for a constant current density even below the value of the equilibrium segregation coefficient. Since, in the presence of convection, the contribution of the Peltier effect to the growth process becomes significant, and since Peltier cooling increases with increasing substrate thickness, the value of the effective segregation coefficient depends on the substrate thickness for a constant current density and solution height.

From the epitaxial data the diffusion coefficient and the electromigration velocity of Sn in Ga-As solution at 900 °C were determined on the basis of the theoretical model. The values obtained were $D = 4\times10^{-5}\,\mathrm{cm^2/s}$ and $\mu E\,|_{10\ \mathrm{A/cm^2}} \simeq 2\times10^{-5}$ cm/s.

ACKNOWLEDGMENTS

The authors are grateful to the National Aeronautics and Space Administration for financial support and to Professor August F. Witt for valuable discussions.

APPENDIX: SEGREGATION OF IMPURITIES MIGRATING IN AN ELECTRIC FIELD

In most instances electroepitaxial growth proceeds with a growth velocity, v, which is independent of time. Under such conditions, the impurity distribution in the liquid phase $C_i(x,t)$ can be obtained in an analytical form. In the absence of convectional flow, the pertinent set of equations becomes:

diffusion and electromigration

$$D_i \frac{\partial^2 C_i}{\partial x^2} + u\frac{\partial C_i}{\partial x} = \frac{\partial C_i}{\partial t}, \tag{A1}$$

where $u = v + \mu_i E$;
conservaton of fluxes at interface ($x = 0$)

$$vC_{is} - uC_i\Big|_{x=0} = D_i \frac{\partial C_i}{\partial x}\Big|_{x=0}; \tag{A2}$$

boundary conditions:

$$C_i = C_{io} \quad \text{for } t = 0$$

and

$$C_i = C_{io} \quad \text{for } x = \infty \text{ for any } t. \tag{A3}$$

By introducing a quantity C^* defined as

$$C^* = C_i \exp\left(\frac{u}{2D_i}x + \frac{u^2}{4D_i}t\right), \tag{A4}$$

Eq. (A1) reduces to a standard diffusion equation

$$D_i \frac{\partial^2 C^*}{\partial x^2} = \frac{\partial C^*}{\partial t} \tag{A5}$$

and the equation of fluxes becomes

$$RC^*|_{x=0} = D_i \frac{\partial C^*}{\partial x}\Big|_0 \tag{A6}$$

where

$$R = (k_0 - 1)v + \frac{v - \mu_i E}{2}. \tag{A7}$$

and

$$k_0 \equiv C_{is}/C_i\,|_{x=0}.$$

Equation (A5) will be solved using the Laplace transform method. The Laplace transform of C^* is

$$\bar{C}^* = \int_0^\infty \exp(-pt)C^*\,dt. \tag{A8}$$

Multiplying both sides of Eq. (A5) by $\exp(-pt)$ and integrating over time one obtains

$$D_i \frac{\partial^2}{\partial x^2}\int_0^\infty \exp(-pt)C^*\,dt = \exp(-pt)C^*\,|_0^\infty + p\int_0^\infty \exp(-pt)C^*\,dt. \tag{A9}$$

However, $\exp(-pt)C^*$ vanishes for $t = \infty$ and for $t = 0$ it equals $C_{io}\exp[(u/2D_i)x]$. Thus (A9) leads to

$$D_i \frac{\partial^2 \bar{C}^*}{\partial x^2} = p\bar{C}^* - C_{io}\exp\left(\frac{u}{2D_i}x\right). \tag{A10}$$

Similarly, the equation of fluxes (A6) becomes

$$D_i \frac{\partial \bar{C}^*}{\partial x}\Big|_{x=0} = R\bar{C}^*\Big|_{x=0}. \tag{A11}$$

The solution of Eq. (A10) is

$$\bar{C}^* = A \exp[-(p/D_i)^{1/2}x] + \frac{C_{io}\exp(u/2D_i)x}{p - u^2/4D_i} \tag{A12}$$

where the constant A is obtained from the boundary condition (A11)

$$A = \frac{C_{io}(u-2R)}{2D_i^2} \frac{1}{(p/D_i - \beta^2)[\alpha + (p/D_i)^{1/2}]}, \tag{A13}$$

where $\alpha = R/D_i$ and $\beta = u/2D_i$. Thus

$$\bar{C}^* = \frac{C_{io}(u-2R)\exp[-(p/D_i)^{1/2}x]}{2D_i^2(p/D_i - \beta^2)(\alpha + (p/D_i)^{1/2})} + \frac{C_{io}\exp(\beta x)}{D_i(p/D_i - \beta^2)}. \tag{A14}$$

Expansion of Eq. (A14) in partial fractions leads to

$$\bar{C}^* = \frac{C_{i0}(u-2R)(D_i)^{1/2}}{2D_i^2}\left(\frac{1}{2(\alpha+\beta)\beta}\frac{\exp[-(p/D_i)^{1/2}x]}{(p^{1/2} - \beta D_i^{1/2})} + \frac{1}{2\beta(\beta-\alpha)}\frac{\exp[-(p/D_i)^{1/2}x]}{p^{1/2} + \beta(D_i)^{1/2}} + \frac{1}{\alpha^2 - \beta^2}\frac{\exp[-(p/D_i)^{1/2}x]}{p^{1/2} + \alpha(D_i)^{1/2}}\right) + C_{i0}\frac{\exp[-(ux/2D_i)]}{(p - \beta^2 D_i)}. \tag{A15}$$

For all components of Eq. (A15) the inversions of Laplace transforms are readily obtainable.[25] Using the tabulated forms of the inversions of corresponding Laplace transforms and the relation (A4) one obtains from Eq. (A15) the solution for the impurity distribution $C_i(x,t)$ as follows:

$$C_i(x,t) = C_{i0}\left[1 - \frac{1}{2}\operatorname{erfc}\left(\frac{x}{2(D_i t)^{1/2}} + \beta(D_i t)^{1/2}\right) + \frac{(\beta-\alpha)\exp(-2x\beta)}{2(\alpha+\beta)} \times \operatorname{erfc}\left(\frac{x}{2(D_i t)^{1/2}} - \beta(D_i t)^{1/2}\right) + \frac{\alpha}{\alpha+\beta}\exp[x(\alpha-\beta) + D_i t(\alpha^2 - \beta^2)] \times \operatorname{erfc}\left(\frac{x}{2(D_i t)^{1/2}} + \alpha(D_i t)^{1/2}\right)\right]. \tag{A16}$$

The effective segregation coefficient k_{eff} and the interface segregation coefficient, k_0 are defined as

$$k_{\text{eff}} = \frac{C_{is}}{C_{i0}} \quad \text{and} \quad k_0 = \frac{C_{is}}{C_i(0,t)}. \tag{A17}$$

Thus taking Eq. (A16) for $x = 0$ and multiplying both sides by $k_0 k_{\text{eff}}/C_{is}$ one obtains

$$k_{\text{eff}} = k_0\left(1 - \tfrac{1}{2}\operatorname{erfc}[\beta(D_i t)^{1/2}] + \frac{\beta-\alpha}{2(\alpha+\beta)}\operatorname{erfc}[-\beta(D_i t)^{1/2}] + \frac{\alpha}{\alpha+\beta}\exp[D_i t(\alpha^2 - \beta^2)]\operatorname{erfc}[\alpha(D_i t)^{1/2}]\right). \tag{A18}$$

Equation (A18) describes the segregation behavior for isothermal electroepitaxial growth at equilibrium temperature T_0. If, due to the current flow, the interface temperature changes (Peltier effect) by ΔT_p, the interface segregation coefficient k_0 in Eq. (A18) be replaced by $k_0^1 = k_0 + \partial k_0/\partial T|_{T_0}\Delta T_p$.

[1] A.F. Joffe, Zh. Tekh. Fiz. 26, 478 (1956).
[2] W.G. Pfann, K.E. Benson, and J.H. Wernick, Electron. Control 2, 597 (1957).
[3] S.E. Bresler and G.E. Pikus, Zh. Tekh. Fiz. 26, 109 (1956); 28, 2282 (1958).
[4] J. Angus, D.V. Ragone, and E.E. Hucke, Metall. Soc. Conf. (Proc.) 8, 833 (1961).
[5] W.G. Pfann and R.S. Wagner, Trans. Metall. Soc. AIME 224, 1139 (1962).
[6] L. Gold, Jpn. J. Appl. Phys. 2, 131 (1963).
[7] M. Kumagawa, A.F. Witt, M. Lichtensteiger, and H.C. Gatos, J. Electrochem. Soc. 120, 583 (1973); L.V. Golubyev, T.V. Pakhomova, O.A. Khatchatunian and Y.V. Shmouvtzev, Proc. IV Nat. Conf. on Crystal Growth; Yerevan, 1972, Izdatielstuo Armenskoy Ak. Nauk. Vol. 1 p. 164 (in Russian).
[8] L. Jastrzebski, J. Lagowski, H.C. Gatos, and A.F. Witt, J. Appl. Phys. 49, 5909 (1978). The derivation given in Appendix A contains errors which are corrected in an erratum. However, the expressions for electroepitaxial growth velocity in metallic solutions [Eqs. (10) and (11) in Ref. 8] which appear in the present paper are correct.
[9] G.M. Blom, J.J. Daniele, T. Kyros, and A.F. Witt, J. Electrochem. Soc. 122, 1541 (1975).
[10] D.J. Lawrence and L.F. Eastman, J. Cryst. Growth 30, 267 (1957); J. Electron. Mater. 6, 1 (1976).
[11] L. Jastrzebski and H.C. Gatos, J. Cryst. Growth 42, 309 (1977).
[12] L. Jastrzebski and H.C. Gatos, Inst. Phys. Conf. Ser. B 33, 88 (1976).
[13] Y. Imamura, L. Jastrzebski and H.C. Gatos, J. Electrochem. Soc. (to be published).
[14] M.B. Small and J.F. Barnes, J. Cryst. Growth 5, 9 (1969); D.L. Rode, J. Cryst. Growth 20, 13 (1973).
[15] See for example, J.N. Pratt and R.G.R. Sellors, *Electrotransport in Metals*, (Trans. Tech. SA, Riehen, Switzerland, 1973), and references quoted therein.
[16] L. Jastrzebski, Y. Imamura, and H.C. Gatos, J. Electrochem. Soc. 125, 1140 (1978).
[17] V.G. Smith, W.A. Tiller, and J.W. Rutter, Can. J. Phys. 33, 723 (1955).
[18] L. Jastrzebski, H.C. Gatos, and A.F. Witt, J. Electrochem. Soc. 124, 633 (1977).
[19] J.A. Burton, R.C. Prim, and W.P. Slichter, J. Chem. Phys. 21, 1987 (1953).
[20] See for example, H. Kressel, J. Electron. Mater. 3, 747 (1974) and references quoted therin.
[21] W. Walukiewicz, J. Lagowski, M. Lichtensteiger, and H.C. Gatos, J. Appl. Phys. 50, 899 (1979).
[22] D.L. Spears and A.J. Strauss, Solid State Res. Rep. 3, 9 (1974).
[23] L. Jastrzebski, J. Lagowski, and H.C. Gatos, J. Electrochem. Soc. 126, 260 (1979).
[24] V.A. Mikhaylov, R.A. Polovinkina, S.I. Drakin, and G.M. Fredova, Phys. Met. Metallogr. 22, 63 (1966).
[25] See, for example, *Tables of Integral Transforms*, edited by A. Erdelyi (McGraw-Hill, New York, 1954), Vol. 1, Chap. V.

Electroepitaxy of multicomponent systems: ternary and quarternary compounds

T. Bryskiewicz,[a] J. Lagowski, and H. C. Gatos
Department of Materials Science and Engineering, Massachusetts Institute of Technology, Cambridge, Massachusetts 02139

(Received 8 June 1979; accepted for publication 21 September 1979)

A theoretical model is presented which accounts for the electroepitaxial growth kinetics and composition of multicomponent compounds in terms of mass transport in the liquid and phase diagram relationships. The mass transport in the interface is dominated by electromigration in the absence of convection and by diffusion in the presence of convection. The composition of the solid is controlled by the Peltier effect at the growth interface and by the diffusion and mobility constants of the solute components and the growth velocity (current density). Thus, for a given solution composition, the composition of the solid can be varied by varying the current density. For a given current density the composition remains constant even in the case of relatively thick epitaxial layers. All aspects of the model were found to be in good agreement with the growth and composition characteristics of $Ga_{x-1}Al_xAs$ layers.

PACS numbers: 61.50.Ci, 81.15.Lm, 64.75. + g, 71.25.Tn

I. INTRODUCTION

Electroepitaxy represents a novel approach to liquid phase epitaxy (LPE) of semiconductor compounds in which growth is achieved by passing an electric current through the substrate solution interface while the overall temperature of the system is maintained constant.[1]

The feasibility of achieving precise control of the crystal growth process by simply controlling the current density has stimulated extensive experimental and theoretical studies of electroepitaxy.[2-6]

In recent theoretical investigations of binary systems a model of the growth kinetics[5] and impurity segregation[6] has been developed. This model defines the contribution of the Peltier effect at the solid-solution interface and that of solute electromigration to the overall growth process. Thus, it has been shown that electromigration of solute species to the growth interface is the primary means of mass transport required for supersaturation and continued growth; the contribution of electromigration to growth is dominant in the absence of significant convection in the liquid. The presence of convection in the solution enhances the contribution of the Peltier effect (cooling or heating at the growth interface) which otherwise is of importance only in the initial stages of growth. The primary reason for this enhancement is the formation of a boundary layer (at the interface) with pronounced concentration gradients which increase mass transport by diffusion.

The presence of electromigration and of the Peltier effect render electroepitaxial growth sensitive to the direction and density of the electric current, to the electrical resistivity of the solution, to the conductivity type (n or p) of the substrate, and to the thickness of the substrate; as has been shown,[5] these parameters provide a high flexibility in controlling and studying the growth process which is unattainable in standard LPE.

Electroepitaxial growth of multicomponent systems (i.e., $Ga_{1-x}Al_xAs$), with a remarkable stabilization of the composition in the direction of growth and improved properties of related optoelectronic structures, has been reported[7-9]; however, these studies, by and large, are of an empirical nature. Yet multicomponent systems play a key role in optoelectronic device structures, and their technology relies exclusively on epitaxial growth. Standard LPE provides only limited flexibility in controlling the microscopic growth velocity; thus, precise control of the composition of ternary and quarternary compound layers is still a problem.

In the present study it is shown that the same phenomena which dominate the electroepitaxial growth of binary compounds are also of fundamental importance in the growth of ternary and quarternary semiconductor compounds. Thus, a theoretical electroepitaxial growth model of multicomponent systems is developed based on electromigration in the solution and the Peltier effect at the growth interface. Quantitative relationships are derived for the dependence of the growth velocity and the composition of the layers on the current density and other growth parameters. The model is successfully used for the analysis of experimental results on the electroepitaxial growth of $Ga_{1-x}Al_xAs$.

II. MASS TRANSPORT MODEL

A. Processes and phase diagram relationships

Electric current flow through the substrate (seed) in contact with a liquid solution of its components leads to a change ΔT_p at the interface temperature due to the Peltier effect; ΔT_p is proportional to the current density and also depends on substrate characteristics such as the Peltier coefficient, thickness, and thermal conductance. In addition, the electric current flow leads to an electric field E in the solution, which is also proportional to the current density; this field causes electromigration of the species in the solutions with a velocity μE, where μ is the effective mobility. In gallium liquid solutions, nearly all solutes migrate under an electric field toward the anode.[10] If the substrate has a posi-

[a] Permanent address: Institute of Physics, Polish Academy of Sciences, Warsaw, Poland.

 0021-8979/80/020988-09$01.10

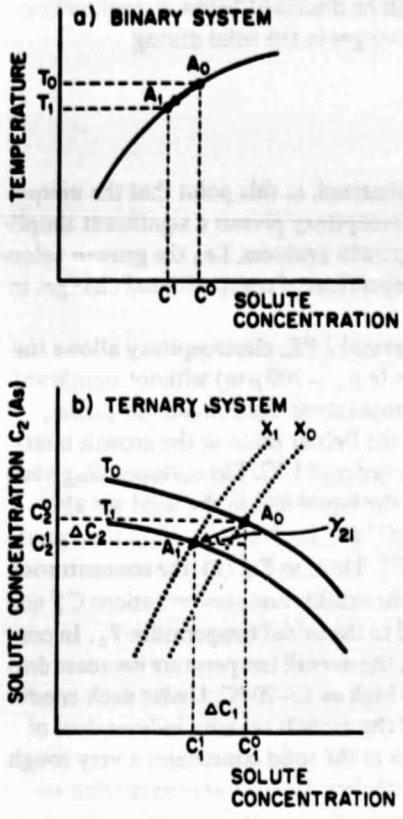

FIG. 1. Schematic representation of the pertinent part of the phase diagram of a (a) binary and a (b) ternary system and transitions involved in electroepitaxial growth; x_0 and x_1 are the solidus lines (see text).

tive polarity, electromigration provides an effective means of solute transport to the substrate leading to supersaturation and continued growth. It is thus apparent that electric current affects two key factors in epitaxial growth, i.e., the interface temperature and solute transport.

The above two factors have been modeled[5] quantitatively in the electroepitaxial growth of binary compounds utilizing the widely accepted treatment of isothermal transport in LPE.[11,12] Considering the binary phase diagram in Fig. 1(a), electroepitaxial growth is approximated as a transition from point A_0 (which is defined by the original equilibrium temperature T_0 and solute concentration C^0) to point A_1 on the liquidus which is uniquely determined by the new interface temperature $T_1 = T_0 + \Delta T_p$ (ΔT_p is negative when $T_1 < T_0$) and defines a new solute concentration C^1 at the interface. The solid composition of a binary compound is known, by definition, and thus the growth velocity can be obtained by solving the solute transport equations which in electroepitaxial growth are modified by including a current-dependent electromigration transport term. The basic assumption made here is that growth proceeds under thermal quasieqilibrium, i.e., the transition $A_0 \rightarrow A_1$ follows the liquidus line; the validity of this assumption in electroepitaxial growth has been experimentally verified.[5]

LPE of multicomponent systems (e.g., ternary and quarternary compounds) is more complex than that of binary ones. Consider, for example, a ternary compound $Ga_{1-x}Al_xAs$ in equilibrium with the (Ga-rich) Ga-Al-As solution. For a given temperature (e.g., T_0) the concentration of the two solutes As and Al is not fixed (more degrees of freedom than in binary compounds), but can vary along the corresponding liquidus isotherm (T_0) as illustrated in Fig. 1(b). The requirement that the solution be in equilibrium with a solid of a given composition x_0 defines the equilibrium solute concentration C_1^0 and C_2^0, and thus the starting point A_0.

If solution A_0 [Fig. 1(b)] is thermally equilibrated at T_0 and the interface temperature is decreased to T_1, the growth point A_1 (in contrast to the case of a binary compound) is not uniquely defined but lies somewhere on the new liquidus isotherm T_1, depending on the composition x_1 of the growing solid. In order to determine the growth path $A_0 \rightarrow A_1$ and, thus, ΔC_1, ΔC_2, and the new solid composition x_1, an additional quantity must be introduced such as the differential growth path function, $\gamma \equiv \Delta C_2 / \Delta C_1$. It is apparent that the ratio $\Delta C_2 / \Delta C_1$ (at the growth interface) will depend on the rates at which the solutes are transported to the growth interface. In thermal LPE, these rates are determined by the diffusion process. In electroepitaxy they depend also on the electromigration properties of the two solutes.

In the present treatment the differential growth path functions are obtained through a consistent treatment of the solute transport (diffusion and electromigration) to the interface and the phase diagram (liquidus and solidus isotherms) relationships. As in the case of the binary system,[5] here also a thermal quasiequilibrium approximation at the growth interface will be used.

Since the Peltier effect-induced changes of the interface temperature are small[13] (of the order of 1 °C) the corresponding compositional changes of the solution are also small (i.e., $|\Delta C_i| \ll C_i^0$). Accordingly, the quasiequilibrium approximation of the growth transition $A^0 \rightarrow A_1$ can be expressed in a differential form:

$$\Delta T = \frac{\partial T}{\partial C_1}\Delta C_1 + \frac{\partial T}{\partial C_2}\Delta C_2 + \cdots + \frac{\partial T}{\partial C_{n-1}}\Delta C_{n-1} \quad (1)$$

or

$$\Delta T = \sum_{i=1}^{n-1} \alpha_i \Delta C_i, \quad (2)$$

where $\alpha_i \equiv \partial T / \partial C_i|_{C_i = C_i^0, T_0}$ are the liquidus slope components ΔC_i is the change in concentration of a given solute component at the interface, n is the number of elements in the compound, and in the liquid phase the solvent concentration is C and the solute concentrations are C_i, where $i = 1,\ldots,n-1$. It is apparent that the change of the solvent concentration is determined by the changes of the solute concentrations, i.e., $\Delta C = -\sum_{i=1}^{n-1} \Delta C_i$. Thus, in formulating mass transport in the solution only the solute components need to be taken into account, or only $n-1$ elements.

B. Solute transport

Assuming a dilute solution, the transport of each solute component can be treated independently. Thus, the transport equation for thermal LPE [14] modified to include the electromigration term is expressed as

$$D_i \frac{\partial^2 C_i}{\partial z_2} + v \frac{\partial C_i}{\partial z} + \mu_i E \frac{\partial C_i}{\partial z} = \frac{\partial C_i}{\partial t}$$
$$\text{for } i = 1,\ldots,n-1, \quad (3)$$

where z is the distance from the advancing growth interface, D_i is the diffusion constant, v is the growth velocity, μ is the mobility, and t is the time. The sign of $\mu_i E$ depends on the direction of current flow and is taken positive when the solute species electromigrates toward the growth interface (for convenience, the convention used here for the sign of μE is opposite to that used in Ref. 5).

The boundary conditions for solute concentration are as follows:

at $t = 0$

$$C_i = C_i^0 \quad \text{for } \textit{all } z, \quad (4a)$$

at $t > 0$

$$C_i = C_i^0 \quad \text{for } z = \infty \text{ (absence of convection)}, \quad (4b)$$

or at $t > 0$

$$C_i = C_i^0 \quad \text{for } z > \delta \text{ (presence of convection)}, \quad (4c)$$

(δ is the solute boundary layer thickness), and at $t > 0$ and $z = 0$,

$$C_i = C_i^1, \quad (4d)$$

(superscript 1 denotes values at the interface).

Flux conservation at the interface requires that

$$vC_i^1 = D_i \frac{\partial C_i}{\partial z}\Big|_{z=0} + (v + \mu_i E) C_i^1, \quad (5)$$

where C_i^1 is the concentration in the solid.

Neglecting the term $v(\partial C_i/\partial z)$ in Eq. (3) as very small in comparison with the electromigration and the diffusion terms,[5] the solution of Eq. (3) for conditions defined by Eqs. (4) is (see Ref. 5)

$$D_i \frac{\partial C_i}{\partial z}\Big|_{z=0} = -\Delta C_i \left(\frac{D_i}{\pi t}\right)^{1/2} f_i, \quad (6)$$

where $f_i(E,\delta,t)$ is similar to the function $f_k(E,\delta,t)$ defined in Ref. 5.

In the low electric field approximation $[\mu_i E \ll 2(D_i/t)^{1/2}]$ which is valid for metallic solutions such as those presently considered, the function f_i reduces to

$$f_i = 1 \quad \text{in the absence of convection} \quad (7a)$$

$$f_i = (\pi D_i t)^{1/2}/\delta \quad \text{in the presence of convection.} \quad (7b)$$

From Eqs. (5) and (6) one obtains ΔC_i, and substituting the resulting expression for ΔC_i into Eq. (2), one obtains for the growth velocity

$$v = -\frac{\Delta T_0}{(\pi t)^{1/2}} \left(\sum_{i=1}^{n-1} \frac{\alpha_i (C_i^1 - C_i^1)}{(D_i)^{1/2} f_i}\right)^{-1} + \left(E \sum_{i=1}^{n-1} \frac{\mu_i \alpha_i C_i^1}{(D_i)^{1/2} f_i}\right)\left(\sum_{i=1}^{n-1} \frac{\alpha_i (C_i^1 - C_i^1)}{(D_i)^{1/2} f_i}\right)^{-1}. \quad (8)$$

In general, since C_i^1 and C_i^1 in Eq. (8) are not known, a complete treatment of the problem must involve the growth path function $\gamma_{kl} = \Delta C_k/\Delta C_l$ (for components k and l) and the solidus relationships. Expressions for γ_{kl} can be readily obtained, and they will be discussed below in conjunction with compositional changes in the solid during electroepitaxy.

C. Growth velocity

It should be emphasized, at this point that the unique characteristics of electroepitaxy permit a significant simplication of the crystal growth problem, i.e., the growth velocity can be treated independent of compositional changes in the solid.

In contrast to thermal LPE, electroepitaxy allows the growth of thick layers (e.g., $\sim 100\,\mu$m) without significant change in interface temperature. As pointed out earlier, ΔT_p, associated with the Peltier effect at the growth interface, is typically of the order of 1 °C. The coresponding compositional changes in the liquid and in the solid are also small, and ΔC_i^1 and ΔC_i^1 are much smaller than the equilibrium values C_i^{10} and C_i^0. Thus, in Eq. (8), the concentration can be substituted by the equilibrium concentrations C_i^{10} and C_i^0, which correspond to the initial temperature T_0. In contrast, in thermal LPE, the overall temperature decrease during growth is often as high as 15–20 °C. Under such conditions the treatment of the growth velocity independent of compositional changes in the solid constitutes a very rough approximation. Nevertheless, such an approximation reduces the extent of numerical calculations and is often used in thermal LPE.[15]

In the low electric field approximation, the electroepitaxial growth velocity, in the absence of convection is

$$v \simeq -\frac{\Delta T_0}{(\pi t)^{1/2}} \left(\sum_{i=1}^{n-1} \frac{\alpha_i (C_i^{10} - C_i^0)}{(D_i)^{1/2}}\right)^{-1} + \left(E \sum_{i=1}^{n-1} \frac{\mu_i \alpha_i C_i^0}{(D_i)^{1/2}}\right)\left(\sum_{i=1}^{n-1} \frac{\alpha_i (C_i^{10} - C_i^0)}{(D_i)^{1/2}}\right)^{-1}, \quad (9a)$$

and in the presence of convection it is

$$v \simeq -\frac{\Delta T_p}{\delta} \left(\sum_{i=1}^{n-1} \frac{\alpha_i (C_i^{10} - C_i^0)}{D_i}\right)^{-1} + \left(E \sum_{i=1}^{n-1} \frac{\mu_i \alpha_i C_i^0}{D_i}\right)\left(\sum_{i=1}^{n-1} \frac{\alpha_i (C_i^{10} - C_i^0)}{D_i}\right)^{-1}. \quad (9b)$$

It is apparent that for $n = 2$, Eqs. (9a) and (9b) become identical to those derived for the electroepitaxial growth velocity of binary systems[5]; if, in addition, $\mu_i = 0$, they, then reduce to the standard LPE expressions for diffusion-controlled growth of a binary compound.[11,12] It is of interest to note that for $\mu_i = 0$ *or* $E = 0$ (no electromigration), and $\Delta T_p \equiv \Delta T$, Eqs. (9a) and (9b) become

$$v = -\frac{\Delta T}{(\pi t)^{1/2}} \left(\sum_{i=1}^{n-1} \frac{\alpha_i (C_i^{10} - C_i^0)}{(D_i)^{1/2}}\right)^{-1} \quad (10a)$$

and

$$v = \frac{\Delta T}{\delta} \left(\sum_{i=1}^{n-1} \frac{\alpha_i (C_i^{10} - C_i^0)}{D_i}\right)^{-1}. \quad (10b)$$

They represent generalized expressions for standard thermal LPE growth velocity of multicomponent systems. They can be used in conjunction with step-cooling thermal growth of

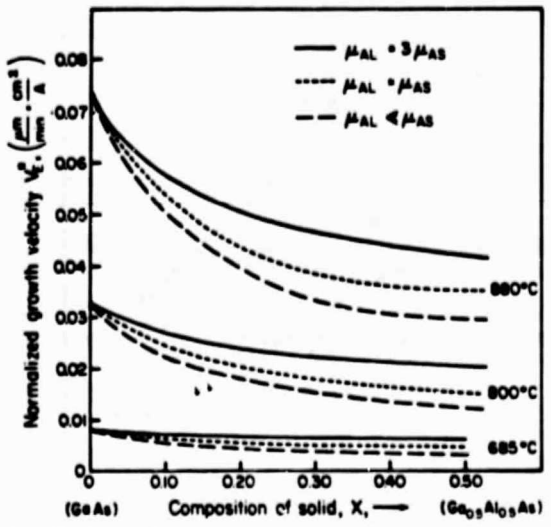

FIG. 2. Electromigration contribution to growth velocity of $Ga_{1-x}Al_xAs$ v_E^0 per unit current density calculated from Eq. (9a), taking $D_{Al} = D_{As} = 5\times10^{-5}$ cm^2/s and $\mu_{As}E/J = 1.1\times10^{-4}$ (cm/s)(A/cm^2)$^{-1}$.

ternary or quarternary compounds provided that ΔT is reasonably low (of the order of 1 °C).

The first terms in Eqs. (9a) and (9b) define the Peltier contribution v_T to the growth velocity, while the second terms define the contribution from electromigration v_E. Both terms are proportional to the electric current density J (through ΔT_p and E, respectively, as pointed out above). In the absence of convection, the Peltier contribution v_T decreases with time, while the electromigration term v_E is independent of time. Thus, the Peltier contribution is of significance during the initial stages of growth. When prolonged electroepitaxial growth is performed on thin substrates (of the order of (0.1 mm), the electroepitaxial growth velocity is dominated by the electromigration term v_E. The presence of convection in the solution enhances the contribution from the Peltier effect, which is proportional to $1/\delta$.

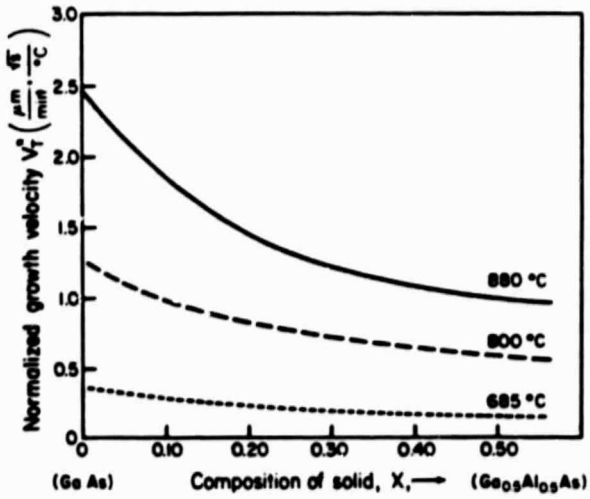

FIG. 3. The Peltier effect contribution to electroepitaxial growth velocity of $Ga_{1-x}Al_xAs$ v_T^0 (see text), calculated from Eq. (9a), taking $D_{As} = 5\times10^{-5}$ cm^2/s and $D_{Al} = 3D_{As}$.

D. $Ga_{1-x}Al_xAs$

In order to calculate the electroepitaxial growth velocity in ternary or quarternary compounds, knowledge of such parameters as the diffusion constants D_i, the mobilities μ_i, and the resistivity of the solution is required. These parameters are not known even for the most commonly used compounds. For this reason, the discussion of Eqs. (9a) and (9b) will be limited primarily to the role of the phase diagram, using $Ga_{1-x}Al_xAs$ as an example.[16]

The electromigration growth velocity v_E, normalized with respect to the electric current density, is given in Fig. 2 as a function of the solid composition x for different growth temperatures. In these calculations the diffusion constant of Al is taken equal to the diffusion constant of As in Ga-rich solutions; the mobilities of As and Al are assigned relative values. It is seen that the electromigration growth velocity decreases with increasing Al concentration and decreases with decreasing temperature.

It is also seen in Fig. 2 that for the assumed Al mobility, equal to that of As, the growth velocity of $Ga_{1-x}Al_xAs$ is smaller than in the case of pure GaAs. This fact is primarily due to the decrease of the As solubility in the liquid when Al is present; it clearly indicates that the Al cannot be treated as an impurity even when the concentration ratio C_{Al}/C_{As} in the solution is of the order of 10^{-2}.

The contribution of the Peltier effect to the growth velocity [Eq. (9a)], normalized with respect to time and Peltier cooling (i.e., $v_T t^{1/2}/\Delta T_p$), is plotted in Fig. 3 as a function of x. Here also there are marked differences between binary and ternary compounds.

It should be noted that the Peltier-induced change of the interface temperature ΔT_p is determined primarily by the properties of the substrate (GaAs in the present case). The contribution of the solution to ΔT_p seldom exceeds 10%. In the present case, ΔT_p, corresponding to a given current density, substrate thickness, and electron (hole) concentration, can be determined from the experimental data given in Ref. 5.

An unusual feature of electroepitaxy is that growth can be carried out even in the presence of Peltier heating at the

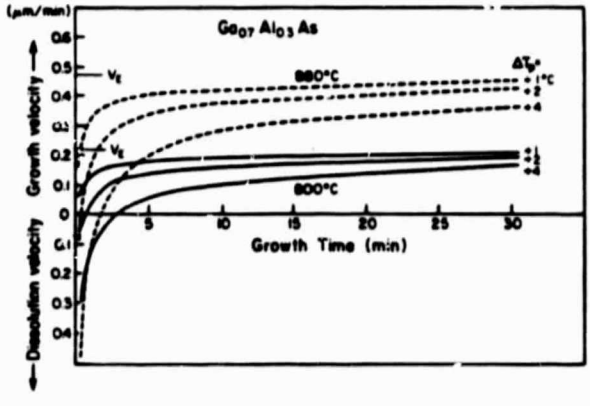

FIG. 4. Total electroepitaxial growth velocity of $Ga_{0.7}Al_{0.3}As$ versus growth time for different values of the Peltier heating ($\Delta T_p > 0$) at the interface. The parameters used in calculations were $D_{Al} = 3D_{As}$, $\mu_{Al} = \mu_{As}$, $D_{As} = 5\times10^{-5}$ cm^2/s, and $\mu_{As}E/J = 1.1\times10^{-4}$ (cm/s)(A/cm^2)$^{-1}$.

interface (ΔT_p positive). This feature is illustrated in Fig. 4 where the growth velocity of $Ga_{1-x}Al_xAs$, calculated from Eq. (9b), is plotted as a function of time. Such behavior can be realized for $Ga_{1-x}Al_xAs$ by utilizing thin p-type GaAs substrates and "plus" polarity on the substrate.

It should be noted that the calculations shown in Figs. 2 and 3 can be very readily extended to the evaluation of the electroepitaxial growth velocity of $Ga_{1-x}Al_xAs$ in the presence of convection, where a boundary layer of thickness δ is present. The required modification are apparent from Eqs. (9a) and (9b); this case will not be discussed further.

$$\gamma_{kl} = \left(\frac{D_l}{D_k}\right)^p \frac{C_k^s - (1+\mu_k E/v)\,C_k}{C_l^s - (1+\mu_l E/v)\,C_l}, \tag{11}$$

where $p = \frac{1}{2}$ or 1 in the absence and in the presence of convection, respectively.

By denoting one specific solute component by C_1, one obtains from Eq. (2)

$$\Delta T_p = \Delta C_1 \sum_{i=1}^{n-1} \alpha_i \gamma_{i1}. \tag{12}$$

Utilizing the common notation $A_{1-x}C_xB_yD_{1-y}$ for the solid phase of the compound (for ternary compound y or x equals 1) and introducing differential segregation coefficients $k_i^x = \partial x/\partial C_i|_{C_i = C_{i0}, T_0}$ and $k_i^y = \partial y/\partial C_i|_{C_i = C_{i0}, T_0}$, the change of solid composition due to small changes of solute concentrations ΔC_i becomes

$$\Delta x = \sum_{i=1}^{n-1} k_i^x \Delta C_i, \quad \Delta y = \sum_{i=1}^{n-1} k_i^y \Delta C_i. \tag{13}$$

From this expression, the definition of γ_{kl}, and Eq. (11), one obtains

$$\frac{\Delta x}{\Delta T_p} = \left(\sum_{i=1}^{n-1} k_i^x \gamma_{i1}^0\right)\left(\sum_{i=1}^{n-1} \alpha_i \gamma_{i1}^0\right)^{-1} \tag{14a}$$

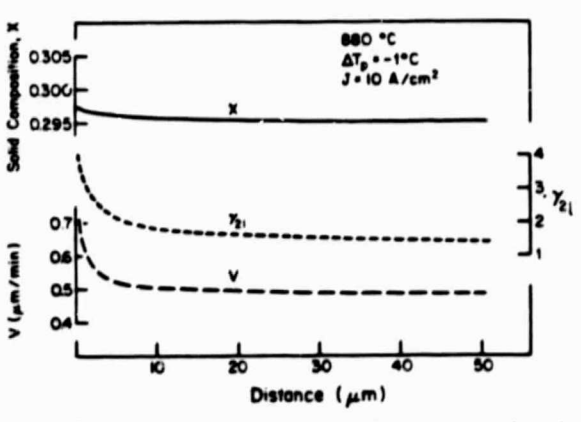

FIG. 5. The microscopic values of the aluminum concentration x in $Ga_{1-x}Al_xAs$, the differential growth path function γ_{21}, and the growth velocity calculated versus distance. The initial temperature $T_0 = 880$ °C, the Peltier-induced change in interface temperature $\Delta T_p = -1$ °C, and current density $J = 10$ A/cm^2. Other parameters are the same as in Fig. 4.

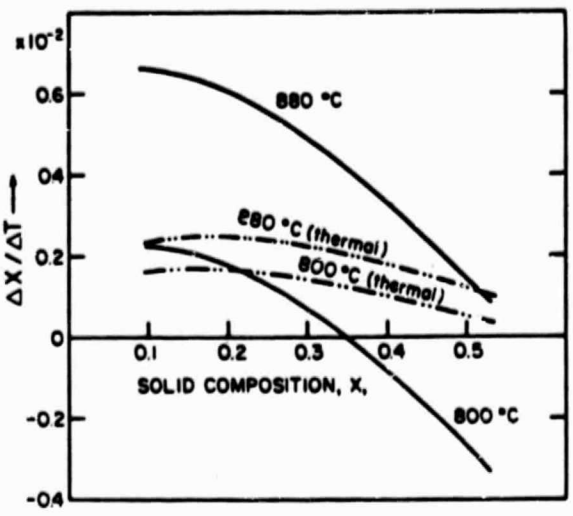

FIG. 6. $\Delta x/\Delta T$ versus solid composition x of $Ga_{1-x}Al_xAs$ calculated from the present model for electroepitaxial growth (solid lines) and thermal growth by step cooling (broken lines). For electroepitaxial growth the Peltier effect contribution to the average growth velocity was taken as $v_J = 0.25v_E$. Other parameters are $D_{Al} = 3D_{As}$, $\mu_{Al} = 3\mu_{As}$, $D_{As} = 5\times10^{-5}$ cm^2/s, and $\mu_{As}E/J = 1.1\times10^{-6}$ (cm/s)(A/cm^2)$^{-1}$.

and

$$\frac{\Delta y}{\Delta T_p} = \left(\sum_{i=1}^{n-1} k_i^y \gamma_{i1}^0\right)\left(\sum_{i=1}^{n-1} \alpha_i \gamma_{i1}^0\right)^{-1}, \tag{14b}$$

where γ_{i1}^0 [Eq. (11)] is taken at the initial equilibrium point [A^0 in Fig. (1b)], where $T = T_0$, $C_i^s \simeq C_i^{s0}$, and $C_i \simeq C_i^0$. For the reference solute component C_1, it is convenient to select the element characterized by the largest differential segregation coefficient k_i (e.g., Al in the case of $Ga_{1-x}Al_xAs$).

Equations (14a) and (14b), together with Eqs. (9a), (9b), and (10), describe the composition, growth path, and growth velocity in electroepitaxial growth of multicomponent semiconductors.

It is of interest to note that in the low mobility limit $\mu_i \to 0$, Eq. (10) reduces to the simpler form,

$$\gamma_{kl} = \left(\frac{D_l}{D_k}\right)^p \frac{C_k^s - C_k}{C_l^s - C_l} \simeq \left(\frac{D_l}{D_k}\right)^p \frac{C_k^s}{C_l^s}, \tag{15}$$

which describes the differential growth path function in thermal LPE (in most instances convection is negligible and $p = \frac{1}{2}$). This growth path function is independent of the growth velocity. It is always positive and in most LPE cases its value is determined by the composition of the solid; usually $(D_l/D_k)^{1/2}$ is a weak function of the relative concentrations in the solution. It is thus evident that in diffusion-limited thermal LPE, control of the composition during growth is primarily limited to the control of the cooling rate $\Delta T(t)$.

In electroepitaxy, on the other hand, the differential growth path functions depend on the solute electromigration and the growth velocity [Eq. (11)]. The ratio of the electromigration velocity to growth velocity is typically about 10, and thus, the solute concentrations C_k and/or C_l also contribute to the value of γ_{kl}. Another unique feature of

electroepitaxy is that the differential growth path functions can be varied by varying the conductivity type (n or p) and the thickness of the substrate. The overall electroepitaxial growth velocity v is the sum of the Peltier effect and electromigration contributions; the magnitude and the sign of Peltier effect contribution can be varied by varying the substrate parameters. Utilizing Eqs. (9a), (11), and (14), the solid composition x was calculated as a function of distance from the original interface using parameters corresponding to $Ga_{1-x}Al_xAs$ growth from Ga-rich solutions, and the results are shown in Fig. 5, together with corresponding values of the microscopic growth velocity v and the differential growth path function γ_{21}. It is seen that electroepitaxial growth leads to a remarkable stabilization of the solid composition. Thus, in electroepitaxy, it becomes feasible to obtain thick layers with very small compositional gradients in the growth direction. It should be noted that this finding is in contrast to the originally proposed advantages of current-controlled growth, whereby the composition of the solid (dopant concentration) could be varied (concentration gradients) by varying the current density.[17]

The composition stabilizing effect illustrated in Fig. 5 indicates that an electroepitaxial layer grown from a solution equilibrated at temperatures T_0 with a solid composition x_0 will exhibit essentially a constant composition $x = x_0 + \Delta T_\rho (\Delta x/\Delta T)_{T_0}$, where ΔT_ρ is determined by the Peltier effect at the interface (it is a linear function of the electric current density and depends on the thickness, conductivity, and conductivity type of the substrate), whereas $(\Delta x/\Delta T)_{T_0}$ can be obtained from Eqs. (9), (11), and (14). The values of $(\Delta x/\Delta T)_{T_0}$ corresponding to electroepitaxial growth of $Ga_{1-x}Al_xAs$ in the absence of convection are given in Fig. 6 as a function of solid composition for two values of the initial temperature T_0. For comparison $(\Delta x/\Delta T)_{T_0}$ in thermal LPE, obtained from Eq. (15), is also shown.

It is seen that the value of $\Delta x/\Delta T$ and, thus, the magnitude of the current-induced change in solid composition increases with increasing temperature and also increases with decreasing x. Thus, the optimum conditions for observing compositional changes as a function of current density can be defined as $T_0 \simeq 880$ °C and solid composition 0.1 –0.2. At $T_0 = 800$ °C, and for solid compositions of 0.3–0.4, $\Delta x/\Delta T$ is 10^{-3} °C^{-1}, or less. The low magnitude of $\Delta x/\Delta T$ explains why in previous electroepitaxy experiments performed with low current density (<30 A/cm^2), the current-induced changes in the composition of $Ga_{1-x}Al_xAs$ could not be consistently resolved.[6-9]

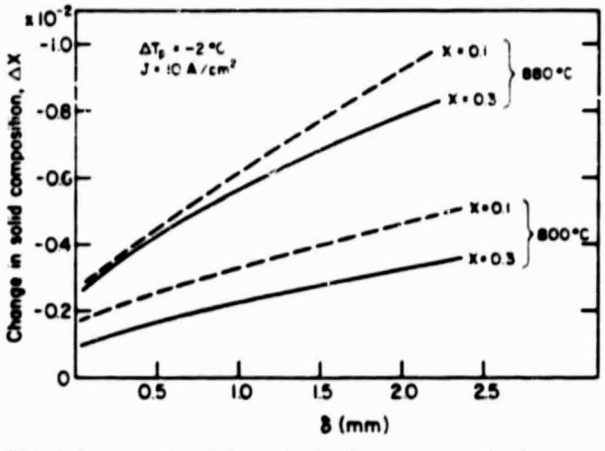

FIG. 7. Current-induced change in aluminum concentration in $Ga_{1-x}Al_xAs$ for electroepitaxial growth in the presence of convection in the solution, calculated from the present (see text) as a function of the boundary layer thickness δ. Diffusion constants and mobilities ar ethe same as in Fig. 6.

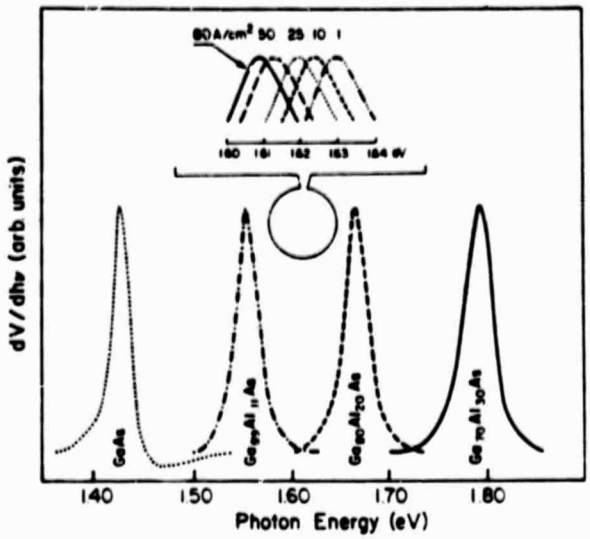

FIG. 8. First-derivative photovoltage peaks of bandgap transitions in $Ga_{1-x}Al_xAs$. In the upper portion of this figure the peaks are shown in an expanded energy scale for electroepitaxial layers grown with different current density.

It is also seen in Fig. 6 that not only the magnitude, but also the sign of $\Delta x/\Delta T$ depends on the initial growth conditions. Thus, for relatively low growth temperature, $\Delta x/\Delta T$ can be positive in a region of low aluminum concentration and negative for higher values of x. This behavior clearly illustrates the significance of the phase diagram relationships in current-induced compositional changes of $Ga_{1-x}Al_xAs$.

In Fig. 7, the current-induced compositional changes of $Ga_{1-x}Al_xAs$ are presented for electroepitaxial growth in the presence of convection leading to a boundary layer thickness δ. It is seen that the value of Δx decreases with decreasing δ and decreasing growth temperature T_0. Thus, when growth is performed at relatively low temperatures and under pronounced convection in the liquid, the effect of the electric current on solid composition can be below the limit of experimental detection.

In summary, it is seen from the present model that in electroepitaxy, the solid composition x can be increased or decreased since the sign ΔT_ρ can be changed without impairing the growth process. For certain solute composition and solute mobility ranges, the sign of $\Delta x/\Delta T$ can also be reversed. This flexibility of changing the growth path in electroepitaxy by selecting the growth parameters, e.g., the conductivity type of the substrate, n or p, (which are of no consequence in the thermal LPE) renders electroepitaxy particularly promising for studying the growth process.

III. EXPERIMENTAL

Electroepitaxial growth experiments were carried out with Ga-rich Ga-Al-As solutions in a standard LPE apparatus (horizontal graphite boat) modified to permit passage of electric current through the solution-substrate interface.[18] The effect of current density on the growth velocity and on the solid composition was studied in a growth configuration in which convectional flow in the solution was essentially eliminated.[18] Preliminary experiments were also carried out in a configuration where convection was intentionally introduced by superimposing a horizontal temperature gradient across the solution. The layers grown in such configuration exhibited noticeable compositional inhomogeneities along the growth plane and were found unsuitable for a meaningful analysis in terms of the theoretical model.

The initial growth conditions, i.e., temperature T_0 and composition of solution C_1^0, were selected so that (a) high current-induced relative changes or aluminum content in the solid, $\Delta x/x_0$, could be obtained, (b) knowledge of the phase diagram was assured, and (c) sufficient amounts of Al and As were present in the solution for the growth of layers about 20 μm thick without noticeable depletion of Al and As in the solution. Accordingly, experiments were performed at $T_0 = 870$ °C, from a Ga-rich solution containing 2 g of Ga, 1.47 mg of Al, and equilibrated with GaAs ($C_{Al}^0 \simeq 1.6\times10^{-3}$, $C_{As}^0 \simeq 4\times10^{-2}$). Current densities up to 80 A/cm^2 were employed. In order to keep the total current at a level not exceeding 25 A (to avoid Joule heating in various parts of the growth system[18]), layers of only 0.5 cm in diameter were grown.

For the verification of the electroepitaxy model, very precise measurements of compositional changes are required. In $Ga_{1-x}Al_xAs$, for small values of x, the energy gap increases linearly with x and thus changes of energy gap provide a sensitive measure of Δx. In the present study, derivative photovoltage spectroscopy[19] was employed to determine the energy gap transitions. For the analysis of the transitions in the vicinity of the energy gap, the photovoltage generated on a MOS structure or on a Schottky barrier can be used. The advantage of the derivative (wavelength modulated) technique in comparison to a standard photovoltage threshold measurement (as used, e.g., in Ref. 20) is that it permits a direct and a far more accurate determination of the energy gap changes. These advantages are apparent from Fig. 8 in which typical first-derivative spectra obtained with Schottky barriers are given for $Ga_{1-x}Al_xAs$ with different compositions. As shown in Fig. 8, the resolution of this approach is sufficiently accurate for the determination of the current-induced changes of the energy gap (and thus of the composition) in electroepitaxially grown layers.

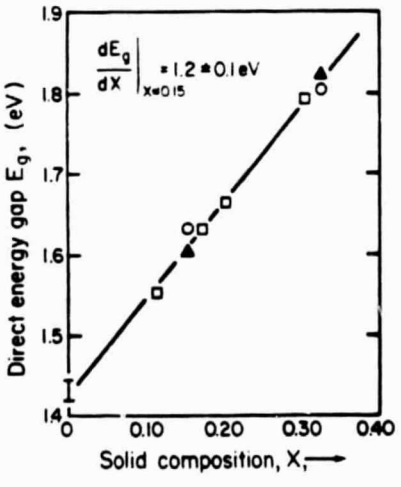

FIG. 9. Energy gap of $Ga_{1-x}Al_xAs$ versus solid composition x. □ indicates the present results, ▲ is from Ref. 20, ○ is from Ref. 21; and I is from Ref. 19.

In addition to derivative photovoltage spectroscopy, electron microprobe and Auger analysis, combined with ion milling, were employed for the compositional study of the electroepitaxial layers.

The results obtained on the energy gap as a function of composition (determined by electron microprobe analysis) are shown in Fig. 9, together with corresponding literature data.[20,21] Note that dE_g/dx, determined from Fig. 9, is 1.2 ± 0.1 eV. This value is used for the precise determination of current-induced compositional changes in $Ga_{1-x}Al_xAs$ from the small changes in the energy position of the first-derivative photovoltage peak. The electron microprobe itself could not be used for such measurements since a typical error in microporbe measurements of x was about 0.01.

IV. RESULTS AND DISCUSSION

A. Growth velocity

The experimental results on the electroepitaxial growth velocity of $Ga_{1-x}Al_xAs$ as a function of electric current density is shown in Fig. 10; current density was the only parameter varied in these experiments. All experimental points correspond to the same initial composition of the solution, the same initial temperature ($T_0 = 870$ °C) of the system, and the same substrate characteristics, i.e., (100) orientation, 500 μm thick, n-type, Si doped with electron concentration $n = 1\times10^{18}$ cm^{-3}, at room temperature. Peltier effect-induced change in interface temperature per unit current density $\Delta T_p/J$ was found to be about -5×10^{-2} °C cm^2/A. The results of Fig. 10 correspond to the average growth velocity v_{av}, defined as $v_{av} = d/t$, where d is the layer thickness and t is the growth time. The variation of growth thickness in the growth plane (typically ± 10%) is responsible for experimental errors, which are marked with vertical bars.

For a quantitative analysis of the results of Fig. 10 in terms of the theoretical growth velocity expressions, it should be noted that

$$v_{av} = \frac{1}{t}\int_0^t v\,dt = 2v_T + v_E\,, \tag{16}$$

where v_T and v_E are given by the first and second term, respectively, on the right-hand side of Eq. (9a). The calculated average growth velocity as a function of current density is represented by the dashed line in Fig. 10. A very good agreement between theory and experiment is obtained by taking the diffusion and mobility constants of Al about three times greater than those of As. The diffusion constant of Al in the

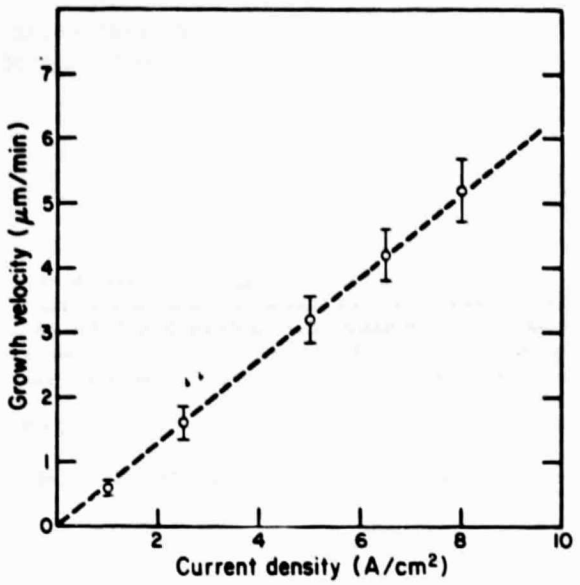

FIG. 10. The average electroepitaxial growth velocity of $Ga_{1-x}Al_xAs$ as a function of current density. Points indicate experimental and lines were calculated from Eq. (16) (see text).

Ga-rich solution is not available in the literature. However, it has been suggested, in conjunction with thermal growth of $Ga_{1-x}Al_xAs$, that it should be greater than the diffusion constant of As.[22,23] Other parameters, i.e., $\mu_{As}E/J$ and D_{As}, used in the growth velocity calculations, are 1.1×10^{-6} $[(cm/s)/(A/cm^2)]^{-1}$ and 5×10^{-5} cm^2/s, respectively; they are essentially the same as those previously reported for binary Ga-As solutions.[5,24,25]

In the context of the compositional analysis discussed below, it should be noted that the value of $\mu_{As}E/v$ obtained from the results of Fig. 10 is 10 ± 2. It is also of interest to note that the Peltier effect contribution to the average growth velocity (i.e., $2v_T$) of $Ga_{1-x}Al_xAs$ was about 25%. This finding is consistent with the general characteristics of electroepitaxial growth kinetics in the absence of convection in the solution, whereby growth is expected to be dominated by solute electromigration.

B. Composition

Electroepitaxially grown $Ga_{1-x}Al_xAs$ layers were found to be highly homogeneous along the growth direction. Electron microprobe compositional profiles taken on surfaces cleaved perpendicular to the growth plane, derivative photovoltage measurements (combined with chemical etching), and Auger microprofiles combined with argon-ion milling showed that macroscopic or microscopic compositional changes across the layer thickness did not exceed $\Delta x/x_{av}\approx3\%$. It should be noted that similar results have been reported in previous electroepitaxial experiments with $Ga_{1-x}Al_xAs$.[7]

This remarkable stabilization of composition in the growth direction is in excellent agreement with the present theoretical model of electroepitaxy (see Fig. 6 and related discussion in Sec. III.), and it is readily explained considering that the major factors affecting the solid composition, i.e., interface temperature and growth velocity, are essentially constant during electroepitaxial growth carried out under constant electric current density. The interface temperature is determined by the Peltier effect ΔT_p, while the growth velocity is controlled by the electromigration term v_E, which is independent of time.

Experimental results on the composition of electroepitaxial growth of $Ga_{1-x}Al_xAs$ as a function of current density are shown in Fig. 11. The experimental points correspond to the layers which have been analyzed with respect to growth velocity in Fig. 10. It is seen that the Al content in the electroepitaxial layers decreases with increasing current density, in agreement with the present theoretical model. The energy gap for a given layer was determined with derivative photovoltage spectroscopy using the value of $dE_g/dx = 1.2\pm0.1$ eV (see Fig. 9). This procedure may involve some uncertainty in the determination of the absolute value of x; however, the composition changes Δx as a function of current density are determined with an error comparable to the error of dE_g/dx, i.e., better than 10%. This error is much smaller than the sum of other experimental errors such as those associated with the preparation of the solution, the measurements of T_0, and the determination of the energy position of the derivative photovoltage peak.

For a quantitative analysis of the results given in Fig. 11, it is convenient to rewrite Eq. (14a) for $Ga_{1-x}Al_xAs$ in an explicit form:

$$\Delta x = \Delta T_p\,(k_1^x + k_2^x\gamma_{21})/(\alpha_1 + \alpha_2\gamma_{21}), \qquad (17)$$

where the suffixes 1 and 2 refer to Al and As, respectively. For the substrate employed here, $|\Delta T_p|$ per unit current density is 5×10^{-2} C/A cm^2. Accordingly, $\Delta x/\Delta T_p$, corre-

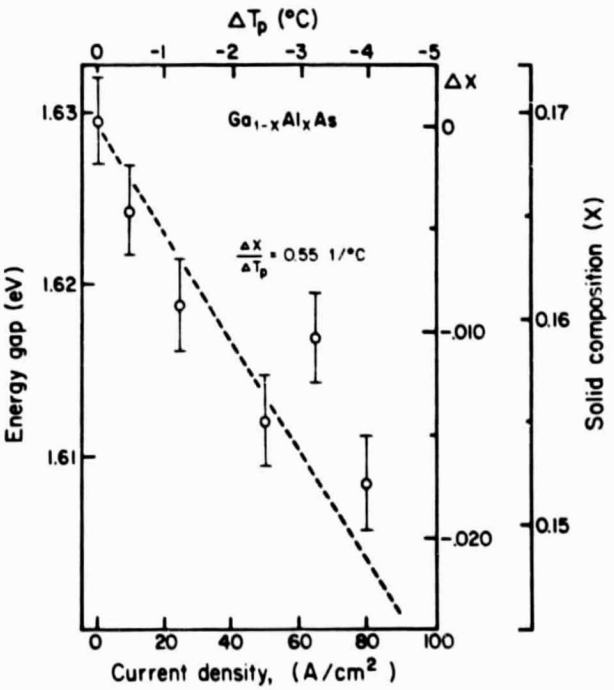

FIG. 11. The energy gap and corresponding compositional changes of electroepitaxially grown $Ga_{1-x}Al_xAs$ as a function of current density (lower horizontal scale) and of Peltier effect-induced change in interface temperature ΔT_p (upper scale).

sponding to the dotted line in Fig. 11, is 0.55 ± 0.15 l/°C. Utilizing the phase diagram relationships[16] of $Ga_{1-x}Al_xAs$ and the above value of $\Delta x/\Delta T_\rho$, one obtains from Eq. (16) $\gamma_{21} = 3.2 \pm 1$, which, according to Eq. (10), yields $\mu_{As}E/v = 8 \pm 2$, taking $D_{Al}/D_{As} = 3$ and $\mu_{Al}/\mu_{As} = 3$, as in the growth velocity analysis. Thus, it is evident that the current-induced compositional changes and the growth velocity characteristics are satisfactorily accounted for on the basis of the present model utilizing a consistent set of parameters (mobilities and diffusion constants) and the phase diagram data.

V. SUMMARY

A theoretical model of electroepitaxial growth of multicomponent semiconductor compounds was developed. It is based on diffusion, as well as electromigration mass transport in the liquid, and on phase diagram relationships. Mass transport by electromigration is dominant in the absence of convection, whereas in the presence of convection the contribution of diffusion-driven transport is enhanced. The resulting growth velocity is proportional to the current density.

The composition of the solid is controlled by the Peltier effect-induced change of the interface temperature, by the mobility and diffusion constants of the solute components, and by the growth velocity. A unique feature of electroepitaxy is that the composition of the solid remains constant even for prolonged crystal growth, provided the current density is kept constant. On the other hand, for a given solution composition, the composition of the solid can be varied by varying the current density, the variation of the composition depends on the phase diagram, and for $Ga_{1-x}Al_xAs$ it is more pronounced at higher temperatures and for lower values of x (e.g., 880 °C, $x \simeq 0.1$–0.2).

Electroepitaxial growth experiments were carried out employing the $Ga_{1-x}Al_xAs$ system. The results on growth velocity and solid composition were analyzed on the basis of the model and were found to be quantitatively consistent with all aspects of the model.

ACKNOWLEDGMENTS

The authors are grateful to the National Aeronautics and Space Administration and to the National Science Foundation for financial support. They are also grateful to Dr. L. Jastrzebski for his contribution in the early stages of this investigation.

[1]Application of an electric current for LPE has been proposed independently by L.V. Golubyev, T.V. Pakhomova, O.A. Khatchaturian, and Y.V. Shmartzev, [*Proc. IV National Conf. on Crystal Growth, Yerevan* (Izdatielstvo Armenskoy A.K. Nauk, Moscow, 1972), Vol. 1, p. 164 (in Russian)]; M. Kumagawa, A.F. Witt, M. Lichtensteiger, and H.C. Gatos, J. Electrochem. Soc. **120**, 583 (1973).
[2]V.A. Gevorkyan, L.V. Golubyev, S.G. Petrosyan, A.Ya. Stchik, and Y.V. Shmartzev, Zh. Tekh. Fiz. **47**, 1306 (1977).
[3]V.N. Demin, Ya.M. Buzhdan, and F.A. Kuznetsov, Zh. Tekh. Fiz. **48**, 1442 (1978).
[4]W. Bryskiewicz, in *Proc. of 2nd Int. School on Sem. Optoelectronics Cetniewo*, 1978 (Polish Scientific Publishers, Warsaw, 1979); see also references quoted therein.
[5]L. Jastrzebski, J. Lagowski, H.C. Gatos, and A.F. Witt, J. Appl. Phys. **49**, 5909 (1978).
[6]J. Lagowski, L. Jastrzebski, and H.C. Gatos, J. Appl. Phys. **51**, 364 (1980).
[7]J.J. Daniele, Appl. Phys. Lett. **27**, 373 (1975).
[8]J.J. Daniele, D.A. Cammack, and P.M. Asbeck, J. Appl. Phys. **48**, 914 (1977).
[9]J.J. Daniele and C. Michel, Inst. Phys. Conf. Ser. No. **24**, 155 (1975).
[10]J.N. Pratt and R.G.R. Sellors, *Electrotransport in Metals* (Trans. Tech. SA, Riehen, Switzerland, 1973).
[11]M.B. Small and J.F. Barnes, J. Cryst. Growth **5**, 9 (1969).
[12]D.L. Rode, J. Cryst. Growth **20**, 13 (1973).
[13]See Appendix B in Ref. 5.
[14]I. Crossley and M.B. Small, J. Cryst. Growth **15**, 268 (1972).
[15]See, for example, S. Isozumi, Y. Komatsu, N. Okazaki, S. Koyama, and T. Kotani, J. Cryst. Growth **41**, 166 (1977) and references quoted therein.
[16]The phase diagram relationships used at present were calculated after M. Ilegems and M.B. Panish [J. Phys. Chem. Solids **35**, 409 (1974)].
[17]W.G. Pfann, K.E. Benson, and J.H. Wernick, J. Electron. **2**, 597 (1957).
[18]L. Jastrzebski, Y. Imamura, and H.C. Gatos, J. Electrochem. Soc. **125**, 1140 (1978).
[19]J. Lagowski, W. Walukiewicz, M.M.G. Slusarczuk, and H.C. Gatos (unpublished).
[20]H.C. Casey and M.B. Panish, J. Appl. Phys. **40**, 4910 (1969).
[21]O. Borelo and J.C. Woolley, Can. J. Phys. **49**, 1335 (1971).
[22]G.H.B. Thompson and P.A. Kirkby, J. Cryst. Growth **27**, 70 (1974).
[23]H. Ijuin and Shun-ichi Gonda, J. Cryst. Growth **33**, 215 (1976).
[24]T. Bryskiewicz, J. Cryst. Growth **43**, 567 (1978).
[25]R.P. Gale, Ph.D. thesis MIT, 1978.

Minority-carrier mobility in *p*-type GaAs

W. Walukiewicz,[a] J. Lagowski,[a] L. Jastrzebski,[b] and H. C. Gatos

Department of Materials Science and Engineering, Massachusetts Institute of Technology, Cambridge, Massachusetts 02139

(Received 3 January 1979; accepted for publication 12 February 1979)

Theoretical calculations of electron mobility in *p*-type GaAs were carried out taking into consideration the screening effects and all major scattering processes. Calculated values of mobility are presented as a function of carrier concentration, compensation ratio, and temperature. The basic differences between minority-carrier mobility in *p*-type GaAs and electron mobility in *n*-type GaAs are pointed out. A practical procedure is also presented for the evaluation of minority-carrier mobility from available electron-mobility data.

PACS numbers: 72.10. – d, 72.20.Fr, 72.20.Jv

Although minority-carrier mobility is recognized as a key electronic parameter for device application, theoretical treatments of minority-carrier mobility in GaAs and related compounds have thus far been very limited. As a result, it has been a common practice to assume that the electron mobility in *p*-type GaAs is equal to the electron mobility in *n*-type GaAs with the same free-carrier concentration.[1,3] Such practice ignores the presence of additional scattering centers (heavy holes) in *p*-type material.[4] Furthermore, it neglects differences in screening effects and electron statistics in *n*-type and *p*-type material.

The present mobility calculations utilize the variational method[5,6] of solving the Boltzmann equation without involving the relaxation-time approximation. This method has recently been used to evaluate electron mobility in *n*-type GaAs as a function of carrier concentration and compensation ratio. Comparison of these calculations with experimental values of electron mobility has made possible the determination of the compensation ratio in *n*-GaAs. It has also been shown[7] that the compensation ratios obtained from mobility measurements are in good agreement with those determined from free-carrier absorption measurements. In the present paper the method used in Ref. 7 is extended to the calculation of the minority-carrier mobility in *p*-type GaAs. This extension involves some modifications and additional assumptions. First it is assumed that the minority-carrier statistics in the conduction band are given by a nondegenerate distribution function described by the crystal-lattice temperature. In the case of photoexcited electrons this assumption requires that the electrons become thermalized within the conduction band prior to recombining with holes or being trapped at localized centers. For GaAs in the temperature range presently considered, this assumption is justified since the effective relaxation time is several orders of magnitude smaller than the minority carrier lifetime.

In addition to the major scattering mechanisms considered in Ref. 7, namely, ionized impurity, optical phonon, piezoelectric scattering, and acoustical phonon, electron scattering by heavy holes will be taken into account. Because of their large effective mass, heavy holes will be regarded as fixed scattering centers.[8] Thus, the overall concentration of ionized scattering centers is given by $N_i \simeq p_h + N_A^- + N_D^+$, where p_h is the concentration of heavy holes and N_A^- and N_D^+ are the concentrations of ionized acceptors and donors, respectively. Neglecting the contribution from light holes and assuming that the minority-carrier concentration is much smaller than p_h one obtains $p_h = N_A^- - N_D^+$ and thus $N_i \simeq 2N_A^-$.

Another modification of the approach of Ref. 7 centers about screening effects. For a parabolic heavy-hole band, the screening length L_D is given by the following expression[7]:

$$\frac{1}{L_D^2} = 5.80\times 10^{13}\,\frac{(m_h/m_0)^{3/2}T^{1/2}F_{-1/2(\eta_p)}}{\epsilon_0}, \qquad (1)$$

where m_h is the heavy-hole effective mass, ϵ_0 is the static dielectric constant, $F_n(\eta_p)$ is the nth-order Fermi-dirac integral, and $\eta_p = E_F^{(p)}/k_0T$ is the reduced-hole Fermi energy. The reduced screening energy, a, which describes screening of the electron-ionized impurity interaction is given by

$$a = \frac{h_2}{2m_e L_D^2 k_0 T}, \qquad (2)$$

where m_e is the conduction-band electron effective mass. The screening energy of the electron-optical phonon interactions has the following form[8]:

$$a_\infty = \frac{a\epsilon_\infty}{\epsilon_0}, \qquad (3)$$

where ϵ_∞ is the high-frequency dielectric constant. The screening effects arising from the conduction-band electrons and the valence-band light holes are negligible as the concentrations of these carriers are much smaller than the concentration of the heavy holes.

Compensation is included in the present calculations by introducing the compensation ratio θ_p defined as $\theta_p = N_D^+/N_A^-$. The hole concentrations enters into the calculation through the reduced-hole Fermi energy η_p; the

[a] On leave from Institute of Physics, Polish Academy of Sciences, Warsaw Poland.

[b] Present address: *RCA* Laboratories, Princeton, N.J. 08540.

 0021-8979/79/075040-03$01.10

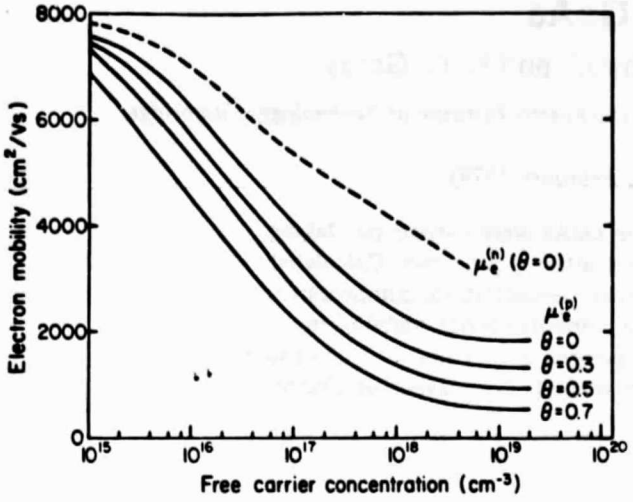

FIG. 1. Room-temperature electron mobility as a function of carrier concentration. Solid curves represent minority-carrier mobility in p-type GaAs for different compensation ratios. Dashed curve shows the electron mobility in n-type GaAs.

compensation ratio affects the total concentration of ionized impurities as follows:

$$N_i = \frac{2p_h}{1-\theta_p}. \tag{4}$$

The values of GaAs parameters used in Ref. 7 have also been adopted in the present case. The hole Fermi energy $E_F^{(p)}$ has been determined from the hole concentration taking the following effective masses for the heavy (m_h) and light holes (m_l): $m_h = 0.54m_0$ and $m_l = 0.089m_0$.

The minority-carrier mobility $\mu_e^{(p)}$ as a function of hole concentration is shown in Fig. 1, together with the electron-mobiiity, $\mu_e^{(n)}$, results reported in Ref. 7. It is seen that the values for $\mu_e^{(p)}$ are lower than those for $\mu_e^{(n)}$ in n-type material with the same carrier concentration. Furthermore, $\mu_e^{(p)}$ decreases more rapidly with carrier concentration than $\mu_e^{(n)}$. The calculated room-temperature mobility ratios $\mu_e^{(p)}/\mu_e^{(n)}$ as a function of carrier concentration is given in Fig. 2. It is seen

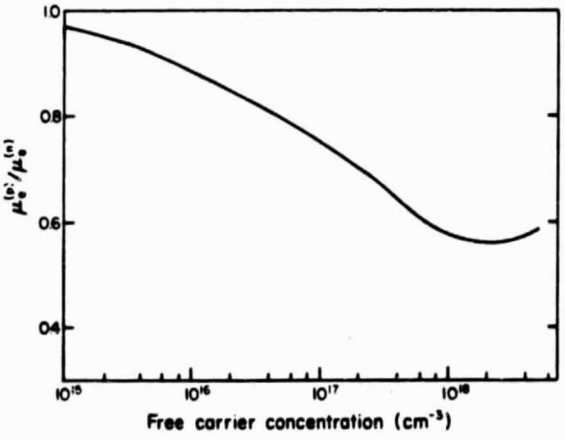

FIG. 2. Ratio of electron mobility in p-type GaAs, $\mu_e^{(p)}$, to the electron mobility in n-type GaAs, $\mu_e^{(n)}$, as a function of free-carrier concentration for $\theta = 0$.

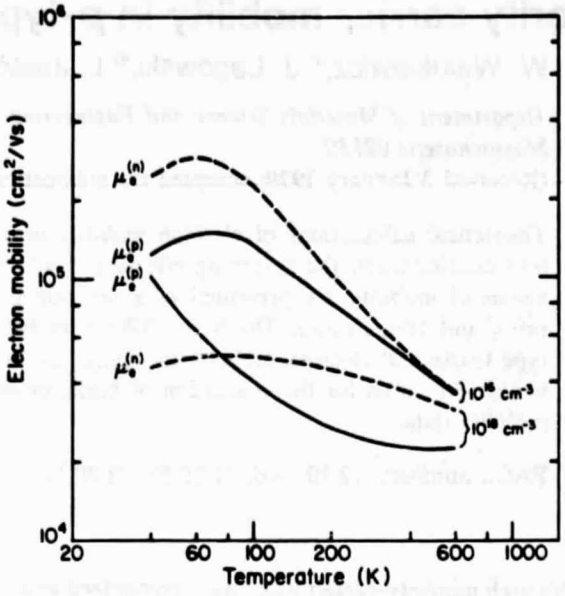

FIG. 3. Temperature dependence of the electron mobility in p-type (solid curves) and n-type (dashed curves) GaAs for two different carrier concentrations: 10^{16} and 10^{18} cm^{-3} and $\theta = 0$.

that for high concentrations this ratio is as low as 0.6, which clearly indicates that the previously reported procedures [1-3] for determining $\mu_e^{(p)}$ from values of $\mu_e^{(n)}$, corresponding to the same free-carrier concentration, are not reliable for carrier concentrations exceeding 10^{16} cm^{-3}.

The calculated temperature dependence of $\mu_e^{(p)}$ and $\mu_e^{(n)}$ is given in Fig. 3. For the low concentrations the difference between $\mu_e^{(p)}$ and $\mu_e^{(n)}$ is more significant at low temperatures. This behavior is apparently due to an increased contribution of the electron scattering by heavy holes relative to that by the lattice. For higher carrier concentrations the screening effects become of greater significance and lead to a temperature dependence of $\mu_e^{(p)}$ entirely different from that of $\mu_e^{(n)}$. Actually, for sufficiently low temperatures $\mu_e^{(p)}$ becomes greater than $\mu_e^{(n)}$.

The above behavior of the minority-carrier mobility can be understood if one considers the fact that with an increase in the hole concentration, there is (a) an increase of the total concentration of the scattering centers and (b) an increase of the heavy-hole screening. At room temperature the contribution from (a) is more significant than from (b), and the mobility decreases with increasing concentration. At lower temperatures the mean electron energy in the conduction band becomes much smaller than the screening energy of the valence-band holes. Accordingly, screening is strongly enhanced and, consequently, (b) dominates (a). Thus, in contrast to n-type material, in p-type GaAs there is a temperature and hole-concentration region in which the electron mobility increases rapidly with decreasing temperature (Fig. 3) and also with increasing carrier concentration.

The effect of compensation on the room-temperature electron mobility in p-type GaAs has been found to be slightly weaker than in n-type material. The computed values of $\mu_e^{(p)}$ with the compensation ratio as a parameter are given in Fig. 1 for hole concentrations ranging from 10^{15} to 10^{19} cm^{-3}.

A comparison of the present results on $\mu_e^{(p)}$ with those on $\mu_e^{(n)}$ (Ref. 7) showed that at room temperature $\mu_e^{(p)}$ can be approximated with $\mu_e^{(n)}$ as follows:

$$\mu_e^{(p)}(p_h,\theta_p) = \mu_e^{(n)}(n,\theta_n), \tag{5}$$

taking $n = p_h$ and $\theta_n = (1 + \theta_p)/(3 - \theta_p)$ where θ_n and θ_p are the compensation ratios in n- and p-type material, respectively. Thus, for example $\mu_e^{(p)}$ in uncompensated p-type GaAs with a hole concentration p_h is equal to the electron mobility $\mu_e^{(n)}$ in n-type GaAs with an electron concentration $n = p_h$ and with compensation ratio $\theta_n = 0.33$. This approximation is particularly valid for low-carrier-concentration material where screening effects are negligible. However, even for the higher concentration considered in this study the error associated with this approximation does not exceed 10%.

From a practical point of view it should be noted that the validity of the above procedure is not limited to GaAs. Expression (5) can be applied to any p-type material with GaAs-like energy-band structure and scattering properties. For instance, in the case of indium phosphide the electron mobility values reported for n-type material [10,11] can be utilized for obtaining the electron mobility values in p-type material.

In summary, it has been shown that the minority-carrier mobility in p-type GaAs is significantly affected by the presence of heavy holes which act as additional scattering centers. The present analysis shows that only at high temperatures and at low carrier concentrations the minority-carrier mobility in p-type GaAs equals the electron mobility in n-type material. For higher concentrations the room-temperature minority-carrier mobility in p-type material can be significantly lower than the electron mobility in n-type material. The minority-carrier mobility was found to exhibit an anomalous dependence on temperature and on carrier concentration. A practical procedure was presented which permits the estimation of the minority-carrier mobility using available data on electron mobility in n-type material.

The authors are grateful to the National Aeronautics and Space Administration for financial support.

[1] J. Vilims and W.E. Spicer, J. Appl. Phys. 36, 2815 (1965).
[2] L.W. Aukerman, M.F. Millea, and M. McColl, J. Appl. Phys. 38, 685 (1967).
[3] M. Ettenberg, H. Kressel, and S.L. Gilbert, J. Appl. Phys. 44, 827 (1973).
[4] For early treatments of minority-carrier mobility see, for example, T.F. McLean and E.G.S. Paige, J. Phys. Chem. Solids 16, 220 (1960), and references quoted therein.
[5] D. Howarth and E.H. Sondheimer, Proc. Phys. Soc. London A 219, 53 (1953).
[6] H. Ehrenreich, J. Appl. Phys. 32, 2155 (1961), and references quoted therein.
[7] W. Walukiewicz, J. Lagowski, L. Jastrzebski, M. Lichtensteiger, and H.C. Gatos, J. Appl. Phys. 50, 899 (1979).
[8] H. Ehrenreich, J. Phys. Chem. Solids 8, 130 (1959).
[9] R.W. Shaw, Phys. Rev. 3, 3283 (1971).
[10] D.L. Rode, Phys. Rev. B 2, 1012 (1970).
[11] W. Walukiewicz, J. Lagowski, L. Jastrzebski, M. Lichtensteiger, and H.C. Gatos (unpublished).

Derivative surface photovoltage spectroscopy; a new approach to the study of absorption in semiconductors: GaAs

J. Lagowski,[a] W. Walukiewicz,[a] M. M. G. Slusarczuk, and H. C. Gatos
Department of Materials Science and Engineering, Massachusetts Institute of Technology, Cambridge, Massachusetts 02139

(Received 18 December 1978; accepted for publication 12 February 1979)

Derivative surface photovoltage spectroscopy was achieved with wavelength modulation; it was applied to GaAs and permitted, in a single experiment, the determination of changes in the absorption coefficient over an energy range of 0.5 to 4.3 eV. Photoionization characteristics of deep levels were determined. All known critical-point transitions up to 4.3 eV were clearly obtained from second-derivative spectra. In addition, previously unresolved transitions were observed at about 2.6 eV. Oscillatory photovoltage in high magnetic fields was observed, and it was used to identify the transitions in the vicinity of the energy gap.

PACS numbers: 78.20. – e, 78.50. – w, 71.25.Tn, 72.40. + w

This communication reports on the absorption changes in GaAs, over a wide energy range, involving photoionization of deep levels, interface states, transitions in the vicinity of the energy gap, and higher-energy critical points. Simultaneous determination of these transitions was made possible with a simple experimental approach combining wavelength modulation and surface photovoltage spectroscopy with strikingly enhanced sensitivity through utilization of the MOS structure characteristics.

Surface photovoltage spectroscopy has been employed primarily for surface state studies.[1] Its inherently low sensitivity in all standard experimental configurations does not permit derivative measurements. Wavelength modulation of photovoltaic effects associated with *p-n* junctions and metal-semiconductor barriers has been reported for indirect-gap semiconductors.[2,3] However, *p-n* junction studies[2] have been limited strictly to the indirect-absorption edge. The metal-semiconductor photovoltage spectroscopy has been extended to the vicinity of direct edges.[3] Extension of this approach well above or below the energy gap is not possible because of the high recombination velocity of minority carriers at the metal interface and the appreciable photoinjection of carriers from the metal to the semiconductor. None of the above limitations is encountered in derivative surface photovoltage.

GaAs *n*-type single crystals and epitaxial layers with room-temperature carrier concentration 1.0×10^{15} to 3.0×10^{16} cm^{-3} and with mobility 6900 to 3000 cm^2/Vsec were employed in the present study. The surface photovoltage (illumination-induced change of the surface barrier) was measured with respect to a transparent reference gold electrode, evaporated on an oxide layer (800 to 1000 Å thick) grown anodically[4] on the GaAs. With this insulating layer a sensitivity of 50 nV was achieved in the surface photovoltage measurements (i.e., two to four orders of magnitude higher than previously reported) permitting the determination of relative changes in the surface barrier as small as about 10^{-7}.

The illumination system consisted of a quartz-halogen light source and a double-prism monochromator with a vibrating slit. The illumination intensity and amplitude of the wavelength modulation were experimentally selected at levels (small) not affecting the measured spectra; typically $\Delta\lambda/\lambda_0$ was of the order of 10^{-3}. Precautions were taken to eliminate the interference of spurious signals (arising, for example, from light-intensity modulation). The measurements were carried out in the temperature range 95–300 K.

A typical sub-band-gap derivative surface photovoltage spectrum obtained with a melt-grown GaAs is shown in Fig. 1. The three-peak structure was found to be characteristic of all melt-grown GaAs crystals studied, although the relative amplitude of the peaks was found to vary with the supplying source of the crystals. In high-purity LPE layers, only the intermediate energy peak (~0.9 eV) was observed, and its amplitude was about two orders of magnitude smaller. Accordingly, the observed transitions are associated with bulk levels rather than with interface states. No photoionization transitions related to interface states were observed. Thus, the surface states in GaAs-oxide interfaces previously reported on the basis of capacitance measurements[5] apparently are not optically active.

By extending the surface photovoltage treatment of surface states[6] to the transitions involving bulk levels (in the surface space-charge region) it is shown that the derivative surface photovoltage ($dV/dh\nu$) is directly proportional to the derivative of the photoionization cross section ($d\sigma/dh\nu$) and thus to the derivative of the absorption coefficient.

The basic features of the deep-level absorption characteristics (Fig. 1) coincide with the extensively studied emission characteristics employing photoluminescence.[7] Thus, the sensitivity of the magnitude of the peaks to the crystal-growth technique and the doping level are identical in both cases; similarly, in both cases the position of the peaks is not sensitive to the nature of the donor dopant. Furthermore, the position of the minimum (1.02 eV) and that of the zero value of the derivative (1.23 eV) in Fig. 1 are similar to the observed energy positions of photoluminescence maxima. Thus, the two high-energy peaks (E_{t1}, E_{t2}) correspond to the same deep levels, previously observed by luminescence and

[a] On leave from Institute of Physics, Polish Academy of Sciences, Warsaw, Poland.

 0021-8979/79/075059-03$01.10

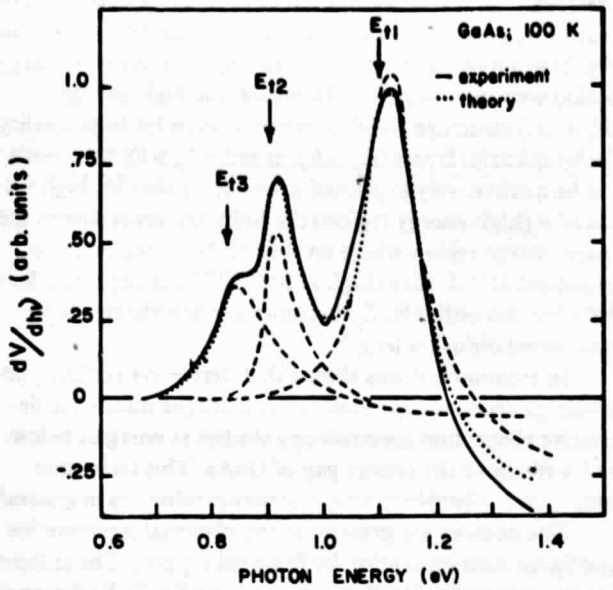

FIG. 1. First-derivative spectrum of subbandgap surface photovoltage of (100) GaAs (melt-grown) with $n = 6\times10^{15}\,\mathrm{cm}^{-3}$. The contribution of the individual transitions is shown by dashed lines. Parameters used in fitting procedure: $E_t = 1.10$, 0.905, and 0.83 eV below conduction band edge; $\Gamma = 40$, 15, and 40 meV, respectively; the Bohr radius of the shallow acceptor $a_s = 3.5\times10^{-7}$cm; the ionization energy of shallow acceptor $E_s = 24.7$ meV was adopted from Ref. 10.

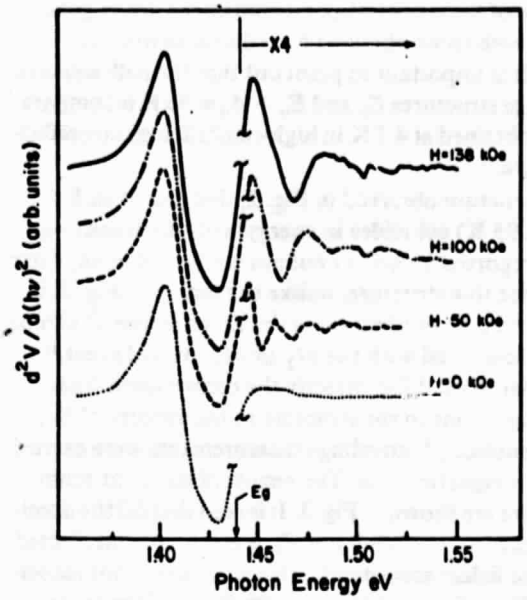

FIG. 3. Second-derivative surface photovoltage of (100) GaAs epitaxial layer ($n = 10^{15}\,\mathrm{cm}^{-3}$) taken in magnetic fields at 300 K. The direction of the magnetic field and that of the light propagation were perpendicular to the surface.

attributed to complexes involving gallium vacancies and donor impurities; the similarity of the absorption and emission energies is significant, as it proves directly that there is no measurable Stokes shift associated with these levels, contrary to the literature report on Ge-doped GaAs.[8] In view of the above, the spectrum of Fig. 1 can be analyzed on the basis of the quantum-defect model of an impurity-band photoionization cross section,[9] modified by the introduction of the Lorentzian broadening Γ.

The results calculated from this model are shown in Fig. 1. It is seen that they are in good agreement with experiment; furthermore, the present treatment enables the separation of the individual contributions of the three deep levels and the accurate determination of the binding energies, E_t. It should be pointed out that with the same set of fitting parameters (given in the caption of Fig. 1) it was possible to obtain good agreement with experiment for all samples studied in spite of the fact that the relative magnitudes of the experimental peaks were quite different. It is thus concluded that the optically active deep centers in n-type GaAs can be approximated in the quantum-defect model as acceptor centers, without invoking configurational changes.

In the region of band-gap transitions second-derivative photovoltage spectra can be directly obtained. A typical spectrum is shown in Fig. 2. The photogenerated transition in the vicinity of the energy gap E_0, the spin-orbit splitting $E_0 + \Delta_0$, and the higher-energy structures E_1 and $E_1 + \Delta_1$, are clearly resolved. The energy positions and temperature

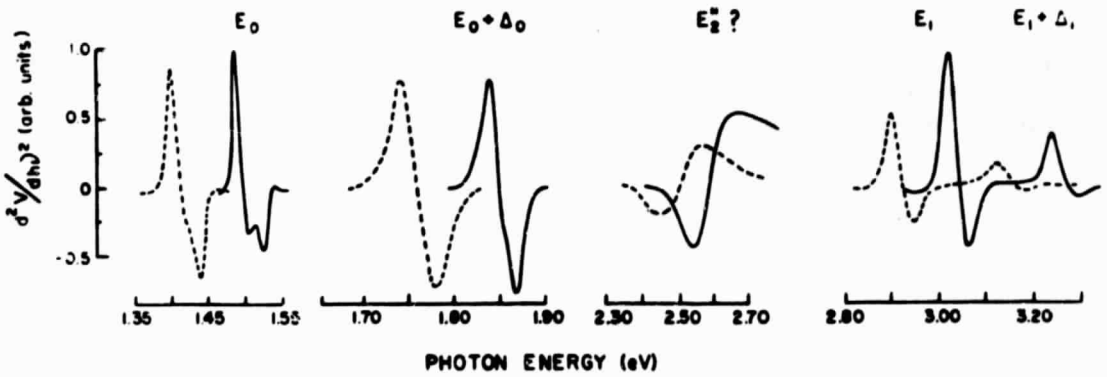

FIG. 2. Second-derivative surface photovoltage spectra of (100) GaAs ($n = 6\times10^{15}\,\mathrm{cm}^{-3}$, $L_p \simeq 10^{-4}$ cm, at room temperature); dashed line 293 K; solid line 95 K. The amplitude of the peaks for $E_0 + \Delta_0$, E_2'', E_1, and $E_1 + \Delta_1$ has been multiplied by a factor of 50, 20, 3, and 3, respectively.

dependence of these critical-point transitions are in good agreement with those obtained by reflectance measurements.[11,12] It is important to point out that the half-width of photovoltage structures E_0 and $E_0 + \Delta_0$ at 95 K is comparable to that obtained at 4.2 K in high-resolution electroreflectance spectra.[13]

The structure observed in Fig. 2, designated as E_2'', (2.59 eV at 95 K) coincides in energy with the transition originally reported in Ref. 11 but not confirmed in any later study.[12] Since this structure, unlike the others in Fig. 2, is characterized by a minimum-maximum sequence, it can be tentatively identified with the M_2 or M_3 critical point.[14]

In order to establish directly the contribution from $\Gamma_8 - \Gamma_6$ transitions to the structure in the vicinity of E_0, derivative surface photovoltage measurements were carried out in high magnetic fields. The results obtained at room termperature are shown in Fig. 3. It is seen that (a) the dominant structure in the vicinity of E_0 is essentially unaffected by magnetic fields; accordingly, this structure is not associated with $\Gamma_8 - \Gamma_6$ transitions or with free-exciton transitions, but rather with residual impurities and/or defects. Thus, the structure at E_0 cannot be identified with the energy gap. (b) For higher photon energies magnetic field leads to an oscillatory magnetophotovoltage with the minima and maxima shifting toward higher energies with increasing magnetic field. The quantitative account of the involved Landau-levels transitions is complicated in GaAs by the complex nature of its valence band. However, from the convergence of the magnetophotovoltage oscillations at zero magnetic field the energy gap at 300 K of high-quality GaAs is precisely obtained as $E_g = 1.440 \pm 0.002$ eV.

In view of the above, it is not surprising that this value is greater than those previously obtained from the derivative spectral in the vicinity of E_0 (1.420–1.427 eV).[15] Transitions in the vicinity of E_0 have been extensively studied in GaAs, as they are important in understanding laser action. However, due to uncertainties in the identification of transitions at room temperature, the energy-gap values obtained by various methods range from 1.38 to 1.445.[15]

The present results (Figs. 2 and 3) clearly show that derivative surface photovoltage is highly sensitive to band-structure optical transitions. This sensitivity can be qualitatively explained by the theory of surface photovoltage arising from trapping of photogenerated holes by surface (interface) states.[16] The spectral response of surface photovoltage is determined by $\alpha L_p/(1 + \alpha L_p)$ where α is the absorption coefficient. Thus, for small values of the minority-carrier diffusion length L_p (e.g., 10^{-5} cm) the surface photovoltage is essentially proportional to the absorption coefficient; as L_p increases the sensitivity of photovoltage to absorption coefficient decreases. Consistent with this model the amplitude of high-energy peaks in the spectra (as those shown in Fig. 2) was found to decrease (with respect to the low-energy peaks) with increasing L_p. However, the high-energy ($E_1 + \Delta_1$) structure could be resolved even for high-quality GaAs epitaxial layers ($L_p \simeq 6\,\mu$m and $\alpha L_p \gg 1$); this result can be qualitatively explained considering that for high values of α (high-energy region) the holes are generated in the space-charge region where an electric field (neglected in treatment of Ref. 16) as high as 10^3–10^4 V/cm opposes their diffusion; accordingly, L_p becomes a much shorter field-contracted diffusion length.[17]

In summary, it was shown that derivative surface photovoltage spectroscopy constitutes a unique means for derivative absorption spectroscopy studies at energies below and well above the energy gap of GaAs. This technique should be applicable to unipolar semiconductors in general.

The authors are grateful to the National Aeronautics and Space Administration for financial support. The authors are also grateful to Dr. R.E. Enstrom and Dr. D. Richman of RCA Laboratories for providing the high-quality epitaxial material and the Francis Bitter National Magnet Laboratory for providing the high magnetic field facilities.

[1] H.C. Gatos and J. Lagowski, J. Vac. Sci. Technol. **10**, 130 (1973).
[2] T. Nishino and Y. Hamakawa, Phys. Status Solidi B **50**, 345 (1972).
[3] T. Nishino, M. Takeda, and Y. Hamakawa, Surf. Sci. **37**, 404 (1973).
[4] H. Hasegawa and H.L. Hartnagel, J. Electrochem. Soc. **123**, 713 (1976).
[5] L.A. Chesler and G.Y. Robinson, J. Vac. Sci. Technol. **15**, 1525 (1978).
[6] C.L. Balestra, J. Lagowski, and H.C. Gatos, Surf. Sci. **64**, 457 (1977).
[7] G.P. Peka and V.A. Brodovoi, Sov. Phys. Semicond. **7**, 1100 (1974); S. Metz and W. Fritz, Inst. Phys. Conf. Ser. B **33a**, 66 (1976).
[8] E.W. Williams and A.M. White, Solid State Commun. **9**, 279 (1971).
[9] H.B. Bebb, Phys. Rev. **185**, 1116 (1969).
[10] N.O. Lipardi and A. Baldareschi, *Proceedings Eleventh Internat'l. Conf. Phys. Semicond.*, Warsaw (Polish Scientific Publishers, Warsaw, 1972), p. 1009.
[11] D.L. Greenway, Phys. Rev. Lett. **9**, 97 (1962).
[12] D.D. Sell and S.E. Stokowski, *Proceedings Tenth Internat'l. Conf. Phys. Semicond.*, Cambridge, Mass. (U.S. Atomic Energy Commission, Oak Ridge, Tenn., 1970), p. 417; J.P. Walter, R.R.L. Zucca, M.L. Cohen, and Y.R. Shen, Phys. Rev. Lett. **24**, 102 (1970); Y.R. Shen, Surf. Sci. **37**, 522 (1973).
[13] D.E. Aspnes and A.A. Studna, Surf. Sci. **37**, 631 (1973).
[14] B. Batz, in *Semiconductors and Semimetals*, edited by R.K. Willardson and Albert C. Beer (Academic, New York, 1972), p. 315.
[15] See for example, J. Camassel, D. Auvergne and H. Mathieu, J. Appl. Phys. **46**, 2683 (1975) and references quoted therein.
[16] N.L. Dimitriuk, V.I. Lyashenko, A.K. Tereshenko, and S.A. Spektor, Phys. Status Solidi A **20**, 53 (1973).
[17] N.J. Harrick, Solid-State Electron. **1**, 234 (1960).

WAVELENGTH MODULATED PHOTOCAPACITANCE SPECTROSCOPY

E. Kamieniecki,[(a)] J. Lagowski and H. C. Gatos
Department of Materials Science and Engineering
Massachusetts Institute of Technology
Cambridge, Massachusetts 02139

Abstract

Derivative deep level spectroscopy was achieved with wavelength modulated photocapacitance employing MOS structures and Schottky barriers. The energy position and photoionization characteristics of deep levels of melt-grown GaAs and the Cr level in high resistivity GaAs were determined. The advantages of this method over existing methods for deep level spectroscopy are discussed.

Journal of Applied Physics, in press.

Capacitance measurements have recently received a great deal of attention as a means for determining deep levels in semiconductors.[1-3] The most effective and sensitive of these methods rely almost exclusively on measurements of thermal emission of carriers trapped by deep levels.[3,4] The photoionization of deep traps has been utilized in conjunction with capacitance measurements, however, with much less success due to ambiguities in the experimental and theoretical determination of photionization cross-sections.

In the present paper it is shown that a reliable determination of photoionization characteristics of deep levels can be achieved by a simple approach combining high sensitivity photocapacitance measurements with wavelength modulation of the incident light. The advantages of wavelength modulation for studying deep levels have recently been demonstrated in derivative surface photovoltage spectroscopy as applied to GaAs MOS structures.[5] It will be presently shown that the derivative wavelength modulated photocapacitance spectroscopy is applicable to MOS as well as to structures simpler than MOS, e.g., metal-semiconductor Schottky barriers and p-n junctions.

The basic capacitance measurements were performed with a 1 MHz commercial capacitance meter in a differential mode. The changes of capacitance induced by wavelength modulation of the incident light (with frequencies ranging from 1 to 25 Hz) were detected using a lock-in amplifier, synchronized with the frequency and phase of the light modulation. In this way the first derivative of the capacitance with respect to the photon energy was obtained. The system employed permitted the detection of capacitance changes smaller than 10^{-4} pF and of relative changes in the total capacitance as small as 10^{-7}-10^{-8}. The illumination system consisted of a tungsten light source and a double prism

monochromator with a vibrating slit. The illumination intensity was experimentally selected at small levels not affecting the measured spectra. The amplitude of the wavelength modulation, $\Delta\lambda/\lambda$, was typically of the order of 10^{-2}. In certain measurements a reduction of $\Delta\lambda/\lambda$ to about 10^{-3} was found necessary in order to reveal a fine structure of photoionization transitions. Precautions were taken to eliminate the interference of spurious signals (arising, for example, from light intensity modulation).

Derivative photocapacitance measurements were performed on n-type GaAs utilizing MOS structures and Schottky barriers. The MOS structures were made by evaporating a transparent gold electrode on an oxide layer (about 1000 Å thick) grown anodically on GaAs.[6] Schottky barriers (MS) were made by evaporating a transparent gold film on GaAs.

Typical subbandgap derivative photocapacitance spectra ($dC/dh\nu$) obtained with MOS and MS structures are shown in the upper part of Fig. 1 (the lower part of Fig. 1 will be discussed below); these structures were prepared on adjacent areas of the same melt-grown GaAs wafer (room temperature carrier concentration $6 \times 10^{15} cm^{-3}$ and mobility 4.500 $cm^2/Vsec$). Both spectra exhibit the same well-defined three-peak structure. The similarity of the derivative photocapacitance spectra of MOS structure and Schottky barrier is significant, as it constitutes a direct proof of the fact that the transitions involved are associated with bulk levels rather than with interface states. Furthermore, the positive sign of the corresponding subbandgap photocapacitance identifies these transitions as photo-excitations of electrons from deep levels into the conduction band.

The three-peak structure observed in derivative photocapactiance was found previously to be characteristic of all melt-grown n-type GaAs.[5]

It is also of interest to note that the position of the 1.0 eV minimum and that of the zero value of the capacitance derivative (1.25 eV) in Fig. 1 correspond to the peak energies observed in luminescence.[7] Thus, the high energy peaks, E_1 and E_2, correspond to the same deep levels previously observed by luminescence and attributed to complexes involving gallium vacancies and donor impurities.[7] It should be noted, however, that high resolution measurements of derivative photocapacitance have revealed a fine three-peak structure of peak E_2 (see insert of Fig. 1) which has not been resolved in any previous studies. The lowest energy peak, E_3, (due to a level at 0.8 eV below the conduction band edge) can be attributed to a level commonly identified with oxygen, although there is no unambiguous proof of this identification.[8,9]

The same three-peak structure as in derivative photocapacitance (Fig. 1) was observed in derivative surface photovoltage measurements performed on the same MOS devices (Fig. 2). However, the derivative photovoltage spectrum obtained with a Schottky barrier (Fig. 2) does not exhibit this structure. In this case the spectrum is dominated by injection of electrons (threshold at $h\nu \approx 0.8$ eV) and of holes ($h\nu \gtrsim 1$ eV) from the metal into the semiconductor which masks the photoionization transitions from deep levels. The advantage of photocapacitance measurements with Schottky barriers is thus apparent.

The quantitative treatment of derivative photocapacitance is simplified significantly by the fact that the interface charge is not modulated by subband-gap illumination (as concluded from the similarity between results obtained with Schottky barriers and MOS structures). By extending earlier photocapacitance and photovoltage treatments[10,11] to transitions involving photoionization of bulk levels (in the depletion space charge region) it is readily shown that small signal derivative photocapacitance, $dC/dh\nu$, is directly proportional to the derivative of the photoionization cross-section, $d\sigma/dh\nu$,

$$\frac{dC}{dh\nu} = \frac{1}{2} C_{eff} \, I \, A \, \frac{n_t}{N_D - N_A} \frac{d\sigma}{dh\nu} \qquad (1)$$

where I is the incident photon flux, n_t is the concentration of occupied traps being probed, and N_D-N_A is the net doping concentration, $C_{eff} = C$ for a Schottky barrier and $C_{eff} = C[1-(C/C_{ox})^2]$ for an MOS structure; C_{ox} is the oxide capacitance. With the exception of very low temperatures, n_t changes only slightly under low intensity subbandgap illumination and thus for the states located below the Fermi level, n_t practically equals the concentration of traps, N_t. Similarly, the derivative photovoltage, $dV/dh\nu$, is given by

$$\frac{dV}{dh\nu} = - V\ I\ A \frac{n_t}{N_D-N_A} \frac{d\sigma}{dh\nu} \qquad (2)$$

The coefficient A in eqs. (1) and (2) depends on the thermal generation and on the recombination rates which characterize the interaction of deep levels with conduction and valence bands. In general it is also dependent on the rate of optical generation.

For sufficiently high temperatures and low intensity of incident illumination, whereby a transient response of deep levels can be approximated by a relaxation time, τ, the coefficient A has a simple form $A = \langle\tau/(1 + \omega^2\tau^2)^{1/2}\rangle$, where ω is the angular frequency of wavelength modulation. A in Eqs. (1) and (2) represents an average value since τ depends on the location of the traps in the space charge region. The approximation of small illumination intensity was verified in the present experiments by the observed linear dependence of the signal on illumination intensity. The coefficient A was also found to be inversely proportional to the frequency of light modulation, i.e., $\omega\tau >> 1$. At lower temperatures ($\lesssim$80°K) the derivative photocapacitance (and surface photovoltage) decreased significantly because under illumination the occupation of states decreases rapidly due to the increase of the relaxation time. No measurable derivative signals could be detected at temperature

50°K. The similarity of Eqs. (1) and (2) shows that the derivative photocapacitance spectra of Fig. 1 can be quantitatively analysed on the basis of the quantum defect photoionization model employed for the analysis of the derivative photovoltage spectra.[5] Such a procedure enables the separation of the individual contributions of the deep levels and the accurate determination of their binding energies, E_t. The presently obtained values for peaks E_1 and E_3 are 1.1 and 0.83 eV, respectively, i.e., identical to the values obtained from surface photovoltage measurements. The high resolution measurements performed with MOS structures showed, however, that the E_2 peak in all investigated samples exhibited a fine structure which cannot be accounted for by existing photionization models.

Since the derivative photocapacitance is directly proportional to the derivative of the photoionization cross-section (Eq. 1) it must also be proportional to the derivative of the absorption coefficient. A typical subbandgap absorption spectrum of GaAs[12] is shown in the lower part of Fig. 1. It is seen that the derivative maxima indeed coincide with the highest absorption slopes. Although the absorption spectrum corresponds to a lower temperature (21°K), its comparison with the derivative photocapacitance spectra is valid in view of the weak temperature dependence of the energy position of the derivative peaks and of the corresponding thresholds.[12]

According to equations (1) and (2), the ratio of the derivative photocapacitance to the photovoltage signal for MOS structures, $(dC/dh\nu)/(dV/dh\nu)$, is equal to $1/2\ (C_{eff}/V)$. For a depletion layer, a decrease of the surface barrier height, V, corresponds to an increase in capacitance C and thus C_{eff} (for $C/C_{ox} < 1$). Accordingly, the ratio $(dC/dh\nu)/(dV/dh\nu)$ should increase with decreasing the surface barrier. This marked difference between surface photovoltage and photocapacitance has been verified by experiments in which

the surface barrier height was decreased by low intensity background illumination with $h\nu > E_g$. As expected, both derivative spectra decreased in magnitude due to the decrease in the occupation of the deep traps by electrons (capture of photoexcited holes). However, the ratio $(dC/dh\nu)/(dV/dh\nu)$ increased under background illumination; furthermore, the derivative photocapacitance spectrum could still be clearly observed when the photovoltage signal essentially vanished. This result indicates again the advantage of photocapacitance measurements under conditions of low surface barrier and/or when interaction of deep centers with minority carriers is significant.

In view of its high sensitivity to deep levels, derivative photocapacitance spectroscopy was applied to high resistivity Cr-doped GaAs. Typical derivative spectra obtained at room temperature and at 100 K are shown in the upper part of Fig. 3. In the lower part of Fig. 3 typical absorption spectra[13] for similar material are shown. The zero crossing point of the derivative photocapacitance spectra at 0.9 eV clearly coincide with the absorption peak observed at the low temperature. The shape of the derivative spectrum is consistent with a transition between two discrete states, rather than between a localized state and the conduction band. This conclusion is in agreement with results of previous investigations.[13]

In summary, it was shown that derivative photocapacitance spectroscopy permits the detection of small changes of optical absorption associated with photoionization of deep levels in semiconductors. The technique can be used with MOS structures, Schottky barriers, and undoubtedly with p-n junctions. It permits the detection of deep bulk levels in GaAs-MOS structures in the presence of a high density GaAs-oxide interface state. According to a realistic estimation, deep levels with a concentration two orders of magnitude

smaller than shallow impurity doping can be detected.

ACKNOWLEDGEMENTS

The authors are grateful to the National Science Foundation and the National Aeronautics and Space Administration for financial support. The authors are also grateful to Dr. L. C. Kimerling of Bell Telephone Laboratories for valuable discussions on capacitance measurements.

REFERENCES

(a) On leave from Institute of Physics, Polish Academy of Sciences, Warsaw, Poland.

1. C. T. Sah, Solid-State Electron. 19, 975 (1976).
2. H. G. Grimmeiss, Ann. Rev. Mat. Sci. 7, 341 (1977).
3. G. L. Miller, D. V. Lang and L. C. Kimerling, Ann. Rev. Mat. Sci. 7, 377 (1977).
4. D. V. Lang, J. Appl. Phys. 45, 3023 (1974).
5. J. Lagowski, W. Walukiewicz, M. M. G. Slusarczuk and H. C. Gatos, J. Appl. Phys. 50, 5059 (1979).
6. H. Hasegawa and H. L. Hartnagel, J. Electrochem. Soc. 123, 713 (1976).
7. See for example, S. Metz and W. Fritz, Inst. Phys. Conf. Ser. 33a, 66 (1977).
8. P. K. Vasuder and R. H. Bube, Solid-State Electron. 21, 1095 (1978).
9. A. M. Huber, N. T. Linh, M. Valladon, J. L. Debrun, G. M. Martin, A. Mitonneau and A. Mircea, J. Appl. Phys. 50, 4022 (1979).
10. E. Kamieniecki, Solid-State Electron. 16, 1487 (1973).
11. C. L. Balestra, J. Lagowski and H. C. Gatos, Surface Sci. 64, 457 (1977).
12. M. D. Sturge, Phys. Rev. 127, 768 (1962).
13. A. L. Lin and R. H. Bube, J. Appl. Phys. 47, 1859 (1976).

FIGURE CAPTIONS

Fig. 1 Derivative photocapacitance spectra of melt-grown GaAs ($n = 6 \times 10^{15} cm^{-3}$) for MOS and MS structures (upper portion of Fig.) obtained with wavelength modulation $\Delta\lambda/\lambda$ of about 10^{-2}. The insert shows a fine structure of peak E_2 as revealed by high resolution measurements on MOS structures employing $\Delta\lambda/\lambda$ of about 10^{-3}. In lower portion of Fig. a typical absorption spectrum is given (Ref. 12).

Fig. 2 Derivative surface photovoltage spectra for the same samples as in Fig. 1. The amplitude of wavelength modulation $\Delta\lambda/\lambda \sim 10^{-2}$. The MOS spectrum is multiplied by a factor of 10.

Fig. 3 Derivative photocapacitance (upper portion of Fig.) and absorption spectra (see Ref. 13) of Cr-doped GaAs. The amplitude of wavelength modulation $\Delta\lambda/\lambda$ was about 10^{-2}.

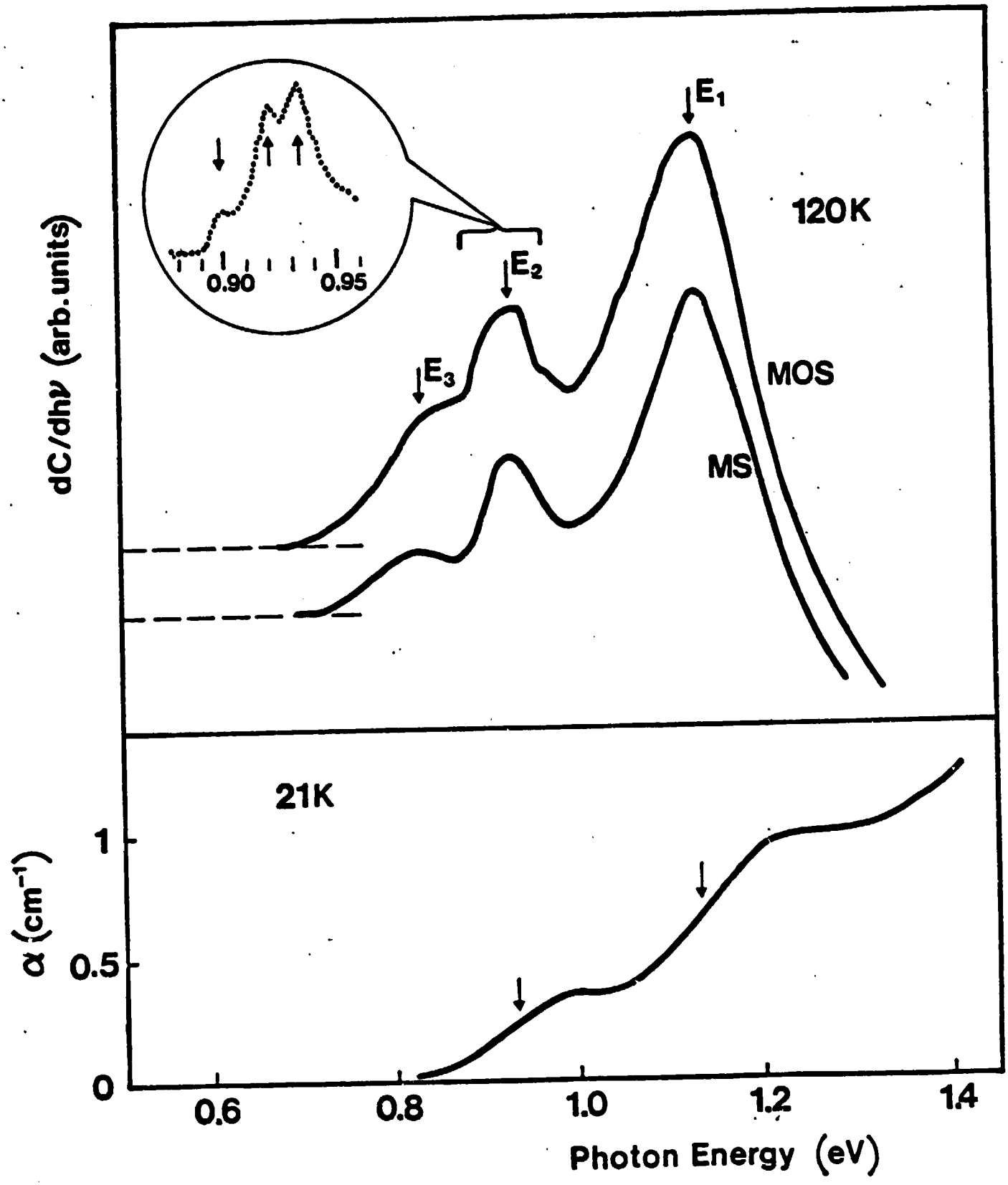
dC/dhν (arb.units)
E1
E2
E3
0.90
0.95
120K
MOS
MS
21K
α (cm⁻¹)
1
0.5
0
0.6
0.8
1.0
1.2
1.4
Photon Energy (eV)

Fig. 2

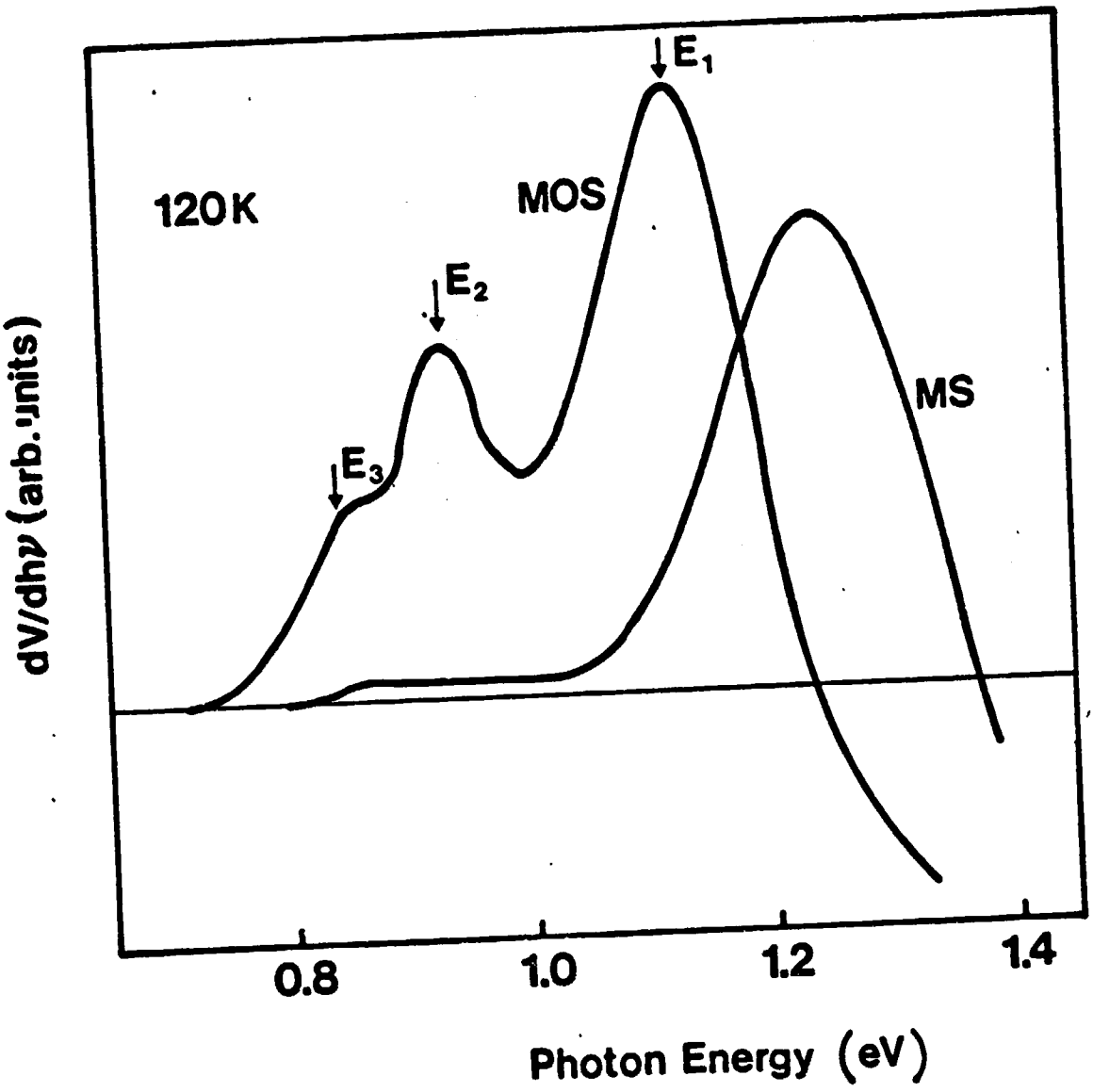
120K
MOS
MS
E_1
E_2
E_3
dV/dhν (arb. units)
0.8
1.0
1.2
1.4
Photon Energy (eV)

Fig. 3

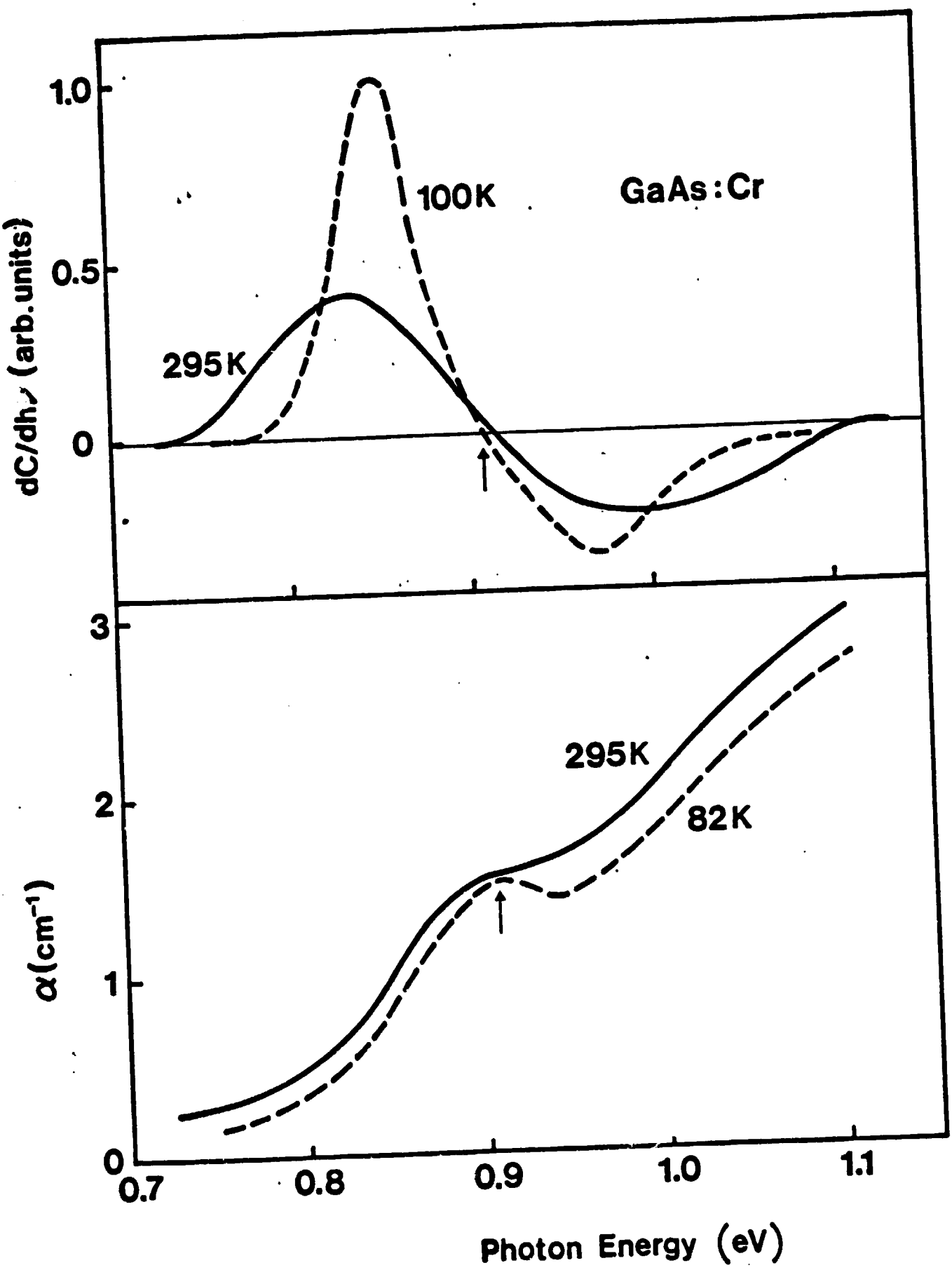
1.0
0.5
0
dC/dhν (arb.units)
100K
GaAs:Cr
295K
3
2
1
0
α(cm⁻¹)
295K
82K
0.7
0.8
0.9
1.0
1.1
Photon Energy (eV)

A STUDY OF GaAs-OXIDE INTERFACE BY TRANSIENT CAPACITANCE SPECTROSCOPY: DISCRETE ENERGY INTERFACE STATES

E. Kamieniecki, T. E. Kazior, J. Lagowski and H. C. Gatos
Massachusetts Institute of Technology
Cambridge, Massachusetts 02139

ABSTRACT

Interface states and bulk GaAs energy levels were simultaneously investigated in GaAs MOS structures prepared by anodic oxidation. These two types of energy levels were successfully distinguished by carrying out a comparative analysis of deep level transient capacitance spectra of the MOS structures and MS structures prepared on the same samples of epitaxially grown GaAs ($n \simeq 10^{15}cm^{-3}$). The identification and study of the interface states and bulk levels was also pursued by investigating the transient capacitance spectra as a function of the filling pulse magnitude. It was found that in the GaAs-anodic oxide interface there are states present with a discrete energy (0.65 eV below the conduction band) rather than with a continuous energy distribution as previously reported. The value of the capture cross-section of the interface states was found to be 10^{-14} to $10^{-15}cm^2$, which is far more realistic than the extremely large values of 10^{-8} to $10^{-9}cm^2$ reported on the basis of conductance measurements.

Proceedings of Seventh Annual Conference on Physics of Compound Semiconductor Interfaces, Estes Park, Colo., January 1980.

I. INTRODUCTION

The rapidly increasing interest in the growth and properties of native oxide layers on GaAs stems primarily from the importance of these layers in electronic device applications such as MOS devices and integrated circuits. The electronic properties of GaAs-oxide interfaces have so far been investigated utilizing primarily C-V measurements.[1-6] Commonly, GaAs MOS structures exhibit carrier-injection type hysteresis and large frequency dispersion which are considered to be due to the high density interface states and/or to traps in the oxide.[3-6] These interface characteristics are undesirable for active device applications and thus, the importance of the quantitative characterization of the interface states and of the understanding of their origin is quite apparent. Precise determination of the interface state parameters from the conventional C-V or conductance methods involves ambiguities related to the very broad time-constant dispersion of GaAs MOS structures.[6] In the case of silicon MOS structures the time constant dispersion is commonly attributed to surface potential fluctuations.[7] It is conceivable that in GaAs MOS structures also such fluctuations influence significantly the results of C-V and conductance measurements.

In this investigation deep-level transient spectroscopy (DLTS)[8,9] was applied to study the parameters of GaAs-native oxide interface states. Unlike C-V and conductance methods, transient capacitance measurements are independent of the surface potential fluctuations.[10] Recently DLTS has been applied to the investigation of interface states in GaAs MOS structures[11] having an oxide layer prepared by plasma oxidation; in the present study the oxide layer was obtained by anodic oxidation in a solution of glycol and water. The experimental approach permitted the investigation of interface states as well as residual bulk levels.

II. EXPERIMENTAL

GaAs LPE layers, n-type 45 μm thick, grown on Cr-doped semi-insulating substrates with an (100) orientation, were used in this study. At room temperature the layers exhibited an electron concentration of 1.1×10^{15} cm^{-3} and a Hall mobility of 6900 cm^2/V-sec. A similar value of net impurity concentration ($N_D^+ - N_A^- = n$) was obtained from C-V measurements.

Anodic oxidation of GaAs was carried out in two different electrolytes: (a) a mixture of propylene glycol and 3% aqueous solution of tartaric acid (buffered by NH_4OH to pH of about 6.2) in a volume ratio 3:1,[12] and (b) a mixture of diethylene glycol + 5% by weight water + 0.5% by weight Na_3PO_4.[13] Oxidation was initiated under a constant current density of 1 mA/cm^2 for electrolyte (a) and 0.1 mA/cm^2 for electrolyte (b), until a predetermined voltage was reached; than a constant voltage was maintained until the current decayed to about 10% of the initial value. During oxidation the GaAs samples were illuminated with a collimated beam of light from a tungsten lamp in order to generate holes required for the anodic reaction.[12] Prior to anodic oxidation the samples were etched in concentrated HCl to remove the as-grown oxide. The thickness of the anodic oxides employed was typically between 2000 and 2500 Å. The MOS structure was prepared by vacuum deposition of gold through a metal mask. The MS structures were prepared from the same GaAs samples used for the MOS structures after dissolving the anodic oxide.

In the C-V and dC/dV measurements an 1MHz commercial capacitance meter was used. The DLTS measurements were performed in a standard experimental arrangement.[8,9] The rate window was implemented with a double boxcar averager. The sampling times were selected so that $t_2 = 2t_1$; t_1 was varied from 0.5 to 25 ms.

III. RESULTS AND DISCUSSION

3.1 Capacitance-Voltage Measurements

Typical C-V characteristics of MOS structures prepared by employing the propylene glycol electrolyte are shown in Fig. 1. Very similar results were obtained with MOS structures prepared by using diethylene glycol, although the resistivity of the oxides prepared in the former electrolyte was higher than the resistivity of those prepared in the latter. As seen in Fig. 1, GaAs MOS structures reveal several distinct features consistent with previous findings:[6] (1) The capacitance-voltage characteristics show carrier-injection type hysteresis; (2) the 1-MHz capacitance of the MOS structures under forward bias is much lower than the oxide capacitance; (3) at high reverse bias the samples show a deep-depletion type characteristic.

The deep-depletion type behavior is especially important for DLTS measurements and its validity was tested in more detail. Measurements of the total capacitance, C, and the derivative of the capacitance, dC/dV, (dV = 10 to 100 mV, frequency of voltage modulation 10 to 100 Hz) were carried out in the temperature range of 80 to 500 K. Provided that the MOS structure is in the deep depletion state these measurements allow the determination of the net doping concentration, $N_D - N_A$, according to the relation:

$$N_D - N_A = (C^3/q\,\varepsilon_s A^2)\,(dC/dV)^{-1}, \qquad (1)$$

where q is the electronic charge, ε_s is the dielectric permittivity of GaAs, and A is the area of the field electrode.

It was established that the net concentration of ionized impurities, as determined from room temperature C-V results under deep-depletion conditions, were in excellent agreement with values obtained from Hall-effect measurements. The doping concentration determined from eq. (1) changed only slightly with temperature and was consistent with that obtained from measurements with MS

structures. These results clearly show that in the temperature range presently studied the MOS structures under high reverse bias were indeed in the deep-depletion state.

3.2 DLTS Measurements

DLTS measurements on MOS structures were carried out under deep-depletion conditions. Typical results are shown in Fig. 2. At low filling pulse voltages (up to 20 volts) only a high temperature (about 390 K) peak is observed. By increasing the filling pulse voltage an additional peak is revealed at a lower temperature (about 360 K). In general increasing the filling pulse voltage should enhance the contribution from traps located close to the interface;[8,9] thus, the lower temperature peak observed only for filling pulses exceeding 20 volts can be attributed to interface states. Consistent with this interpretation, the lower temperature peak was not observed in MS structures prepared with the same samples; the high temperature peak (390 K) was clearly observed which indicates that this peak is associated with bulk traps.

Thermal activation plots of $T^2\tau_m$ (where T is the temperature and $\tau_m = (t_2-t_1)[\ln(t_2/t_1)]^{-1}$, i.e., the inverse of the rate window[8]) are shown in Fig. 3. It is seen that the activation energy of the emission rate of bulk levels is the same for MOS and MS structures, and equal to 0.81 eV. The activation energy of the interface states is found to be 0.65 eV. The corresponding capture cross-sections determined from transient capacitance spectra (assuming that they are independent of temperature) are about $10^{-13}cm^2$ and 10^{-14} to $10^{-15}cm^2$ for bulk and interface states, respectively. The present value of the capture cross-section of the interface states is far more realistic than the extremely large values of 10^{-8} to $10^{-9}cm^2$ reported on the basis of conductance measurements.[6,14]

The transient capacitance spectra as a function of the filling pulse voltage in Fig. 2 show that the high temperature peak associated with 0.81 eV bulk states saturates at about 20 V. The lower temperature peak, associated with interface states, is negligible at low filling pulse voltages, but it increases sharply for pulses exceeding 20 volts. This markedly different behavior of the bulk traps and interface states permits the quantitative determination of their contributions to the total DLTS spectra. For a single energy level the temperature dependence of the DLTS signal, measured at sampling times $t_2 = 2t_1$, $\Delta C(T) = C(t_2) - C(t_1)$, is described by equations:[8,9]

$$\Delta C(T) = 4\Delta C \exp(-t_1/\tau)\,[1 - \exp(-t_1/\tau)]$$
$$\tau^{-1} = \sigma_n v_{th} N_c \exp[-(E_c - E_t)/kT], \qquad (2)$$

where ΔC is the DLTS signal at the peak maximum, σ_n is the electron capture cross-section, v_{th} is the thermal velocity of electrons, N_c is the density of states in the GaAs conduction band, $E_c - E_t$ is the activation energy of states, and k is the Boltzmann's constant.

As shown in Fig. 4, $\Delta C(T)$ calculated from eq. (2) assuming $E_c - E_t = 0.807$ eV, $\sigma_n = 8.94 \times 10^{-14}\,cm^2$, and typical temperature dependence of v_{th} and N_c is in excellent agreement with the experimentally determined transient capacitance spectrum obtained with a 20V/20 μsec filling pulse, associated with the bulk states. To separate the DLTS peak associated with the interface states, this saturation value of the bulk peak was subtracted from the total DLTS signal at higher filling pulse voltages. As shown in Fig. 5, the resulting interface peak is in good agreement with theoretical calculation assuming a discrete energy level at $E_c - E_t = 0.651$ eV, characterized by an electron capture cross-section $\sigma_n = 7.0 \times 10^{-15}\,cm^2$.

By extending earlier treatments of the capacitance transients in MOS structures[15] to DLTS measurements, it is readily shown that the concentration of the bulk states N_t is given by

$$N_t = 8 \frac{\Delta C}{C} \frac{N_D - N_A}{1-(C/C_{ox})^2} \qquad (3)$$

while the density of interface states N_{ss} is

$$N_{ss} = 4\Delta C(N_D - N_A)A\epsilon_s C_{ox}/C^3 \qquad (4)$$

where C is the total capacitance of the structure, C_{ox} is the oxide capacitance, and $N_D - N_A$ is the net doping concentration. The concentration of the 0.81 eV bulk states was found to be about $10^{14}cm^{-3}$ in all measured MOS and MS structures (in the case of MS structure C/C_{ox} in eq. 3 is equal to zero) and was independent of depth. The density of the 0.65 eV interface states evaluated from the saturation value of the DLTS signal was of the order of $10^{12}cm^{-2}$.

The position of the discrete interface level reported in this paper is consistent with the energy-density distribution of the oxide-GaAs interface states previously obtained by using Berglund's[2] and Terman's[6] methods as well as by the saturation photovoltage technique.[16] As shown in Fig. 6, these results show an increase of the interface state density towards the energy corresponding to the position of the presently observed discrete interface level. It should be noted, however, that recent DLTS measurements of GaAs MOS structures prepared by oxidation in an oxygen plasma, induced by high-frequency discharge, revealed interface states with continuous energy distribution (about $10^{13}cm^{-2}eV^{-1}$), exhibiting a peak at 0.43 eV below the conduction band edge and an increase in density toward the valence band edge.[11] These results were obtained below room temperature. In the present study, transient

C-2

capacitance measurements carried out under conditions similar to those reported in ref. 11 revealed no measurable DLTS signal below room temperature. Thus, it is concluded that the interface states at 0.43 eV are characteristic of MOS structures prepared by plasma oxidation rather than by anodic oxidation.

IV. SUMMARY

Interface states and bulk GaAs levels were simultaneously investigated in GaAs MOS structures prepared by anodic oxidation in propylene and diethylene glycol electrolytes. They were successfully distinguished by carrying out a comparative analysis of deep level transient capacitance spectra of MOS and MS structures prepared on the same samples of epitaxially grown n-type GaAs. The transient capacitance spectra of both MOS and MS structures exhibited a peak corresponding to a bulk level at 0.81 eV below the conduction band and with a concentration of about $10^{14}cm^{-3}$, independent of depth. The electron capture cross-section σ_n, of these states was found to be of the order of $10^{-13}cm^2$, assuming σ_n to be independent of temperature. The 0.81 eV bulk states can be attributed to a level commonly identified with oxygen,[17] although there is no unambiguous proof of this identification.[18] An additional DLTS peak observed only in the case of MOS structures was found to be very sensitive to the filling pulse voltage consistent with the behavior of interface states. The results can be readily accounted for on the basis of interface states with a discrete energy at 0.65 eV below the conduction band, with an electron capture cross-section of 10^{-14} to $10^{-15}cm^2$ and a density of about $10^{12}cm^{-2}$. Thus, it is concluded that in the GaAs-anodic oxide interface near the mid-gap, there are interface states with a discrete energy level rather than with a continuous energy distribution as previously reported.

The authors are grateful to the National Aeronautics and Space Administration and the National Science Foundation for financial support.

REFERENCES

1. H. Hasegawa, K. E. Forward and H. L. Hartnagel, Appl. Phys. Lett. 26, 567 (1975).
2. C. R. Zeisse, L. J. Messick and D. L. Lile, J. Vac. Sci. Technol. 14, 957 (1977).
3. L. A. Chesler and G. Y. Robinson, J. Vac. Sci. Technol. 15, 1525 (1978).
4. F. Koshiga and T. Sugano, Thin Solid Films 56, 39 (1979).
5. G. Weimann, ibid. 56, 173 (1979).
6. T. Sawada and H. Hasegawa, ibid. 56, 185 (1979).
7. See e.g., A. Goetzberger, E. Klausmann and M. Schulz, CRC Rep. 1, 1 (1976).
8. D. V. Lang, J. Appl. Phys. 45, 3023 (1974).
9. G. L. Miller, D. V. Lang and L. C. Kimerling, Ann. Rev. Mater. Sci., 1977, p. 377.
10. M. Schulz and N. M. Johnson, Solid State Commun. 25, 481 (1978).
11. K. Yamasaki and T. Sugano, Appl. Phys. Letters, to be published.
12. H. Hasegawa and H. L. Hartnagel, J. Electrochem. Soc. 123, 713 (1976).
13. M. Croset, J. Diaz, D. Dieumegard and L. M. Mercandalli, ibid. 126, 1543 (1979).
14. K. Yamasaki and T. Sugano, Proc. 25th Int. Sci. Cong. Electronics, Roma, 1978, p. 418.
15. See e.g., E. Kamieniecki, Solid-State Electron. 16, 1487 (1973).
16. A. Shimano, A. Moritani and J. Nakai, Japan J. Appl. Phys. 15, 939 (1976).
17. D. V. Lang and R. A. Logan. J. Electronic Materials 4, 1053 (1975).
18. A. M. Huber, N. T. Linh, M. Valladon, J. L. Debrun, G. M. Martin, H. Mitonneau and A. Mircea, J. Appl. Phys. 50, 4022 (1979).

FIGURE CAPTIONS

Fig. 1. Typical capacitance-voltage characteristics of GaAs MOS structures prepared by anodic oxidation in propylene glycol electrolyte for two sweep rates.

Fig. 2. Dependence of transient capacitance spectra of MOS structures on filling pulse voltage; sampling times t_1/t_2 = 5/10 msec.

Fig. 3. Typical thermal activation plots for MOS and MS structures.

Fig. 4. Comparison of measured (t_1/t_2 = 5/10 msec) and calculated transient capacitance spectra of bulk traps. Parameters used in the fitting procedure: E_C-E_t = 0.807 eV and $\sigma_n = 8.94 \times 10^{-14} cm^2$.

Fig. 5. Comparison of measured and calculated transient capacitance spectra. Total DLTS signal was obtained with sampling times t_1/t_2 = 5/10 msec and filling pulses 40 V/0.5 msec. The experimentally determined (see text) contribution of the bulk and interface traps is shown by dashed lines. Parameters of interface states used in the fitting procedure are: E_C-E_t = 0.651 eV and $\sigma_n = 7.0 \times 10^{-15} cm^2$.

Fig. 6. The interface state distribution in the energy gap as measured by Terman's method (after Sawada and Hasegawa - ref. 6) and saturation surface photovoltage technique (after Shimano, Moritani and Nakai - ref. 16).

Fig. 1

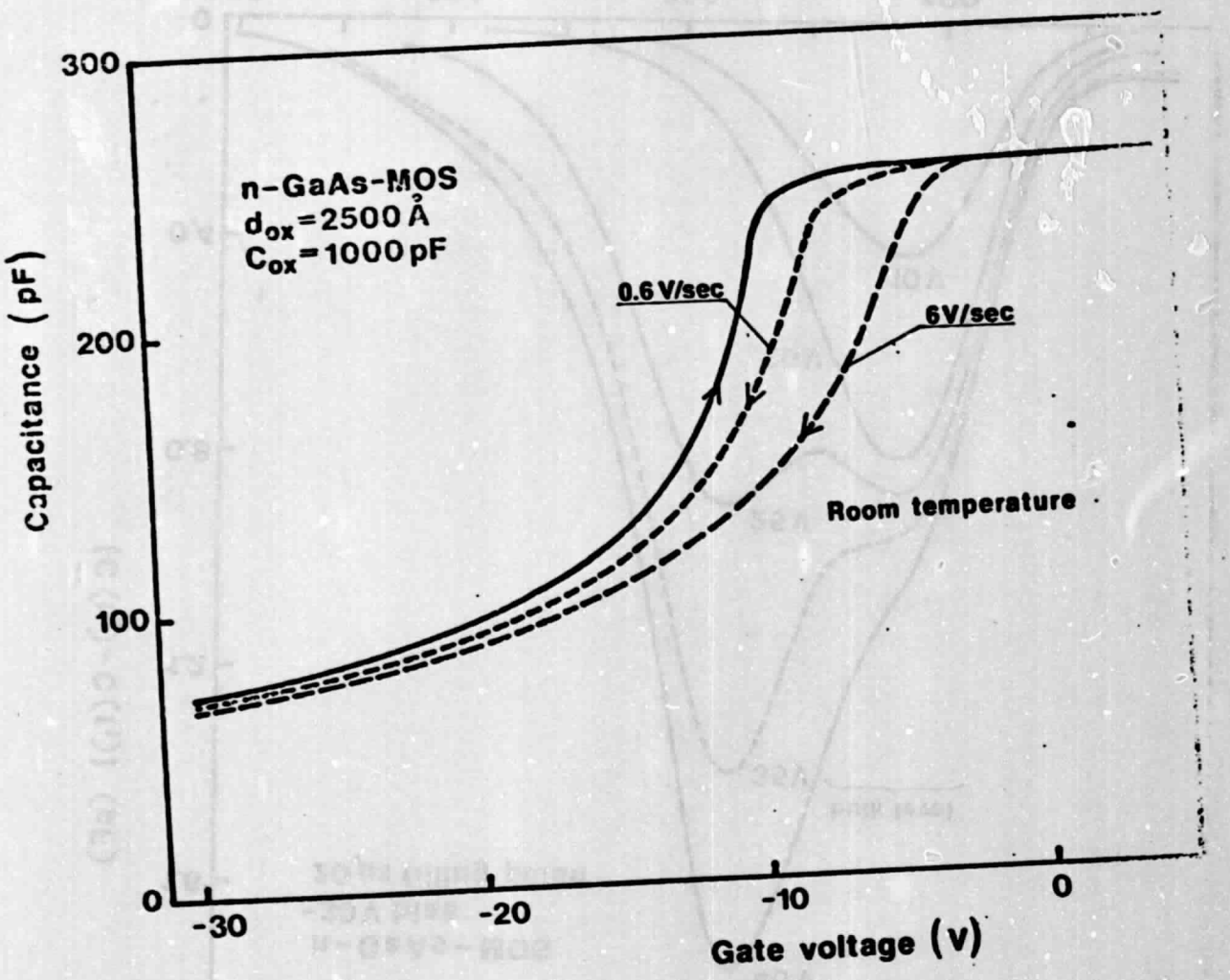
n-GaAs-MOS
d_{ox}=2500 Å
C_{ox}=1000 pF
0.6 V/sec
6V/sec
Room temperature
Capacitance (pF)
300
200
100
0
-30
-20
-10
0
Gate voltage (V)

Fig. 2

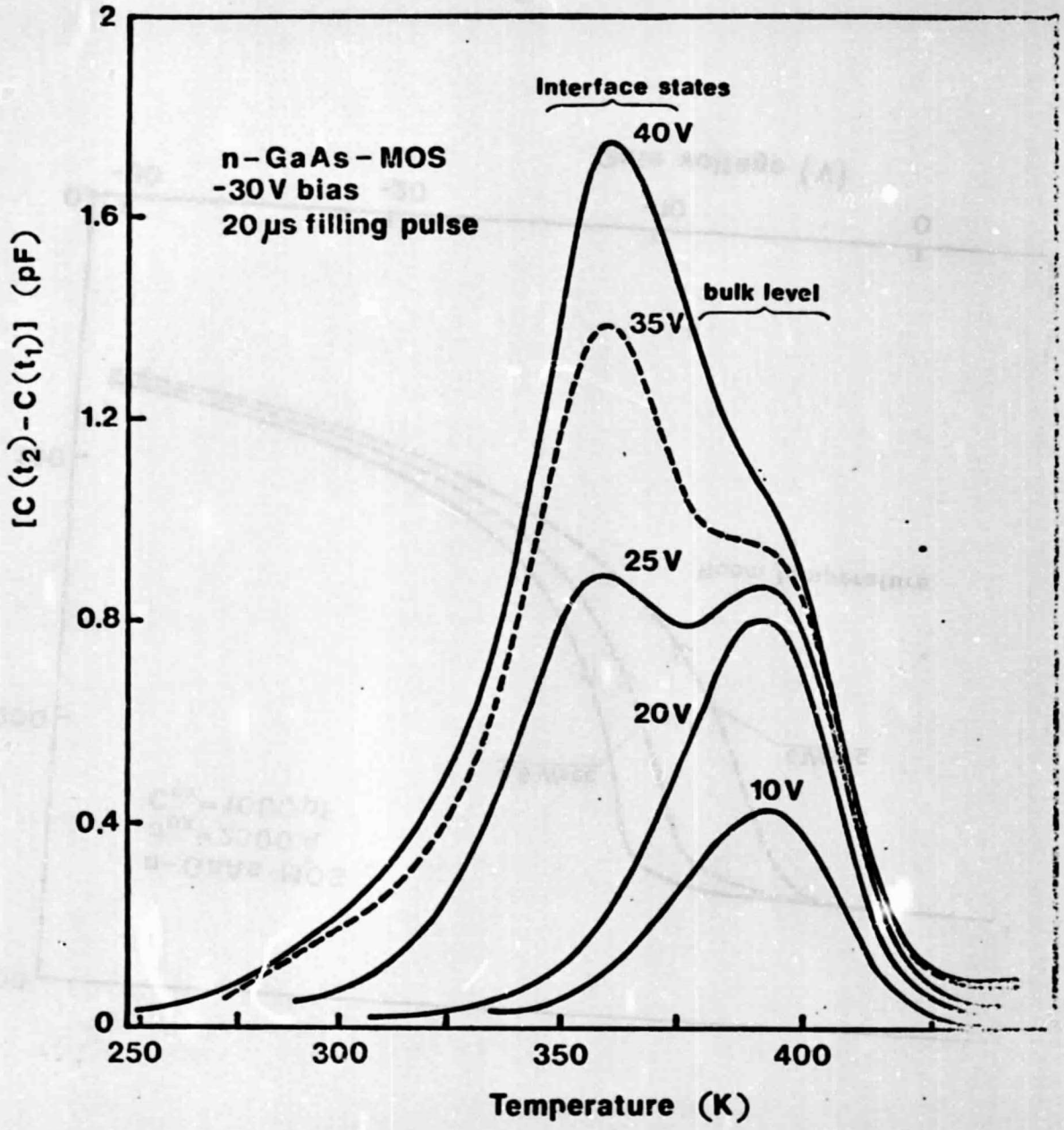
Interface states
40V
n-GaAs-MOS
-30V bias
20μs filling pulse
bulk level
35V
25V
20V
10V
2
1.6
1.2
0.8
0.4
0
250
300
350
400
Temperature (K)
[C(t2)-C(t1)] (pF)

Fig. 3

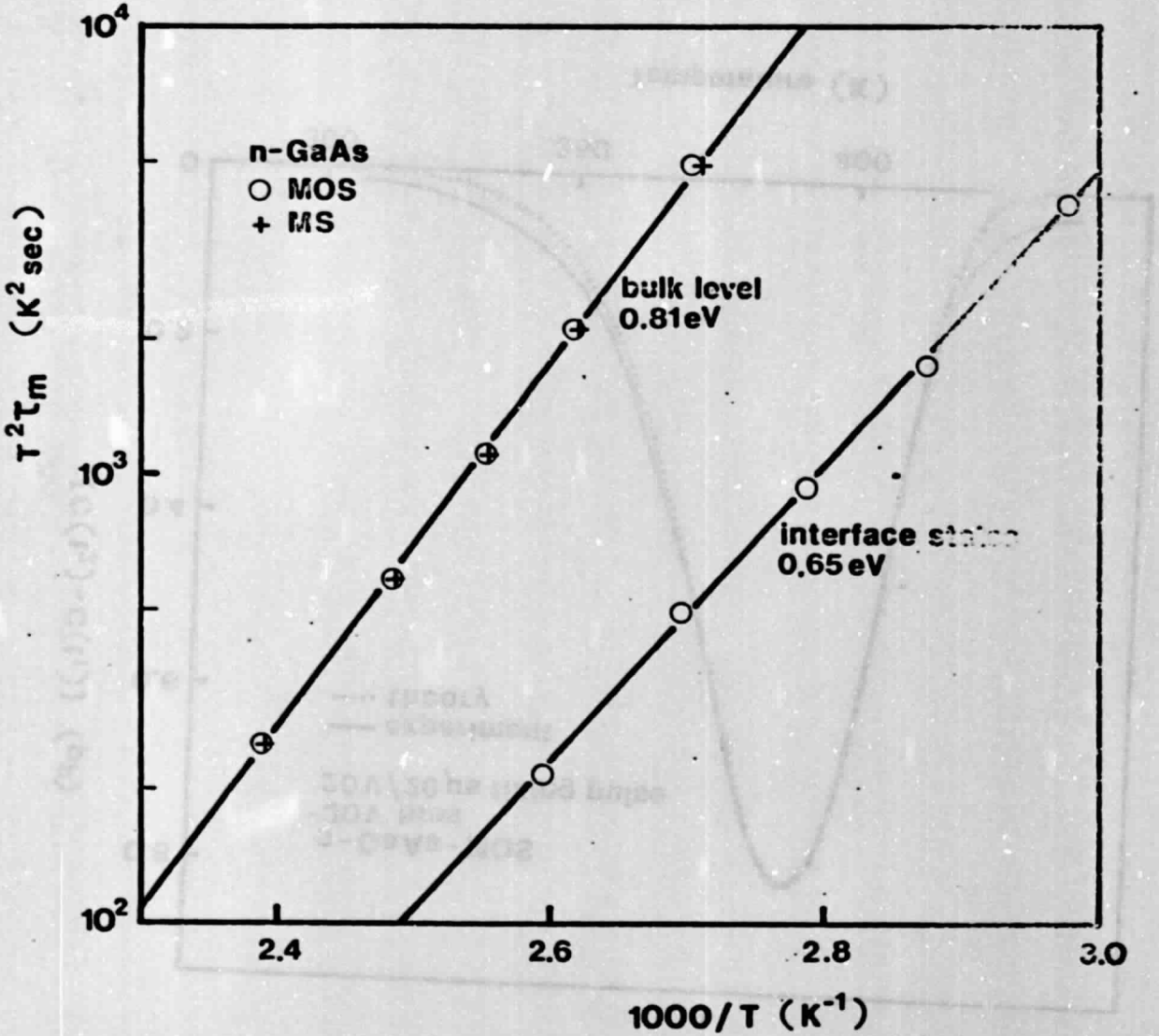
10^4
10^3
10^2
$T^2\tau_m$ (K^2 sec)
n-GaAs
○ MOS
+ MS
bulk level
0.81eV
interface state
0.65eV
2.4
2.6
2.8
3.0
1000/T (K^{-1})

Fig. 4

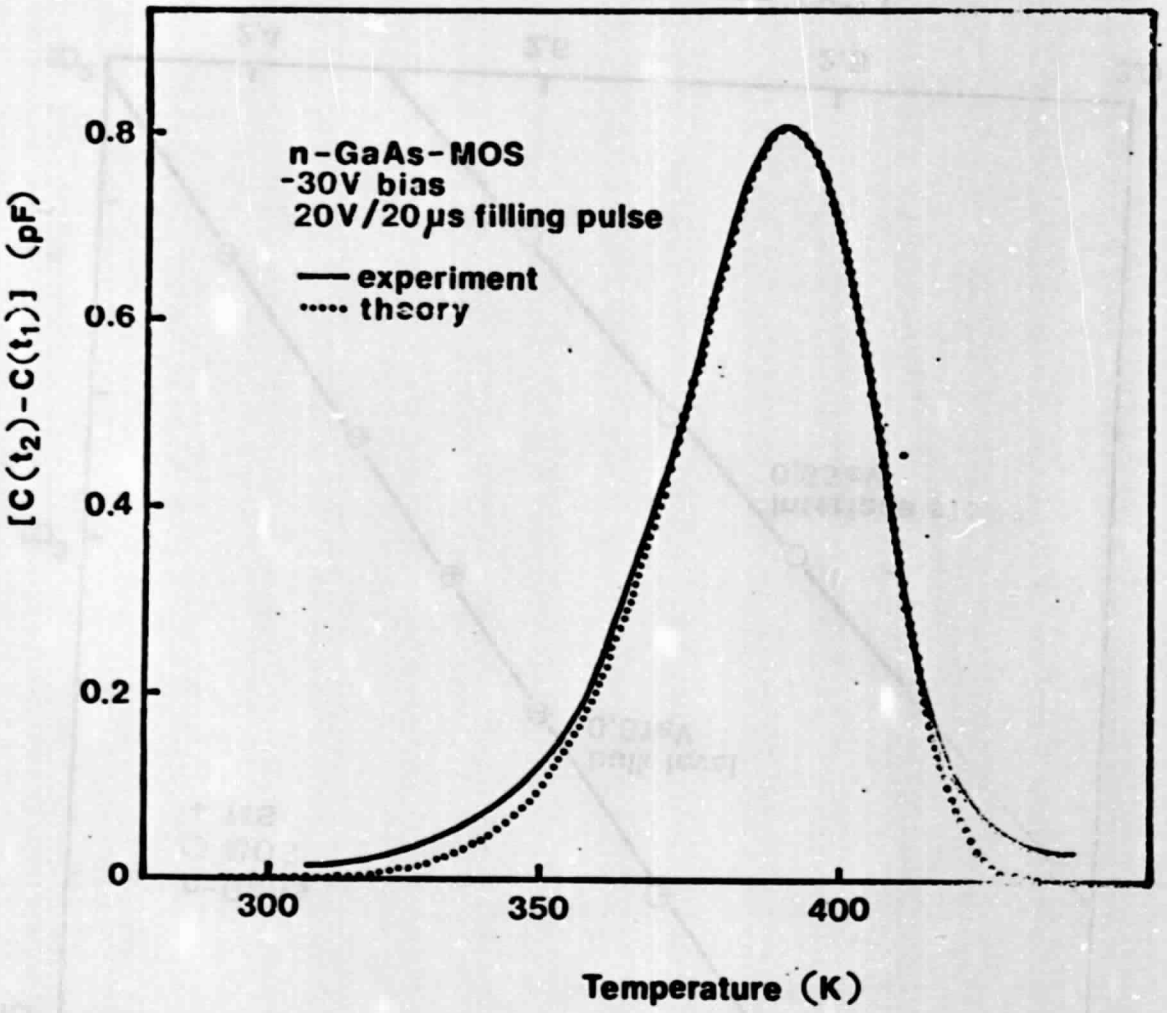
n-GaAs-MOS
-30V bias
20V/20μs filling pulse
experiment
theory
[C(t2)-C(t1)] (pF)
0.8
0.6
0.4
0.2
0
300
350
400
Temperature (K)

Fig. 5

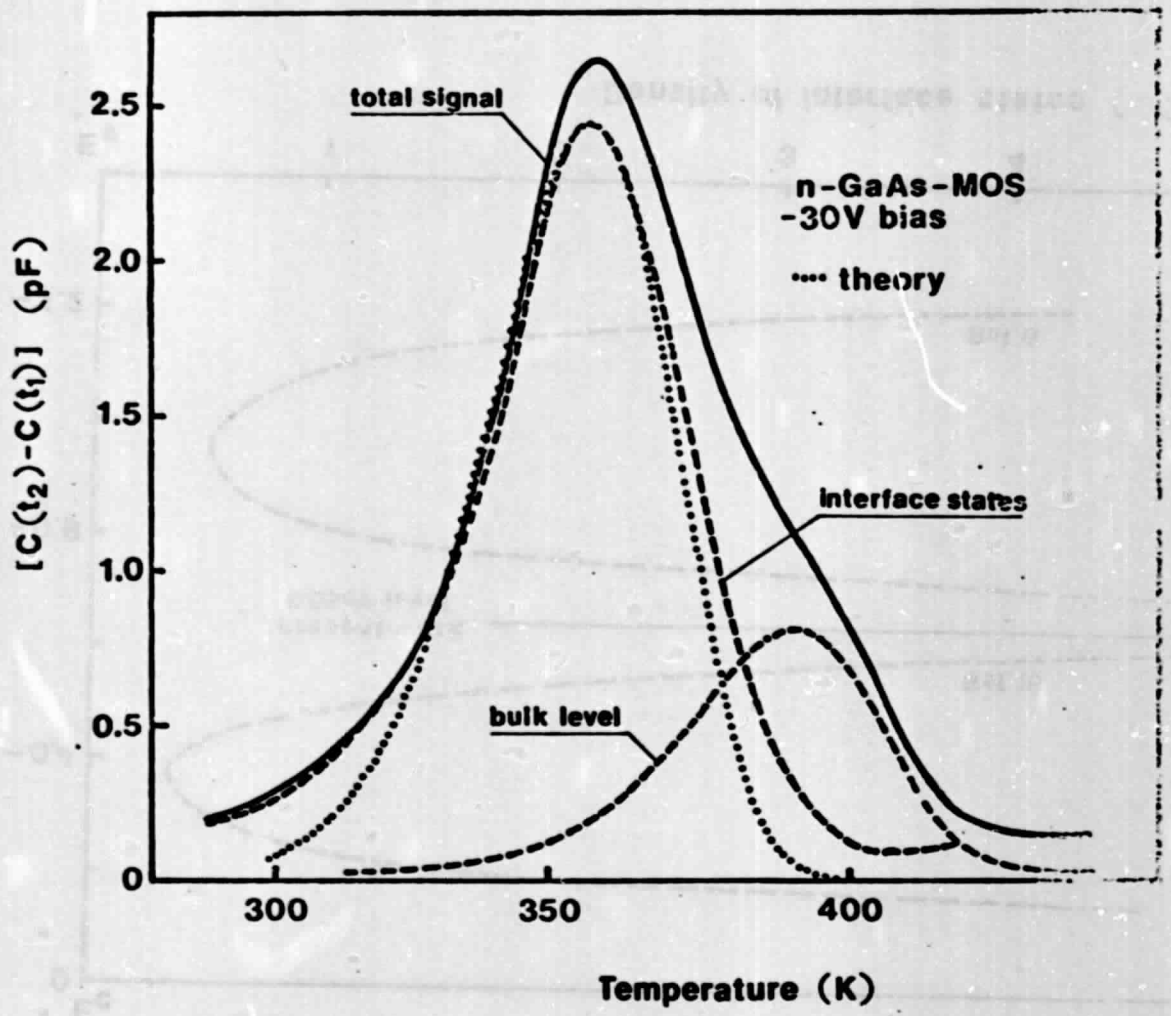
total signal
n-GaAs-MOS
-30V bias
···· theory
interface states
bulk level
2.5
2.0
1.5
1.0
0.5
0
300
350
400
[C(t2)-C(t1)] (pF)
Temperature (K)

Fig. 6

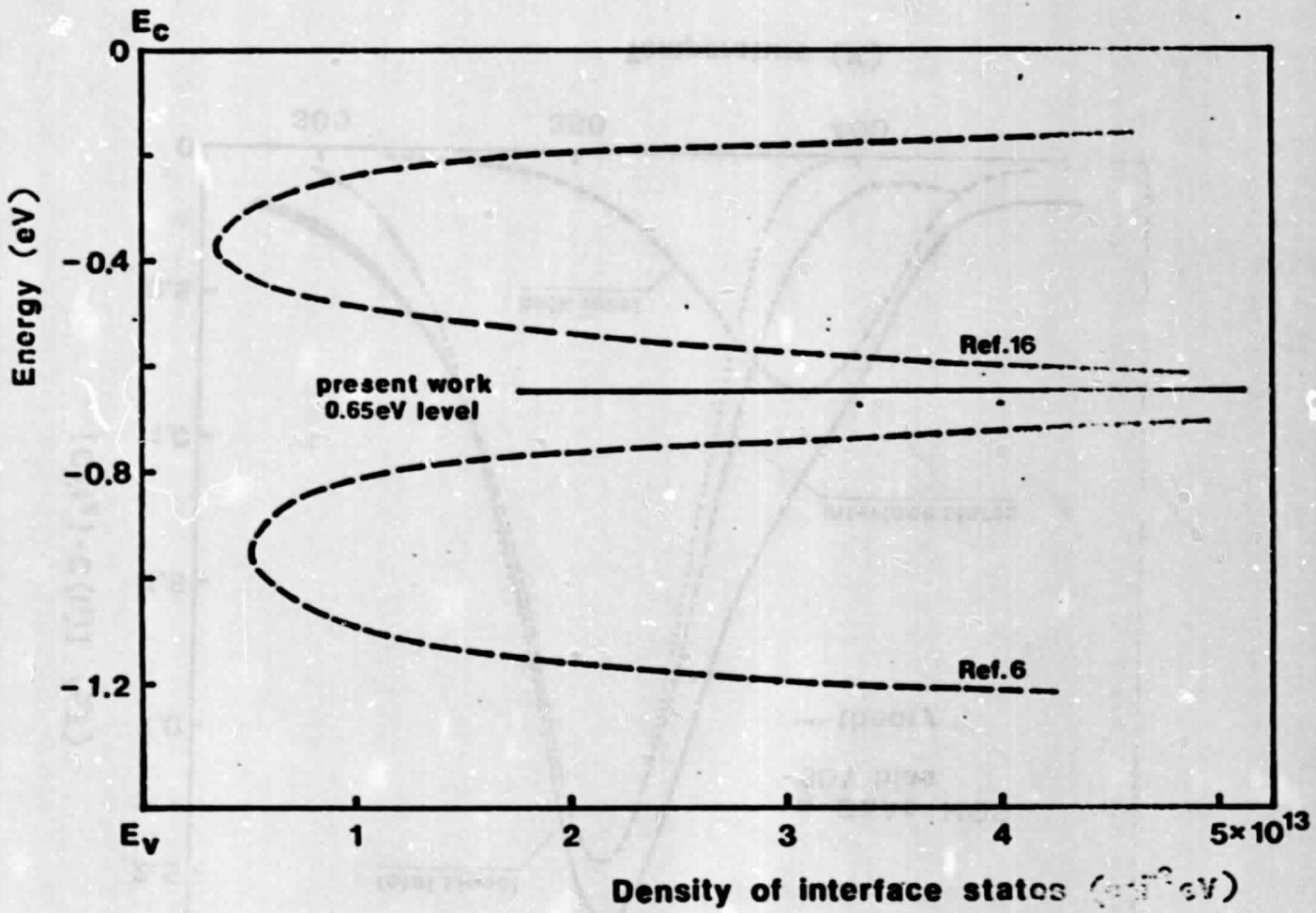
E_c
0
-0.4
-0.8
-1.2
Energy (eV)
Ref.16
present work
0.65eV level
Ref.6
E_v
1
2
3
4
5×10^{13}
Density of interface states

ELECTRON MOBILITY AND FREE-CARRIER ABSORPTION IN InP; DETERMINATION OF THE COMPENSATION RATIO

W. Walukiewicz,[a] J. Lagowski, L. Jastrzebski,[b] P. Rava
M. Lichtensteiger,[c] C. H. Gatos,[d] and H. C. Gatos
Department of Materials Science and Engineering
Massachusetts Institute of Technology
Cambridge, Massachusetts 02139

ABSTRACT

Theoretical and experimental studies of the electron mobility and the free-carrier absorption of n-type InP were carried out in the temperature range of 77-300°K. All major scattering processes and screening effects were taken into consideration. It was found that the experimental dependence of electron mobility and free-carrier absorption on temperature and/or on carrier concentration can be consistently explained only when the effect of compensation is quantitatively taken into account. Convenient procedures are presented for the determination of the compensation ratio from the values of electron mobility and from the free-carrier absorption coefficient. The high contribution of optical phonon scattering in InP limits the applicability of the free-carrier absorption approach to electron concentration $n > 10^{17}cm^{-3}$. Electron mobility, however, can be reliably employed for the determination of the compensation ratio for $n > 10^{17}cm^{-3}$ at 300°K and $n > 10^{15}cm^{-3}$ at 77°K.

Journal of Applied Physics, in press.

I. INTRODUCTION

The compensation ratio is a very important parameter in the characterization of semiconducting materials. In recent years a number of procedures for evaluating this parameter in n-type semiconductors have been proposed. Some of these methods require extensive low temperature measurements and therefore are of limited practical importance.[1,2] The simplest and most widely used methods are based on the finding that kinetic phenomena such as electron mobility and/or free electron absorption depend on the total concentration of ionized impurities and, thus, on the compensation ratio.[3] For III-V compound semiconductors, the relevant theoretical analysis is complicated, since a relaxation time cannot be introduced except at very low temperatures. Accordingly, one has to rely on numerical calculations, including the compensation ratio, as a parameter.

This type of theoretical analysis of electron mobility and free-carrier absorption in n-type GaAs has been carried out recently in conjunction with an experimental study.[4] It has led to the formulation of practical procedures for the determination of the compensation ratio over a wide range of free electron concentrations. In the present study this approach is extended to InP, which recently has been receiving a great deal of attention as a potential substitute for GaAs in a number of microwave and optoelectronic applications.

The electron mobility in InP has been extensively studied, both theoretically and experimentally.[5-22] Thus, it has been shown that theoretical mobility limits agree with experimental data obtained with good quality uncompensated material.[20] Only a limited effort has been directed toward the study of free-carrier absorption in InP. There are just two pertinent experimental reports.[16,17] Furthermore, the materials parameters used in the

theoretical analysis of free-carrier absorption[18] have since been revised.

In the present calculations of the electron mobility and the free-carrier absorption a set of up-dated materials parameters is employed. The mobility calculations are based on a variational procedure[23] while the free-carrier absorption is calculated utilizing the expression of ref. 18, derived with a perturbation theory.

II. THEORETICAL CONSIDERATIONS

Electron mobility and free-carrier absorption depend on the band structure parameters and the scattering processes which determine the momentum relaxation of the free electrons. In III-V compound semiconductors the following scattering mechanisms play the most important role: electron-optical phonon, electron-acoustical phonon (including piezoelectric scattering) and electron-ionized impurity scattering. For InP the conduction band parameters and the electron-phonon coupling constants are fairly well known. Thus, InP is a direct and wide gap semiconductor (E_g ~ 1.35 eV at 300°K) with the conduction band minimum located at the Γ point of the Brillouin zone. The conduction band dispersion relation is well described within the spherical and parabolic approximation with a constant effective mass m*. This approximation allows direct application of the relationships for the mobility and free-carrier absorption in the form given in ref. 4.

All major scattering mechanisms, namely polar optical, deformation potential acoustical and ionized impurity, are included in these calculations. The piezoelectric acoustical phonon scattering is neglected since in InP the piezoelectric coupling parameter p^2 is ~16 times smaller than that of GaAs in which the piezoelectric scattering contribution to the room temperature mobility does not exceed 2%. The deformation potential-optical phonon scattering (not considered in ref. 4) will also be neglected here, since in most

compound semiconductors this scattering process is efficiently masked by the much stronger polar interaction.

The values of InP parameters used in the computations are given in Table I. It was assumed that all parameters other than the effective mass are temperature independent in the temperature range considered.

A. Electron Mobility

Due to the large optical phonon energy the electron-optical phonon scattering is an inelastic process and thus the relaxation time approximation cannot be used in the mobility calculations.[19-22] Accordingly, the variational procedure in the form given in ref. 23 with modifications introduced for free-electron screening effects is used. This procedure does not invoke the Matthiessen rule (according to which average macroscopic mobilities resulting from different scattering mechanisms are summarized, $1/\mu = \Sigma_i 1/\mu_i$) since in III-V compounds it leads to unacceptable errors.[4,19] Thus, in order to find the electron mobility as a function of free carrier concentration and compensation ratio it is necessary to perform numerical computations.

Figure 1 shows the calculated temperature dependence of the total electron mobility in InP with two different free electron concentrations. In addition, the temperature dependence of the two most important component mobilities is plotted. The ionized impurity contribution to the total mobility rapidly increases with increasing temperature. For the material with the lower dopant concentration the room temperature mobility is practically insensitive to ionized impurity scattering and its value is determined mainly by optical phonon scattering. In such a case, more reliable results for the compensation ratio can be obtained from the mobility value at the liquid nitrogen temperature.

The calculated room and liquid nitrogen temperature mobilities as a function of

free-carrier concentrations and compensation ratio are presented in Tables II and III.

The results for the lattice mobility limits obtained in the present study, i.e., ~3 x 10^5 cm^2/Vs at liquid nitrogen and ~4800 cm^2/Vs at room temperature, are in good agreement with those reported in ref. 19, i.e., ~3.2 x 10^5 and ~4700 cm^2/Vs, respectively, where an iterative procedure was used to obtain numerical solution of the Boltzmann equation and the same set of InP parameters as in the present calculations.

B. Free Electron Absorption

In contrast to the mobility, the free-carrier absorption may be represented as a sum of absorption coefficients associated with various scattering processes considered in the present paper; the total absorption coefficient is:

$$\alpha_i = \alpha_{op} + \alpha_{ac} + \alpha_{imp} \quad (1)$$

where α_{op}, α_{ac} and α_{imp} are the absorption coefficients associated with electron-optical phonon, electron-acoustical phonon and electron-ionized impurity interaction, respectively.

Numerical calculations of absorption coefficients were carried out employing appropriate expressions for the component absorption coefficients as given in refs. 18 or 4. The results for room and liquid nitrogen temperatures at a wavelength of 10 μm are given in Tables II and III, respectively.

As in the case of GaAs,[4] it can be shown that the component absorption coefficients at any wavelength, λ, can be obtained from the following approximate relationships:

$$\alpha_{op,\lambda} = \alpha_{op,\lambda_o} (\lambda/\lambda_o)^{2.5} \quad (2a)$$

$$\alpha_{imp,\lambda} = \alpha_{imp,\lambda_o} (\lambda/\lambda_o)^{3.5} \quad (2b)$$

$$\alpha_{ac,\lambda} = \alpha_{ac,\lambda_o} (\lambda/\lambda_o)^{1.5} \quad (2c)$$

This approximation is valid for n-type InP with free-carrier concentrations up to about $10^{18}cm^{-3}$ and for wavelengths $\lambda < 10$ μm. The above expressions are valid at larger wavelengths for lower dopant concentrations.

The results of Tables II and III can be used to determine the absorption coefficient in samples with a given ionized impurity concentration, namely

$$\alpha_{exp} = \frac{N_{imp}}{n} \alpha_{imp} + \alpha_{op} + \alpha_{ac} \qquad (3)$$

where N_{imp} is the total concentration of ionized impurities and n is the free electron concentration. Using the above relation one can express the compensation ratio in terms of the experimental and theoretical component absorption coefficients

$$\theta = \frac{\alpha_{exp} - (\alpha_{op} + \alpha_{ac} + \alpha_{imp})}{\alpha_{exp} + \alpha_{imp} - (\alpha_{op} + \alpha_{ac})} \qquad (4)$$

where $\theta = N_A^-/N_D^+$, i.e., the ratio of the ionized acceptor to the ionized donor concentrations.

III. EXPERIMENTAL

Hall-effect measurements, conductivity and infrared absorption have been carried out on n-type InP samples cut from melt-grown single crystals with electron concentrations in the range of 3×10^{15} to $2.5 \times 10^{18}cm^{-3}$. Assessment of the sample homogeneity was found necessary in order to obtain consistent and meaningful results. The measurements carried out for this assessment, namely the carrier concentration profiling with IR laser scanning[28,29] and the Hall-constant measurements as a function of magnetic field up to 150 KOe, are presented in Appendix I. In considerable portions of melt-grown crystals the spatial variation of the absorption coefficient, at $\lambda = 10.6$ μm was found to exceed 30% of the average value. In such inhomogeneous samples the Hall

constant exhibited an anomalous magnetic field dependence consistent with the Hall-effect analysis of Ref. 25. A reliable interpretation of electron mobility and free carrier absorption on the basis of average macroscopic values is not possible for inhomogeneous material. Accordingly, only selected samples with carrier concentration inhomogeneities not exceeding 10% and exhibiting the standard Hall constant dependence on magnetic field are considered in this study. For these samples, the electron mobility and electron concentration were obtained from conductivity and Hall-effect measurements. The saturation value of the Hall constant, in high magnetic field, at which the Hall factor, $r = 1$, was used to determine the electron concentration. In this way common ambiguities associated with the value of the Hall factor, r, were eliminated. The measured parameters of the samples employed are listed in Table IV.

A. Electron Mobility

In the present theoretical treatment, the electron drift mobility was taken as $\mu = \sigma/en$, where σ is the low DC electric field conductivity. Thus, a comparison between theory and experiment requires experimental data of drift mobility rather than of the commonly measured Hall-effect mobility, $\mu_H = r\mu$. Since the present measurements of the Hall constant, R_H, were determined in a high magnetic field, where $r = 1$, the electron concentration ($n = r/eR_H$) and the drift mobility can be reliably determined. The results on the room temperature mobility as a function of electron concentration are presented in Fig. 2, together with the theoretically calculated values for different compensation ratios, θ. It is seen that the presently determined mobility values are below the theoretical limit for uncompensated InP ($\theta = 0$). Utilizing Table III, the values of compensation ratios were determined for these samples and are given in Table IV.

The literature mobility data[5,10-15] plotted in Fig. 2 represent Hall mobilities, and thus it is not surprising that in the region of low electron concentrations, some values exceed slightly the limit of the drift mobility. According to theoretical considerations presented in ref. 26, the Hall factor, r, in pure InP at room temperature is about 1.25. With increasing electron concentration the value of r decreases, approaching r = 1 for degenerate material. Thus, for high electron concentrations, the Hall mobility approaches the drift mobility value, and the literature results fall below the theoretical curve corresponding to uncompensated material.

Mobility data at 77°K are given in Fig. 3. At this temperature the difference between the Hall-effect and drift mobility does not exceed 5%,[26] i.e., it is within the experimental accuracy of Hall-effect measurements. Thus, the present results and the literature data fall below the theoretical curve of $\theta = 0$ over the entire electron concentration range. The compensation ratios determined from Table III are given in Table IV. A comparison with the results obtained at 300°K shows that there is a noticeable increase in the compensation ratio at 77°K for the samples in which the electron concentration decreases at 77°K (samples 4, 5 and 7). For the other samples the differences in compensation ratio do not exceed the experimental error. However, it should be noted that for electron concentrations below 10^{16}, the mobility at 77°K is much more sensitive to ionized impurities than at 300°K.

The necessity to include the compensation ratio in the theoretical analysis of the mobility is especially evident in the dependence of mobility on temperature. Thus, in Fig. 4 the experimentally determined mobility is shown as a function of temperature for two InP samples with different free electron concentrations. The theoretical curves for uncompensated samples lie well above the experimental

values and exhibit a distinctly different temperature dependence. On the other hand, as shown in the same figure, there is a very reasonable agreement between theory and experiment if the compensation ratio is taken into account in the theoretical calculations.

It is of interest to note that, according to the present analysis, melt-grown InP exhibits much lower compensation than that encountered in melt-grown GaAs. This difference is evident in Fig. 5 where the normal range of N_{imp}/n is plotted as a function of electron concentration for commercially available high-quality GaAs[4] and for InP. In the low electron-concentration region the melt-grown GaAs is highly compensated, with a total concentration of ionized impurities exceeding by an order of magnitude the free carrier concentration. InP, on the other hand, even at low concentrations can be obtained by melt growth with a concentration of ionized impurities of the same order of magnitude as the electron concentration. This marked difference is probably related, in part, to the lower melting point of InP (1062°C for InP and 1238°C for GaAs) and thus to the lower concentration of native point defects; point defects in compound semiconductors are known to participate in the formation of compensation centers. Furthermore, the covalent radii of In and P differ by about 40%, whereas those of Ga and As are about the same; thus, a dopant impurity is more likely to occupy preferentially In or P sites in InP than Ga or As sites in GaAs (amphoteric or compensating doping).

B. Free Carrier Absorption

Room temperature IR absorption was determined from transmittance measurements employing a Fourier spectrometer. The absorption coefficient, α, is obtained from the relationship:

$$T = \frac{(1-R)^2 \exp(-\alpha d)}{1-R^2 \exp(-2\alpha d)} \qquad (5)$$

where T is the transmittance, d is the thickness of the sample, and R is the reflectance. Values of R as a function of wavelength, λ, for InP are given in Ref. 27.

The present experimental results on the absorption coefficient at $\lambda = 10$ μm together with those in Ref. 16 are presented in Fig. 6 as a function of electron concentration. The theoretical values of the total absorption coefficient and the absorption components associated with different scattering mechanisms are also shown in this figure. It is seen that the major contribution to free carrier absorption in InP is provided by optical phonon scattering. The ionized impurity scattering is of significance only at high concentrations, $n > 10^{17} cm^{-3}$.

As pointed out in Ref. 4, a comparison between the experimental and theoretical dependence of free carrier absorption on the electron concentration (for samples having different compensation ratios) can be achieved by reducing the experimental absorption coefficient, α_{exp}, to an absorption coefficient corresponding to zero compensation, $\alpha^*_{exp} \equiv \alpha_{exp} - (\frac{N_{imp}}{n} - 1)\alpha_{imp}$; which according to ref. (4) is:

$$\alpha^*_{exp} = \alpha_{exp} - \alpha_{imp} 2\theta/1-\theta \qquad (6)$$

The values of α^*_{exp} were calculated using the values of compensation ratio determined for each sample from its electron mobility (Table IV) and from the computed values of α_{imp} given in Table II. In Fig. 7, α^*_{exp} is plotted as a function of carrier concentration together with the theoretical dependence $\alpha_T(n)$. It is seen that good agreement is obtained between theoretical and experimental results.

Using Eq. (4) and the theoretical values of the absorption coefficient given in Table II, values of the compensation ratios for the samples investigated

were obtained. The results are summarized in Table IV. It is seen that the values obtained by the optical method are in satisfactory agreement with those determined from electron mobilities.

The theoretically calculated values of the absorption coefficient at 77°K are shown in Fig. 8 as a function of carrier concentration. A comparison with the room temperature results in Fig. 6 shows that the optical phonon contribution to the total absorption coefficient does not decrease significantly with decreasing temperature. Thus, low temperature IR absorption is not appreciably more sensitive to the ionized impurity scattering than room temperature absorption. This behavior is significantly different from that of the electron mobility discussed in the previous section. The optical phonon contribution to the total mobility decreases rapidly with decreasing temperature and thus the low temperature mobility is very sensitive to the ionized impurity scattering. This different behavior of two closely related processes can be explained as follows: At low temperatures when the optical phonon occupation number is very small the main contribution to electron optical phonon scattering consists of transitions in which optical phonons are emitted by electrons. In low DC fields phonon emission requires a transition of an electron from an occupied state at a given energy E to an empty state at an energy lower by the phonon energy, $\hbar\omega_o$. Such a process is hardly possible at low temperatures ($kT \ll \hbar\omega_o$) whereby the density of final unoccupied states is essentially negligible. Free carrier absorption involves additional interaction with an incident photon. Thus, even at low temperatures the photon emission is energetically possible provided that the energy of the absorbed photon, $h\nu$, is higher than the energy of the emitted phonon $\hbar\omega_o$.

IV. SUMMARY

The electron mobility and IR free electron absorption in n-type InP have been investigated theoretically and experimentally. Theoretical calculations of mobility based on a variational procedure agree very well with previously published results. The room temperature mobility in pure InP is dominated by optical phonon scattering, a contribution of less than 10% made by acoustic phonon scattering. On the other hand, the room temperature absorption coefficient of pure InP is entirely determined by electron-optical phonon interactions; the contribution from the other scattering processes is negligible. With increasing doping the ionized impurity contribution to the total scattering increases, which permits the ionized impurity concentration to be determined from the mobility and free carrier absorption measurements. At lower temperatures the optical phonon scattering contribution to the mobility decreases; thus, the interaction between electrons and ionized impurities becomes the main process controlling the electron mobility over a wide range of free electron concentrations.

In contrast, in free carrier absorption, the absorption coefficient resulting from the optical phonon scattering decreases slowly with decreasing temperature, and its value at liquid nitrogen temperature is smaller only by a factor of two than its room temperature value. A comparison of theory with experimental data showed that the experimental values of the room temperature mobility and of the free carrier absorption coefficient, as well as the temperature dependence of the mobility can be consistently explained if the compensation ratio of the investigated material is taken into account.

The tabulated values of electron mobilities and free carrier absorption coefficients provide a practical means for the determination of the compensation

ratio in n-type InP, with $n > 10^{17} cm^{-3}$ from room temperature measurements of either the mobility or the free carrier absorption coefficient. For free carrier concentrations ranging from 10^{14} to $10^{18} cm^{-3}$ the compensation ratio is determined from mobility measurements at the liquid nitrogen temperature.

As shown recently, under certain conditions the mobility calculations for n-type GaAs can be utilized to estimate minority carrier mobility in p-type GaAs.[30] This method can be directly applied to InP.

Finally, it was found that data on mobility in InP are very close to theoretical values obtained for uncompensated material; in contrast, for GaAs with similar free carrier concentrations the free carrier mobilities indicate compensation ratios in the range of 0.6 to 0.8.

ACKNOWLEDGEMENTS

This work was initiated with support from the Deputy for Electronic Technology of the U. S. Air Force. The authors acknowledge with gratitude the financial support of the National Aeronautics and Space Administration. They are also grateful to the administration of the Francis Bitter National Magnet Laboratory of M.I.T. for making possible the performance of the high magnetic field experiments.

Appendix I

ASSESSMENT OF HOMOGENEITY OF InP

The electron concentration profiles of InP samples were measured with the IR laser scanning technique.[28,29] The experimental arrangement consisted of a CO_2 laser (tunable from 9.2-11.8 μm), a stage with x-y motion, an optical system for monitoring the power and wavelength of the laser beam, and an IR detector. The optically flat wafer was mounted on the stage and the intensity of a collimated beam (~30 μm in diameter) passing through the wafer was measured as a function of the position along the sample. The IR transmission scans were converted into an absorption coefficient utilizing Eq. (3). The measurements were repeated for different wavelengths of the laser radiation in order to separate possible interference effects resulting from slight variations in wafer thickness.

The electron concentration profiles were determined from absorption coefficient profiles utilizing the tabulated theoretical values of the free carrier absorption coefficient. Typical results obtained with melt-grown InP are given in Fig. 9. It is seen that local changes in electron concentration are as high as $\pm$30% from the average value. Similar large fluctuations of carrier concentration were found in about 20% of the melt-grown InP crystals obtained from various sources. Reliable analysis of such inhomogeneous material on the basis of the average optical and electrical properties is not possible.

As shown in Fig. 10, inhomogeneous InP samples exhibit anomalous Hall constant dependence on the magnetic field: In samples 1 and 2 the Hall constant increases in high magnetic fields and in sample 3 it even passes through a minimum. In n-type homogeneous samples the Hall factor r (and

thus the Hall constant R = r/en) should decrease monotonically to the value of r = 1 (or R = 1/en) with increasing magnetic field.

This anomalous Hall constant behavior is in excellent agreement with a recent treatment of the Hall effect in inhomogeneous semiconductors[25] where it is shown that the standard analysis of DC conductivity and low magnetic field Hall constant applied to inhomogeneous material can lead to false mobility values noticeably exceeding theoretical limits. It should also be noted that the standard analysis of the average free carrier absorption and low field Hall constant leads for inhomogeneous samples to an IR absorption coefficient which is appreciably smaller than the theoretical value.

In the present study of the electron mobility and the free carrier absorption only selected samples were employed which exhibited standard Hall constant dependence on the magnetic field, and fluctuations of electron concentration not exceeding $\pm$10%.

REFERENCES

(a) On leave from Institute of Physics, Warsaw, Poland.

(b) Present address: RCA, David Sarnoff Research Center, Princeton, New Jersey 08540.

(c) Present address: Coulter Systems Corporation, Bedford, Mass. 01730.

(d) Present address: Brown University, Providence, R. I. 02192

1. A. Raymond, J. L. Robert and B. Pistoulet, Proc. VI Intern. Symp. on GaAs and Related Compounds, Edinburgh, Sept., 1976, edited by C. Hilsum (The Institute of Physics, London 1976). p. 105.
2. Takeshi Kamiya and Elmar Wagner, J. Appl. Phys. 48, 1928 (1977).
3. G. E. Stillman and C. M. Wolfe, Thin Solid Films 37, 69 (1976).
4. W. Walukiewicz, J. Lagowski, L. Jastrzebski, M. Lichtenstein and H. C. Gatos, J. Appl. Phys. 50, 899 (1979).
5. V. V. Galavanov and N. V. Siukaev, Phys. Stat. Sol. (b), 36, [illegible] (1970).
6. Ming-Jong Tsai and R. H. Bube, J. Appl. Phys. 49, 3392 (1978).
7. J. Leloup, H. Djerassi, J. H. Albany and J. B. Mullin, J. Appl. Phys. 49, 3359 (1978).
8. J. S. Barrera and R. J. Archer, IEEE Trans. Electron Devices, ED-22, 1023 (1975).
9. R. L. Henry and E. M. Swiggard, J. Electron. Materials 7, 647 (1978).
10. O. Röder, U. Heim and M. H. Pilkuhn, J. Phys. Chem. Solids 31, 2625 (1970).
11. R. C. Clarke, B. D. Joyce and W. H. E. Wilgoss, Sol. State Comm. 8, 1125 (1970).
12. G. G. Kovalevskaya and S. V. Slobodchikov, Phys. Stat. Sol. 30, 441 (1968).
13. J. Kudman and E. F. Steigmeier, Phys. Rev. 133, A1665 (1964).
14. D. Richman, Compound Semiconductors, Vol. 1, eds. R. K. Willardson and H. L. Goering, p. 214.

15. M. Glicksman and K. Weiser, J. Electrochem. Soc. 105, 729 (1958).

16. R. Newman, Phys. Rev. 111, 1518 (1958).

17. W. P. Dumke, M.R Lorenz and G. H. Pettit, Phys. Rev. B1, 4668 (1970).

18. E. Haga and H. Kimura, J. Phys. Soc. Japan 19, 658 (1964).

19. D. L. Rode in "Semiconductors and Semimetals", eds. R. K. Willardson and A. C. Beer, Academic Press, New York 1975, Vol. 10, Ch. 1.

20. D. L. Rode, Phys. Rev. B2, 1012 (1970).

21. D. L. Rode, Phys. Rev. B3, 3287 (1971).

22. B. R. Nag and G. M. Dutta, J. Phys. C 11, 219 (1978).

23. D. Howarth and E. H. Sondheimer, Proc. Phys. Soc. A219, 53 (1953).

24. J. M. Chamberlain, P. E. Simmonds, R. A. Stradling and C. C. Bradley, J. Phys. C 4, L38 (1971).

25. C. M. Wolfe and G. E. Stillman in ref. 19, Chap. 3.

26. D. L. Rode, Phys. Stat. Sol. (b) 55, 687 (1973).

27. B. O. Seraphin and H. E. Bennett in ref. 19, Vol. 3, Chap. 12.

28. D. L. Spears and A. J. Strauss, Solid State Research Report, Lincoln Laboratory, M.I.T., 3, 9 (1974).

29. L. Jastrzebski, J. Lagowski and H. C. Gatos, J. Electrochem. Soc. 126, 260 (1979).

30. W. Walukiewicz, J. Lagowski, L. Jastrzebski and H. C. Gatos, J. Appl. Phys. 50 5040 (1979).

Table I. InP parameters used in the present computations (after Ref. 7 and 10)

Low-freqency dielectric constant ε_o	12.38	
High-frequency dielectric constant ε_∞	9.55	
Optical-phonon energy $\hbar\omega_o$	42.8 meV	
Deformation potential, E_1	6.8 eV	
Longitudinal elastic constant, C_l	12.1×10^{11} dyne/cm^2	
Effective mass, m^*/m_o	0.082 (77°K)	0.078 (300°K)

Table IIa. Electron mobility, carrier concentration and compensation ratio in n-type InP at 300°K

Concentration	Compensation Ratio 0	.1	.2	.3	.4	.5	.6	.7	.75	.80	.85	.90	.95
	Electron Mobility (cm^2/Vsec)												
$1.0x10^{15}$	4710	4690	4660	4620	4570	4510	4410	4270	4160	4020	3820	3490	2900
1.5	4670	4630	4590	4540	4480	4390	4270	4090	3970	3800	3560	3210	2610
2	4640	4600	4550	4490	4410	4300	4160	3960	3810	3630	3380	3010	2420
3	4570	4510	4450	4370	4270	4140	3970	3730	3570	3360	3090	2720	2150
4	4520	4450	4370	4280	4160	4010	3820	3560	3380	3170	2900	2530	1980
5	4460	4390	4300	4190	4060	3900	3690	3410	3230	3020	2750	2380	1840
6	4420	4340	4240	4120	3980	3810	3590	3300	3120	2900	2620	2270	1740
7	4380	4290	4180	4060	3910	3730	3500	3200	3010	2790	2520	2170	1650
8	4330	4230	4120	3990	3830	3640	3410	3110	2920	2700	2440	2090	1570
9	4300	4200	4080	3940	3780	3580	3340	3030	2850	2630	2360	2020	1510
$1.0x10^{16}$	4250	4140	4010	3870	3700	3500	3250	2950	2760	2550	2290	1950	1450
1.5	4080	3950	3800	3640	3460	3240	2990	2690	2500	2300	2044	1720	1240
2	3960	3820	3660	3480	3290	3070	2810	2510	2330	2120	1880	1560	1100
3	3770	3610	3440	3250	3050	2820	2570	2270	2100	1900	1660	1360	918
4	3630	3460	3280	3090	2880	2660	2400	2110	1940	1750	1510	1220	800
5	3530	3350	3170	2970	2770	2540	2290	2000	1830	1640	1410	1120	718
6	3440	3270	3080	2880	2670	2440	2190	1900	1740	1550	1320	1040	654
7	3370	3190	3000	2800	2590	2360	2120	1830	1660	1480	1250	973	604
8	3310	3130	2940	2730	2530	2300	2050	1770	1600	1410	1190	920	563
9	3260	3070	2880	2680	2470	2250	2000	1710	1550	1360	1140	875	530
$1.0x10^{17}$	3220	3030	2830	2630	2420	2200	1950	1660	1500	1320	1100	835	501
1.5	3090	2900	2700	2490	2280	2060	1800	1520	1360	1180	970	723	423
2	2960	2760	2560	2350	2140	1910	1660	1370	1210	1040	839	611	345
3	2840	2640	2430	2210	1990	1750	1500	1220	1060	896	712	507	277
4	2770	2560	2340	2120	1890	1650	1400	1120	967	806	633	444	239
5	2720	2500	2270	2050	1820	1570	1320	1040	896	741	577	400	213
6	2680	2450	2220	1990	1760	1510	1260	987	844	694	536	369	194
7	2650	2410	2180	1940	1710	1460	1210	942	802	657	505	346	181
8	2620	2380	2140	1900	1660	1420	1160	900	764	623	477	325	169
9	2590	2350	2110	1860	1630	1380	1130	867	733	596	455	309	160
$1.0x10^{18}$	2570	2320	2080	1830	1590	1350	1100	839	708	573	436	295	152
1.5	2470	2210	1960	1710	1460	1220	979	737	617	495	373	250	128
2	2390	2130	1870	1620	1380	1140	904	674	561	448	336	224	113
3	2290	2010	1750	1500	1260	1030	811	598	495	393	293	194	98
4	2210	1930	1670	1420	1190	965	755	553	456	361	268	177	89
5	2150	1880	1610	1360	1140	920	717	523	431	340	252	166	83
6	2100	1830	1560	1320	1100	886	687	501	411	325	241	158	79
7	2070	1790	1530	1290	1070	861	667	484	398	314	232	152	76
8	2040	1760	1500	1260	1040	838	647	470	386	304	225	148	74
9	2010	1740	1480	1240	1020	821	635	462	378	296	219	144	72
$1.0 x10^{19}$	1990	1710	1460	1230	1010	809	624	452	370	289	215	141	71

Table IIb. Free carrier absorption

Concentration cm^{-3}	300°K, $m^* = 0.078$			77°K, $m^* = 0.082$		
	α_{imp}	α_{ac}	α_{op}	α_{imp}	α_{ac}	α_{op}
1.0×10^{16}	0.004	0.034	0.623	0.003	0.005	0.320
1.5	0.008	0.052	0.932	0.007	0.008	0.476
2	0.014	0.069	1.239	0.012	0.011	0.629
3	0.031	0.104	1.850	0.028	0.016	0.928
4	0.056	0.139	2.456	0.048	0.022	1.217
5	0.086	0.173	3.051	0.075	0.028	1.503
6	0.123	0.208	3.646	0.106	0.033	1.780
7	0.167	0.243	4.240	0.143	0.039	2.053
8	0.217	0.278	4.815	0.185	0.045	2.321
9	0.273	0.313	5.397	0.232	0.050	2.588
1.0×10^{17}	0.314	0.325	5.578	0.284	0.056	2.849
1.5	0.690	0.491	8.227	0.617	0.086	4.127
2	1.201	0.660	10.79	1.066	0.117	5.366
3	2.602	1.005	15.75	2.296	0.181	7.793
4	4.474	1.360	20.52	3.949	0.250	10.19
5	6.790	1.726	25.16	6.009	0.322	12.60
6	9.510	2.100	29.65	8.460	0.398	15.02
7	12.64	2.488	34.11	11.27	0.476	17.41
8	16.13	2.879	38.44	14.49	0.560	19.90
9	20.00	3.285	42.75	18.05	0.646	22.38
1.0×10^{18}	24.22	3.699	47.01	21.96	0.736	24.89
1.5	50.28	5.912	67.80	46.69	1.229	37.69
2	83.91	8.354	88.02	78.85	1.798	50.91
3	170.3	13.87	127.0	165.13	3.147	78.60
4	276.7	20.12	164.1	276.8	4.751	98.46
5	396.1	26.98	199.6	405.0	6.57	118.6
6	522.8	34.34	233.4	533.3	8.527	137.7

Table III. Computed values of electron mobility in n-type InP at 77°K

Concentration	Compensation Ratio: 0	.1	.2	.3	.4	.5	.6	.7	.75	.8	.85	.9	.95
	Electron Mobility ($cm^2/Vsec$)												
$1.0x10^{13}$	$3.06x10^5$	$2.98x10^5$	$2.88x10^5$	$2.77x10^5$	$2.63x10^5$	$2.46x10^5$	$2.25x10^5$	$1.99x10^5$	$1.83x10^5$	$1.64x10^5$	$1.42x10^5$	$1.15x10^5$	$8.01x10^4$
1.5	2.91	2.80	2.68	2.54	2.39	2.20	1.98	1.72	1.56	1.39	1.19	$9.58x10^4$	6.64
2	2.77	2.65	2.52	2.37	2.20	2.01	1.79	1.53	1.39	1.23	1.05	8.41	5.78
3	2.56	2.42	2.27	2.11	1.94	1.74	1.53	1.30	1.17	1.03	$8.76x10^4$	6.97	4.72
4	2.38	2.24	2.08	1.92	1.75	1.56	1.36	1.15	1.03	$9.05x10^4$	7.68	6.09	4.05
5	2.25	2.09	1.94	1.77	1.61	1.43	1.24	1.04	$9.33x10^4$	8.19	6.92	5.47	3.58
6	2.13	1.98	1.82	1.66	1.49	1.32	1.15	$9.60x10^4$	8.60	7.54	6.36	5.00	3.22
7	2.03	1.87	1.72	1.56	1.40	1.24	1.07	8.96	8.02	7.02	5.91	4.62	2.94
8	1.92	1.77	1.62	1.47	1.31	1.16	1.00	8.35	7.47	6.52	5.48	4.26	2.68
9	1.87	1.71	1.56	1.41	1.26	1.11	$9.60x10^4$	8.00	7.15	6.23	5.23	4.04	2.51
$1.0x10^{14}$	$1.80x10^5$	$1.65x10^5$	$1.50x10^5$	$1.35x10^5$	$1.21x10^5$	$1.06x10^5$	$9.16x10^4$	$7.62x10^4$	$6.81x10^4$	$5.93x10^4$	$4.96x10^4$	$3.81x10^4$	$2.35x10^4$
1.5	1.55	1.41	1.27	1.14	1.02	$8.91x10^4$	7.65	6.33	5.63	4.87	4.02	3.03	1.80
2	1.38	1.25	1.13	1.01	$8.97x10^4$	7.85	6.72	5.53	4.89	4.20	3.44	2.55	1.48
3	1.17	1.06	$9.49x10^4$	$8.46x10^4$	7.50	6.33	5.55	4.52	3.97	3.37	2.71	1.96	1.10
4	1.04	$9.36x10^4$	8.39	7.47	6.60	5.72	4.84	3.90	3.40	2.86	2.27	1.62	$8.95x10^3$
5	$9.46x10^4$	8.50	7.60	6.75	5.95	5.14	4.32	3.45	2.99	2.50	1.97	1.39	7.58
6	8.76	7.86	7.02	6.22	5.47	4.71	3.93	3.12	2.69	2.34	1.75	1.23	6.62
7	8.21	7.36	6.56	5.80	5.09	4.36	3.63	2.86	2.46	2.03	1.58	1.10	5.91
8	7.74	6.93	6.17	5.44	4.76	4.07	3.37	2.64	2.26	1.86	1.44	1.00	5.33
9	7.36	6.58	5.85	5.15	4.49	3.83	3.16	2.46	2.10	1.72	1.33	$9.20x10^3$	4.88
$1.0x10^{15}$	7.04	6.29	5.58	4.91	4.27	3.63	2.98	2.31	1.97	1.61	1.24	8.53	4.51
1.5	5.87	5.22	4.60	4.01	3.46	2.90	2.35	1.80	1.52	1.23	$9.37x10^3$	6.37	3.33
2	5.16	4.56	4.00	3.47	2.97	2.47	1.98	1.50	1.26	1.01	7.67	5.18	2.70
3	4.27	3.74	3.25	2.79	2.36	1.95	1.54	1.15	$9.58x10^3$	$7.67x10^3$	5.77	3.87	2.00
4	3.72	3.25	3.80	2.39	2.01	1.64	1.29	$9.56x10^3$	7.93	6.32	4.74	3.17	1.63
5	3.33	2.89	2.48	2.11	1.76	1.43	1.12	8.24	6.82	5.42	4.05	2.71	1.39
6	3.05	2.64	2.26	1.90	1.59	1.28	1.00	7.34	6.06	4.81	3.59	2.39	1.23
7	2.82	2.43	2.07	1.74	1.45	1.67	$9.07x10^3$	6.63	5.47	4.34	3.23	2.15	1.10
8	2.63	2.26	1.92	1.61	1.34	1.07	8.34	6.08	5.01	3.97	2.95	1.96	1.01
9	2.48	2.13	1.80	1.51	1.25	1.00	7.76	5.65	4.65	3.68	2.74	1.82	$9.30x10^2$
$1.0x10^{16}$	$2.35x10^4$	$2.01x10^4$	$1.70x10^4$	$1.42x10^4$	1.17	$9.39x10^3$	$7.26x10^3$	$5.28x10^3$	$4.34x10^3$	$3.43x10^3$	$2.53x10^3$	$1.70x10^3$	$8.66x10^2$
1.5	1.92	1.63	1.37	1.14	$9.32x10^3$	7.42	5.70	4.12	3.38	2.67	1.98	1.31	6.67
2	1.67	1.41	1.18	$9.73x10^3$	7.95	6.31	4.83	3.48	2.86	2.25	1.67	1.10	5.58
3	1.38	1.15	$9.55x10^3$	7.86	6.39	5.05	3.86	2.77	2.27	1.78	1.32	$8.69x10^2$	4.38
4	1.20	1.00	8.30	6.81	5.52	4.36	3.32	2.38	1.95	1.53	1.13	7.42	3.73
5	1.08	$9.04x10^3$	7.48	6.12	4.96	3.91	2.97	2.13	1.74	1.36	1.00	6.60	3.31
6	1.00	8.34	6.89	5.64	4.56	3.59	2.73	1.95	1.59	1.25	$9.20x10^2$	6.03	3.02
7	$9.36x10^3$	7.79	6.43	5.25	4.24	3.34	2.53	1.81	1.48	1.16	8.53	5.58	2.79
8	8.68	7.22	5.96	4.87	3.94	3.10	2.36	1.69	1.38	1.08	7.99	5.24	2.62
9	8.44	7.02	5.78	4.72	3.81	2.99	2.27	1.62	1.32	1.03	7.59	4.97	2.48
$1.0x10^{17}$	8.08	6.71	5.53	4.51	3.64	2.85	2.16	1.54	1.26	$9.84x10^2$	7.23	4.72	2.35
1.5	6.92	5.73	4.71	3.84	3.09	2.42	1.83	1.30	1.06	8.29	6.08	3.97	1.97
2	6.22	5.15	4.22	3.44	2.76	2.16	1.63	1.16	$9.45x10^2$	7.38	5.40	3.52	1.75
3	5.38	4.45	3.65	2.96	2.38	1.86	1.40	$9.96x10^2$	8.09	6.31	4.62	3.01	1.49
4	4.90	4.04	3.31	2.69	2.16	1.68	1.27	8.99	7.30	5.69	4.16	2.71	1.34
5	4.63	3.82	3.12	2.53	2.03	1.58	1.19	8.43	6.84	5.33	3.90	2.53	1.25
6	4.31	3.55	2.91	2.36	1.89	1.47	1.11	7.86	6.38	4.97	3.63	2.36	1.17
7	4.09	3.38	2.76	2.24	1.79	1.40	1.05	7.46	6.05	4.72	3.45	2.24	1.11
8	3.96	3.27	2.67	2.16	1.73	1.35	1.02	7.20	5.84	4.55	3.33	2.16	1.07
9	3.88	3.19	2.61	2.11	1.69	1.32	$9.91x10^2$	7.01	5.68	4.42	3.23	2.10	1.04
$1.0x10^{18}$	3.74	3.07	2.51	2.04	1.63	1.27	9.57	6.78	5.48	4.28	3.12	2.03	1.01
1.5	3.37	2.79	2.26	1.83	1.47	1.14	8.61	6.12	4.98	3.85	2.81	1.82	$9.00x10^1$
2	3.71	2.61	2.12	1.72	1.38	1.09	8.02	5.79	4.64	3.63	2.64	1.67	8.50
3	2.70	2.37	2.00	1.48	1.34	$9.16x10^2$	7.51	5.33	4.34	3.34	2.36	1.59	7.60

Table IV. Compensation ratios determined from mobility and IR absorption measurements

Sample No.	Electron concentration, cm^{-3} 300°K	77°K	Electron mobility, cm^2/Vs 300°K	77°K	Compensation ratio, θ mobility 300°K	77°K	absorption 300°K
1	$1.9x10^{15}$	$1.9x10^{15}$	3950	20000	0.5[a]		
2	$3.5x10^{15}$	$3.0x10^{15}$	4340	30500	0.23	0.22	-
3	$4.2x10^{15}$	$3.6x10^{15}$	3850	18500	0.57	0.48	-
4	$1.1x10^{16}$	$7.0x10^{15}$	2220	5150	0.86	0.76	-
5	$5.7x10^{16}$	$3.9x10^{16}$	2800	3850	0.35	0.56	-
6	$6.3x10^{16}$	$4.6x10^{16}$	2710	3740	0.37	0.54	-
7	$3.3x10^{17}$	$3.3x10^{17}$	2130	2210	0.33	0.40	0.38
8	$4.1x10^{17}$	$3.2x10^{17}$	2390	2970	0.17	0.29	0.29
9	$7.0x10^{17}$	$6.6x10^{17}$	2050	2100	0.27	0.34	0.4
10	$8.0x10^{17}$	$8.0x10^{17}$	1800	1650	0.36*		
11	$2.45x10^{18}$	$2.4x10^{18}$	1620	1650	0.28	0.3	0.31

[a] Compensation determined from mobility vs. temperature.

FIGURE CAPTIONS

Figure 1. Theoretical temperature dependence of electron mobility in uncompensated InP (see text).

Figure 2. Theoretical (solid lines) and experimental values of mobility at 300°K as a function of electron concentration in n-type InP for various compensation ratios; + - present results (drift mobility); other experimental results correspond to measured Hall mobility; I - ref. 5; o - Ref. 10; ▲ - Ref. 11; x - Ref. 12; ▽ - Ref. 13; ● - Ref. 14; △ - Ref. 15.

Figure 3. Theoretical (solid lines) and experimental values of mobility at 77°K as a function of electron concentration in n-type InP for various compensation ratios; + - present results (drift mobility); other experimental points correspond to reported Hall mobility values: I - Ref. 5; ■ - Ref. 9, ▲ - Ref. 11; ▽ - Ref. 13; ● - Ref. 14; △ - Ref. 15.

Figure 4. Experimental (+) and theoretical (lines) values of electron mobility in n-type InP as a function of temperature. Dashed lines correspond to uncompensated material. Solid lines represent electron mobilities calculated using a compensation ratio Θ independent of temperature.

Figure 5. Normal range of N_{imp}/n as a function of electron concentration in available melt-grown InP and GaAs (see text).

Figure 6. Theoretical and experimental values of the room temperature (300°K) absorption coefficient as a function of electron concentration in InP (for λ = 10 μm. ● - present results; x - Ref. 16.

Figure 7. Theoretical (solid line) and experimental values) obtained in present study) of the absorption coefficient reduced to zero compensation (see text).

Figure 8. Theoretical and experimental (Ref. 16) values of low temperature (77°K) free carrier absorption coefficient in n-type InP.

Figure 9. Typical electron concentration microprofile of InP obtained with scanning IR absorption.

Figure 10. Hall constant dependence on magnetic field for inhomogeneous n-type InP.

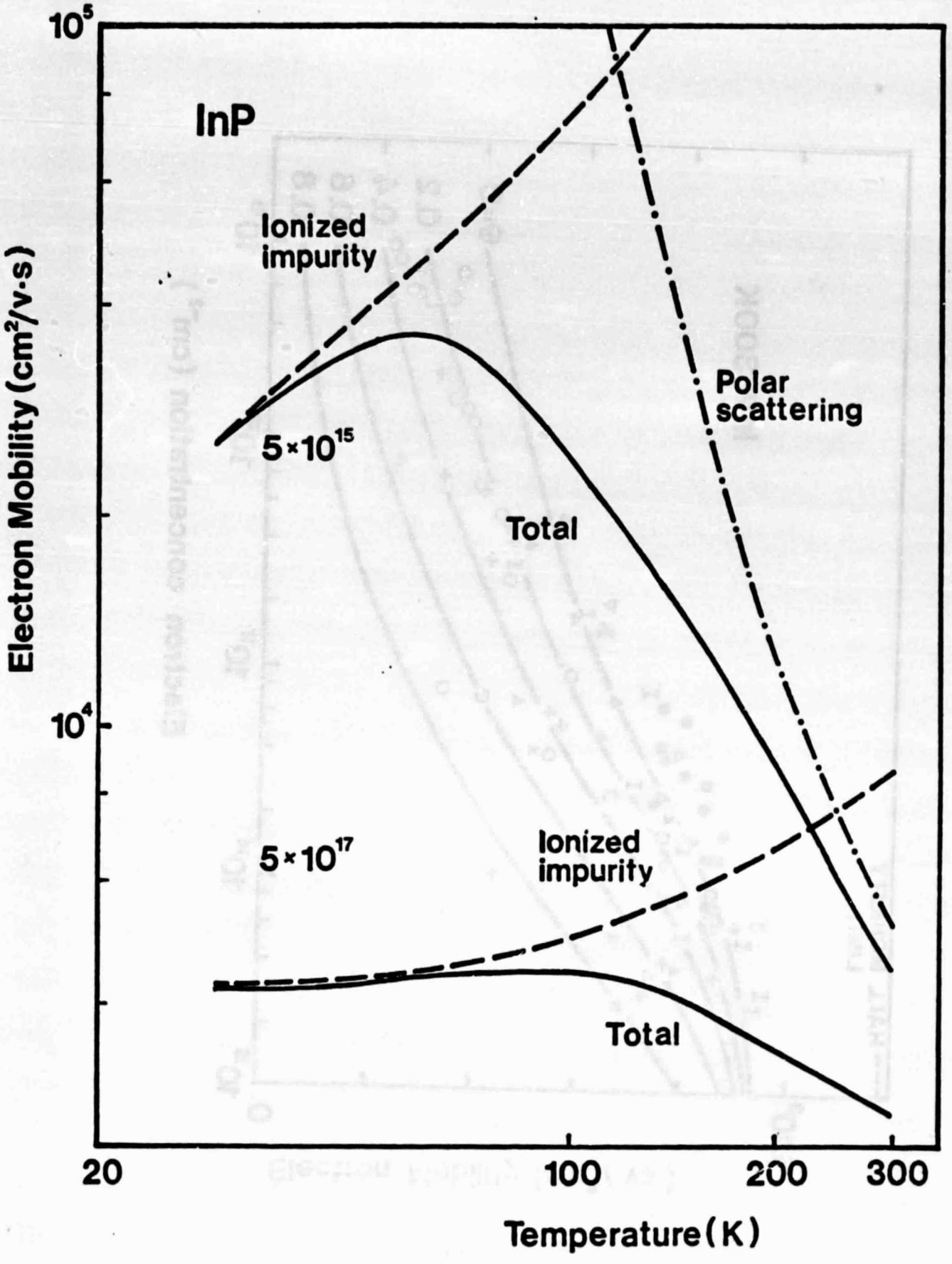
InP
Ionized impurity
Polar scattering
5×10^15
Total
5×10^17
Ionized impurity
Total
Electron Mobility (cm²/v·s)
10^5
10^4
20
100
200
300
Temperature (K)

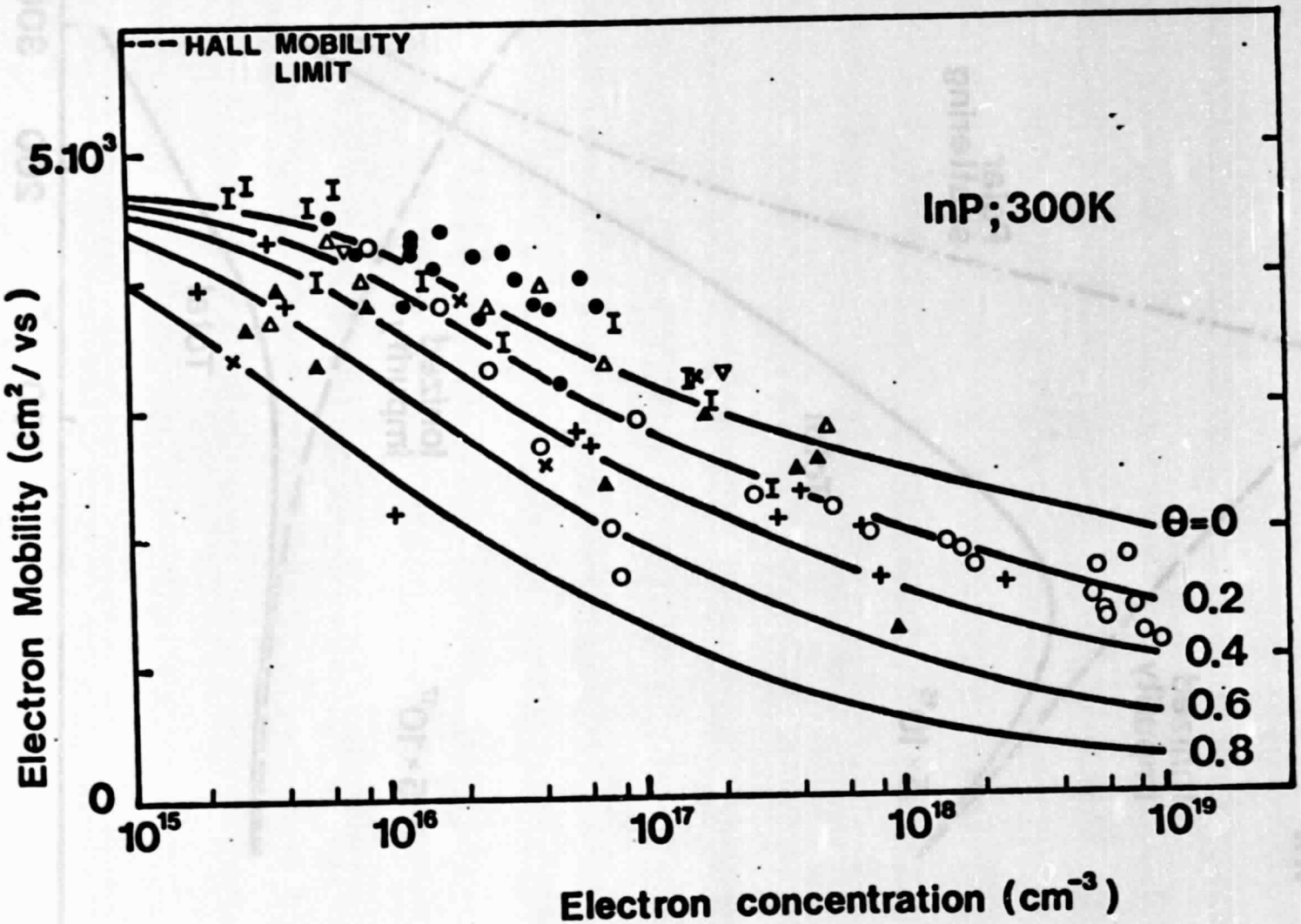
HALL MOBILITY LIMIT
InP;300K
5.10³
0
Electron Mobility (cm²/ vs)
θ=0
0.2
0.4
0.6
0.8
10¹⁵
10¹⁶
10¹⁷
10¹⁸
10¹⁹
Electron concentration (cm⁻³)

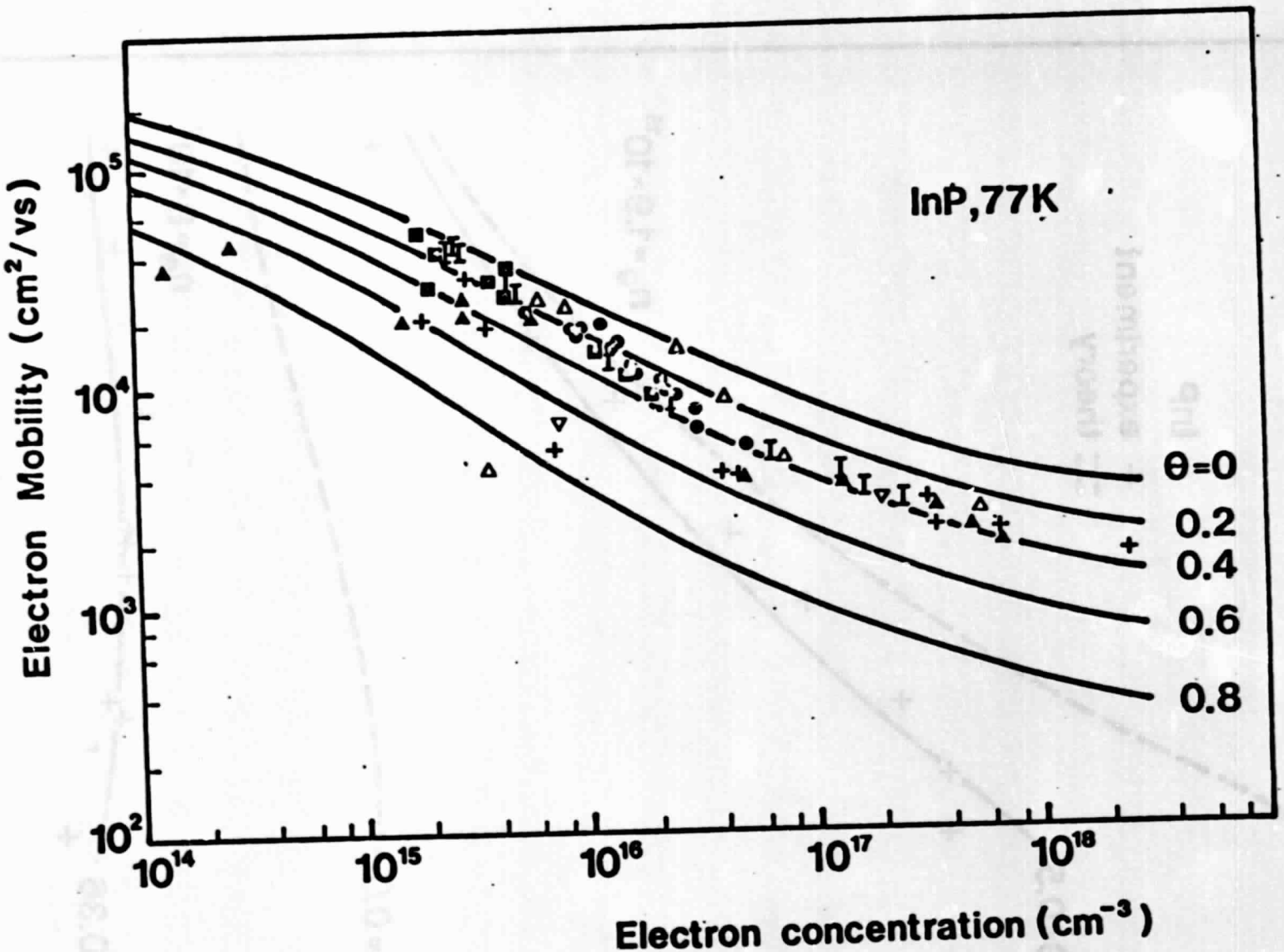
InP,77K
Electron Mobility (cm²/vs)
10⁵
10⁴
10³
10²
θ=0
0.2
0.4
0.6
0.8
10¹⁴
10¹⁵
10¹⁶
10¹⁷
10¹⁸
Electron concentration (cm⁻³)

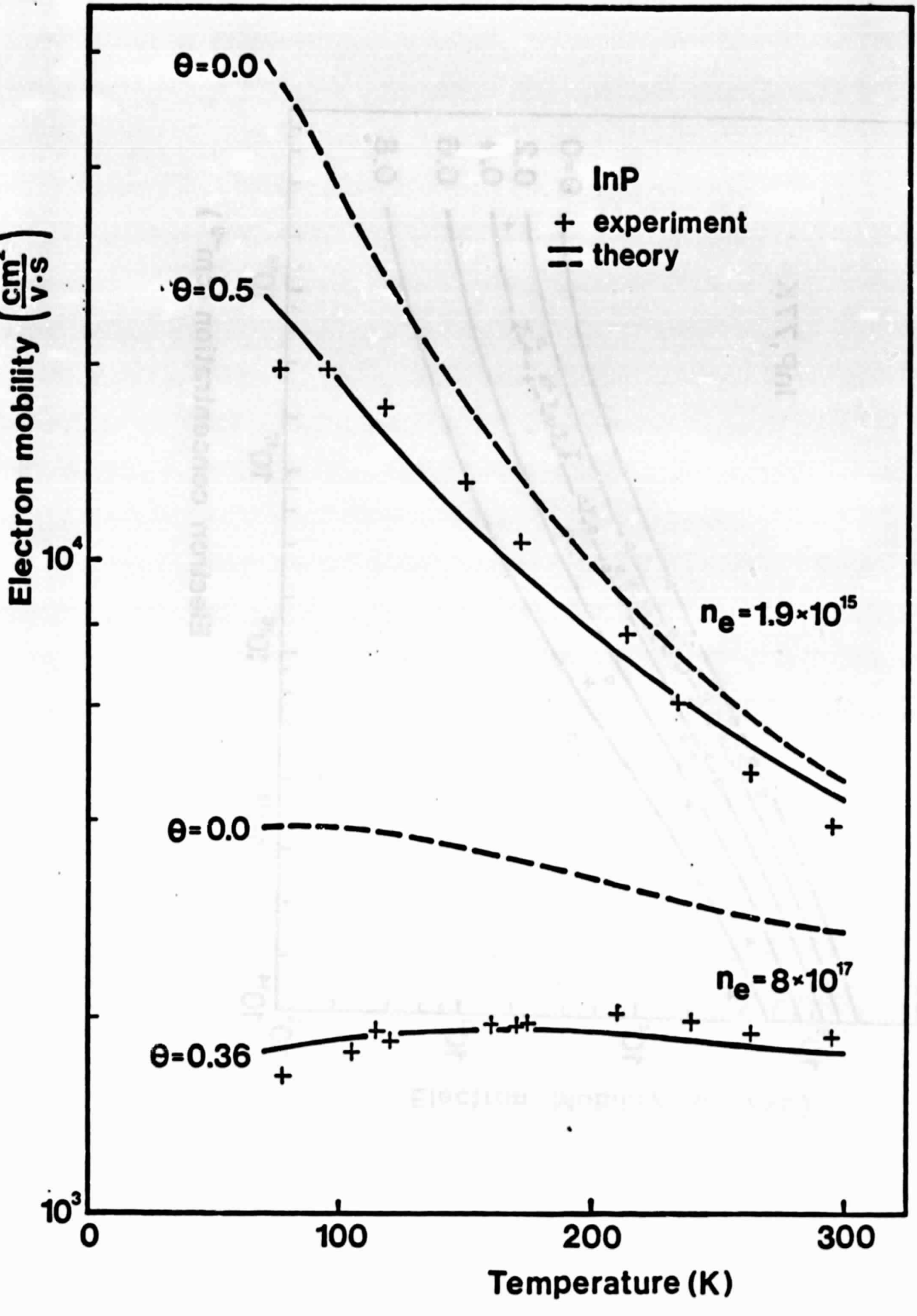
θ=0.0
InP
+ experiment
= theory
θ=0.5
Electron mobility $\left(\frac{cm^2}{V \cdot s}\right)$
10^4
$n_e = 1.9 \times 10^{15}$
θ=0.0
$n_e = 8 \times 10^{17}$
θ=0.36
10^3
0
100
200
300
Temperature (K)

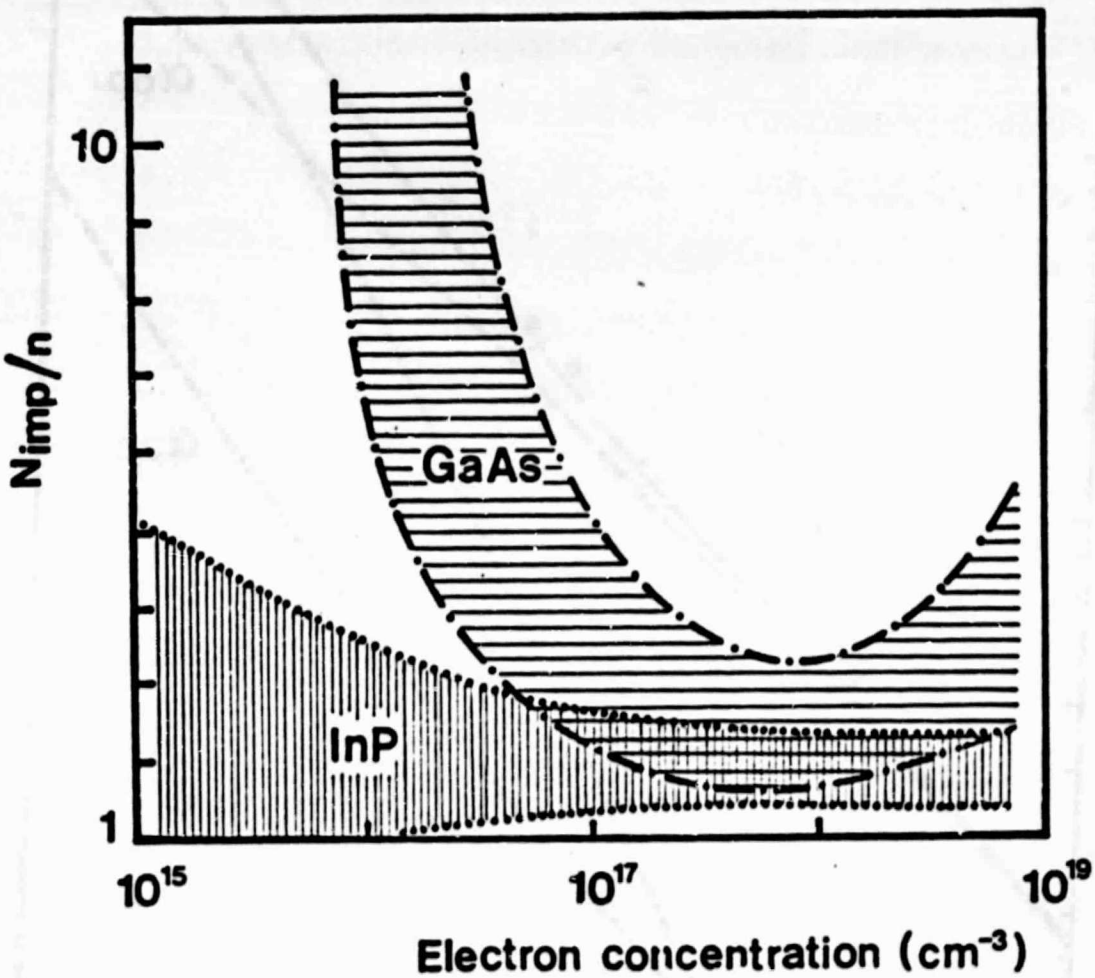
10
1
Nimp/n
GaAs
InP
10^15
10^17
10^19
Electron concentration (cm^-3)

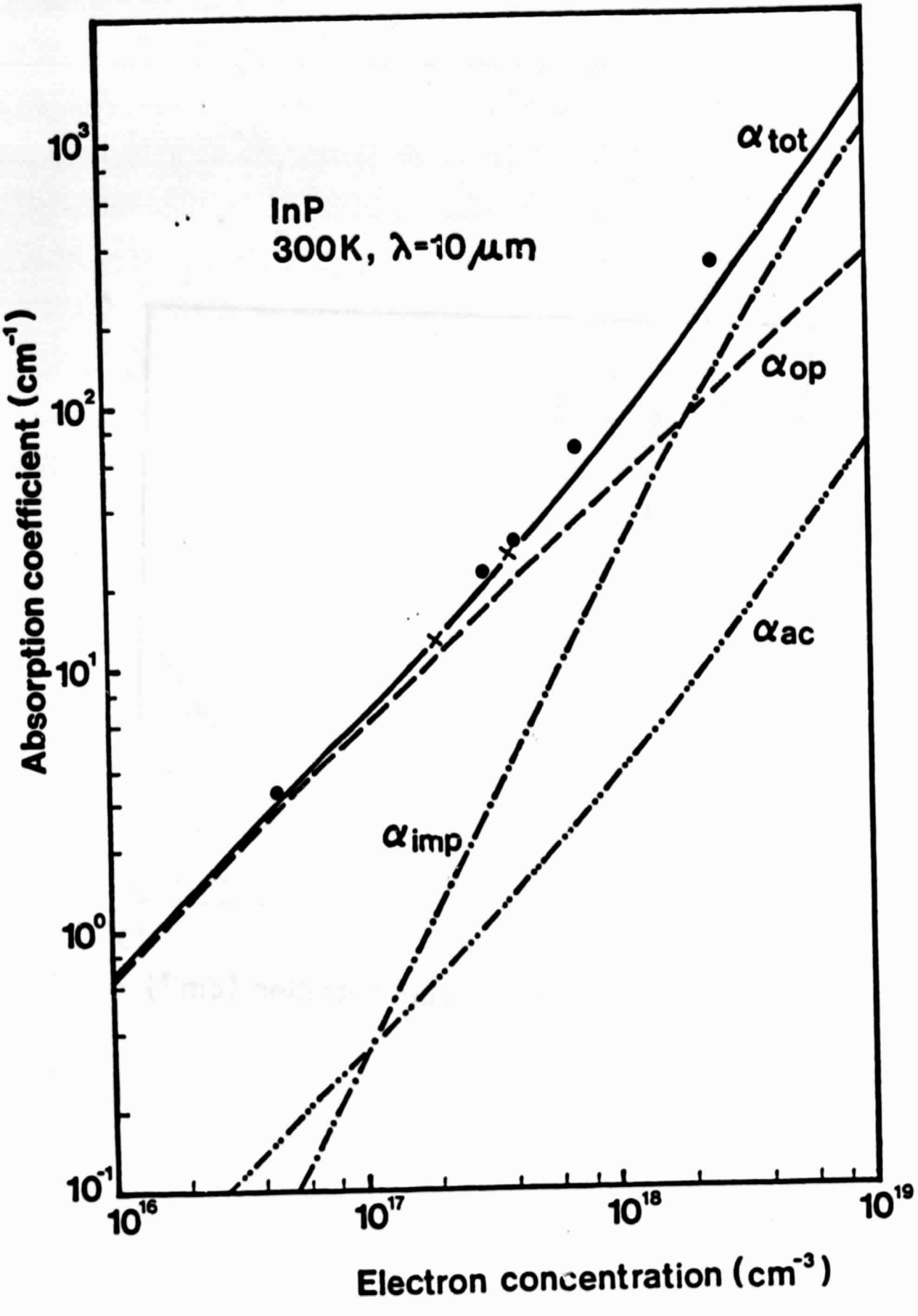
InP
300K, λ=10μm
α_{tot}
α_{op}
α_{ac}
α_{imp}
Absorption coefficient (cm^{-1})
10^3
10^2
10^1
10^0
10^{-1}
10^{16}
10^{17}
10^{18}
10^{19}
Electron concentration (cm^{-3})

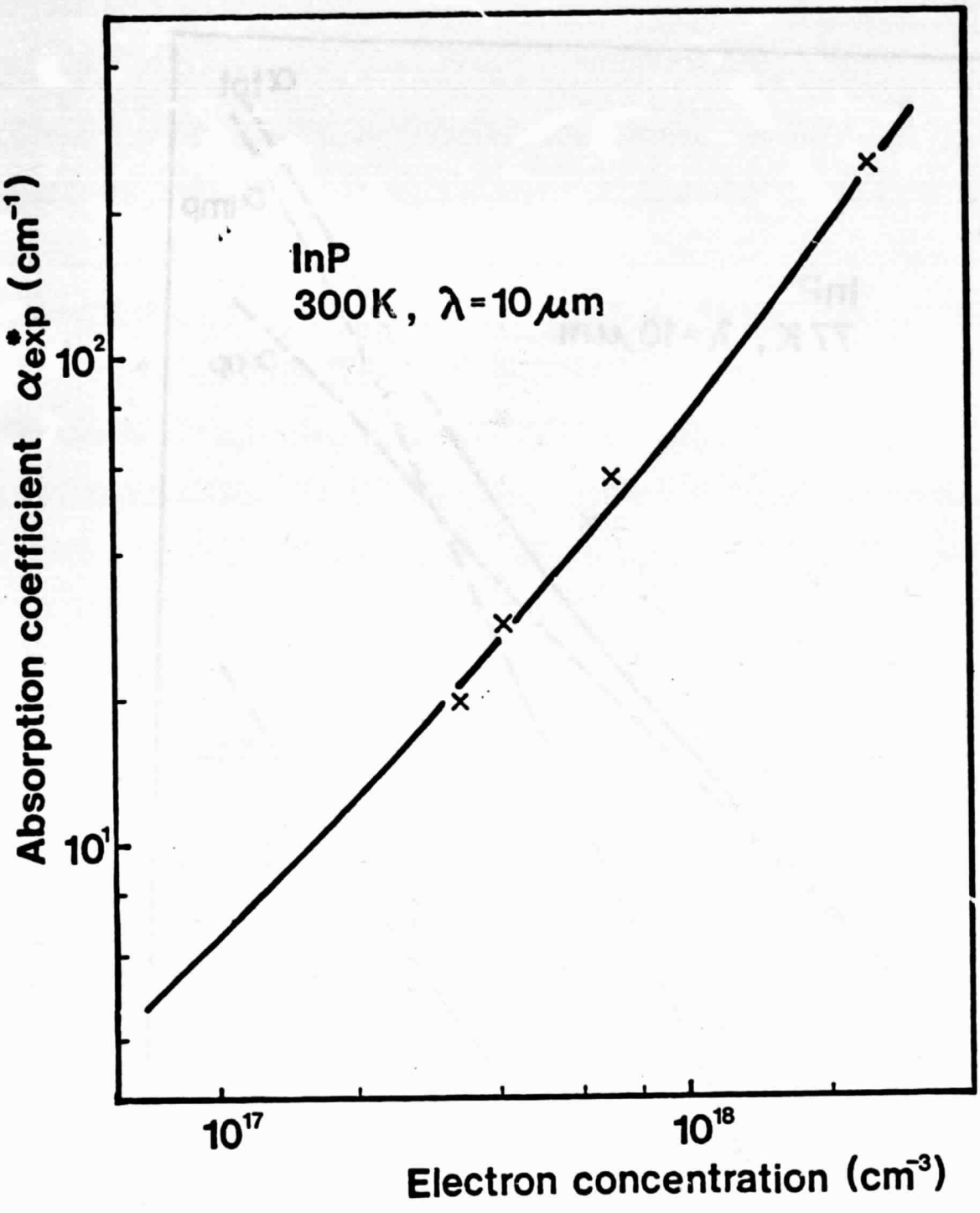
InP
300K, λ=10μm
Absorption coefficient α^{*}_{exp} (cm^{-1})
10^{2}
10^{1}
10^{17}
10^{18}
Electron concentration (cm^{-3})

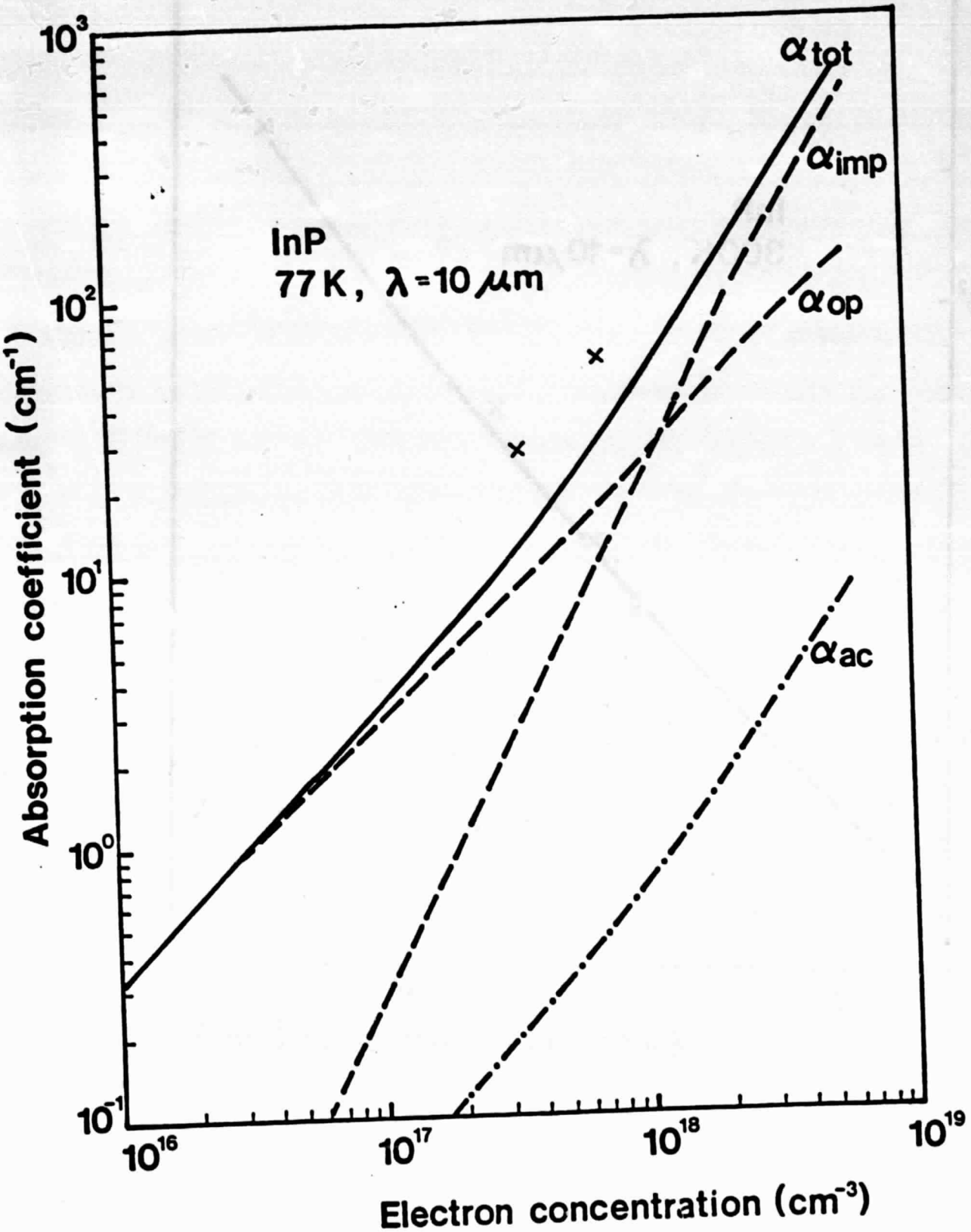
InP
77 K, λ = 10 μm
α_{tot}
α_{imp}
α_{op}
α_{ac}
Absorption coefficient (cm^{-1})
Electron concentration (cm^{-3})
10^{3}
10^{2}
10^{1}
10^{0}
10^{-1}
10^{16}
10^{17}
10^{18}
10^{19}

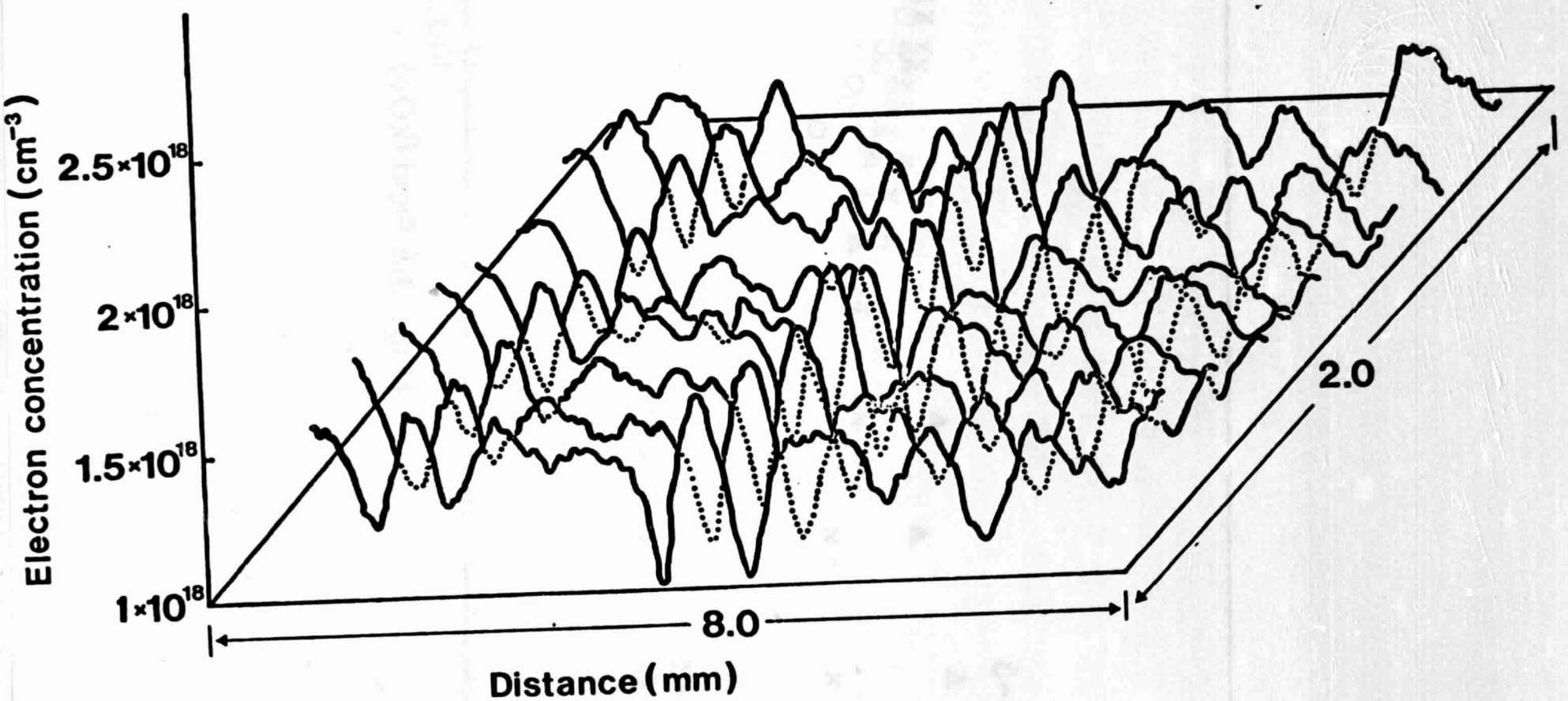
Electron concentration (cm^{-3})
2.5×10^{18}
2×10^{18}
1.5×10^{18}
1×10^{18}
8.0
2.0
Distance (mm)

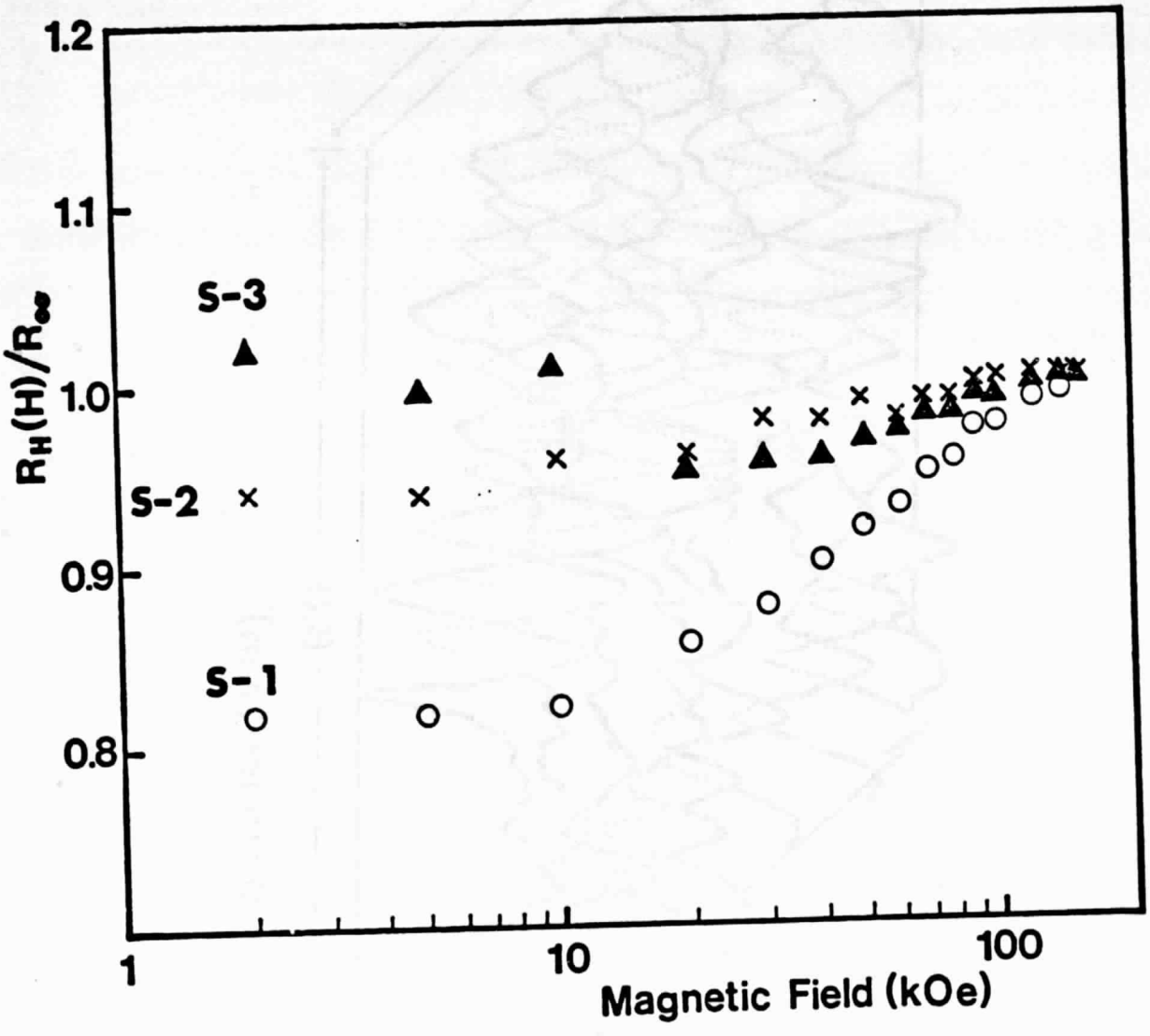
1.2
1.1
1.0
0.9
0.8
$R_H(H)/R_\infty$
S-3
S-2
S-1
1
10
100
Magnetic Field (kOe)

DETERMINATION OF CARRIER CONCENTRATION AND COMPENSATION MICROPROFILES IN GaAs

L. Jastrzebski,[a] J. Lagowski, W. Walukiewicz[b] and H. C. Gatos
Department of Materials Science and Engineering
Massachusetts Institute of Technology
Cambridge, Massachusetts 02139

Simultaneous microprofiling of semiconductor free carrier, donor and acceptor concentrations was achieved for the first time from the absolute value of the free carrier absorption coefficient and its wavelength dependence determined by IR absorption in a scanning mode. Employing Ge- and Si-doped melt-grown GaAs, striking differences were found between the variations of electron concentration and those of ionized impurity concentrations. These results showed clearly that the electronic characteristics of this material are controlled by amphoteric doping and deviations from stoichiometry rather than by impurity segregation.

Journal of Applied Physics, in press

The simultaneous determination of the donor and acceptor concentrations is of particular importance in III-V semiconductor compounds which exhibit an appreciable degree of compensation. A number of techniques utilizing spreading resistance,[1] Schottky barriers,[2] EBIC,[3,4] electroreflectance[5] and IR absorption[6-9] or topography[10,11] have been developed for profiling the carrier concentration in semiconductors. However, these techniques essentially fail to distinguish between changes in impurity concentration and in compensation ratio. The present method is an application of the recent quantitative studies of the free carrier absorption in GaAs[12] and InP[13] as a means of determining the compensation ratio. The principle of the method is understood by considering that the absolute value and the wavelength dependence of the free carrier absorption coefficient are experimentally measured quantities which contain only two unknown parameters, namely the electron concentration $n = N_D - N_A$ and the compensation ratio $\theta = N_A/N_D$. (N_D and N_A are the concentrations of ionized donors and acceptors, respectively.)

The experimental arrangement for microprofile determinations consists of a CO_2 tunable laser (with about 90 lines in the spectral range of 9.16-11.02 μm), a stage with x-y scanning motion, an optical system for monitoring the power and wavelength of the laser beam, and an IR detector. Optically flat samples were mounted on the stage, and the intensity of a collimated beam (~ 30 μm in diameter) transmitted through the wafer was measured as a function of its position along the sample.

From the IR transmission scans the absorption coefficient, α, was obtained utilizing the standard relationship:

$$T = \frac{(1-R)^2 \exp(-\alpha d)}{1-R^2 \exp(-2\alpha d)} \qquad (1)$$

where T is the transmittance, d is the thickness of the sample, and R is the reflectance (values of R are tabulated in Ref. (14)). Measurements were performed with different wavelengths of the laser radiation in order to determine the wavelength dependence of the absorption coefficient.

Common difficulties encountered in scanning IR absorption measurements arise from interferenc e effects. The large refractive index of semiconductors in the infrared region (usually for $\lambda \simeq 10$ μm, the refractive index exceeds 3) enhances the interference due to slight variations of the wafer thickness. For thicker wafers, the temperature dependence of the refractive index can also lead to interference effects in the presence of temperature gradients. These effects were essentially eliminated by careful polishing of the wafers, by utilizing a small power incident laser beam (to prevent heating of the wafer) and by performing the measurements under conditions of low transmittance ($\alpha d > 2$, eq. 1). The negligible role of interference effects was verified by carrying out scanning IR absorption measurements at different wavelengths and for different values of incident beam power.

In ref. (12) the study of free carrier absorption was primarily addressed to the determination of the compensation ratio, θ, from measured values of the absorption coefficient, α_{exp}. The simultaneous determination of the electron concentration, $n = N_D - N_A$, can be obtained if the logarithmic slope $p \equiv \frac{d\ell n\alpha}{d\ell n\lambda}$ is also available.

For n-type GaAs at room temperature, α_{exp} can be expressed as[15,12]

$$\alpha_{exp} = \alpha_{op} + \alpha_{ac} + \alpha_{imp} N_{imp}/n \qquad (2)$$

where α_{op} and α_{ac} are the absorption coefficients corresponding to electron interaction with screened optical phonons and acouston phonons, respectively;

α_{imp} is the absorption coefficient due to the interaction of electrons with screened ionized impurities in uncompensated material, and N_{imp} is the actual total concentration of ionized impurities $N_D + N_A$. For a given temperature and wavelength λ the component absorption coefficients, α_{op}, α_{ac} and α_{imp} are determined knowing the electron concentration, n. Values of these coffiecients for $\lambda = 10$ μm are tabulated in ref. 12 as a function of n.

The component absorption coefficients are characterized by different wavelength dependences. In the vicinity of $\lambda_o = 10$ μm they can be expressed as[12]

$$\alpha_{op}\Big|_{\lambda} = \alpha_{op}\Big|_{\lambda_o} \cdot \left(\frac{\lambda}{\lambda_o}\right)^{2.5} \quad ; \quad \alpha_{ac}\Big|_{\lambda} = \alpha_{ac}\Big|_{\lambda_o} \cdot \left(\frac{\lambda}{\lambda_o}\right)^{1.5} \quad ; \text{ and}$$

$$\alpha_{imp}\Big|_{\lambda} = \alpha_{imp}\Big|_{\lambda_o} \cdot \left(\frac{\lambda}{\lambda_o}\right)^{3.5} \tag{3}$$

By differentiating equations 2 and 3 it is shown that the slope $p \equiv \frac{d\ell n\alpha}{d\ell n\lambda} = \frac{\lambda}{\alpha}\frac{d\alpha}{d\lambda}$ in the vicinity of λ_o satisfies the relationship

$$(3.5 - p) = \frac{\alpha_{op} + 2\alpha_{ac}}{\alpha_{exp}} \tag{4}$$

Computed values of $\alpha_{op}+2\alpha_{ac}$ as a function of electron concentration are shown in Fig. 1. In the range of n considered, α_{op} exhibits a slightly sublinear dependence on n (screening effects) while α_{ac} increases stronger than linearly with increasing n (effect of degeneracy). However, as seen in Fig. 1, $\alpha_{op}+2\alpha_{ac} = 3.33\times10^{-17}n$. Thus eq. (4) can be rewritten in the convenient form

$$n[cm^{-3}] = 3.10^{16}(3.5-p)\alpha_{exp}[cm^{-1}] \tag{5}$$

which permits the direct determination of n from the measured values of p and α_{exp}.

As shown in Fig. 2, the values of p in n-type GaAs can vary between 2.5 and 3.5, depending on the electron concentration and compensation ratio (or total concentration of ionized impurities). These changes of p with n and/or θ were neglected in previous treatments of scanning IR absorption[6-9] and topography[10,11] where direct proportionality between α_{exp} and n was assumed; such simplified relationship is justified only when scattering by ionized impurities is negligible. However, it is evident from eq. 5 and Fig. 2 that for $n > 10^{17}$ the reliable determination of the electron concentration in GaAs requires the measurement of the absorption coefficient and its wavelength dependence. When the electron concentration, n, is determined, the total concentration of ionized impurities, N_{imp}, can be obtained from expression 2, using the values of α_{op}, α_{ac}, and α_{imp}, tabulated in ref. 12. Knowledge of n and N_{imp} permits the determination of the compensation ratio θ and/or the concentration of ionized donors N_D and acceptors N_A.

Microprofiles of free carrier, donor and acceptor concentrations obtained with melt-grown (horizontal Bridgman) Ge- and Si-doped GaAs are presented in figures 3 and 4, respectively. The inhomogeneities seen in these figures, although of an amplitude larger than average, are typical of all crystals obtained from several sources. Actually, as a general rule, all presently available melt-grown GaAs is highly compensated and exhibits pronounced variations in free carrier concentration.[12,16]

A striking feature of the results of Fig. 3 is that the electron concentration exhibits large fluctuations of a magnitude comparable to its average value, while the total concentration of ionized impurities remains essentially constant. The average compensation ratio of this material was found to be about 0.4, which is a typical value for GaAs with an electron concentration in the range of $10^{18} cm^{-3}$.[12] It is also seen in Fig. 3 that the spatial

variations of donor and acceptor concentration are out of phase, i.e., maxima in N_D coincide with minima of N_A.

The variations of the donor and acceptor variations shown in Fig. 3 cannot be explained on the basis of standard impurity segregation behavior controlled by the crystal growth velocity or the diffusion boundary layer thickness.[17] If it is assumed that the donor concentration variations reflect standard segregation behavior, the maxima in donor concentration must correspond to maxima in growth rate or diffusion boundary layer thickness, since the distribution coefficient of Ge is smaller than one.[18] In that case the acceptor impurity must be an unintentionally added impurity with a distribution coefficient greater than one, since its concentration maxima coincide with the Ge concentration minima. However, there are no known impurities with a distribution coefficient greater than one in the GaAs system.[18] Nor is it likely that an unintentionally added impurity is present at as high a level as $10^{18}cm^{-3}$. Thus, both donor and acceptor levels must be attributed to Ge (amphoteric doping). Accordingly, the segregation of Ge ($N_D + N_A$) undergoes only small fluctuations, and the free carrier variations are due to the variations of the relative Ge concentration in Ga (donor) sites and in As (acceptor) sites. Such variations (which are consistent with free carrier concentration fluctuations) must be associated with factors affecting the relative concentrations of Ga and As vacancies or stoichiometry of GaAs. No correlation between point defect formation and growth parameters is available.[16]

Similarly, the free carrier concentration profiles in Si-doped GaAs cannot be accounted for by standard segregation behavior. Thus, in Fig. 4a the donor and acceptor concentration changes are not nearly as pronounced. The results of Fig. 4b were obtained from the same Si-doped crystal as those of Fig. 4a, but a different segment. In this case, the fluctuations of the free carrier,

the donor and the total ionized impurity ($N_D + N_A$) concentrations are of similar nature and magnitude, but the ionized acceptor concentration undergoes relatively small variations.

It is apparent from figures 3 and 4 that fluctuations in the individual profiles of carrier, donor, acceptor and total ionized impurity concentration can readily be mistaken as related to standard impurity segregation behavior as they resemble well established impurity segregation variations, particularly in elemental semiconductors. Thus, all of these microproifles must be simultaneously considered in assessing the origin of inhomogeneities in compound semiconductors.

In summary, a method is developed for the simultaneous determination of free carrier, donor and acceptor microprofiles. It is also shown that in Ge- and Si-doped melt-grown GaAs dopant inhomogeneities are not controlled by standard impurity segregation behavior, but rather by growth factors affecting amphoteric doping and stoichiometry, which cannot be as yet unambiguously defined.

ACKNOWLEDGEMENT

The authors are grateful to the National Aeronautics and Space Administration for financial support.

REFERENCES

(a) Present address: RCA David Sarnoff Research Center, Princeton, New Jersey 08540.

(b) Present address: Institute of Physics, Polish Academy of Sciences, Warsaw, Poland.

1. See for example, J. R. Ehrstein, in "Semiconductor Silicon 1977," H. R. Huff and E. Sirtl, Editors, p. 327, The Electrochemical Society Softbound Symposium Series, Princeton, N. J. (1977).
2. M. F. Matare, Solid State Technol. 20, 56 (1977).
3. A. J. R. deKock, S. D. Ferris, L. C. Kimerling and H. J. Leamy, J. Appl. Phys. 48, 301 (1977).
4. J. Y. Chi and H. C. Gatos, J. Appl. Phys. 50, 3433 (1979).
5. R. Sittig, Surface Sci. 37, 987 (1973).
6. V. T. Prokopenko and A. D. Yaskov, Prib. Tekh. Eksp. 3, 215 (1974).
7. V. T. Prokopenko, V. S. Rondarev, A. V. Semenov and A. D. Yaskov, Zavadskaya Laboratoriya 43, 986 (1977).
8. D. L. Spears and A. J. Strauss, Solid State Research Report, Lincoln Laboratory, MIT 3, 9 (1974).
9. L. Jastrzebski, J. Lagowski and H. C. Gatos, J. Electrochem. Soc. 126, 260 (1979)
10. F. E. Roberts, Solid-State Electron. 1, 93 (1960).
11. B. Sherman and J. F. Black, Appl. Opt. 9, 802 (1970).
12. W. Walukiewicz, J. Lagowski, L. Jastrzebski, M. Lichtensteiger and H. C. Gatos, J. Appl. Phys. 50, 899 (1979).
13. W. Walukiewicz, J. Lagowski, L. Jastrzebski, P. Rava, M. Lichtensteiger, C. H. Gatos and H. C. Gatos, submitted to J. Appl. Phys.
14. B. O Seraphin and H. E. Bennett in "Semiconductors and Semimetals," eds. R. K. Willardson and A. C. Beer, Academic Press, New York 1967, vo. 3, ch. 12.
15. E. Haga and H. Kimura, J. Phys. Soc. Japan 19, 658 (1964).

16. H. C. Gatos, J. Lagowski and L. Jastrzebski, "Present Status of GaAs," NASA Report 3090, (1979).

17. J. A. Burton, R. C. Prim and W. P. Slichter, J. Chem. Phys. 21, 1987 (1953a).

18. S. Skalski, in "Compound Semiconductors," editors R. K. Willardson and H. L. Goering, Reinhold Publishing Corp., New York 1962, vol. I, p. 385

FIGURE CAPTIONS

Figure 1. Dependence of $\alpha_{op} + 2\alpha_{ac}$ on electron concentration (see text).

Figure 2. Calculated logarithmic slope, p, of the free carrier absorption coefficient of n-type GaAs as a function of compensation ratio, θ, in n-type GaAs at room temperature.

Figure 3. Electron concentration and ionized impurity microprofiles of Ge-doped melt-grown GaAs.

Figure 4. Electron concentration and ionized impurity microprofiles of Si-doped melt-grown GaAs. (a) and (b) correspond to different segments of the same crystal.

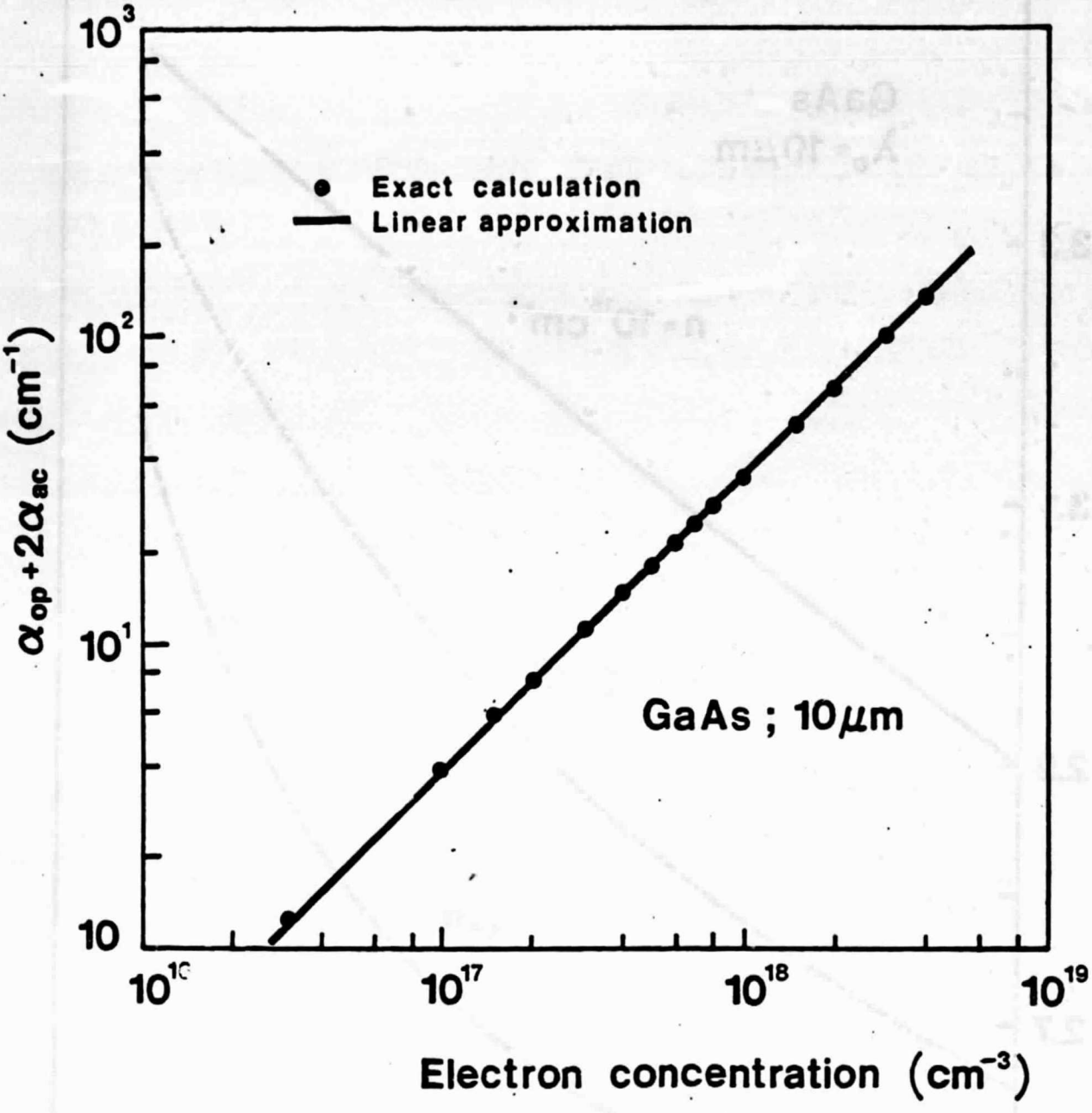
Exact calculation
Linear approximation
GaAs ; 10μm
$\alpha_{op}+2\alpha_{ac}$ (cm^{-1})
Electron concentration (cm^{-3})
10^3
10^2
10^1
10
10^{16}
10^{17}
10^{18}
10^{19}

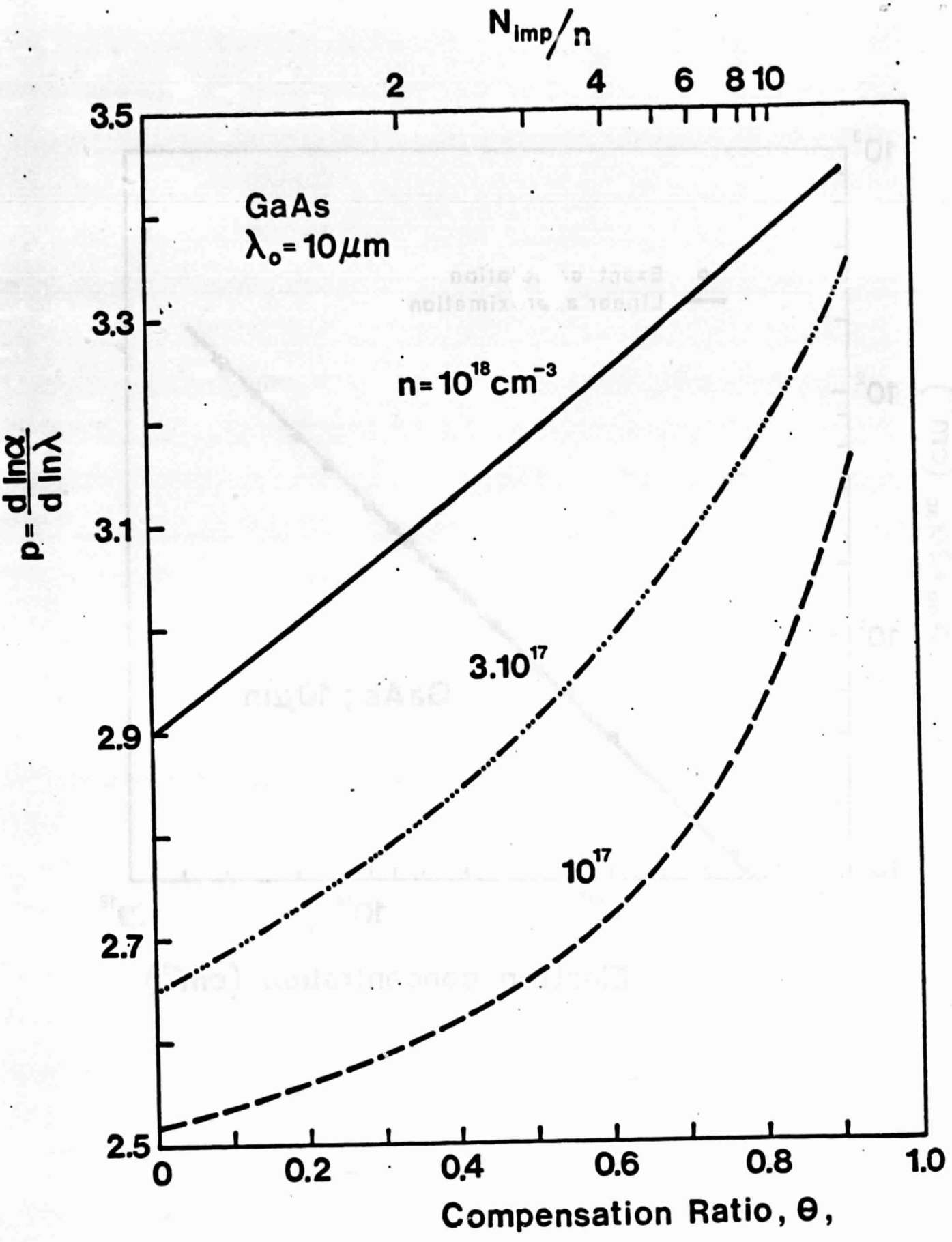
N_{imp}/n
2
4
6
8
10
3.5
3.3
3.1
2.9
2.7
2.5
GaAs
$\lambda_o = 10\mu m$
$n = 10^{18} cm^{-3}$
3.10^{17}
10^{17}
$p = \frac{d \ln \alpha}{d \ln \lambda}$
0
0.2
0.4
0.6
0.8
1.0
Compensation Ratio, θ,

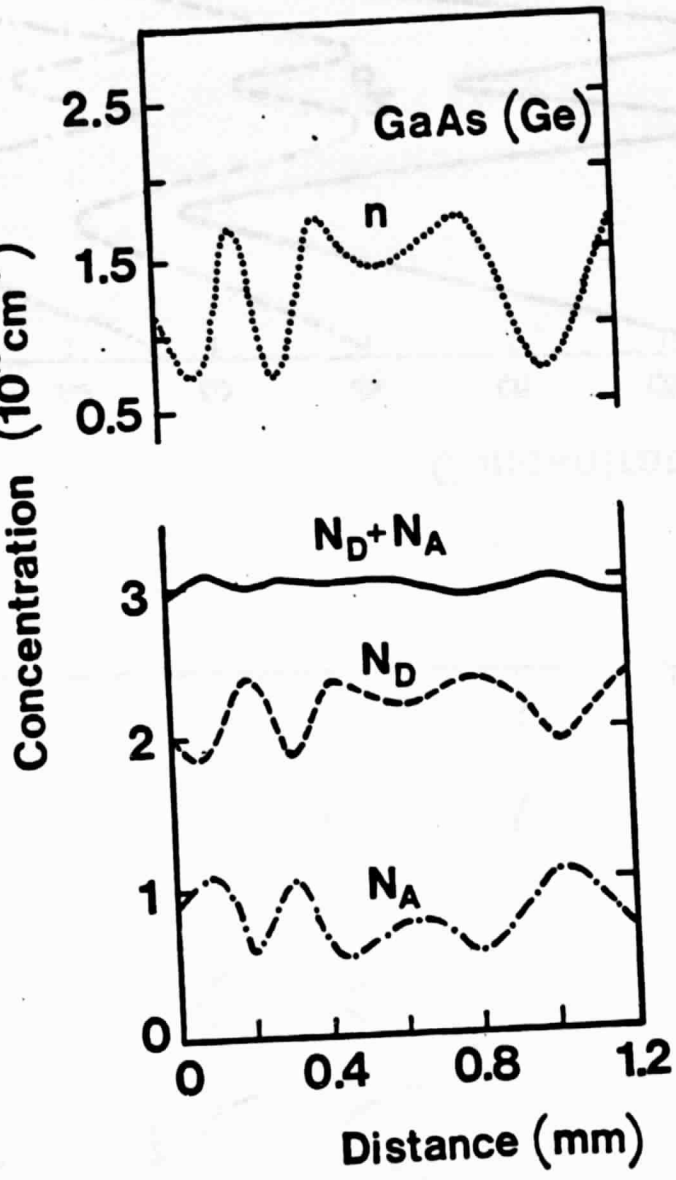
GaAs (Ge)
n
2.5
1.5
0.5
Concentration (10^{18}cm^{-3})
N_D+N_A
N_D
N_A
3
2
1
0
0
0.4
0.8
1.2
Distance (mm)

Fig. 3